Technical Report

TR-06-23

Climate and climate-related issues for the safety assessment SR-Can

Svensk Kärnbränslehantering AB

November 2006

Svensk Kärnbränslehantering AB
Swedish Nuclear Fuel
and Waste Management Co
Box 5864
SE-102 40 Stockholm Sweden
Tel 08-459 84 00
+46 8 459 84 00
Fax 08-661 57 19
+46 8 661 57 19

Climate and climate-related issues for the safety assessment SR-Can

Svensk Kärnbränslehantering AB

November 2006

Preface

This document compiles information on climate and climate related issues relevant for long-term safety of a KBS-3 repository. It supports the safety assessment SR-Can, which is a preparatory step for a safety assessment that will support the licence application for a final repository in Sweden.

The report has been compiled by Jens-Ove Näslund, SKB. A number of authors have contributed to various sections of the report as listed in Table 1-1.

The report has been reviewed by Mike Thorne, Mike Thorne and Associates Ltd, UK.

Stockholm, October 2006

Allan Hedin
Project leader SR-Can

Contents

1 Introduction

1.1 Purpose and structure of the report

The purpose of this report is to document current scientific knowledge of the climate-related conditions and processes relevant to the long-term safety of a KBS-3 repository to a level required for an adequate treatment in the safety assessment SR-Can. The report also includes a concise background description of the climate system. The report includes three main chapters:

- A description of the climate system (Chapter 2).
- Identification and discussion of climate-related issues (Chapter 3).
- A description of the evolution of climate-related conditions for the safety assessment (Chapter 4).

Chapter 2 includes an overview of present knowledge of the Earth climate system and the climate conditions that can be expected to occur in Sweden on a 100,000 year time perspective. Based on this, climate-related issues relevant for the long-term safety of a KBS-3 repository are identified. These are documented in Chapter 3 “Climate-related issues” to a level required for an adequate treatment in the safety assessment. Finally, in Chapter 4, “Evolution of climate-related conditions for the safety assessment” an evolution for a 120,000 year period is presented, including discussions of identified climate-related issues of importance for repository safety. The documentation is from a scientific point of view not exhaustive, since such a treatment is neither necessary for the purposes of the safety assessment nor possible within the scope of a safety assessment.

As further described in the /**SR-Can Main Report**/ and in the /**FEP report**/ (Features Events and Processes report) the content of the present report has been audited by comparison with FEP databases compiled in other assessment projects. This report follows as far as possible the template for documentation of processes regarded as internal to the repository system. However, the term processes is not used in this report, instead the term *issue* has been used. Each issue includes a set of processes together resulting in the behaviour of a system or feature. For instance, “ice sheet dynamics” is the result of several climatological, hydrological, and mechanical processes. But as the ice sheet can be seen as one entity in its interaction with the bed, these processes are jointly accounted for under the heading “ice sheet dynamics”.

The experts involved in assembling the basic information about the climate system and climate-related issues are listed in Table 1-1. In addition, the sections “Handling in the safety assessment SR-Can” and “Handling of uncertainties in SR-Can” have been produced by Jens-Ove Näslund and Lena Morén, SKB, in collaboration with the expert that assembled the information on the issue in question. All experts contributing to the present report are included in the SR-Can expert database.

Table 1-1. Authors of individual chapters and sections, including experts responsible for the documentation of climate-related issues (Sections 3-1 to 3-5).

Chapter/Section	Responsible author
1 Introduction	Lena Morén, SKB; Jens-Ove Näslund, SKB
2 The climate system (Sections 2.1–2.3)	Jörgen Bogren and Torbjörn Gustavsson, Klimator AB, Göteborg university
Climate variability and change (in Section 2.3.4)	Moberg et al. 2006
2.4 Climate in Sweden	Hans Alexandersson, SMHI
3.1 Ice sheet dynamics	Jens-Ove Näslund, Stockholm university, SKB
3.2 Ice sheet hydrology	Peter Jansson, Stockholm university
3.3 Isostatic adjustment and shoreline migration	Pippa Whitehouse, University of Durham
3.4 Development of permafrost	Juha Hartikainen, Helsinki University of Technology; Thomas Wallroth, Bergab
3.5 End-glacial faulting	Björn Lund, Uppsala university
4.1–4.4 Evolution of climate-related conditions	Jens-Ove Näslund and Lena Morén, SKB
4.4.1 Extremes within the permafrost domain	Juha Hartikainen, Helsinki University of Technology; Jens-Ove Näslund, SKB
4.4.2 Extremes within the glacial domain	Jens-Ove Näslund, SKB

1.2 Structure for description of climate-related issues

In discussing each of the various climate-related issues, the following standardised structure has been adopted.

1.2.1 Overview/general description

Under this heading, a general description of the current knowledge regarding the climate-related issue is given.

A table summarising the influence of the climate-related issue on the geological barrier of the repository is produced. The table includes the geosphere variables influenced by the system/feature and the variables associated with the system/feature that are required to be known to quantify the interaction between the system/feature and the repository system, e.g. for "ice sheet dynamics" basal temperature and melt-rate. In this context, the repository system includes both the geosphere and the engineered barriers.

1.2.2 Controlling conditions and factors

The external and internal conditions and factors that control or govern each "issue" are discussed. External refers to systems that are not part of the described system/feature and that the described system/feature interacts with. For example, for "ice sheet dynamics", the atmosphere and the bed are external factors and relevant aspects of them are described. Internal refers to conditions and factors governing system/feature behaviour and that are generally included in models of the system/feature, e.g. for "ice sheet dynamics" the creep process of ice. The external and internal conditions and factors are those that relate to the described behaviour of the system/feature, e.g. for "ice sheet dynamics" air temperature, geothermal heat flow and ice properties.

1.2.3 Observations in nature and present-day natural analogues

Under this heading observations in nature and – when applicable – present-day natural analogues regarding the process are summarised.

1.2.4 Model studies

Model studies of the process are summarised. This documentation focuses on process understanding and for instance includes sensitivity analyses. The handling of external and internal controlling conditions and factors are described. Are e.g. spatially and temporally varying internal conditions considered?

1.2.5 Time perspective

The time scales on which the system/feature operates and changes are documented.

1.2.6 Handling in the safety assessment SR-Can

The handling of the documented interactions with the repository is discussed. As a result of the information under this subheading, a mapping of the climate system-related issues to method of treatment and, in relevant cases, applicable models are produced, see the Interim main report /SKB 2004a/ for an example. The mapping is characterised on various time scales.

1.2.7 Handling of uncertainties in SR-Can

Given the adopted handling in the safety assessment SR-Can as described above, the treatment of different types of uncertainties associated with the process, within that general framework, is summarised under the following headings.

Uncertainties in mechanistic understanding: The uncertainties in the general understanding of the process are discussed based on the available documentation and with the aim of answering the question: Are the basic scientific mechanisms governing the process understood to a level necessary for the suggested handling? Alternative models may sometimes be used to illustrate this type of uncertainty.

Model simplification uncertainties: In most cases, the quantitative representation of a process contain simplifications, for instance in a numerical model. These may result in a significant source of uncertainty in the description of the system evolution. Alternative models or alternative approaches to simplification for a particular conceptual model may sometimes be used to illustrate this type of uncertainty.

Input data and data uncertainties: The input data necessary to quantify the process for the suggested handling are documented. The further treatment of important input data and input data uncertainties described in the /**Data report**/, to which reference are made as appropriate.

1.3 Strategy for managing climate-related issues in safety assessments

1.3.1 Climate and climate-related changes

Climate-related changes such as shoreline migration and the development of permafrost and ice sheets are the most important naturally occurring external factors affecting the repository in a time perspective from tens to hundred of thousands of years. Most of the processes occurring in the biosphere and geosphere regarded as internal to the repository system are likely to be affected by climate and climate-related changes. In very long time perspectives, millions to several millions of years, geological processes like plate tectonic movements and uplift or downwarping (additional to those crustal displacements due to glacial loading and unloading) will affect both the repository and the Earth climate system.

Studied time frame

The SR-Can safety performance assessment need to address timescales up to one million years /**SR-Can Main Report**/. For the past 2.5 million years, Fennoscandia has experienced several cycles of growth and decay of ice sheets. Periods during which ice sheets gradually grow to a maximum extent are known as *glacials*. Periods with warm climate when the ice sheets wane to an extent similar to that at the present day are called *interglacials*. A *glacial cycle* consists of a glacial and an interglacial. Within the generally cool glacial, warmer *interstadial* periods occur, as well as cool *stadial* periods. The shifting between glacials and interglacials is depicted for instance in the variation of the content of the heavy oxygen isotope, ^{18}O, in deep sea sediments which reflect the temperature of the sea and, more importantly, the volume of water that has been bound in land-based ice sheets and glaciers all over the world, see Figure 1-1.

Over the last 700,000 years, glacial-interglacial cycles of about 100,000 year duration have dominated climate variation. Such a glacial-interglacial cycle is considered to give rise to the extremes of climate conditions that the repository should be designed to withstand. The time frame of a glacial-interglacial cycle, 100,000 years, is also similar to the time it takes for the radioactivity in the spent fuel to decay to levels comparable to the activity in the natural uranium that was once used to manufacture the fuel /**SR-Can Main Report**/. The time scale of a safety assessment for a final repository for spent nuclear fuel should be one million years. For the period up to approximately 100,000 years, the reporting is required to be based on a quantitative risk analysis /**SR-Can Main Report**/. The 100,000 year time frame, corresponding to the first glacial cycle, is thus chosen as a basis for analysing repository safety. For the remainder of the assessment period, this glacial cycle is assumed to be repeated. An alternative development of the first 100,000 years, including a period of anthropogenic climate warming, is also analysed, see below. A time frame of 100,000 years is also reasonable when determining the extremes of climate conditions the repository should be designed to withstand.

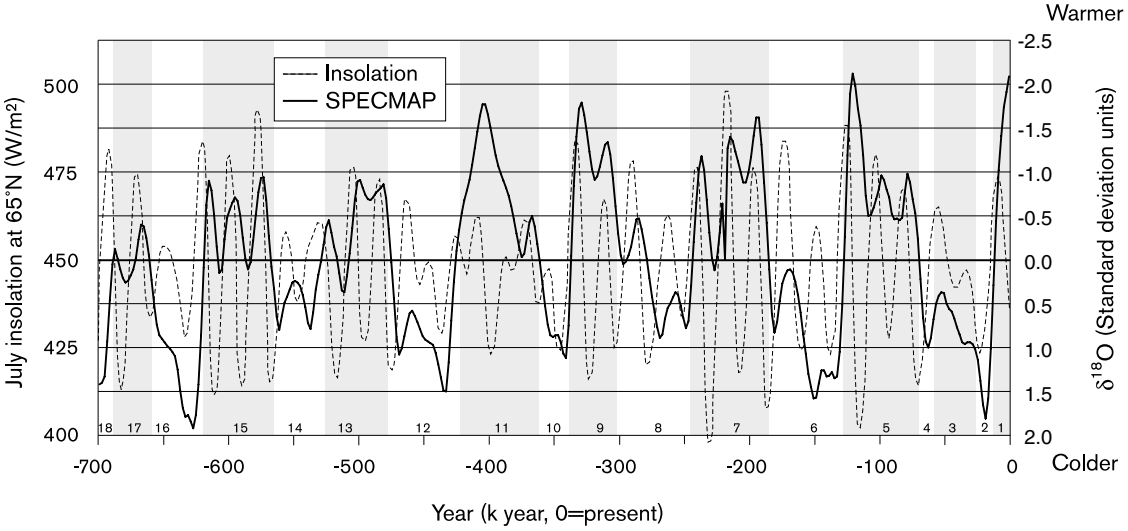

Figure 1-1. *Variations of ^{18}O in deep sea sediments the last 2.5 million years /from Imbrie et al. 1984/. $\delta^{18}O$ is a measure of the isotope fractionation that occurs during changes between condensed and vapour phases of water, expressed as the difference from the isotopic composition of Standard Mean Ocean Water. High $\delta^{18}O$ values indicate large global ice volume and lower sea water temperature, i.e. colder climate conditions, whereas low $\delta^{18}O$ values indicate the opposite.*

1.3.2 Impact on repository performance and safety

Climate changes, permafrost and the growth and decay of ice sheets will alter not only surface but also subsurface conditions. Shore level alterations, freezing, and the presence of ice sheets will change permeability, water turnover, groundwater pressures, groundwater flow and composition. The ice load will alter rock stresses and during different phases of a glaciation the principal stresses will change in both direction and magnitude. This will alter bedrock permeability and as ice sheets melts away, a combination of large horizontal stresses and high water pore pressures may cause end-glacial faulting. In general, the integrated effects of the continuous evolution of climate-related conditions need to be considered, but there are also a number of more specific phenomena of importance for repository safety that require special attention. Based on the results of the earlier and present assessment, these include:

- The maximum hydrostatic pressure occurring at repository depth for glacial conditions.
- The maximum permafrost depth.
- The degree of penetration of oxygen to deep groundwaters during glacial conditions.
- The groundwater salinity occurring at repository depth.
- The potential for end-glacial faulting.
- Factors affecting retardation in the geosphere, like high groundwater fluxes and mechanical influences on permeability.

1.3.3 Strategy for managing the long-term evolution of climate-related conditions

Definition of climate domains

It is not possible to predict the evolution of the climate in a 100,000-year time perspective with confidence enough to use in safety assessments of nuclear waste repositories, and any presented long-term future climate evolution is associated with large uncertainties. However, the extremes within which the climate of Sweden may vary can be estimated with reasonable confidence. Within these limits, characteristic climate-related conditions of importance for repository safety can be identified. The conceivable climate-related conditions can be represented as *climate-driven process domains* /Boulton et al. 2001a/ where such domain is defined as *a climatically determined environment in which a set of characteristic processes of importance for repository safety appear.* In the following these climate driven process domains are referred to as *climate domains.* The identified domains are denominated:

- The temperate domain.
- The permafrost domain.
- The glacial domain.

The purpose of identifying climate domains is to create a framework for the assessment of issues of importance for repository safety associated with particular climatically determined environments that may occur in Sweden. If it can be shown that a repository for spent nuclear fuel fulfils the safety requirements independent of the prevailing climate domain, and the possible transitions between them, then the uncertainty regarding their extent in time and space is of less importance.

The temperate domain is defined as regions without permafrost or the presence of ice sheets. It is dominated by a temperate climate in a broad sense, with cold winters and either cold or warm summers. Precipitation may fall at any time of the year, i.e. there is no dry season. The precipitation falls either as rain or snow. The temperate domain has the warmest climate of the three climate domains. Within the temperate domain, a site may also at times be submerged by the sea or by an ice-dammed lake.

The permafrost domain is defined as periglacial regions that contain permafrost. It is a cold region but without the presence of an ice sheet. The permafrost occurs either in sporadic-, discontinuous-, or continuous form. Although true for most of the time, regions belonging to the permafrost domain are not necessarily the same as regions with a climate that *supports* permafrost. For example, for a certain area, at the end of a period with permafrost domain the climate may be relatively warm, not building or even supporting the presence of permafrost. Instead, permafrost may be diminishing. However, as long as permafrost is present, the region is defined as belonging to the permafrost domain, regardless of the prevailing temperature at the ground surface. This way of defining the domain is used because, in this case the presence of the permafrost is more important for the safety function of the repository than the actual temperature at the ground surface. In general, the permafrost domain has a climate colder than the temperate domain and warmer than the glacial domain. Precipitation may fall either as snow or rain.

The glacial domain is defined as regions that are covered by ice sheets. Within the glacial domain, the ice sheet may in some cases be underlain by sub-glacial permafrost. In line with the definition of the permafrost domain, areas belonging to the glacial domain may not necessarily at all times have a climate that supports the presence of ice sheets. However, in general, the glacial domain has the coldest climate of the three climate domains. Precipitation normally falls as snow in this domain.

It is currently not possible to make confident predictions of future long-term climate, particularly taking into account the potential long-term significance of inferred current human-induced perturbations of the natural climate system. It is, however, likely that the three climate domains will appear repeatedly during the one million year assessment period, i.e. any reasonable evolution will have to address them, and transitions between them.

Safety assessment scenarios

In the safety assessment, the climate domains are first analysed within a *main scenario* aiming at describing a plausible evolution of the repository system. There are two variants of the main scenario. When studying the climate domains, the *base variant* of the main scenario (Figure 1-2) comprises a reconstruction of climate and climate-related processes during the last glacial cycle. This serves as one example of the evolution during a glacial cycle. The motivation for doing this is given in Section 4-1. As a complement to this, the climate domains are also analysed in a *greenhouse variant* of the main scenario, in which inferred current human influence on climate are taken into account (Figure 1-2).

Following the analysis of the main scenario, a number of *additional scenarios* of importance for repository safety are selected, based on the evolution in the main scenario and on the understanding of repository safety. The latter is expressed through a number of safety functions and safety function indicators, and these are used to make a structured selection of additional scenarios (Figure 1-2). Detailed information about the safety function indicators and how the selections are made is found in **SR-Can Main Report**. These additional scenarios essentially address relevant situations not covered by the main scenario.

For example, for the glacial domain the maximum ice sheet thickness is one parameter of interest for the hydrostatic pressure at repository depth. In the *base variant of the main scenario*, the development of ice sheet thickness comes from a reconstruction of the Fennoscandian ice sheet during the last glacial cycle, whereas in an *additional scenario* the effect of ice sheet thicknesses greater than those during the last glacial cycle are studied. In this way, the main scenario describes a plausible evolution of ice sheet thickness, and the additional scenario describes relevant variations of this plausible evolution. Figure 1-2 shows the scenarios and variants in SR-Can, and sections where these are described in the present report.

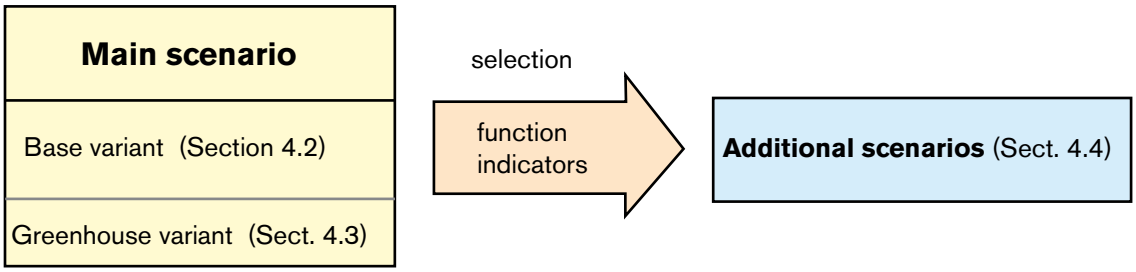

Figure 1-2. *Scenarios and variants in SR-Can, and sections where these are described in the present report.*

It is important to include the climate domains and sequences that have the greatest impact on repository safety. Phenomena that may affect barrier safety functions are mentioned above, the most severe effects are related to the development of permafrost and the advance and decay of ice sheets. It is also important to include sequences covering external conditions yielding, with a high likelihood, the peak risk during the assessment period. Based on results of earlier analyses, the highest risks are likely to occur during temperate periods. Typical situations are i) a terrestrial system that has accumulated radionuclide releases over a long time, possibly at early stages in sea sediment that subsequently is exposed and used for agriculture and ii) a well intruding into the host rock and used for domestic purposes.

The documentation of the climate system and climate variations in Sweden in Chapter 2 has been structured in light of the above. The intention is not to give a complete picture of the Earth climate system but rather a summary sufficient for identification of climate-related conditions and processes with possible impact on repository performance. The interactions between these processes of importance for repository performance and other parts of the climate system set the limits for the documentation of the climate system in this report.

In Chapter 3, there are five sections that in detail describe the climate-related phenomena within the climate domains that may affect repository safety functions. These sections deal with the development and characteristics of ice sheets, glacial hydrology, shore level displacement, permafrost, and faulting in association with ice sheets. The documentation of climate-related conditions and processes in Chapter 3 thus focuses on possible impact on the repository system, and largely follows the structure for documentation of processes regarded as internal to the repository.

In Chapter 4 “Evolution of climate-related conditions for the safety assessment” the evolution over a 120,000 year period is presented, including identified climate-related issues of importance for repository safety. In this context, a short comment on time scales is relevant. Chapter 3 mainly deals with reconstructions of climate-related conditions for the last glacial cycle. Because of this, the time scales used in this chapter runs from 120,000 years before present up to present day. In Chapter 4 on the other hand, the reconstructions from Chapter 3 have been used to construct future scenarios of climate-related conditions. Therefore, the time scale used in Chapter 4 runs from 0 (present day) to 120,000 years into the future.

2 The climate system

The following general description of the climate system is based on information from /Ahrens 1994, Bogren et al. 1998, Burroughs 2001, Ruddiman 2000, Weart 2003/.

Weather and climate has great impact on life on Earth. The always changing weather is determined by the fluctuating state of the atmosphere surrounding us, and characterised and described by weather elements such as air temperature, air pressure, humidity, clouds, precipitation, visibility and wind. The predictability of weather is very limited. The reason for this is that the atmospheric characteristics and processes determining the weather can only be predicted over periods from a few hours up to about a week.

The climate is by definition a summary of weather conditions during a certain period and/or within a certain area. Climate is usually described as mean values of the weather elements and their variability over a specific time-span and covering a distinct area. The climate varies between different places due to factors such as latitude, altitude, distance to the ocean and vegetation. The climate also varies over time on different time scales from seasonal through decadal, centennial, and millennial to several thousands and million of years. The complex range of climatic variability is a result of external forcing acting on the Earth climate system as well as internal factors acting within the system. The climate system includes five major components: the atmosphere, the hydrosphere, the cryosphere, the land surface and the biosphere (Figure 2-1). Within the climate system, there are many physical, chemical, and biological processes that interact on a wide temporal and spatial range of scale both within and between the components.

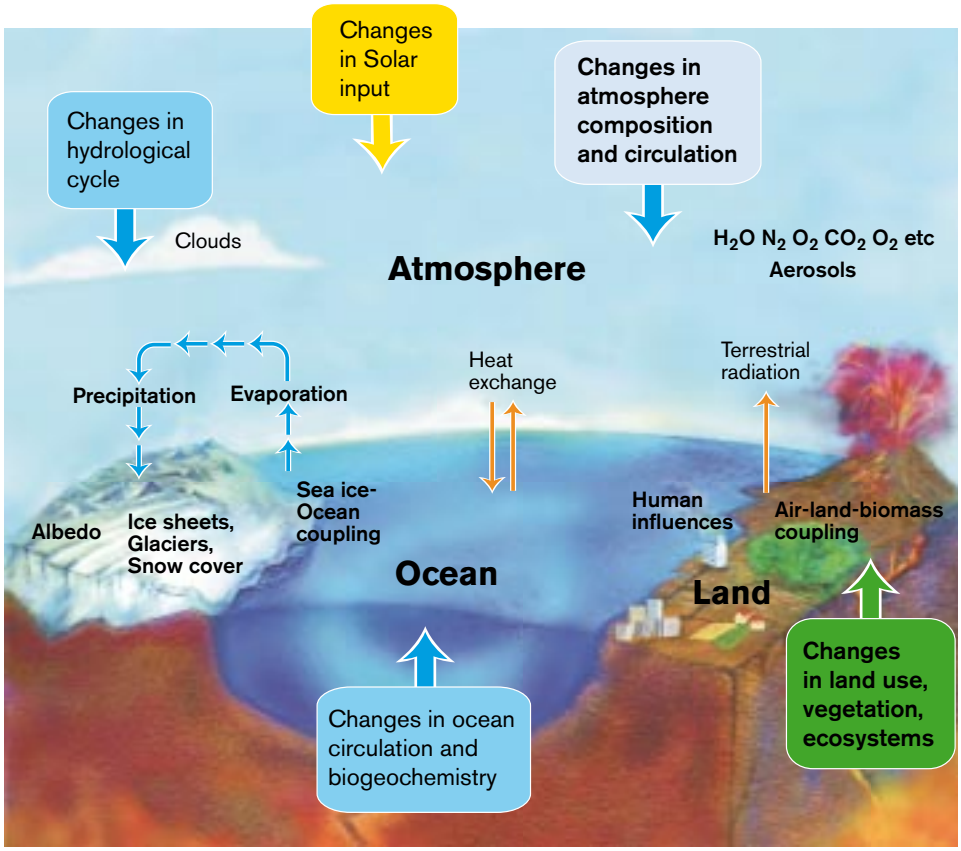

Figure 2-1. *Schematic view of the components of the global climate system, their processes and interactions and some aspects that may change (boxes). Modified from /NSF 2000/.*

2.1 Components of the climate system

2.1.1 The atmosphere

Overview/general characteristics

The atmosphere is the blanket of gases that surrounds the Earth. About half of its mass is to be found in the lowest 5–6 km and more than 99% of the mass is within 40 km from the surface of the Earth. This can be compared with the radius of the Earth which is about 6 400 km. The atmosphere or the air is retained by gravity. The atmosphere is generally considered to be 1,000 km thick. However, it has no distinct outer border but a successive decrease of density as it merges into the inter-planetary medium. The origin of the atmosphere is gases which were released from the interior of the Earth by, for example, volcanic eruptions. The atmosphere has undergone major changes during the evolution of the Earth due to several factors in which changes of solar radiation and biological activities have played important roles. Oxygen was not added to the atmosphere until produced by living organisms throughout photosynthesis.

The Atmosphere can be divided into four major layers: the *troposphere*, the *stratosphere*, the *mesosphere* and the *thermosphere* (Figure 2-2). This division is based upon the temperature structure of the atmosphere. In the lowest layer, the troposphere, all processes that we know as weather take place. The troposphere contains almost all of the water vapour and clouds, and approximately 75% of the total atmospheric mass. The troposphere is characterised by a more or less uniform decrease in temperature with height, averaging 0.65°C per 100 m. Generally, it has an increasing wind speed with height except close to the surface where topography determines the wind. The upper part of the troposphere is limited by the tropopause, which is very important since it prevents convective, vertical air movement. The distance from the Earth surface to the tropopause varies according to latitude and season ranging from 16–17 km at the poles to 8–9 km at the equator.

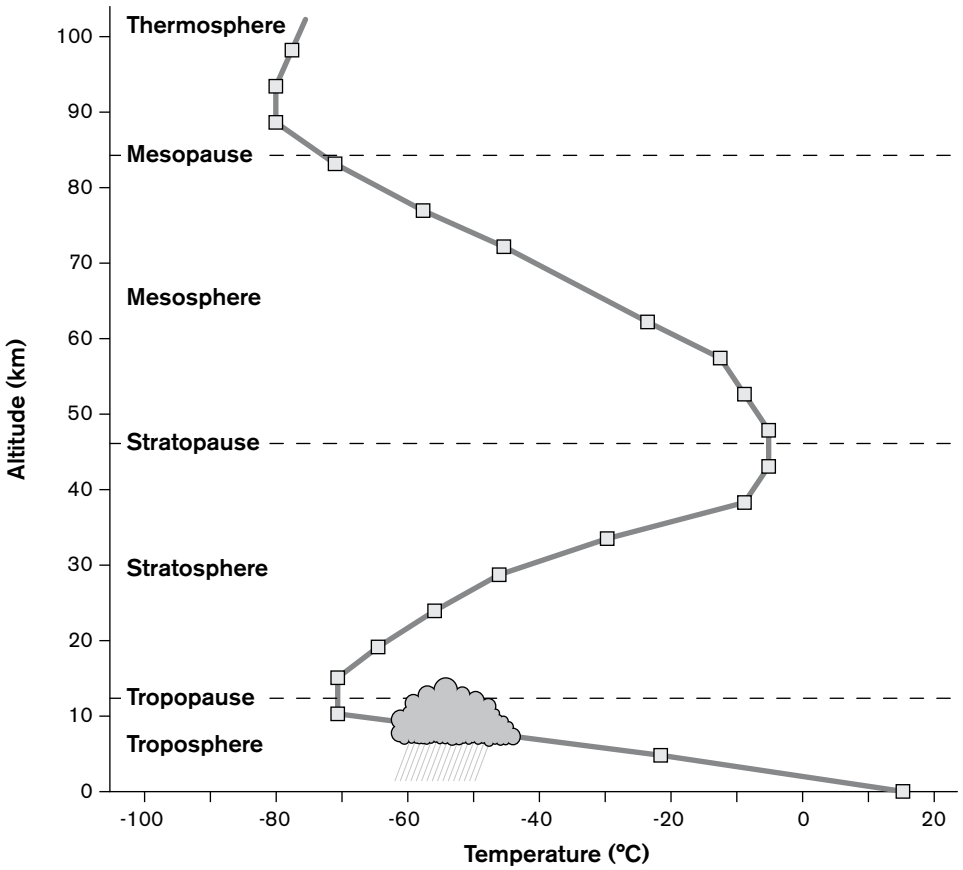

Figure 2-2. *Vertical structure of the atmosphere.*

Composition

The natural atmosphere can be divided into three types of constituents these are: permanent gases, variable gases, non-gaseous constituents. Of the permanent gases, the main components are nitrogen (N_2), 78.1% volume mixing ratio, oxygen (O_2), 20.9% volume mixing ratio and argon (Ar) 0.93% volume mixing ratio. These gases are mostly passive in meteorological processes, they have only limited interactions with the incoming solar radiation and they do not interact with the infrared radiation emitted by the Earth. However, oxygen is highly active chemically; it can combine with other substances and also form ozone (O_3).

The variable gases on the other hand, such as carbon dioxide, methane, nitrous oxide and also ozone, absorb and emit infrared radiation. They are the most important components in terms of meteorological processes. These gases are also called greenhouse gases, and they are sparsely occurring with a total volume mixing ratio in dry air of less than 0.1% by volume. However, these gases play an essential role in the energy budget of the Earth/atmosphere system (Figure 2-3). The atmosphere also contains the natural greenhouse gas water vapour with a volume mixing ratio that is highly variable having a typical value in the order of 1%. These greenhouse gases absorb the infrared radiation emitted by the Earth. Thus they tend to raise the temperature close to the Earth's surface. The greenhouse gases water vapour, carbon dioxide, and ozone also absorb solar short-wave radiation. Water vapour is the strongest greenhouse gas and has a fundamental effect on climate as it exhibits strong spatial and temporal variations in concentration.

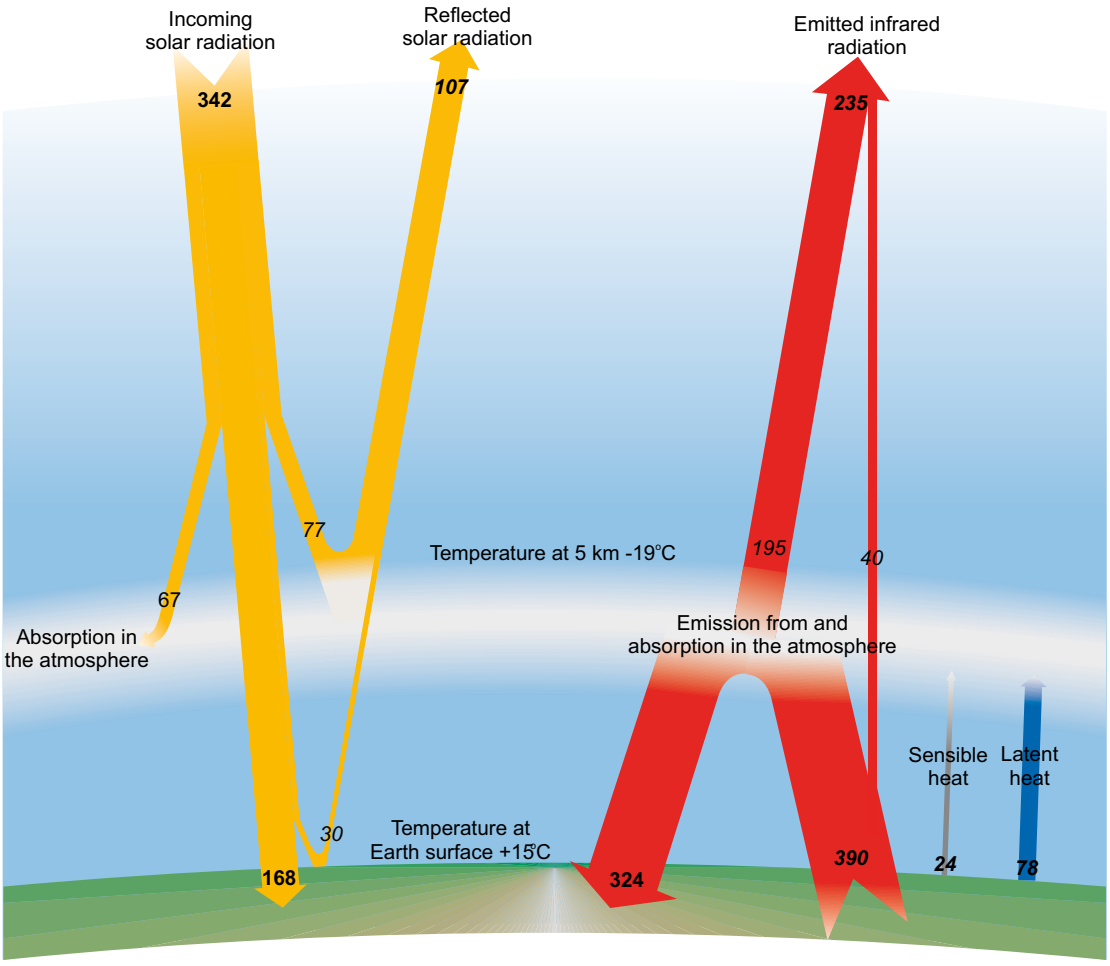

Figure 2-3. *Earth's radiation and energy balance. Units are expressed in* Wm^{-2}.

In the atmosphere, there are also non-gaseous constituents including dust, smoke and salt particles often referred to as aerosols (solid and liquid particles). These are present in different concentrations from a few millions of particles per m^3 of air and they can affect the transmission of radiation through the atmosphere. The effect depends on particle characteristics such as shape, size and colour, and also on the particle distribution and their altitude above the surface. Sulphate aerosols are of utmost importance in the atmosphere, since they directly affect cloud formation, and also on the size of the cloud droplets formed, which in turn has an influence on cloud albedo. The content of aerosols in the atmosphere is altered by volcanic eruptions and human activities. Although most climate-related effects of particles arise in the tropopause, volcanic eruptions can eject particles into the stratosphere.

Dynamics – atmospheric circulation

The atmosphere is in continuous motion. The underlying cause of the circulation is the pressure differences caused by the unequal distribution of solar radiation over the Earth's surface and the unequal heating of land and ocean areas. Averaged over the entire Earth, incoming solar radiation equal outgoing radiation. This energy balance is not maintained for each latitude, since the tropics experience a net radiative gain in energy whereas the Polar Regions suffer a net loss. These inequities are balanced when heat is transported from equatorial regions pole-ward.

The thermal energy in the atmosphere is transferred in different ways. *Convection* means that the heated atmosphere is physically transported from one location to another in, for example, rising thermals. By *conduction,* heat energy is transferred through the medium by molecular impact, whereas the medium itself does not move. *Latent heat transfer* means that the heat energy absorbed by the melting or evaporation of water in one location may be released elsewhere in the atmosphere when the water vapour subsequently condenses or the water freezes. Heat energy may be transferred horizontally by *advection* when the winds cause the mass movement of the atmosphere. Finally, energy is transferred in the atmosphere through the emission and absorption of *radiation* the process of waves moving through the space at the velocity of light.

The motion of the atmosphere is determined by two types of forces; driving forces and steering forces resulting in the pattern of winds. The driving forces exist regardless of whether or not the air is moving. Vertically, gravity is acting downwards whereas the vertical pressure gradient, with lower pressures at higher altitude, tend to force air upwards. Gravity and the vertical pressure gradient are generally close to being in balance. Horizontal pressure gradients forcing air movement are also present, and are both spatially and temporally variable on a range of scales.

The steering forces are related to the motion of the air. The Coriolis force, due to the rotation of the Earth, deflects the air from its initial motion generated by the driving forces. Frictional forces depend on the degree of roughness of the surface the air moves over and act to reduce the wind speed resulting from the prevailing pressure gradient and to produce a component of flow across the isobars. Around curved isobars, the centripetal acceleration produces a force that deflects the inward motion.

The general circulation of the atmosphere is seen in (Figure 2-4).The circulation of the troposphere conforms to a pattern that is characterised by low pressure areas in the tropics where hot air rises. The rising air spreads towards the poles in the upper troposphere and eventually descends in the middle latitudes. This forms part of the so-called Hadley cells. The sinking air leads to the development of large areas dominated by subtropical high pressures. These high-pressure cells are stable and occur over oceans and continents. From these high-pressure areas the trade winds have their origin. Over the poles the coldest air masses, with dense relatively stable air, are found. The cold and dense polar air drifts towards the middle latitudes where, in contact with the warmer air, it gives rise to cyclonic activity. The interaction of cold and warm air masses in the middle latitudes is largely influenced by a belt of high-speed winds at high altitude in the upper troposphere.

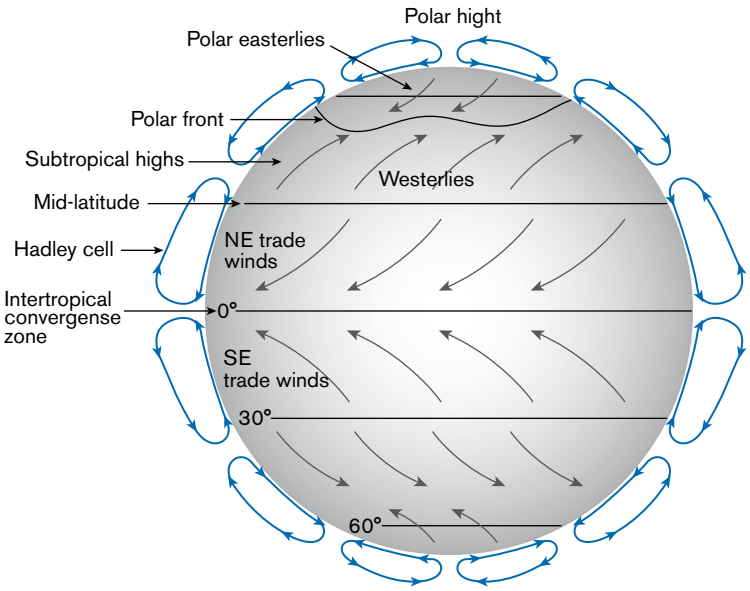

Figure 2-4. *The general circulation of the atmosphere, shown as a three-cell circulation model.*

The atmosphere is the most unstable and rapidly changing part of the climate system. Its response time to forcing mechanisms for climate change is on time scales from months to hundreds of years.

2.1.2 The hydrosphere

General structure

The hydrosphere comprises all liquid water that can be found on Earth. It includes ground-water, surface water in fresh-water lakes and watercourses and saline water in the oceans. Approximately 70% of the Earth's surface is covered by oceans, which make the oceans a very important part of the hydrosphere, and they play a major role within the climate system. The oceans have a large capacity for storing and transporting heat energy, and also serve as storehouses for carbon dioxide. Due to the large thermal inertia of the oceans, the oceans play the role of a dampener of temperature changes.

The significance of the ocean is that it stores a much greater quantity of energy than the atmosphere. This is because of both its larger heat capacity and its much greater density. The vertical structure of the ocean can be divided into two layers, which differ in the scale of their interaction with the overlying atmosphere. The lower layer comprises the cold deep-water sphere, making up 80% of the oceans volume. The upper layer, which has closest contact with the atmosphere, is the seasonal boundary layer, a mixed water layer extending down only about 100 m in the tropics but several kilometres in Polar Regions. The seasonal boundary layer alone stores approximately 30 times as much heat as the atmosphere.

Dynamics – ocean circulation

The hydrosphere, like the atmosphere, is always in motion. The characteristics of the ocean which affect its motion are its temperature and salinity. Warm water is less dense and therefore tends to move up towards the surface, whereas colder water is denser and tends to sink towards the bottom. Saline water is also denser and thus tends to sink, whereas fresh or less saline water is less dense and thus rise toward the surface. Sea salt is left in the water during the formation of sea ice in the Polar Regions, resulting in an increased salinity of the ocean. This cold and saline water is particularly dense and therefore sinks, transporting with it a considerable quantity

of energy. The combination of the water's temperature and salinity determines whether it rises to the surface, sinks to the bottom, or stays at some intermediate depth. This results in the thermohaline circulation.

The transfer of heat between the surface layer and deeper layers of the ocean takes place through different mechanisms: i) diffusion or turbulent mixing which transfers heat from warmer layers to cold layers, ii) convection which happens when surface waters become cold and denser than the water below and thereby switch places often resulting in transferring of heat upwards, and iii) advection which is a large-scale flow transferring water from one place to another.

Advection of heat in the oceans often occurs in the form of currents that move the warm waters in the tropics toward the poles, and colder water from the Polar Regions toward the tropics. These currents exist on the surface and at great depths of up to about 4 km. The currents are driven by the winds, by thermoclines and by the circulation of the Earth. In contrast to the atmospheric circulation and winds, the ocean circulation and currents are more stable and reacts much slower to changes in external forcing than the atmosphere. In the Polar Regions, cold water sinks and spreads throughout the oceans, causing the deep ocean to be cold. In mid latitudes, this is balanced by the upwelling of relatively warm water. Horizontal variations in the density of the water play an important role in driving this large scale overturning, and in this context evaporation of water from the ocean surface are of importance, since it increases the salinity and density of the remaining surface water.

There are linkages between anomalies in sea-surface temperatures and atmospheric long-wave circulation patterns. Shifts in sea-surface temperature anomaly patterns may therefore alter the prevailing circulation and climate. The atmosphere-ocean system involves a two-way interaction. Atmospheric impacts on the ocean are relatively short-term, whereas the oceans' effect on the atmosphere is relatively long-term because of the great thermal stability of the ocean. The response time of the oceans to an external forcing is from days to months regarding the surface layer, whereas the deep ocean exhibits a response time in the range of 100–1,500 years.

An important component of the system that is thought to be involved in abrupt climate change is the ocean circulation (Figure 2-5). Here, the key aspect is the thermohaline circulation in the North Atlantic, though other aspects of the circulation, such as wind-driven components, may

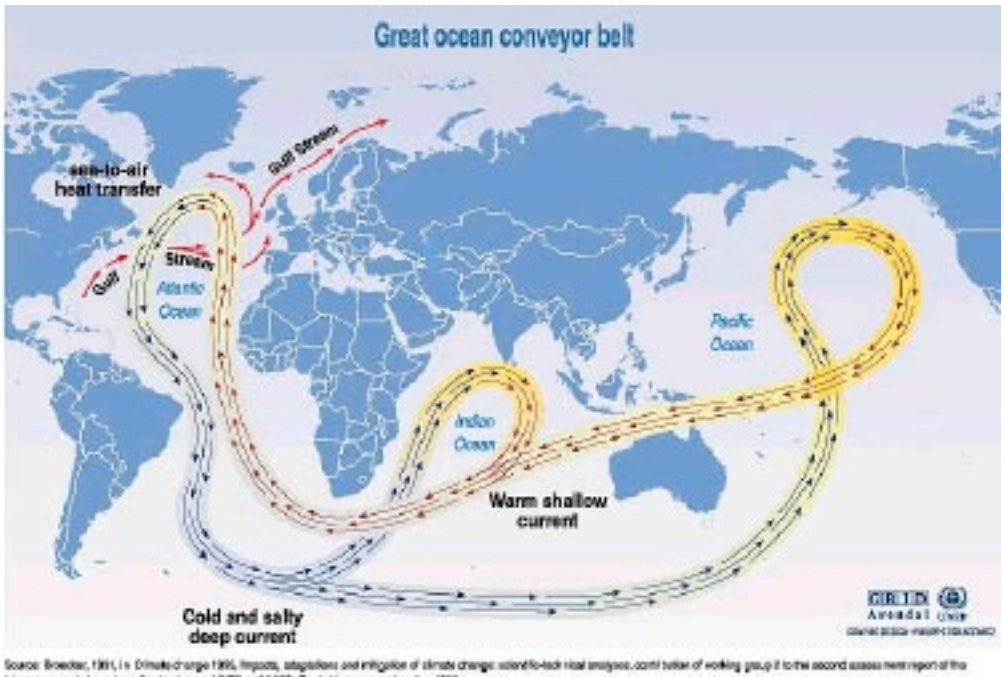

Figure 2-5. *The thermohaline circulation, source /Broecker 1991/.*

also be important. Related to this, land glaciers and sea ice are also of importance. Changes in the basal characteristics of glaciers and ice streams can lead to surging. In turn, this can affect atmospheric circulation patterns, release icebergs to the oceans and, more importantly, release freshwater to the oceans, potentially affecting ocean circulation patterns. Freshwater releases from ice-related processes can be catastrophic, e.g. the breaking of an ice dam leading to the rapid draining of the associated lake. It is believed that the draining of an ice-dammed lake (Lake Agassiz) was at least partly involved in the initiation of the Younger Dryas event and was also responsible for a more limited event 8.2 ka BP /NAS 2002/.

The global thermohaline circulation consists of cooling-induced deep convection; brine rejection and sinking at high latitudes; upwelling at lower latitudes; and the horizontal currents feeding the vertical flows. In the North Atlantic, where much of the deep sinking occurs, the thermohaline circulation is responsible for the unusually strong northward heat transport. The climate in Fennoscandia is in this way to a large extent affected by the presence of the North Atlantic Drift, a northern part of the Gulf Stream. The heat transfer by this ocean current gives a significantly warmer climate in Fennoscandia than if this current was to be absent or reduced.

2.1.3 The cryosphere

The cryosphere comprise all the ice on Earth, snow, sea ice, glaciers and permafrost. Areas that are snow or ice covered through-out the year include for example Antarctica, Greenland, parts of the Arctic Ocean, and the high mountain ranges throughout the world. Snow and ice are important for the climate system since they have a high albedo, or reflectivity. Some parts of the Antarctic reflect as much as 90% of the incoming solar radiation, compared to a global average of about 30%. Without the cryosphere, the global albedo would be considerably lower and mean global temperatures would be higher. Exchange of water between the cryosphere and the atmosphere is considerably less than between hydrosphere and atmosphere. The ice has a low conductivity and a large thermal inertia. The ice, both sea ice and ice sheets, also affects the oceans and ocean circulation. The large amount of freshwater stored in the ice sheets, and variations in the ice sheet volumes, play a major role when it comes to salinity distribution and the eustatic and isostatic processes cause sea-level variations (see further Section 3.3 Global isostatic adjustment and sea-level migration). Through changes in salinity, variations in fresh water discharge from the cryosphere affect the ocean thermohaline circulation.

Snow

Seasonal snow cover is the largest component of the cryosphere and it covers up to 33 percent of the Earth's total land surface. About 98 percent of the total seasonal snow cover is located in the Northern Hemisphere. Snow cover is an important climate variable because of its influence on energy and moisture budgets. The variations in snow cover between summer and winter account for the large differences in surface albedo, both on an annual basis and also between years. Snow may reflect as much as 80 to 90 percent of the incoming solar energy, whereas a snow-free surface such as soil or vegetation may reflect only 10 to 20 percent. Surface temperature is highly dependent on the presence or absence of snow cover, and temperature trends have been linked to changes in snow cover. In addition to the albedo effect, snow cover represents a significant heat sink during the melt period of the seasonal cycle due to a relatively high latent melting heat. As a result, the seasonal snow cover provides a major source of thermal inertia within the total climate system, as it takes in and releases large amounts of energy with little or no fluctuation in temperature.

Sea ice

Floating ice includes sea ice and frozen lake and river water. Sea ice typically covers 14 to 16 million square kilometres of the Arctic Ocean, and 17 to 20 million square kilometres of the Southern Ocean around Antarctica, during their respective winter seasons. The seasonal decrease is much larger in the Antarctic, with only about three to four million square kilometres

remaining at summer's end, compared with approximately seven to nine million square kilometres in the Arctic. Sea ice is formed by the direct freezing of the water on which it floats. If the water is saline, the salt is left in the sea water during the freezing process, making it more saline and dense, whereas sea ice consists of freshwater.

Sea ice is important because it regulates exchanges of heat, moisture, and salinity in the polar oceans. It insulates the relatively warm ocean water from the cold polar atmosphere except where cracks, or leads, in the ice allow exchange of heat and water vapour from the ocean to the atmosphere. The number of leads determines where and how much heat and water are lost to the atmosphere, which may affect local cloud cover and precipitation. Sea ice thickness, its spatial extent, and the fraction of open water within the ice pack can vary rapidly.

The sea ice acts to decouple the atmosphere and oceans, reducing the transfer of moisture and momentum, so stabilising the energy transfers within the atmosphere. The formation of sea ice in Polar Regions can influence global thermohaline circulation patterns in the oceans, which greatly influence the global climate system.

Ocean water covers nearly three-quarters of the Earth's surface. It has a very low albedo, making the oceans the principal absorber of solar radiation. Anything that might change this strong absorption such as fluctuations of sea-ice cover is likely to affect radiative equilibrium and climate.

Glaciers and ice sheets

About 10 percent of the Earth's land area is covered by glaciers and ice sheets. Today two large ice sheets exist on Earth, one in Greenland and one in Antarctica. The Antarctic ice sheet consists of the East Antarctic Ice Sheet (EAIS) and the West Antarctic Ice Sheet (WAIS). In all continents except Australia, ice in the form of mountain glaciers, or ice caps can be found on high altitudes.

A glacier, ice cap or ice sheet gains mass by accumulation of snow, which is gradually transformed to ice. Mass-loss, or ablation, is mainly accomplished by melting at the surface or base, with subsequent runoff or evaporation of the melt water. Some melt water may refreeze within the snow instead of being lost and some snow may sublimate or be blown off the surface. Ice may also be removed by discharge into a floating ice shelf or glacier tongue, from which it is lost by basal melting and calving of icebergs. Net accumulation occurs at higher altitude, net ablation at lower altitude; to compensate for net accumulation and ablation, ice flows by internal deformation and sliding and bed deformation at the base (see further Section 3.1 Ice sheet dynamics).

The Greenland ice sheet is considerably more sensitive to increases in temperature than are the Antarctic ice sheets /Huybrechts and de Wolde 1999/. An increase in annual temperature of ~ 3° or more over Greenland could result in an irreversibly decreasing ice sheet and increased sea-level /Huybrechts et al. 1991/. Excluding complex processes that could counterbalance a simple warming-melting situation, such as changes in oceanic circulation, many studies suggest that the Greenland ice sheet gets drastically reduced in size and contributes considerably to global sea-level rise under various future greenhouse gas scenarios. In a worst-case CO_2 scenario with an 8 degree climate warming by the year of 2100 /IPCC 2001/, the warming would lead to a complete and irreversible collapse of the Greenland ice sheet over the next 1,000 years /Huybrechts and de Wolde 1999, Gregory et al. 2004, Alley et al. 2005a/.

The two most important conditions for ice surface melting involve exposure to radiation and heat exchange with the air in contact with the glacier or ice sheet. Radiation involves short-wave solar radiation as well as long wave radiation from water vapour and carbon dioxide in the atmosphere. The efficiency of solar radiation in melting is, to a large extent, influenced by the albedo of the glacier surface. If the surface is covered with fresh snow then the albedo is typically 0.6 to 0.9 and most solar radiation is reflected. If the surface is glacier ice on the other hand the albedo is 0.2 or 0.4 and melting due to the solar radiation is much more likely to occur.

Heat exchange at the glacier surface with the air takes place mainly in two ways by conduction of heat from the air to the ice and by condensation of water vapour on the ice surface which results in the release of latent heat. Condensation of 1g water vapour on the surface releases enough heat to melt about 7.5 g of ice. Conduction and condensation are both enhanced dramatically when windy conditions cause air turbulence close to the glacier surface.

Finally, ice sheets have a large inertia, their response time to a change external forcing, i.e. a climatic change, is in the range of 100 to 10,000 years whereas glaciers respond much faster, typically in the range of 10 to 100 years.

Permafrost

Permafrost affects climate since it has an impact on vegetation and a role in the storage and release of carbon. Much of the Northern Hemisphere frozen ground is overlain by evergreen boreal forest. These boreal forests comprise both a source and a sink of carbon. The Arctic contains nearly one-third of the Earth's stored soil carbon. If the high northern latitudes were to experience a significant temperature increase, the regional soils would begin to release carbon into the atmosphere, which could lead to increased plant growth, carbon aspiration, and possibly a temperature drop or stabilisation. Alternately, it could lead to higher temperatures, fuelling the cycle of carbon release and temperature rise. The presence of permafrost also has an effect on groundwater flow and composition, both in periglacial regions and under ice sheets. For example, it may stop groundwater recharge from the surface by forming an impermeable upper layer, or it may result in freeze-out of salts in front of an advancing permafrost freeze front.

2.1.4 The land surface

The appearance of the land surface is critical when it comes to transfer of energy received from the sun to the atmosphere. Depending on the vegetation, the porosity and saturation of the soil and its thermal properties the amount of energy that is transferred to the atmosphere can vary. The energy can be returned as long-wave radiation, which will heat the atmosphere, or it can be used for evaporation of water. Soil moisture has a strong influence on the surface temperature since energy is required for its evaporation.

Vegetation and topography determines the roughness of the land surface affecting turbulence and the surface winds. Particles and dust from the surface is suspended into the atmosphere by the winds and affect the radiation balance in the atmosphere. Physical and chemical processes affect certain characteristics of the soil, such as moisture availability and water run-off, and the fluxes of greenhouse gases and aerosols into the atmosphere.

Chemical weathering processes may react to different factors in different areas and function both to initiate climate change and also to regulate it. In regional areas with active chemical weathering, carbon dioxide can in the long-term be removed from the atmosphere, causing a cooling the climate over a much larger area than affected by the weathering.

The presence of mountain ranges also influence global climate. North-south orientated mountain ranges in particular have the ability to influence global atmospheric circulation patterns. In turn, climate also affects mountain ranges, since climate governs important denudation processes, for example fluvial erosion. These processes causes down-wearing of mountain ranges. Orogenic processes and continental drift, forming mountain ranges, are processes acting over time scales of millions of years.

2.1.5 The biosphere

The different ecosystems existing on Earth have significant impact on the composition of the atmosphere when it comes to uptake and release of greenhouse gases. Photosynthesis by both terrestrial plants and marine biota can store significant amounts of carbon from carbon dioxide,

playing a central role in the carbon cycle. Ecosystem characteristics are also of importance to the budgets of many other greenhouse gases, for example methane and nitrous oxide. The exchange and storage of the trace gases are to a great extent influenced by the biosphere which in turn is sensitive to climate.

2.2 Climate forcing

Climate is changing naturally on time scales of 10 to more than 100,000 years, due to 1) alterations of the radiation emitted by the sun, 2) insolation changes caused by variations in the Earth orbit and 3) processes related to tectonism, such as volcanism. In addition to the change and variability from external causes to the global climate system, natural internal variability is a characteristic of the system as well. The latter has often a more regional than global character. In addition to the natural forcing, there is also an anthropogenic forcing of the climate, one example being the burning of fossil fuels that increases the concentration of greenhouse gases in the atmosphere.

2.2.1 Alteration of solar radiation

The sun is the most powerful source of energy that affects the climate system. The energy output of the sun varies over time, being correlated with sunspot activity or magnetic storms. During periods of maximum sunspot activity, the sun emits more energy than during periods with minimum sunspot activity. Solar variation affects the radiation balance of the Earth, but to what degree this impacts global climate is not yet understood. Fluctuations in solar output may account for climate variations over time scales of decades and centuries, and in the long-term on time scales up to billions of years.

2.2.2 Earth-orbital variations

According to the Milankovitch theory, or astronomical climate theory, variations in the Earth's orbit around the sun has been a main forcing factor of the Pleistocene glacial/interglacial cycles (Figure 2-6). Glaciations in the past were principally a function of variations in the Earth's orbital parameters, and the resulting redistribution of solar radiation reaching the Earth. A key to explain how the variation in orbital parameters can trigger ice ages is the amount of solar radiation received at high latitudes during the summer. This is critical to the growth and decay of ice sheets. When summer insolation is strong, more radiation is absorbed at Earth's surface at high latitudes resulting in a warmer climate. In contrast, when insolation is weak, less radiation is received at Earth's surface at high latitudes, and the reduction in radiation cools the regional climate. Latitudinal and seasonal variations in incident solar radiation due to the precession of the equinoxes (19- and 23 ka periodicies) and variations in the tilt (obliquity) of the Earth's axis (41-ka periodicity) (Figure 2-6), together with internal feed-back mechanisms in the atmosphere-ocean system, are sufficient to drive the significant climatic changes observed on these time scales. By comparison, the 100-ka eccentricity periodicity is the weakest of the orbital effects. However, it is these weaker eccentricity variations that have been of primary importance in regulating glacial-interglacial cycles over the last 700,000 years. Prior to this time, precession and obliquity played a larger role in regulating the glacial cycles. The mechanisms by which the weak 100-ka periodicity, is manifested during this period as significant climate changes with growth and decay of major ice sheets on both hemispheres, are ,however, still unsolved. The Milankovitch theory alone is not sufficient to explain many features of the past evolution of climates /e.g. Paillard 2001/. In this context, new ideas involving mechanisms that affect the variations in CO_2 concentration in the oceans through glacial interglacial variations in deep ocean water salinity are of interest /e.g. Paillard and Parrenin 2004/.

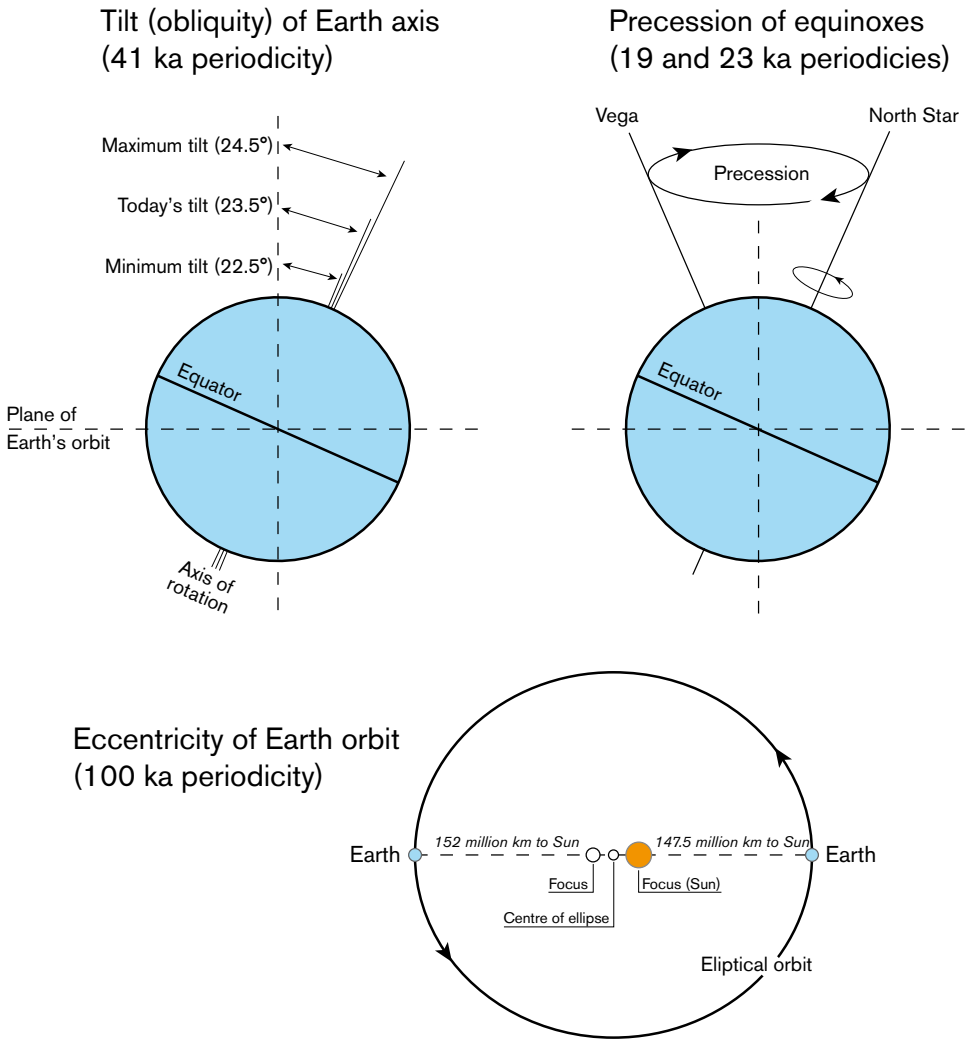

Figure 2-6. *Earth's orbital parameters affecting the seasonal distribution (obliquity and precession) and amount of solar radiation reaching the Earth (eccentricity). After /Tarbuck and Lutgens 1999/.*

2.2.3 Tectonic processes

Tectonic processes alter the configuration of continents and oceans and also the composition of the atmosphere by volcanic eruptions. The configuration of the continents influences the path of the ocean currents and thus has an impact on heat transport from low to high latitudes in the oceans as well as in the global wind system. Orogenic uplift result in mountain ranges, redistribution of land and ocean areas and may also contribute to increase the land surface area permanently covered by snow. Also, if there is a change in the characteristics of land and water surfaces, or in the relative distribution of land and sea, this can affect the radiation balance and, in consequence, the climate.

Volcanism, although driven by the slow movement of the tectonic plates, occurs irregularly on much shorter timescales. Volcanic eruptions replenish the carbon dioxide in the atmosphere, removed by the biosphere, and emit considerable quantities of dust and aerosols. Volcanic activity can therefore affect the energy budget and regulation of the global climate system.

Volcanic eruptions can have an immediate and profound impact on climate when fine particles such as dust and ash together with gases are ejected into the stratosphere. Whereas volcanic modification of the lower atmosphere is removed within days by the effects of rainfall and gravity, stratospheric modification may remain for several years, gradually spreading to cover much of the globe. The amounts of aerosols ejected by volcanic eruption into the atmosphere

may vary on widely different time-scales, causing natural variations in the radiative forcing. The variations can be either negative or positive, but the climate system must react to restore the balance. Generally, a positive radiative forcing tends to warm the surface and a negative radiative forcing tends to cool it.

2.2.4 Anthropogenic forcing

Anthropogenic forcing is a result of human activities that have an impact on the climate. There are three different processes that can be identified that are thought to have the largest effects. The first is release of greenhouse gases, which absorb and re-emit the longwave radiation from Earth, increasing the temperature. Secondly, increased amount of aerosols in the atmosphere reduce the amount of incoming solar radiation at the surface affecting the temperature. Thirdly, by changing the surface characteristics of the Earth the albedo is affected which in turn alters the radiation balance.

Climate scenarios based on global and regional climate models indicate for the 21st century a substantial rise in temperatures, a considerable change in hydrological conditions and a rise in global sea level due to increased greenhouse gas levels /e.g. IPCC 2001/, see below.

2.3 Climate dynamics

Many of the processes and interactions in the climate system are non-linear, meaning that there is no simple proportional relation between cause and effect. A complex, non-linear system may display what is often called chaotic behaviour. The behaviour of the system is critically dependent on very small changes of the initial conditions. This does not necessarily mean that the behaviour of non-linear chaotic systems is unpredictable. The development of the daily weather is a useful example. The development of weather systems creating the daily weather is governed by this non-linear chaotic dynamics. This does not exclude successful weather prediction, but the predictability of the weather becomes limited to a period of approximately two weeks. The climate system is also to a high degree nonlinear.

Climate at the global, regional and local scales is forced or influenced by a wide range of factors. These factors and their characteristic timescales are illustrated in Figure 2-7.

On our short timescale, the climate system is affected by a variety of internal feedbacks (items 6, 9, 11 and 12 in Figure 2-7, counting the oceans to be an integral part of the global climate system). It is these short-term feedbacks that contribute to the natural variability of climate on annual and decadal timescales, in the context of which longer-term trends have to be detected and evaluated. Aperiodic events (such as volcanic activity) can also perturb the climate on these timescales, with individual volcanic eruptions typically affecting climate for a few years at most (though prolonged periods of enhanced volcanism may have more profound effects).

On this short timescale, the orbital characteristics of the Earth do not change substantially, so the main factor forcing an overall trend in climate characteristics is the evolution of the atmosphere, notably the changes in carbon dioxide and other greenhouse gas concentrations and in atmospheric aerosol concentrations that have occurred since about 1,850 AD. On the medium timescale of the next 1,000 years, anthropogenically induced evolution of the atmosphere is thought to remain the main external forcing factor. On both the short and medium timescales, internal feedbacks are known to modify substantially the effects of this external forcing.

On multi-millennial timescales, variations in orbital characteristics interact with changes in greenhouse-gas concentrations to force alterations in climate. The effects of orbital variations have been recognized for many decades (and described as the Milankovitch mechanism). However, more recently, variations in greenhouse-gas concentrations in inclusions in ice cores have been analysed and shown to be an important forcing factor that is correlated with orbital variations.

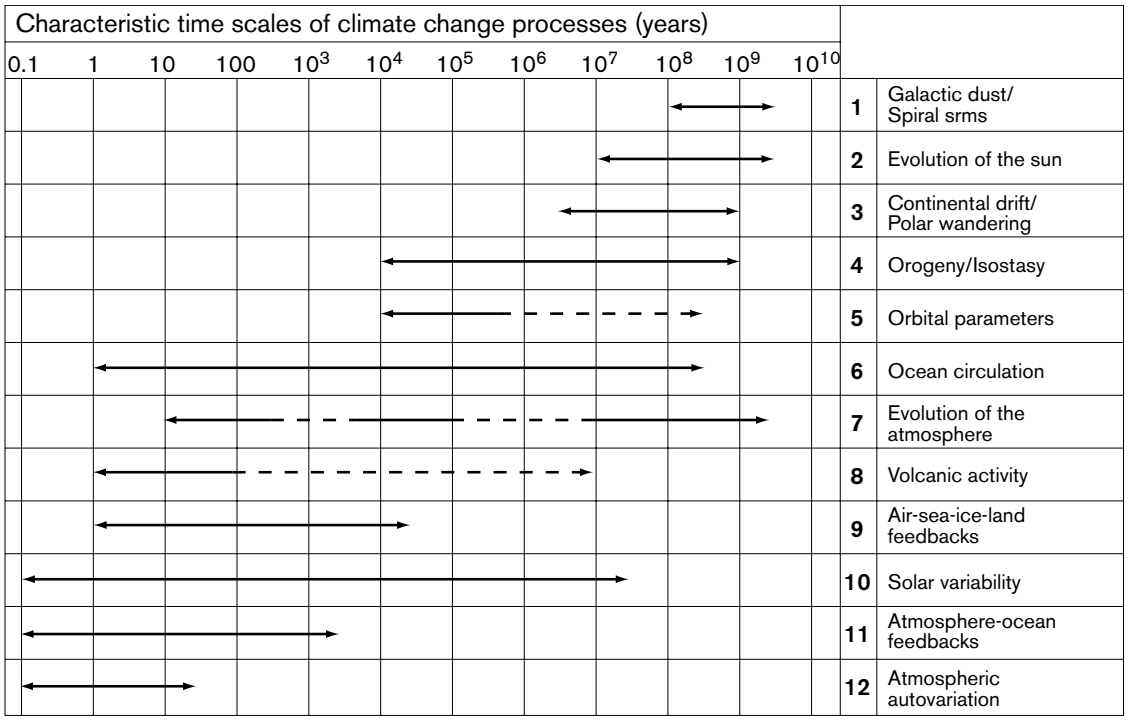

Figure 2-7. *Characteristic timescales of climate change processes /from Goodess et al. 1992/.*

In principle, a comprehensive climate model could be used to calculate variations in greenhouse-gas concentrations by incorporation of a carbon cycle model that was closely coupled to associated atmospheric, oceanic, vegetation and biogeochemical models. However, such models are currently only at an early stage of development, so future variations in natural carbon dioxide concentrations in the atmosphere are typically estimated using statistical regression techniques or simple threshold models /see e.g. BIOCLIM 2001/.

Imposed upon this natural variation are the changes in carbon dioxide concentrations that arise from human activities, primarily the burning of fossil fuels. Between 1850 and 1950, the concentration of atmospheric carbon dioxide rose from a pre-industrial value of 280 ppmv to 300 ppmv and by 1999 the concentration was approximately 370 ppmv /IPCC 2001/. Future increases can be estimated for various emissions scenarios, based on different projections of future fossil fuel use, combined with a model-based relationship between the amount of carbon introduced into the atmosphere as carbon dioxide and the time-dependent increment in the carbon dioxide concentration in the atmosphere arising in consequence /e.g. Archer et al. 1997, 1998/.

2.3.1 Energy budget and radiation balance

The Earth can be considered as a physical system with an energy budget that includes all gains of incoming energy and all losses of outgoing energy. The total flux of power entering the Earth's atmosphere is dominated by solar radiation (99.985%). A small amount is received from geothermal energy (0.0135%), which is produced by stored heat produced by radioactive decay leaking out of the Earth's interior, and tidal energy (0,002%) produced by the interaction of the Earth's mass with the gravitational fields of other bodies such as the moon. The outgoing power from the Earth is determined by the albedo or reflectivity which on average amounts to 0.3. This means that 30% of the incident solar energy is reflected back into space, while 70% is absorbed by the Earth and reradiated as infrared radiation. Of the 30% reflected energy, 6% is reflected from the atmosphere, 20% from the clouds, and 4% is reflected from land, water and ice. The absorbed energy is eventually re-radiated mainly by the clouds and atmosphere (64%) and by the ground (6%).

The radiation budget represents the balance between incoming energy from the Sun and outgoing thermal (longwave) and reflected (shortwave) energy from the Earth (Figure 2-3). Globally, the radiation budget is balanced, i.e. when averaged over a sufficient time interval, the amount of solar radiation absorbed by the atmosphere and the surface beneath it is equal to the amount of heat radiation emitted by the Earth to space. At the local scale, however, the budget is not balanced, whereas tropical areas gain more then they lose and at high latitudes of the winter hemisphere more energy is lost than gained. The global balance is maintained by energy transfers in ocean currents and the atmosphere. For these transfers, radiation energy is transformed to latent heat, sensible heat or kinetic energy (motion). Eventually, all energy forms are converted to thermal energy that is lost as radiation from the Earth-atmosphere system.

The various factors that influence the radiation balance can be divided into internal and external mechanisms. Internal factors are all mechanisms affecting the atmospheric composition (volcanism, biological activity, land use change, human activities). The main external factor is solar radiation. External and internal factors are closely interconnected. Increased solar radiation for example results in higher average temperatures and higher water vapour content of the atmosphere. Water vapour is a heat trapping gas which absorbs infrared radiation emitted by the Earth surface. This absorption can lead to either higher temperatures through radiation forcing or lower temperatures as a result of increased cloud formation which in turn increases the albedo.

2.3.2 The hydrological cycle

The hydrological cycle involves the evaporation and precipitation of water, transport of water vapour by the atmosphere, runoff from the continents to the oceans, and the net transfer of water by ocean currents. Evaporation and precipitation account for some 80% of the required non-radiative energy transfer from the Earth's surface to the atmosphere.

The exchange of water vapour and heat between the atmosphere and oceans has a profound impact on climate. The atmosphere and the ocean are strongly coupled to each other and the exchange between these systems is an important way of feeding energy into the weather systems as well as the oceans. Precipitation, condensation, and cloud formation in the atmosphere is part of the hydrological cycle, which also affects the seas and oceans. Through precipitation and run off the salinity and thus the thermohaline circulation of the oceans can be affected.

2.3.3 The carbon cycle

Carbon dioxide is another important component that is also exchanged between atmosphere and ocean maintaining a balance. The solubility of carbon dioxide in water is temperature dependent and in cold water in the Polar Regions carbon dioxide is dissolved and sinks into the deep ocean. Near the equator, the carbon dioxide is outgassed when the cold water upwells and warms. If there are large quantities of ice present, the exchange between atmosphere and ocean is hindered.

2.3.4 Feedback mechanisms and climate change

Feedback mechanisms refer to processes whereby an initial change or response to an external forcing either reinforces the initial change (positive feedback) or weakens it (negative feedback). Some of the processes involved in climate system feedback-mechanisms is briefly presented in Figure 2-1, and discussed below.

Temperature – water vapour and cloudiness

The most important greenhouse gas is water vapour. It has a concentration in the atmosphere that is strongly correlated to temperature and varies in concentration from 0.2% in very dry air to more than 3% in humid air. The dependence of concentration on temperature results in

positive feedback. A warming of the atmosphere allows the air to hold more water vapour resulting in an increased absorption of heat. This enhanced greenhouse effect increases the warming resulting in even more water vapour in the air. A positive feedback loop is started amplifying the initial warming. If a cooling is initiated, the feedback will result in additional cooling. However there are complications when dealing with water vapour since the atmospheric content of water vapour affects the amount of clouds. There are uncertainties whether an increase of water vapour would lead to an increase in cloud amount or not. Although clouds can have both positive and negative feedback effects, depending on their type, overall an increase in cloudiness is considered to be a negative feedback, so that changes in cloud cover characteristics compensate for more than half of the positive feedback from water vapour and albedo changes.

Temperature – carbon dioxide

Carbon dioxide is a greenhouse gas affecting the temperature and climate of the Earth. Estimates of the effect of increased carbon dioxide on Earth's climate indicates that a doubling of the amount of carbon oxide could lead to an increased temperature in the range of +1.5°C to +4.5°C /IPCC 2001/. A large number of later GCM studies suggest that this range might be too narrow. An increase of greenhouse gases alters the global temperature both by increasing the amount of heat absorbed in a cloud-free atmosphere and by trigging feedback mechanisms, both positive and negative.

Temperature – albedo

When a cooling climate increases the extent of reflective snow and ice the albedo of the snow covered surface will increase. The high albedo causes further cooling and a positive feedback enhances the progress of cooling. Conversely, the same feedback process amplifies climate warming.

Vegetation – albedo and precipitation

During cooling of the climate in high latitude areas, the spruce forest is replaced by tundra increasing the reflectivity of the land during the winter season. This causes an enhanced cooling as a positive feedback. If the climate becomes warmer, the tundra is replaced by forest and the feedback results in more absorbed solar radiation and a warmer climate.

If the climate becomes wetter in the high latitudes, the area of forests might increase. More vegetation results in an increase of water vapour transfer back to the atmosphere. As a positive feedback, rainfall can locally increase. A change towards drier climate will work the opposite way.

Other feedback mechanisms

Increases in atmospheric turbidity (aerosol abundance) will affect the atmospheric energy budget by increasing the scattering of incoming solar radiation. Atmospheric turbidity has been shown to be higher during glacial episodes than in interglacials, with a consequent reduction in direct radiation reaching the Earth's surface. Such a situation will enhance the cooling associated with glacial periods.

Climate variability and change

As previously mentioned, climate is changing naturally on time scales of 10 to more than 100,000 years, due to e.g., solar variability, volcanic eruptions, and insolation changes caused by variations in the earth's orbit. Recent climate changes, however, are also affected by increased atmospheric concentrations of greenhouse gases. It is likely that the recent rise in greenhouse gases is mainly due to human activities /IPCC 2001/. Climate scenarios based on global and regional climate models indicate for the 21st century a substantial rise in

temperatures, a considerable change in hydrological conditions, and a rise in global sea level due to increased greenhouse gas levels /IPCC 2001/. The impact of these changes will likely exhibit distinct and important geographical differences. In addition to the change and variability attributable to causes external to the global climate system, internal variability is a characteristic of the system as well. The latter is often more pronounced on regional scales than in the global mean.

The future climate will be shaped by both anthropogenic and natural forcing, as well as by unforced internal variability. The necessary scenarios for the anthropogenic climate forcing rely on assumptions about future human activities as a result of societal choices, including future population changes and economic development. These scenarios for future anthropogenic climate forcing have been used to force climate models, in order to develop scenarios for the future climate changes towards the end of the current century /IPCC 2001/. Inferences on the internal climate variability can be made both from past data and by means of climate modelling. Scenarios for the future natural climate forcing are, however, impossible to construct as the relevant mechanisms are not understood in any predictive sense. We can, nevertheless, try to estimate the possible magnitude of future natural change, based on inference drawn from natural climate changes in the past /e.g. Moberg et al. 2006/.

For recent ideas on how anthropogenic forcing may modify climate at present and in the future, see for example /IPCC 2001, BIOCLIM 2001, 2003, Rummukainen 2003, Thorne and Kane 2006, and references therein/. Specific climate modelling results, for relevant areas of Sweden, are discussed in Section 4.3.1.

2.4 Climate in Sweden

The following description of the climate in Sweden is from /Ministry of the Environment 2001/.

Sweden is located in the northerly west wind belt, an area where the prevailing winds come from the south and west. The Gulf Stream and the numerous areas of low pressure produce a climate with winters that are 20–30°C warmer than at corresponding latitudes in Siberia and Canada. The precipitation brought by the frequent lows gives fairly plentiful rain and snow, although there is some rain shadow effect east of the Norwegian mountains.

According to the most frequently cited climate classification (Köppen), Sweden has a temperate, moist climate with year-round precipitation. Along the coasts of southern Sweden, the climate is warm-temperate, with a natural cover of deciduous forest. The climate in the rest of the country is cool temperate, the predominate vegetation being coniferous forest. Tundra conditions prevail in the mountains. The battle between areas of warm and cold air along the polar front, and Sweden's location between the Atlantic to the west and the largest continent on earth to the east, results in dramatic changes in the weather, particularly in winter. Often, a change in wind direction will suffice for icy Siberian conditions to be replaced by mild air from the Atlantic.

Summer temperatures are largely governed by altitude, and to a lesser extent by latitude. Thus the mean temperature in July is 15–16°C along the entire coast. The mean temperature in summer drops by 0.6°C with every 100 m of altitude. Even though there is little difference in temperature between southern and northern Sweden in high summer, summer itself (defined as the time of the year when the mean diurnal temperature is above 10°C) is much longer in the south than in the north. For example, in southernmost Sweden, summer lasts for five months, compared with three in the northernmost region. The turn of the seasons in spring and autumn, when the mean temperature is between 0 and 10°C, is also much shorter in the north. So in Lapland in northernmost Sweden, winter lasts for just over half the year, whereas the coast of Skåne, in the far south, only has winter for a few weeks, with temperatures below zero. The vegetation growing season, defined as the part of the year when the mean diurnal temperature is over 5°C, varies considerably over the country. It lasts for between 210 and 220 days in southernmost Sweden (western and southern Skåne and the coast of Halland), but is only half as long in the far north.

Local conditions such as topography and proximity to the sea or large lakes influence the climate locally. The mean temperature can be extremely low in valleys with open terrain in inland areas of northern Sweden (−15 to −17°C). Elsewhere in northern Sweden the January mean temperature is generally between −9 and −14°C, except along the coast in the south of the region where, as in much of the central inland region, the mean January temperature is −5 to −8°C. In the southern and eastern part of central Sweden, the mean temperature is −3 to −5°C in January, while it is −1 to −2°C in southern coastal areas owing to the ameliorating effect of the nearby open sea. The temperature can vary a great deal, from approximately −50 to 38°C. The lowest recorded temperature is −53°C, recorded at two locations in northern Sweden. Elsewhere in Sweden the coldest recorded temperatures are −30 to −40°C, except along some parts of the southern coast, where it has never fallen below −25 to −30°C. The highest recorded temperatures display much less geographical variation than the lowest; in southern and central Sweden and along the northern coast, the records are between 34 and 36°C. Very occasionally, temperatures also rise above 30°C in other parts of the country. Over much of Sweden annual precipitation is between 600 and 800 mm. Annual precipitation in the mountains, most exposed to westerly winds in northern Sweden (western Lapland and Jämtland), is between 1,500 and 2,000 mm. On the western slopes of the southern uplands, maximum annual precipitation is 1,300 mm. The Abisko area in northernmost Sweden has least precipitation, approximately 450 mm per year. This area lies in the rain shadow of the mountains to the west.

In more or less the entire country, precipitation is heaviest during July–November. Most precipitation falls along fronts as areas of low pressure move across the country. But several weeks may sometimes go by in spring and early summer without any rain. Most of Sweden usually has a snow cover in winter. In the mountains of Lapland, the ground has a snow cover for an average of 225–250 days a year. Most of the rest of northern Sweden is covered in snow for more than 150 days a year. In central Sweden and upland areas of the south, there is a snow cover on average between 100 and 150 days each winter. In the rest of southern Sweden, there is a snow cover for between 50 and 100 days, except along the west coast and the far south, where snow lies for less than 50 days each winter. The maximum snow depth averages more than 60 cm throughout almost all of northern Sweden; the mountains generally have more than a metre of snow. Air pressure distribution over the European continent causes winds from south and west to predominate. However, winds from other directions are fairly common because of the numerous areas of low pressure arriving from the west, and the circulation of winds around them. Occasionally, lows reaching Sweden develop into storms so intense that winds reach hurricane force along the coast and above the tree line.

For a more detailed account of climate in Sweden, see /Raab and Vedin 1995/.

The climate at Forsmark and Oskarshamn sites are similar, with typical values for the climate on the Swedish east coast (Table 2-1). Oskarshamn has slightly lower mean annual precipitation, and slightly higher mean annual air temperature than at Forsmark.

An overview of climate proxy data and what they can tell us about climate in Sweden during the last millennium, or in some cases even longer back in time is presented in /Moberg et al. 2006/.

Table 2-1. Present-day climate data for Oskarshamn and Forsmark. Data from /SMHI 2001/. For Forsmark, the precipitation was measured at Östhammar whereas the temperature was measured at Risinge.

Site	Mean annual precipitation (mm/a)	Mean annual air temperature (°C)	Mean summer temperature, JJA (°C)	Mean winter temperature, DJF (°C)
Oskarshamn	553	+6.4	+15.5	−2.0
Forsmark	576	+5.0	+14.9	−4.3

That report also provides more detailed climate information from Swedish instrumental data for the last 260 years. A tentative evolution of climate in Sweden for the last millennium, as simulated by a climate model, is also provided. Taken together, these three basic types of information are used to illustrate possible Swedish climate variations during the last millennium. /Moberg et al. 2006/ provides a benchmark for the likely range within which our regional climate has varied naturally during the last millennium. An example of this is given in the very last analysis presented in that report. In this example, output from a regional climate model simulation is used to illustrate how daily temperature, precipitation, runoff and evaporation at Forsmark and Oskarshamn might have differed between unusually cold and warm 30-year periods during the last millennium.

3 Climate-related issues

3.1 Ice sheet dynamics

3.1.1 Overview/general description

Introduction. Glaciers and ice sheets may form in climate regions where, in places, the winter snow precipitation is not completely melted away during summer. A glacier is an ice mass that has been formed by successive local accumulation of snow, with ice movement due to ice deforming under its own weight. An *ice sheet* is defined as a glacier that spreads out in all directions from a central dome, i.e. a large glacier (> 50,000 km^2 in area) that is not confined by the underlying topography. In reality, the flow pattern of ice sheets is not radial from a single dome. Instead, ice often flows out from a number of elongated *ice divides*, with the ice divides constituting the highest parts of the ice sheet.

Generally, ice flow velocities are moderate to slow within an ice sheet, with ice moving a few tenths of metres per year. However, certain well-defined parts of ice sheets, so called *ice streams*, exhibit significantly faster ice flow. Ice streams are typically some tenths of kilometres wide and several hundreds of kilometres long. Ice velocities within present-day ice streams are several hundred metres per year, in some cases exceeding 1,000 m a^{-1} /cf Joughin et al. 2004/. Since surrounding ice typically move considerably slower, high velocity gradients across the ice stream margins produce distinct *shear zones* with heavy crevassing. Because of the high ice flux in ice streams, these features may drain ice from large portions of ice sheets. Ice streams are often characterised by specific basal thermal and hydrological conditions, differing from those of the surrounding ice sheet.

The margin of an ice sheet may end either on land or in water. If the ice margin is positioned in the sea or in a lake, it is common that the outer part of the ice sheet is floating on the water, constituting an *ice shelf*. The boundary between the floating and grounded ice is the ice sheet *grounding-line*.

If the basal thermal and topographical conditions are favourable, sub-glacial melt water may accumulate in topographic lows beneath the ice, forming *sub-glacial lakes*. These are common features under the present Antarctic ice sheet, whereas none have been found beneath the Greenland ice sheet.

Mass balance. The growth and decay of ice sheets are determined by the *mass balance* of the ice mass. The mass balance constitutes the result of the mass gain, or *accumulation*, and the mass loss, or *ablation*, typically averaged one year. The mass gain of an ice sheet is completely dominated by the process of snow accumulation. Most of the snow falls and accumulates during winter seasons, but snow may also accumulate during summer. For ice sheet ablation on the other hand, a number of important processes may be involved, the two most significant being surface melting of snow and ice (if the summer climate is warm enough) and calving of ice bergs from ice shelves (when the margin is at the sea). In addition, mass may also be lost from the ice sheet by melting of basal ice, and locally on the surface by sublimation of ice and snow. When a certain part of an ice sheet exhibits more accumulation than ablation during one year, that part is said to belong to the *accumulation area* of the ice sheet. This is in contrast to the *ablation area*, where there is a net loss of mass during one year. Central parts of ice sheets typically constitute accumulation areas, whereas in case of surface melting, lower parts of ice sheets constitute ablation areas (Figure 3-1). The line between the accumulation- and ablation area is called the *equilibrium line*.

If the total ice sheet accumulation is greater than the total ablation during one year, the mass balance is said to be positive, whereas the opposite case produces a negative mass balance.

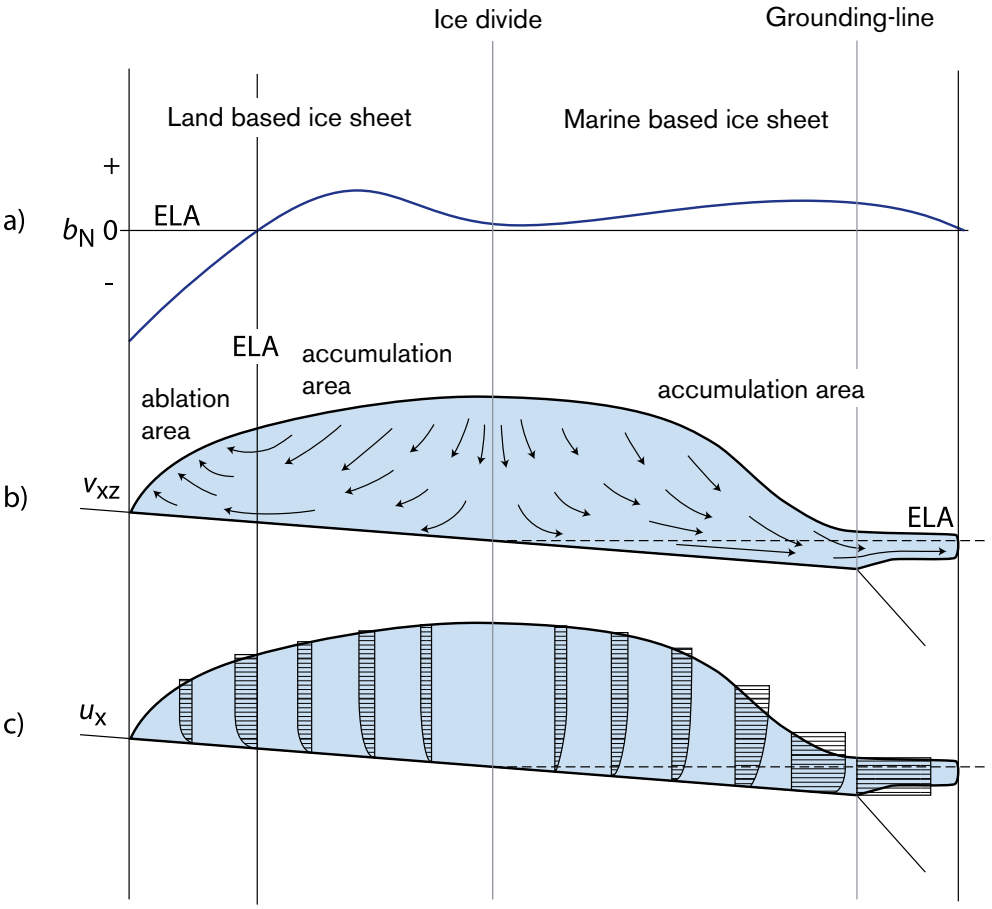

Figure 3-1. *Schematic ice sheet cross section. Panel a) shows the surface net balance distribution (b_N), panel b) shows ice velocity trajectories (v_{xz}) as well as distribution of accumulation- and ablation areas, and panel c) shows the horizontal velocity component (u_x). ELA denotes equilibrium line altitude. Figure modified form /Denton and Hughes 1981/.*

If accumulation and ablation are equal, the mass balance is zero. Large amounts of water are involved in this mass turnover process, for example the mass overturn for the Antarctic ice sheet is today about 2 Gtonnes per year /Church et al. 2001/.

A positive mass balance over a number of years makes an ice sheet grow, whereas a negative mass balances reduces its size. However, changes in the size of ice sheets are very slow processes acting over hundreds and thousands of years. The *response time* of an ice sheet is the time it takes for a steady-state ice sheet to come to a new steady-state condition after a climate change. Since climate is constantly changing, ice sheets are never in true steady-state, but are constantly adjusting their size and shape to the prevailing climate.

Ice temperature. The temperature of the ice is of fundamental importance for the behaviour and characteristics of glaciers and ice sheets. Among other things, it has a strong effect on the movement, dynamics and hydrology of the ice. Two types of glacier ice can be defined based on temperature; 1) *Temperate* (or *warm*) *ice* with the ice temperature at the pressure melting point, and 2) *Polar* (or *cold*) *ice* with the ice temperature below the pressure melting point. Cold ice is harder than temperate ice, and also impermeable to water.

Glaciers and ice sheets are often classified according to their thermal characteristics. In the simple case, a glacier where all ice has a temperature at the pressure melting point throughout the year is called a *temperate glacier* or *temperate ice sheet,* whereas a glacier in which all the ice is below the pressure melting point throughout the year is called a *polar glacier* or *polar ice sheet*. However, an ice sheet or glacier need not consist exclusively of temperate or polar ice. In many cases, it can contain both ice types, and in such a case it is called *polythermal*.

Of particular interest is the temperature of the ice at the ice sheet bed, i.e. the basal thermal condition. An ice sheet can be *cold-based* or *warm-based*. A cold-based ice sheet has cold basal ice, and it is frozen to its bed. There is no free water at the bed, and no sliding of basal ice over the substrate is taking place. A warm-based ice sheet is at the pressure melting point at the bed. Free water is, in this case, present at the ice/bed interface, and the ice may slide over the substrate. This has important consequences both for ice kinematics and landform development. A polar ice sheet may be either cold-based or warm-based. In the case of a warm-based polar ice sheet, it is typically only the lowermost part of the ice that is at the pressure melting point, whereas most of the ice sheet consists of polar ice. One part of a polar ice sheet may thus be cold-based at the same time as other parts are warm-based. This is the present case for the Greenland and Antarctic ice sheets /cf Näslund 1997/. Warm-based and cold-based ice sheets are also called *wet-bed ice sheets* and *dry-bed ice sheets*.

Glaciers and ice sheets experience melting of basal ice where the basal ice temperature is at the pressure melting point. Heat for this melting can be added from geothermal heat flux and from frictional heating by internal deformation of basal ice. The thermodynamic situation at the base of an ice sheet is determined by the thermal properties of ice. Energy can be transferred by diffusion along a temperature gradient in ice as in all materials. However, the solidus of the ice-water vapour phase space has a negative slope, which means that the melting or freezing temperature is depressed with increasing pressure by 0.09 K/Pa. As a general statement, freezing of liquid water occurs when temperature and pressure satisfy the generalised Clapeyron equation /e.g. O'Neill and Miller 1985/:

Equation 3-1
$$\frac{p_w}{\rho_w} - \frac{p_i}{\rho_i} = \frac{L}{273.15} T + \frac{P_o}{\rho_w}$$

where p_w = water pressure, ρ_w = water density, p_i = ice pressure, ρ_i = ice density, L = ice density coefficient of latent heat of fusion, T = temperature in degrees centigrade, and P_0 = osmotic pressure. Equation 3-1 couples the effect of temperature and pressure. It is a general thermodynamic relationship not specific for the case of ice sheets and glaciers. However, the phase change of the ice-water system is not only controlled by temperature and pressure. Two other factors may also be of importance; 1) the presence of solutes in water, and 2) surface tension arising from interface curvature. Just as in the case with an increasing pressure, an increase in solutes in liquid water also depresses the melting/freezing point. This effect is referred to as the osmotic pressure /e.g. Padilla and Villeneuve 1992/, and it is included in Equation 3-1. If liquid water is present at the base of ice sheet, and it contains solutes, this will together with the pressure modify the melting point. The second factor constitutes an ice/water interfacial effect. The finer grains that a sediment has, the higher the curvature of the ice-water interface becomes, which in turn lowers the melting point /Hohmann 1997/. For example, in clays, liquid water has been observed at temperatures down to −10°C /O'Neill and Miller 1985/.

If the effect of phase curvature is taken into consideration the Clapeyron equation may be modified to /Raymond and Harrison 1975/:

Equation 3-2
$$T = -\frac{273.15}{L}\left(\frac{1}{\rho_i} - \frac{1}{\rho_w}\right) p_w - \frac{273.15\sigma_{iw}}{L\rho_i r_p} - \frac{273.15}{\rho_w L} P_o$$

where σ_{iw} = ice-water surface energy, and r_p = characteristic particle radius. Equation 3-2 is the fundamental equation for the ice water phase transition given by /Hooke 1998/. In this equation, the first of the three terms describes the effect of pressure on the ice water phase transition, the second term describes the effect of interfacial pressure, and the third term the effect of osmotic pressure. Equation 3-2 thus gives the complete treatment of the ice water phase transition. Commonly only the first term is used for calculations of the pressure melting point beneath glaciers and ice sheets, often rewritten in glaciological literature to give a simplified expression for calculating the pressure melting point /cf Remy and Minster 1993/:

Equation 3-3
$$T = -\frac{h}{1503}$$

where T = pressure melting point temperature (°C), and h = ice thickness (m). The effect of the lowering of the pressure melting point described above is, in the case of an ice sheet, that the melting point is lowered by c 2 K beneath 3 km of ice. This is very important, since the basal conditions change drastically if the bed of an ice sheet becomes melted or frozen. This affects ice sheet flow by turning on and off basal sliding, governs if glacial erosion can take place or not, and of course has a profound impact on basal hydrology.

To demonstrate the effect of ice sheet surface conditions on the temperature distribution within polar ice sheets, we start with a simplified case of a steady-state ice sheet with no ice flow, corresponding to an artificial situation at an ice divide (no horizontal flow) without any precipitation (no vertical flow). Figure 3-2a shows the vertical temperature profile through such an ice mass given a surface temperature of −20°C and a specified geothermal heat flux at the base. The resulting temperature profile is a straight line from the surface temperature down towards the bed. In this case the vertical temperature profile reaches the pressure melting point temperature near the bed, resulting in a warm-based polar ice sheet.

Next we consider the same case but with snow accumulation at the ice sheet surface, which means we are introducing a vertically downward directed ice movement. Generally, this lowers the temperatures within the ice sheet as seen in (Figure 3-2a). Due to the vertical velocity and

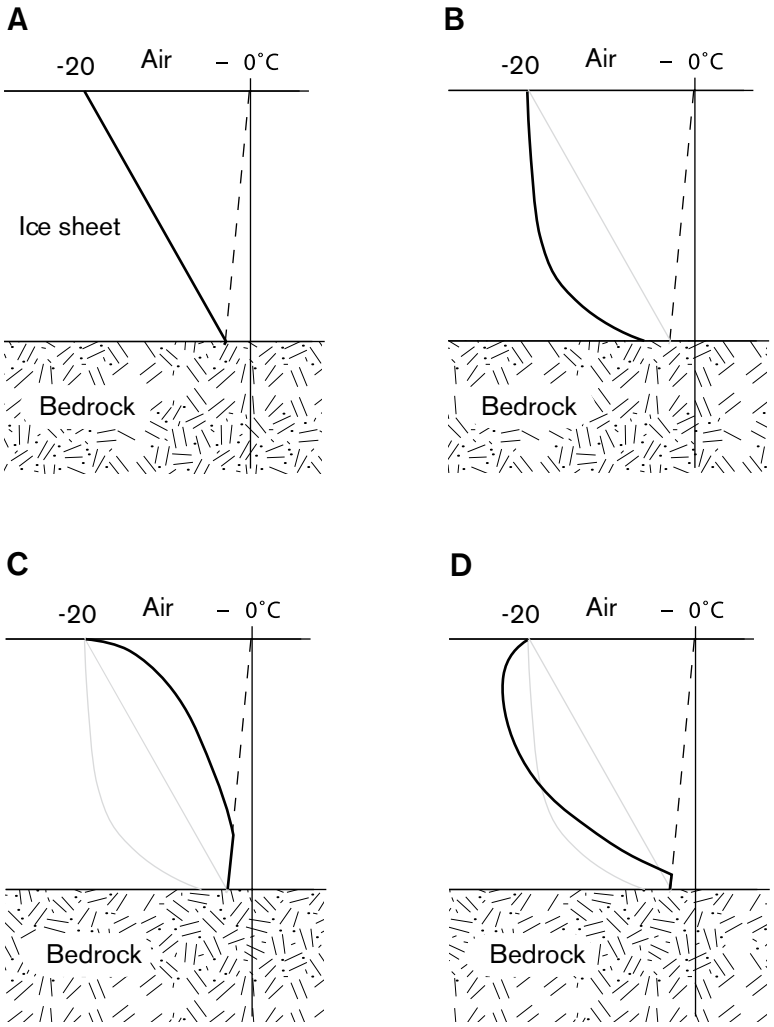

Figure 3-2. *Vertical temperature profiles through a 2,000 m thick theoretical polar ice sheet. The dashed line denotes the pressure melting point temperature. a) No ice flow (dead-ice body), b) Vertical ice flow only – accumulation area (reflecting only a surface accumulation rate), and c) Vertical ice flow only – ablation area, d) Horizontal and vertical ice flow – accumulation area.*

cold surface climate, cold ice is advected downward, while the geothermal heat warms this descending ice. The upper part of the ice sheet develops an almost isothermal zone, whereas the ice warms quickly near the bed. In this example the ice sheet below this accumulation area has become cold-based. Higher precipitation rates at the surface, i.e. higher vertical velocities, result in an increased thickness of the isothermal zone and also decrease the basal temperature. Furthermore, lower air temperatures at the ice sheet surface also decrease the ice column temperatures, and vice versa.

If we instead consider an ablation area, with net mass loss at the surface, the vertical ice movement will be directed upwards. In this case, the upward vertical velocity produces a generally warmer ice column, in this example resulting in temperate conditions at the bed (Figure 3-2c).

The last case to consider is a more common situation, when we also have horizontal ice movement. Figure 3-2d shows a typical situation within the accumulation area of an ice sheet, but not located directly on an ice divide. The horizontal velocity component is advecting cold ice into the site, ice that was formed in higher, colder parts of the ice sheet. Compared to the situation in Figure 3-2b, the minimum temperature is now found at some depth below the surface, since the ice at the surface, formed locally at the site, is warmer (Figure 3-2d). This positive temperature gradient near the surface has been observed in several deep drill holes, see for example the Mirny, Century 13, and Byrd 9 drill hole temperatures in (Figure 3-3). Furthermore, due to the horizontal ice movement, ice in the lower part of the ice sheet is warmed by internal friction, as this is where most of the internal deformation of the ice is taking place. In this example, the ice sheet has again become warm-based.

Including these processes, the resulting englacial and subglacial temperatures along a flow line are as shown in Figure 3-4. Typical polar ice sheet accumulation rates and air temperatures are assumed. The lowest englacial temperatures are found in the highest central parts of the ice sheet, and the highest ice temperatures are found near the front. Basal melting is taking place in the interior part of the ice sheet and close to the margin, with a zone of basal frozen condition in between. A narrow zone of basal frozen conditions at the margin may also occur due to decreasing vertical velocity.

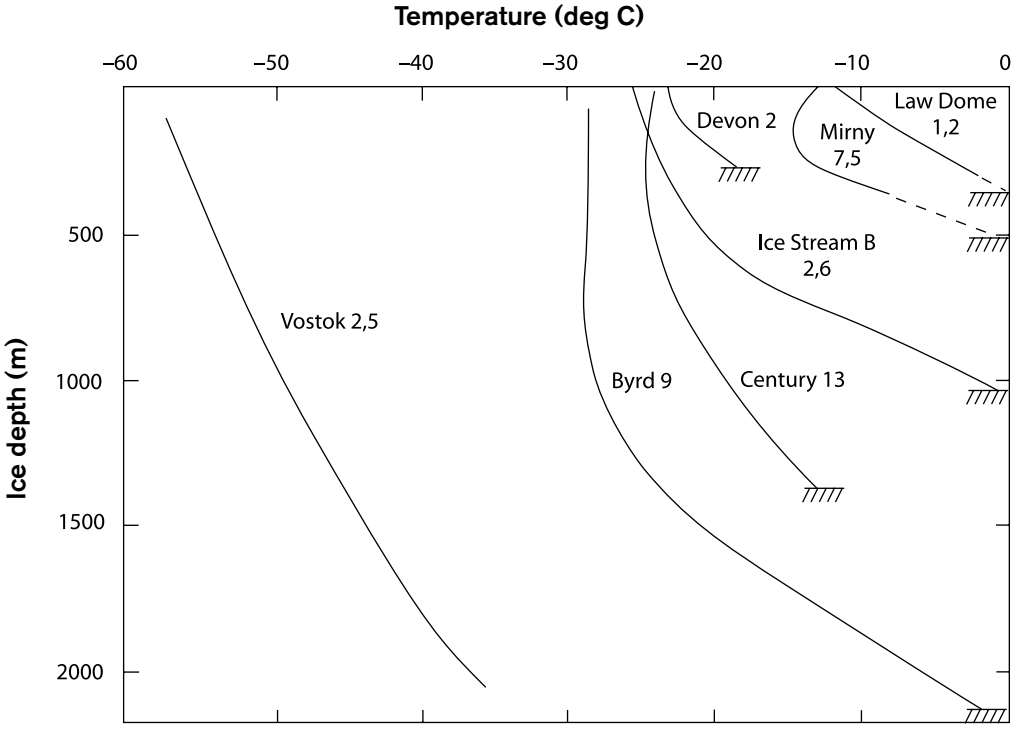

Figure 3-3. *Borehole temperature data from the Greenland and Antarctic ice sheet /from Paterson 1994/.*

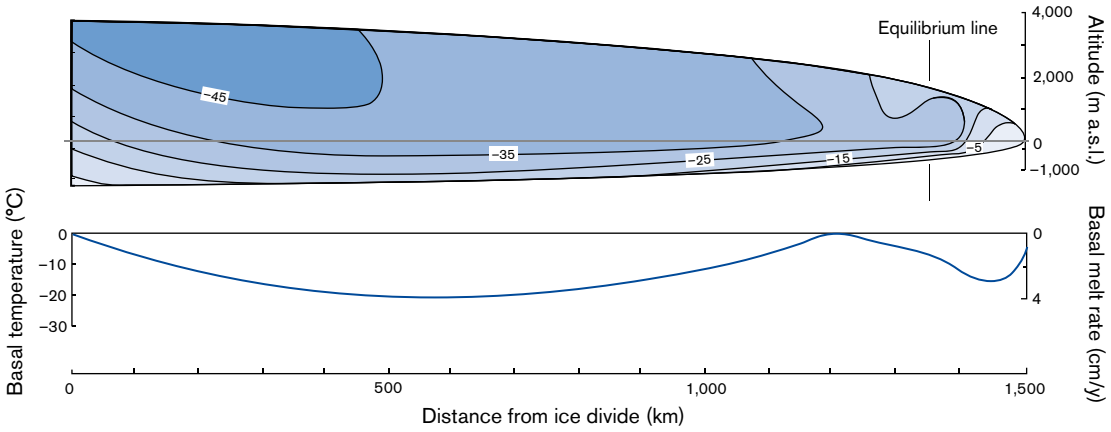

Figure 3-4. *Example of modelled ice sheet temperature distribution along a flow line, modified from /Hooke 1977/. Ice temperatures are in °C. Basal melt rates are high near the terminus because of the strain heating effect from rapid ice flow in the region around the equilibrium line.*

In nature, the topography of the landscape beneath the ice sheet is of great importance for the basal temperature distribution. Topographic lows are more prone to experience basal melting conditions that topographic heights. This is both due to the fact that the pressure melting point is lowered more in depressions (due to the greater ice thickness) than over surrounding higher terrain, and due to the less insulating capacity of thinner ice over topographic heights. The result is for example that a floor of a large valley in general is more likely to have experienced longer periods of basal melting than surrounding elevated areas. This local topographic control on basal temperatures has been observed in the Antarctic ice sheet /Näslund 1997/.

An additional important process affecting ice temperature takes place if the air temperate allows surface melting during spring periods, for example at low elevations of an ice sheet in a warming deglaciation climate, or during times of early ice sheet formation. After the winter period with cold temperatures, the temperature in the upper snow/firn pack of the ice sheet is well below the freezing point. As surface melting starts, meltwater percolates down in to the snow pack and re-freezes at some depth. During the re-freezing process, latent heat is released (334 kJ/kg, corresponding to the latent heat of fusion for ice) which warms the surrounding snow. As the process continues the entire snow pack can be transformed to temperate conditions during a few weeks. This is a very efficient process, and the result is that temperate ice instead of cold ice is formed at the location. This may have been an important process during build-up phases of Fennoscandian ice sheets, having an important effect on the thermal characteristics of those early ice sheets /Näslund 1998/.

Ice movement and thermodynamic feed-back. The stresses enforced by the mass of over-laying ice induce deformation or strain in the ice. The resulting ice movement, often referred to as *internal deformation*, is present in all glaciers (being one of the main criteria for the term *glacier*). The shear stress at the base of an ice sheet is calculated from:

Equation 3-4 $$\sigma = \rho\, gh \sin\alpha$$

where σ is the shear stress, g is the acceleration of gravity, h is the ice thickness, and α is the ice sheet surface slope. The most common flow law of ice describing the strain rate of ice under pressure is Glen's flow law /Glen 1955/:

Equation 3-5 $$\dot{\varepsilon} = \left(\frac{\sigma}{B}\right)^n$$

where $\dot{\varepsilon}$ is the strain rate, σ is the shear stress, B is a viscosity parameter that increases as the ice gets more difficult to deform, a parameter depending on among other things ice temperature and crystal fabric, and n is an empirically determined constant (~ 3) that depends

on the specific creep process that is operating. The main effect of Glen's flow law is that also moderate increases in stress (ice thickness) results in a substantial increase in strain rate. For example, a doubling of the amount of stress results in 2^3, that is 8, times higher deformation rate (Figure 3-5). Glen's flow law assumes that ice is an isotropic material.

In ice sheets the horizontal ice velocity increases from the ice divides, where it is zero toward the margin. The steeper surface slope at the margin induces larger driving stresses which makes the ice deformation rate high. For an ice sheet with an ablation area, i.e. an ice sheet ending on land (Figure 3-1) the maximum horizontal velocity is at the equilibrium line, whereas in the case of a marine ice sheet margin, the maximum velocity is at the ice sheet grounding-line (Figure 3-1).

The stress that acts on the uppermost layer of a glacier does not produce a creep or plastic deformation. Instead the uppermost part of the ice, about 30–100 m thick depending on ice temperature, is brittle, often resulting in typical fractures, or *crevasses*. Most of the internal deformation takes place near the bed where stresses are highest. The overlaying ice moves along more or less as a uniform block on top of the deforming ice. This is indicated as the internal deformation portion of the ice velocity in Figure 3-6.

There is also another process that may contribute to glacier movement. If the ice sheet is wet-based, the ice may slide over the substrate. The surface ice velocity is, in this case, the sum of the component from internal deformation and the component from basal sliding (Figure 3-6). For all practical purposes, one can assume that *basal sliding* does not occur if the bed is frozen. Not all glaciers, or all parts of an ice sheet, necessarily have the sliding ice flow component. However, where it is present, it may be of great importance, for example in ice streams, which are typically warm-based. Here, the observed surface flow may be completely dominated by basal sliding /Engelhardt and Kamb 1998/. High basal water pressures are favourable for intense basal sliding /Engelhardt et al. 1990/, as well as smooth bed topographies and deformable, water-saturated tills /e.g. Kamb 2001, Iverson et al. 1995/.

Within glaciers and ice sheets there are important thermodynamic feedback mechanisms, in the following exemplified by a discussion on ice streams. As seen above, the viscosity of the ice is affected by the ice temperature, with higher ice temperatures giving more easily deformable ice. At the same time, the internal deformation itself produces frictional heat, with higher velocities producing more heat. This gives a positive feedback mechanism; high internal deformation rates increase the temperature of the ice, which in turn makes the ice even easier to deform.

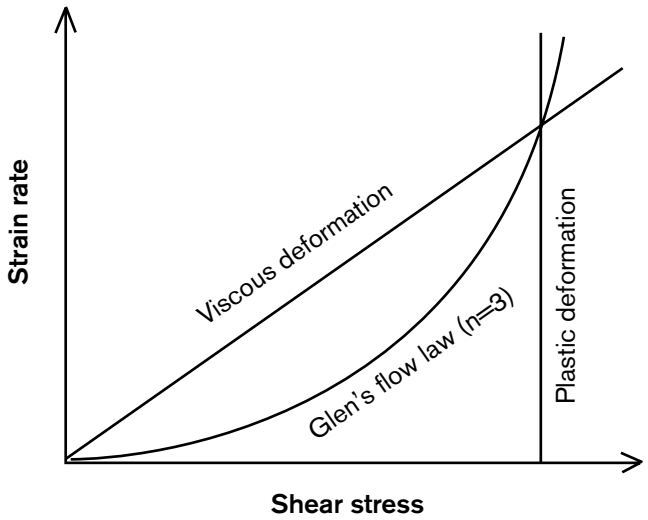

Figure 3-5. *Deformation rate versus shear stress for various flow laws, including Glen's flow law for ice.*

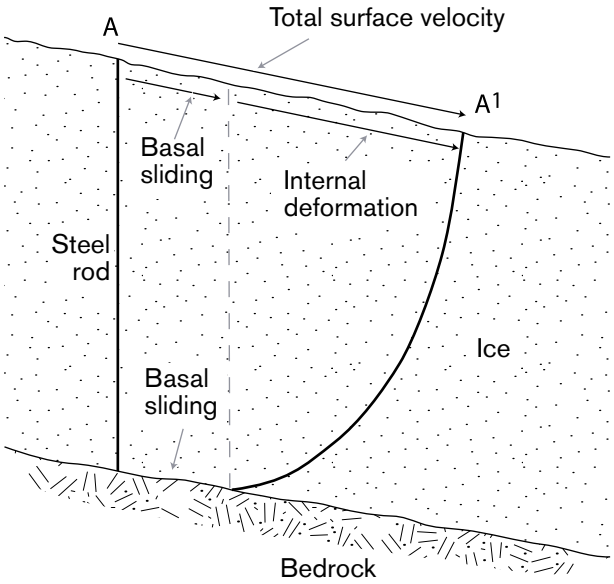

Figure 3-6. *Internal deformation and basal sliding demonstrated by the deforming of a steel rod from time A to A[1].*

On the other hand, looking at the basal thermal conditions of ice streams, there may be additional thermodynamic processes acting. A fast-flowing warm-based ice stream may drain a lot of ice from the ice sheet. Over time this will reduce the thickness of the ice, also over the ice stream itself. The thinner ice insulates less well from cold surface temperatures, which leads to less melting at the bed, and eventually also to a drastic shift from warm-based to cold-based conditions. This reduces the velocity of the ice stream considerably and the ice flux deformational heating reduces accordingly. The ice stream now drains much less ice than before, which in time results in increased ice thicknesses /Payne 1995/. The larger ice thickness warms the bed, which again may become wet-based and basal sliding may start again. This process suggests that ice streams may have an inherited built-in unstable behaviour. It has been suggested as on explanation for the cyclic Dansgaard-Oeschger events recorded in glacial marine sediment /cf Andrews and Barber 2002/.

The ice sheet dynamics described above may affect a number of geosphere variables of importance for a deep geological repository (Table 3-1).

Indirectly fracture geometry is affected by ice sheet dynamics since the fracture geometry is determined by the prevailing rock stresses which in turn depend on ice load and basal conditions of the ice sheet. Generally, the ice load will act to compress the bedrock pores and fractures. In some cases, high water pressures may act to open fractures. There may also be movements along fractures /see further **Geosphere process report**/.

3.1.2 Controlling conditions and factors

The upper boundary of the ice sheet system is the ice sheet surface, whereas the lower boundary is the ice sheet bed, i.e. the interface between basal ice and substrate. In accordance with ice sheet fluctuations the lateral extent of these boundaries changes over time.

Upper boundary condition – Climate. The boundary condition at the ice sheet surface is the prevailing climate, i.e. air temperature and precipitation, including its variation over time. The air temperature at the ice sheet surface is determined mainly by the latitude, altitude and climate changes. The latitude at a site is fixed, but the altitude varies with the local thickness variations of the ice sheet and associated isostatic responses. The typical air temperature pattern over an ice sheet is with the lowest temperatures in the ice sheet interior, and higher surface temperatures closer to the margin. If temperatures are greater than 0°C during summer, surface

Table 3-1. A summary of how geosphere variables are influenced by ice sheet dynamics.

Geosphere variable	Influenced by climate issue variable/s	Summary of influence
Ground temperature	Basal ice temperature	During periods of cold-based ice coverage, low basal ice temperatures contribute to the formation of permafrost.
Groundwater flow	Basal thermal condition Basal melt rate Supply of surface melt water	If the ice sheet is cold-based no free water is available and there will be no groundwater recharge from basal melt water. If the ice sheet is warm-based, basal melting occurs at the ice/bed interface and groundwater recharge takes place. In addition, meltwater from the ice sheet surface will, in both cases, be transported to the bed in frontal-near areas of the ice sheet (see further Section 3.2). Groundwater recharge and flow will be determined by the presence of the ice sheet.
Groundwater pressure	Basal thermal condition Ice sheet thickness Basal melt rate Supply of surface melt water	If the ice sheet is warm-based, the water pressure at the ice/bed interface may correspond to the ice sheet overburden pressure, and in certain cases more. The groundwater pressure also depends on the melt water supply and the flow properties of the en- and sub-glacial hydrological systems (see further Section 3.2). The groundwater pressure is also affected by the ice load compression of the bedrock pores and fractures.
Rock stresses	Basal condition Englacial ice temperatures Ice sheet thickness	Rock stresses will be influenced by the ice load and the hydrostatic pressure. Independently of basal conditions there will be an increase in vertical stresses corresponding to the ice thickness. The horizontal stresses will also increase. If the ice sheet is warm-based the prevailing water pressures at the ice/bed interface will also alter rock stresses. The alteration of rock stresses also depends on the duration of the ice load and the slope of the ice sheet surface (see further Section 3.5). The slope of the ice sheet surface near the front is to a highly dependent on englacial ice temperatures and basal thermal conditions.
Groundwater composition	Glacial melt water composition	The glacial melt water is oxygen rich. The combination of abundant melt water supply and high water pressures may cause injection of glacial melt water to great depths. Also, the consumption of oxygen close to the surface may be limited due to the lack of organic matter and microbiological activity.

melting takes place on the lower parts of the ice sheet surface. This melting typically amounts to several m of ice per year, with large variations according to the prevailing temperature regime. Surface melt rates are lower closer to the equilibrium line. In general, during cold stages of ice sheet growth, the amount of surface melt water production is small compared with the amounts of water produced in warmer climates during ice sheet deglaciation.

Most precipitation that falls on ice sheets falls as snow. During relatively warm climates at low ice sheet elevations, precipitation may occur as rain. Snow accumulation and surface ablation are not distributed evenly over the ice sheet surface. The precipitation pattern reflects ice surface elevation and degree of continentality, often giving a pattern of high accumulation rates close to the ice sheet margin with diminishing values towards the interior. On mid-latitude ice sheets, like the former Fennoscandian ice sheet, the precipitation pattern is strongly

affected by the prevailing west-wind belt and associated low-pressure tracks. This results in an orographic effect which gives most precipitation on the western side of large Fennoscandian ice sheets. Typical coastal accumulation rates of the Antarctic ice sheet are 0.3–0.6 m a^{-1} (water equivalents), whereas the interior parts gets less than 0.1 m a^{-1} in precipitation /Giovinetto and Zwally 2000/, i.e. here polar desert conditions prevail. On an ice sheet surface, regional and local variations of great magnitude in the amount of snow accumulation often occur, mainly due to wind re-distribution of snow in regions close to the ice sheet margin (Figure 3-7).

To initiate ice sheet growth in a non-glaciated region, local climate need to change. That can either occur due to global climate change, towards lower local summer temperatures or higher winter precipitation rates, or, over long time scales, by tectonic uplift, or a combination of climate and tectonics. Generally, ice sheet formation in Fennoscandia involves small alpine glaciers in the Scandinavian mountain range that grow into a mountain centred ice sheet, and then grow to a full-scale ice sheet /Andersen and Mangerud 1989, Lundqvist 1992, Kleman et al. 1997/. Increasing evidence suggests very dynamic ice sheet growth, with growth phases interspersed by extended periods with restricted ice coverage, for example during Marine Isotope Stage 3, see review by /Lokrantz and Sohlenius 2006/.

Lower boundary condition – Ice sheet bed. The lower boundary condition of the ice sheet system is the ice sheet bed. The substrate may either consist of bedrock, in Fennoscandia typically crystalline rocks, or bedrock covered by till. There are two important parameters to consider here; 1) the topography of the landscape, and 2) the amount of geothermal heat flow.

The topography of the bed is of importance for the basal boundary conditions of ice sheets, as discussed above. Above all, an ice sheet bed with strong relief produces basal thermal conditions with stronger lateral temperature gradients than an ice sheet bed with smooth topography. The first case also implies larger spatial variations in basal melt water production.

The geothermal heat flux is also of great importance for the basal condition of ice sheets /e.g. Waddington 1987/, affecting basal ice temperatures, hydrology, ice dynamics, and the erosional capacity of the ice. Typically, for a 3 km thick ice sheet at steady-state, a 20% error in geothermal heat flux generates a 6 K error in calculations of basal ice temperatures. This has direct implications on, for example, numerical ice sheet modelling. If the geothermal heat flow is not realistic in the model setup, ice sheet models will not produce useful data on basal melting

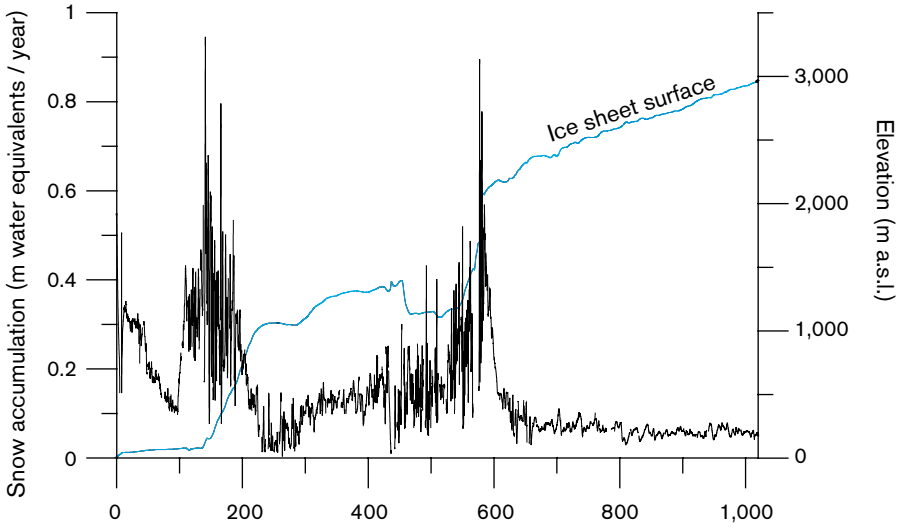

Figure 3-7. *Accumulation rates and ice surface elevations along a profile in over the east Antarctic ice sheet. The accumulation is high in the coastal area and low in the interior. Due to wind redistribution of snow, exceptionally high values with strong variations are found in areas of nunataks and steep surface slope. From /Richardson 2004/.*

and other characteristics. Numerical ice sheet modelling studies have also shown that basal ice temperatures are sensitive to relatively small changes in geothermal heat flow /e.g. Greve and Hutter 1995, Siegert and Dowdeswell 1996/.

For the present study, /Näslund et al. 2005/ calculated a distributed, high-resolution geothermal heat flow data set for an approximate core area of the Fennoscandian ice sheet, and embedded this within lower-resolution data published for surrounding regions. In the following, a brief overview of the geothermal heat flux calculation is given.

The geothermal heat flow, or surface heat flow density (HFD), in cratonic areas consists of two components: (1) heat produced within the mantle and core of the Earth and (2) heat produced within the crust. The contribution from the Earth's interior (so-called Moho- or reduced heat flow) arises from the cooling of the Earth and formation of a solid core, and from radiogenic heat production /Turcotte 1980, Pollack et al. 1993/. The crustal component consists of a radiogenic heat production where heat is produced by the natural radioactive decay of primarily ^{238}U, ^{232}Th, and ^{40}K /Furlong and Chapman 1987/. The Moho heat flow has a smooth spatial variation, possibly depending on mantle convection cell distribution /Beardsmore and Cull 2001/, whereas the spatial variation in concentration of radioactively decaying nuclides in the lithosphere generates a heat flow with large spatial variations. The surface HFD can be estimated by a heat flow-heat production (Q-A) relationship of the form

Equation 3-6 $$Q = q_0 + DA_0$$

/Birch et al. 1968, Lachenbruch 1968, Beardsmore and Cull 2001/ where Q is the surface heat flow density (or geothermal heat flow), q_0 is the Moho heat flow, D represents the vertical distribution of heat producing radionuclides in the lithosphere and A_0 is the radiogenic heat production from near-surface rocks.

The regional HFD pattern does not correlate with gravity variations /Balling 1984/, magnetic anomalies /Riddihough 1972/, or crustal thickness /Čermák et al. 1993/. However, within the Baltic shield, as well as in other areas with similar geological settings, there is close correlation between HFD and regional geological units, with higher heat flow from acid (commonly granitic) areas and lower heat flow values from basic areas /e.g. Landström et al. 1979, Malmqvist et al. 1983/.

The calculation of HFD values for Sweden and Finland were based on detailed data sets from numerous γ-emission measurements from bedrock and till. In Sweden, airborne surveys of γ-emissions have been carried out by the Geological Survey of Sweden (SGU), sampling data at 70 m intervals along flight lines with 17 km separation. In order to avoid shielding effects from vegetation and lakes, only data from exposed bedrock and till surfaces were used in our calculations. The Finnish data set is based on radiometric γ-emission measurements of 1,054 till samples providing full spatial coverage of the country /Kukkonen 1989/.

The calculation of HFD is performed in several steps. First, the concentrations of ^{238}U, ^{232}Th, and ^{40}K are calculated from the γ-emission measurements, using information from detailed reference measurements over calibration plates with well known isotopic concentrations. Near-surface heat production was then calculated from the concentrations of radionuclides. In addition, the Moho heat flow contribution needs to be considered. The distributed Moho heat flow by /Artemieva and Mooney 2001/ was added to the near-surface heat production data set. Finally, the HFD data set was re-sampled to a grid with 5 km resolution. To provide HFD coverage for the entire model domain, data for surrounding areas were added from the much coarser observed global HFD data set provided by /Pollack et al. 1991/. The resulting geothermal heat flow distribution is shown in Figure 3-8.

Within the LGM ice margin, the new data set shows that the geothermal heat flow varies by a factor of as much as 2.8 (geothermal heat flow values ranging between 30 and 83 mW/m^2), with an average of 49 mW/m^2. This average value is 17% higher than 42 mW/m^2, the typical uniform value used in ice sheet modelling studies of Fennoscandia. Using this new distributed

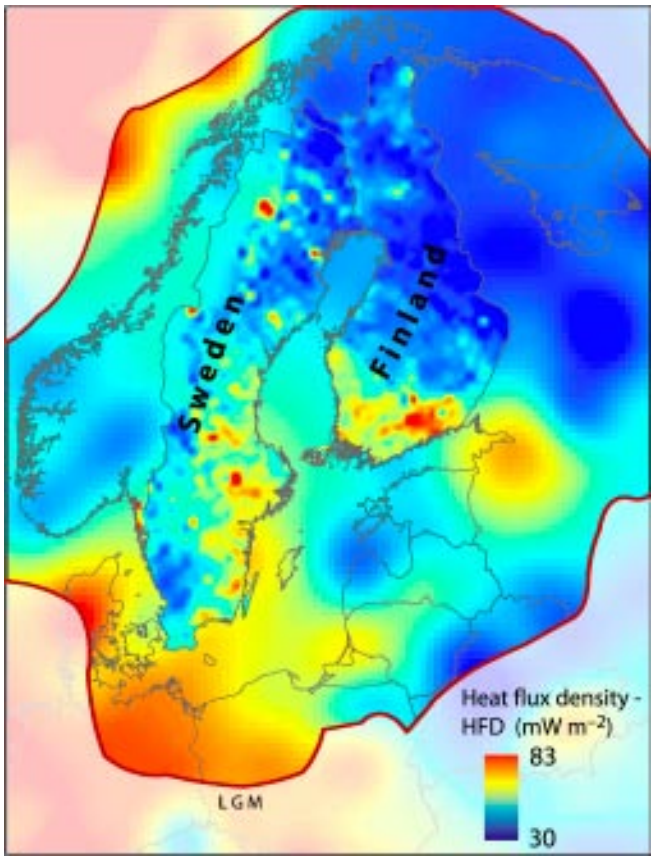

Figure 3-8. *Geothermal heat flow distribution over Fennoscandia. From /Näslund et al. 2005/.*

data set on geothermal heat flow, instead of a traditional uniform value of 42 mW/m^2, yields a factor of 1.4 larger total basal melt water production for the last glacial cycle /Näslund et al. 2005/. Furthermore, using the new data set in high-resolution modelling, results in increased spatial thermal gradients at the bed. This enhances and introduces new local and regional effects on basal ice temperatures and melt rates. The results show that regional to local variations in geothermal heat flow need to be considered for proper identification and treatment of thermal and hydraulic bed conditions under the Fennoscandian ice sheet /Näslund et al. 2005/.

Ice properties. The exponent n in Glen's flow law (Equation 3-5) is dependent on the active creep process. Numerous field experiments and laboratory tests of glacier ice suggest that n should be ~ 3. The typical creep process taken into account is a simple power-law creep, where the creep rate is proportional to the stress raised to some power greater than 1, for example:

Equation 3-7 $$\dot{\varepsilon} \propto \sigma^3$$

On the other hand, with certain temperature, stress, and grain size combinations, diffusional creep instead of power-law creep could take place in ice sheets /Duval et al. 1983/, which would lower the value of n to less than 3. Other recent studies suggest that n should be between 1 and 2 for deformation at low stresses, low temperatures, and low cumulative strains /Alley 1992, Montagnat and Duval 2000/. However, some of these conditions are likely to be important only down to depths of a few hundred metres in the coldest parts of ice sheets.

The viscosity constant B in Glen's flow law is dependent on a large number of parameters. Therefore, various modifications of Glen's flow law have been developed taking into account temperature, hydrostatic pressure, and even crystal orientation. The last case is the most difficult, and it is done by introducing an anisotropy enhancement factor. The c-axes of the ice crystals are, to a large degree, uniformly distributed in the upper part of the ice sheet, i.e. the ice is basically isotropic. When the ice over time is affected by the weight of the accumulating

overlying ice mass, it is vertically compressed and longitudinally stretched, which results in a conical distribution of c-axes orientations. Subsequently, when the ice is affected by the simple shear close to the ice sheet bed, the *c*-axes are typically re-oriented to a preferred single orientation. Development of *c*-axis fabrics has been obtained by re-crystallisation and ice grain rotation. Since we know from ice core studies that the crystal orientation in ice sheets is not isotropic at depth, a non-isotropic flow law of ice should improve, for example, ice sheet modelling. However, this re-crystallisation process in glacier ice is not yet understood well enough to define a well justified empirical non-isotropic flow law.

3.1.3 Observations in nature and present-day natural analogues

Palaeo-ice sheets. The mid-latitudes of the Northern hemisphere have experienced repeated continental scale glaciations during the Late Cenozoic. These periods are referred to as *glacial cycles* or *glaciations*. In north-western Europe, the last glaciation is named the Weichselian. The warm periods between the glacials are called *interglacials* and the present interglacial called the Holocene. Within a generally cool glacial period, there are shorter periods of both relatively warm and cool climates; these are called *interstadials* and *stadials* respectively.

Palaeo-ice sheets have left geological traces in previously glaciated terrain in Fennoscandia, North America and Siberia, as well as abundant glacio-marine traces in adjacent ocean basins. Studies of North Atlantic marine sediments have shown that the first traces of eroding glaciers in Greenland and Fennoscandia date back to between 12 and 6.6 Ma /Jansen and Sjøholm 1991, Fronval and Jansen 1996/, with larger ice sheets present in Fennoscandia from around 2.75 Ma. During the last ~ 700 ka, glaciation cycles have been about 100 ka long /cf EPICA community members 2004, Lisiecki and Raymo 2005/, preceded by a period of shorter (41 ka) glacial cycles /e.g. Raymo et al. 1998, McIntyre et al. 2001/, with presumably smaller ice sheets.

Geological information on till stratigraphy, interstadial deposits, glacial landforms in loose sediments and in bedrock have for a long time been used to try and reconstruct the Weichselian glacial history. A summary of that work is provided in /Lokrantz and Sohlenius 2006/. Various types of glacial landforms may also be used to infer information on basal thermal conditions of palaeo-ice sheets /e.g. Lagerbäck 1988, Kleman et al. 1997, Kleman and Hättestrand 1999/.

Present ice sheets. At present there are two ice sheets present on Earth, the Antarctic (14 Mkm^2) and Greenland (1.7 Mkm^2) ice sheets. Large portions of these quasi-stable ice sheets are more than 3 km thick. In both cases, the ice sheet load has depressed the bed so that large portions are situated below sea-level. Offshore marine sediments have shown traces of waxing and waning Antarctic ice sheets of continental proportions back to 40–36 Ma /Haq et al. 1987, Hambrey et al. 1992/, and Antarctic alpine glaciers may trace back to the Oligocene /Näslund 2001/. The present configuration of the Antarctic ice sheet is thought to have been relatively stable for the last 15–11 Ma /cf Shackleton and Kennett 1975, Marchant et al. 1993/.

The spatial patterns of basal thermal characteristics of the Antarctic and Greenland ice sheets are complex due to ice sheet dynamics, bed topography, and geothermal heat flux variability. For both ice sheets, parts of the bed are cold-based whereas other parts are warm-based, as seen from modelling studies (Figure 3-9) and confirmed by drill hole data. Ice sheet modelling has also, together with geological field observations and remote sensing studies, showed that ice streams are prominent features of the Antarctic ice sheet, penetrating far into the ice sheet interior (Figure 3-10). This has also been shown by remote sensing Interferometric Synthetic Aperture Radar (InSAR) studies /Joughin and Tulaczyk 2002/. The outer coastal-near parts of these ice streams are typically wet-based, whereas their upstream parts, high in the catchments areas, often are cold-based.

During the main Pleistocene glacial periods, the Greenland and Antarctic ice sheets had a larger extent than at present. The major limiting factor on their maximum lateral extent is the bed topography; the Antarctic and Greenland ice sheet margins are both today located close to the coast line. The continental crust does not extend out very far from the present day coast lines,

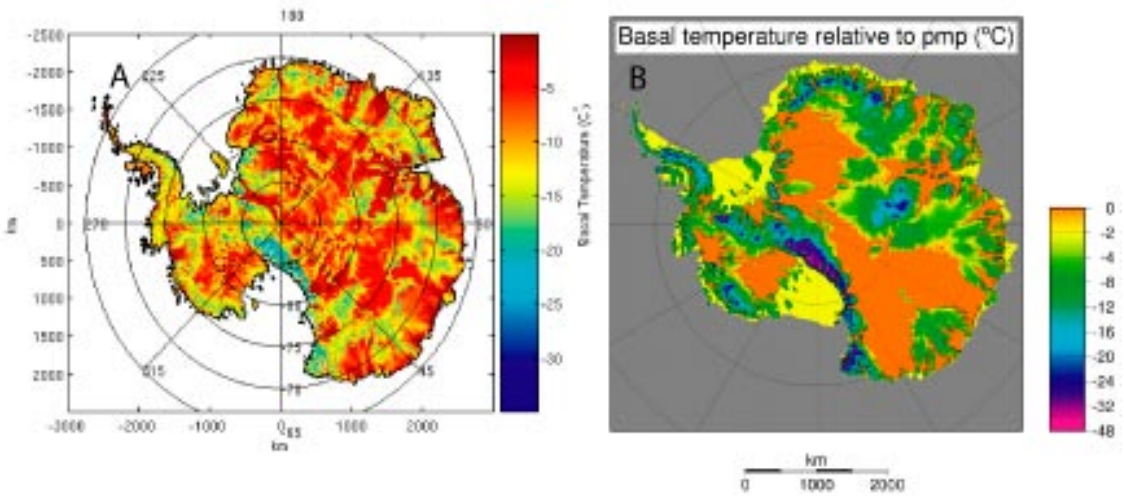

Figure 3-9. *Two examples of modelled present-day Antarctic ice sheet basal temperatures. Temperatures are expressed relative to the pressure melting point (pmp). Figure a) is from /Johnson 2004/ and b) from /Huybrechts 2006/.*

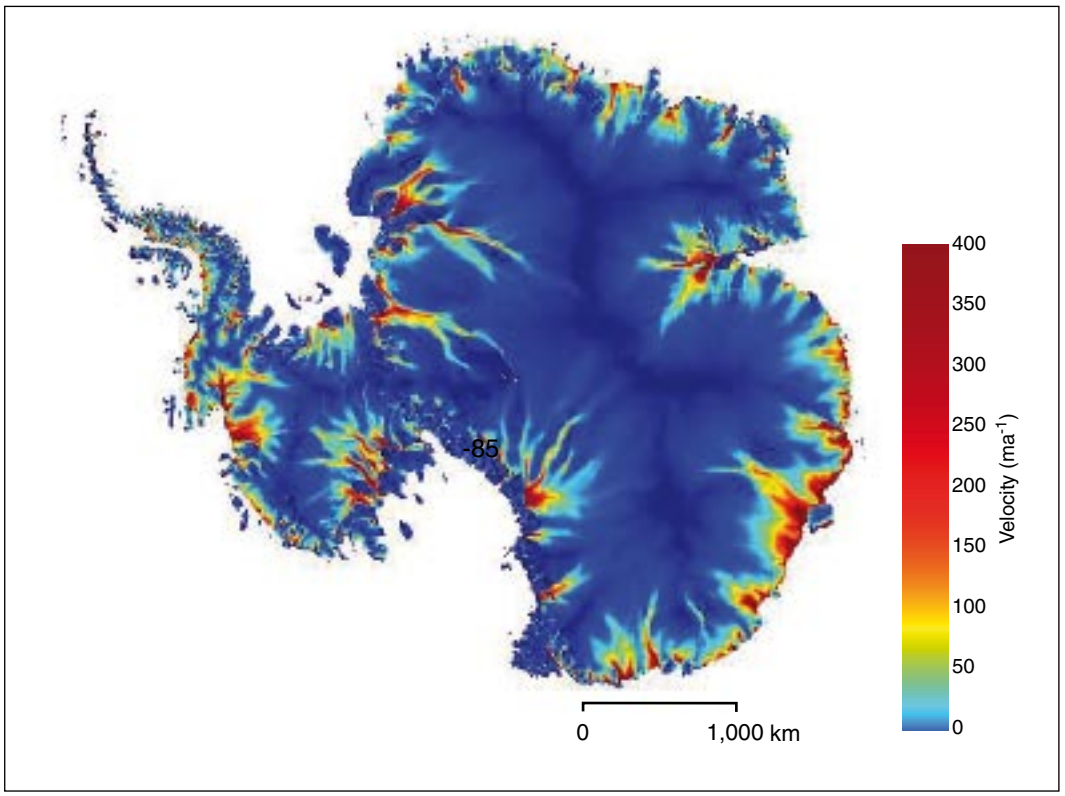

Figure 3-10. *Modelled Antarctic ice surface velocities. Fast-flowing ice streams (red/yellow/green colour) reach far into the ice sheet interior. From /Johnson 2004/ with numerical methods described in /Staiger et al. 2005/.*

and at the continental margin the water depth quickly becomes deeper. When the ice sheets grow larger the grounding-line migrates outward, resulting in a larger area for the grounded part of the ice sheet. The grounding line cannot advance past the continental margin due to the deeper water outside. The continental margin thus constitutes a definite constraint on the maximum size of Antarctic and Greenland ice sheets during Late Cenozoic ice sheet fluctuations. The situation

was similar for part of the Fennoscandian ice sheet. From a bed topography point of view there were no constraints for ice sheet growth from the Scandinavian mountain range towards east (the Baltic depression is not deep enough in this context), but towards the west Fennoscandian ice sheets, including the last Weichselian ice sheet, could not and did not extend farther towards west than the offshore continental margin /Svendsen and Mangerud 1987, Zweck and Huybrechts 2003/.

Although the sizes of the Antarctic and Greenland ice sheets were greater during the Late Pleistocene glacials, the maximum thicknesses need not have been larger. On the contrary, because of atmospheric moisture starvation during the colder climates, the interior parts of the ice sheets probably were thinner during the coldest parts of the glacial cycles /Huybrechts 1990, Näslund et al. 2000/. In contrast, at the ice sheet margins the ice sheet thickness varies considerably during a glacial cycle. Areas where the ice thickness is zero during a warm interglacial period (i.e. at the exact margin) may experience an increase in ice thickness of several hundred metres, up to one kilometre, during a glacial maximum ice configuration /Näslund et al. 2000/.

In turn, this means that the temporal changes in basal conditions of the ice sheets, for example changes in basal ice temperatures from the present interglacial pattern, were highly complex. For example, due to the changed ice configuration affecting ice sheet dynamics, some parts of the Antarctic ice sheet were warmer at the LGM ice configuration than at present, whereas at the same time, other parts were colder (Figure 3-11) /cf Näslund et al. 2000/.

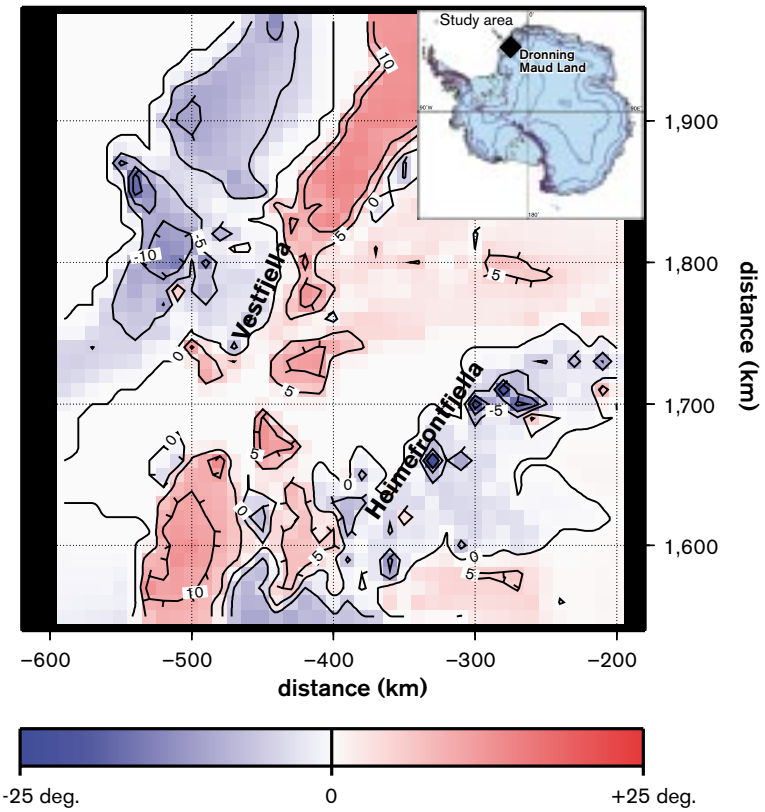

Figure 3-11. *Modelled difference in basal temperature between the present-day ice configuration and a maximum Pleistocene ice sheet configuration for part of the Antarctic ice sheet. For this single change in ice configuration, ice sheet thermodynamics induce complex changes in basal thermal pattern; some parts of the ice sheet become warmer at the bed the same time as other parts become colder. From /Näslund et al. 2000/.*

3.1.4 Model studies

Ice sheet modelling. Thermo-mechanical ice sheet modelling is a well established and useful tool for studying a large array of ice sheet-specific and ice sheet-related issues. It can be used to study characteristics and behaviour of present ice sheets, palaeo-ice sheets, and in some cases also inferred future ice sheets. As computer capacity has increased, more sophisticated models have been able to be run at higher spatial resolutions, which in turn has made it meaningful to compare detailed model output with various types of geological information, both for model verification and testing of glacial-geological hypotheses /Pattyn et al. 1989, Van Tatenhove and Huybrechts 1996, Näslund et al. 2003/.

Ice sheet models are deterministic, i.e. they always generate the same output given the same input and model forcing. Various ice sheet models are available. Two dimensional flow-band models are used to study properties along a glacier or ice sheet flow line, whereas three dimensional ice sheet models describe the entire ice body. Ice sheet models may be either static or dynamic. The first type can only simulate ice sheets in steady-state with the climate, i.e. with climate and ice sheet parameters not changing over time. The latter type can simulate the time transient behaviour of more realistic ice sheets that are not in balance with the prevailing climate.

An ice sheet is a very well defined natural system suitable for numerical modelling. The simulations of the Weichselian ice sheet for the present project used the University of Maine Ice Sheet Model (UMISM) /Fastook and Chapman 1989, Fastook 1990, 1994, Fastook and Prentice 1994, Johnson 1994/. Most of the results were obtained by a version of UMISM as of October 2004. The UMISM was part of the EISMINT model intercomparison experiment and yielded output in agreement with many other ice sheet models /Huybrechts et al. 1996, Payne et al. 2000/. The UMISM has been previously been used for various simulations of Fennoscandian ice sheets /Fastook and Holmlund 1994, Holmlund and Fastook 1995, Näslund et al. 2003/.

The ice sheet system constitutes three main sub-systems, mass-balance, ice movement, and ice temperature. For these three sub-systems the ice sheet model solves differential equations describing conservation of mass, momentum, and energy respectively. In addition the ice sheet model needs to contain a description of climate. A mass balance parameterisation for the spatial pattern of air temperature and precipitation is used. The UMISM model includes a mathematical description of precipitation based on a number of other parameters; distance from the pole, saturation vapour pressure (function of altitude and laps-rate), and surface slope. This is an empirical relationship developed from the Antarctic ice sheet /Fastook and Prentice 1994/. Over a certain model domain, with a topography described by a Digital Elevation Model (DEM), this climate description gives a spatial pattern of air temperatures at ground level and a pattern of precipitation.

The UMISM ice sheet model also includes a simplified isostatic description for the behaviour of deforming bedrock due to the weight of the modelled ice sheet configuration. This is not a full self-gravitational spherical Earth model as used in the GIA modelling in Section 3.3. Instead, it is a hydrostatically supported elastic plate model, adequate for the purpose of placing the ice sheet surface at an appropriate altitude, and hence at an appropriate air temperature, for the mass balance calculations. Furthermore the UMISM also includes a subglacial hydrology model /Johnson 1994/ which is able to transport basal meltwater under the ice sheet according to prevailing pressure potentials governed by ice sheet thickness and basal topography.

A palaeo-temperature record is employed to run the ice sheet model (Figure 3-12). For simulations of the Weichselian ice sheet the temperature proxy record for the last 120 ka from the Greenland GRIP ice core has been used /Dansgaard et al. 1993/. The isotopic record is the one used for the temperature calculations in /Johnsen et al. 1995/. The temperature file used contained 50 year averages of the original series.

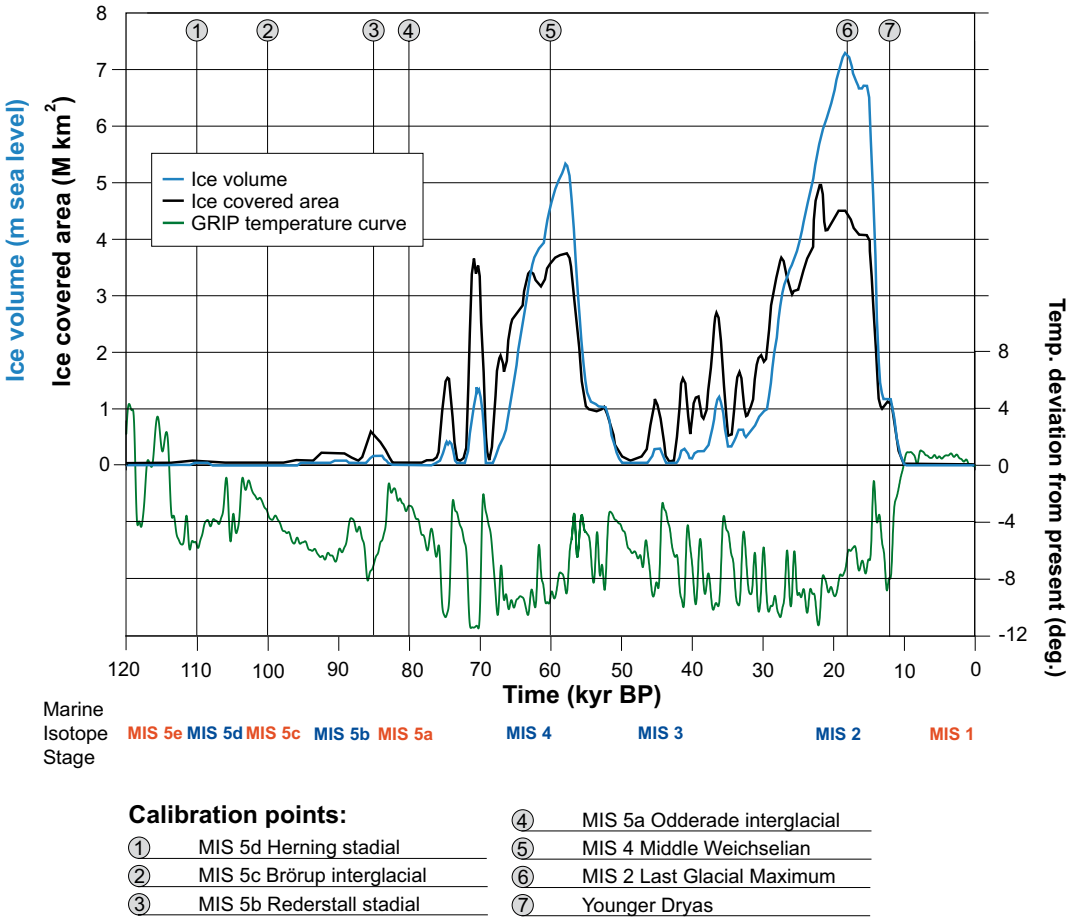

Figure 3-12. *GRIP proxy temperature curve and reconstructed ice covered area and ice volume for the Weichselian reference model run. Times of model calibration are shown, as well as Marine Isotope Stages (warm stages in red and cold stages in blue).*

In the modelling process, the climate curve is used to shift the climate pattern over the model domain (both temperatures and precipitation), according to the variations in the temperature proxy curve. This initiates ice sheet growth in Fennoscandia for the last glacial cycle. Once glaciers/ice sheets are formed, the internal thermodynamic processes of the ice masses become significant and the modelled dynamic ice sheet system starts to evolve over time, with that evolution taking account of the thermodynamic feed-back mechanisms described above. In this way, the ice sheet model simulates the behaviour of the ice sheet as it responds to the external forcing such as changing climate or sea level, as well as internal dynamics, such as ice stream variations caused by internal temperature oscillations at the bed.

The following are input parameters to the ice sheet model in the simulations of the Weichselian ice sheet:

1. The thermodynamic properties of the ice, including flow laws, sliding laws, feedback mechanisms etc.
2. Upper boundary conditions:
   Climate description (annual air temperature, and precipitation rates) from the mass balance parameterisation.
3. Lower boundary conditions:
   A. A DEM over Fennoscandia with a certain spatial resolution. For the reference glacial cycle simulation a grid size of 50 km was used. DEM data were taken from the ETOPO2 data base /ETOPO2 2001/, depicting both continental topography and bathymetry;
   B. Geothermal heat flux at the bed.

4. Sea-level changes during the last 120 ka.
5. Proxy curve of palaeo-air temperatures during the past 120 ka (GRIP data).

The modelling starts at 120,000 years before present, and the model is run at a 2–10 year time step forward in time up to time zero (present). The size of the time step depends on the size of model domain and grid resolution. For each time step, output data are calculated for each grid cell and grid node, for example:

1. Ice thickness.
2. Englacial and basal ice temperatures.
3. Ice velocity.
4. Direction of ice movement.
5. Isostatic depression of crust.
6. Amount of basal melting or freeze-on of water.

Model setup and geothermal heat flow boundary condition. A model domain was selected to cover the maximum extent of the Weichselian ice sheet over Fennoscandia, with a spatial DEM resolution of 50 km. The thermomechanical coupling between ice movement and ice temperature was enabled, as well as a function by which the amount of basal sliding is coupled to the amount of basal meltwater present at the ice sheet bed. No horizontal flow of basal meltwater was allowed at the ice sheet bed. The parameters in Glen's flow law were set to standard values. In the final model run, the model was run with a 5 year time step and data was saved from the model simulation at a 100 year interval.

The traditional way of specifying the basal thermal boundary condition in ice sheet modelling has been to apply a single, uniform value of geothermal heat flow for the entire model domain. The magnitude of this geothermal heat flow value has often been set according to the general geological setting for the area to be studied. Thermodynamic modelling of Fennoscandian ice sheets has, for instance, used a single geothermal heat flow value typical for the Pre-Cambrian shield, the most common reported value being 42 mW/m^2 /e.g. Boulton and Payne 1992, Huybrechts and T'siobbel 1995, Payne and Baldwin 1999/. Others have used higher values, around 50–55 mW/m^2 /e.g. Hindmarsh et al. 1989, Forsström et al. 2003/. However, in several published ice sheet modelling studies of the Fennoscandian and other ice sheets the values on geothermal flow used is not mentioned at all.

For the reference glacial cycle simulation, see below, we used the new geothermal data set of /Näslund et al. 2005/ as the basal boundary condition. For additional tests of using the new realistic high-resolution geothermal heat flux data set in ice sheet modelling, we also used another three-dimensional thermomechanically coupled ice sheet model which, in contrast to most other ice sheet models including UMISM, includes higher-order stress gradients. This is important for reproducing realistic ice flow characteristics close to ice sheet margins and centres /Pattyn 2003/. We used this higher-order model for specific studies of ice flow behaviour in relation to geothermal heat-flow anomalies in Sweden /Näslund et al. 2005/.

Model calibration and reference glacial cycle simulation. In cases when ice sheet modelling aims at simulating realistic palaeo-ice sheets, one need to calibrate the behaviour of the model against known information on ice sheet extents. The reason for this is that we have far from perfect knowledge on a number of the processes and boundary conditions involved, for example on surface climate back in time, or ice sheet basal processes. In the simulation of the Weichselian ice sheet for the reference glacial cycle, the UMISM model was calibrated by making adjustments of the proxy climate curve. The proxy temperature curve was slightly shifted and stretched (Figure 3-13) to obtain as good a fit as possible against dated ice-marginal positions during Weichselian stadials /Lokrantz and Sohlenius 2006/.

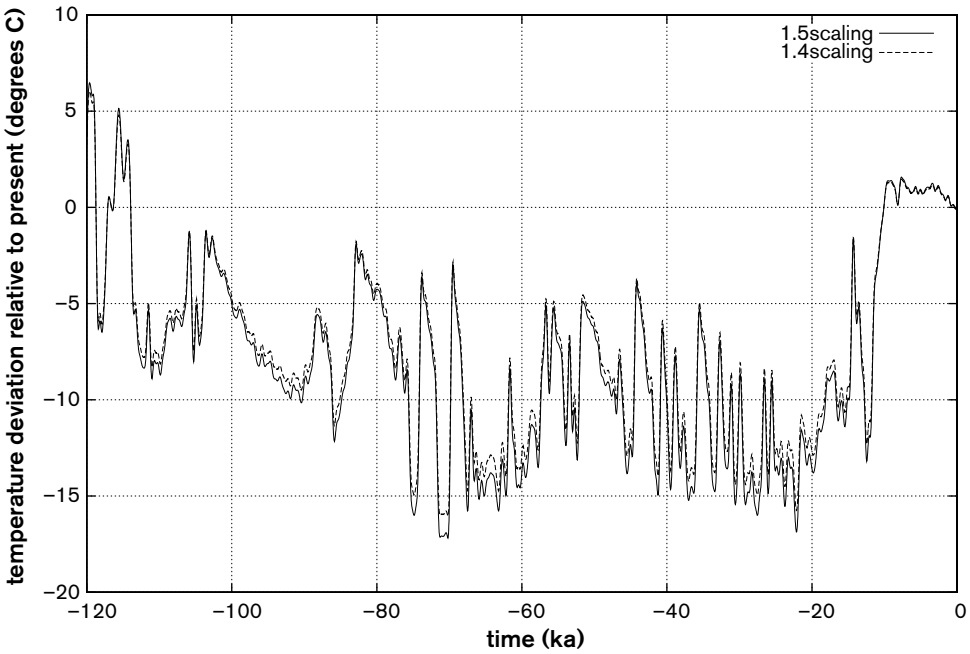

Figure 3-13. *Example of two stretched proxy temperature curves from the calibration process of the UMISM ice sheet mode. This final calibrated curve that was used had a larger amplitude that the original data, i.e. cold periods were even colder in the calibrated curve. The entire curve is always changed in the same way.*

As mentioned above, the forcing in temperature for the ice sheet model is based on the GRIP ice core /Dansgaard et al. 1993/. The isostopic record is the one used for the temperature calculations in /Johnsen et al. 1995/. The temperature file that was used contains 50 year averages of original series. One important thing here is that the approach is to use the climate curve for calibration of the model. The temperature signal is slightly shifted and amplified so as to obtain a calibrated ice sheet model run that fits as well as possible with geological observations on dated marginal positions, for example the LGM and Younger Dryas margins. A very large number of such simulations of the Fennoscandian ice sheet have been dome with the UMISM model using this climate curve over the years, which have given extensive experience of how to perform the model calibration.

One interesting observation in this context is the results from the recent NorthGRIP ice core from Greenland. There is not yet a published proxy temperature curve from the NorthGRIP core, only oxygen isotope values /Andersen et al. 2004/. However, there are some interesting differences between the GRIP and NorthGRIP oxygen isotope values. Both cores are considered to have reliable data (no folding of ice etc) for the period from about 105,000 years ago. In the case of NorthGRIP, reliable data are considered to exist also for a longer period. Comparing the information in the two cores shows that warm periods have basically the same oxygen isotope values during the last glacial cycle, whereas cold periods have significantly lower values in the NorthGRIP core /Andersen et al. 2004/. Thus, the signal in the two cores is not the same although they are located not very far from each other. One reason put forward for the difference is that the two sites had differing moisture sources during the last glacial cycle.

If the same transfer function between oxygen isotope values and temperature is used as for the GRIP core /Dansgaard et al. 1993/, the lower oxygen isotope values in the NorthGRIP core translate into several degrees lower temperatures during cold periods. When calibrating the ice sheet model by modifying the GRIP temperature curve, the result is similar to such a translation to NorthGRIP temperatures. The best modelled ice sheet configurations are obtained by making the amplitude of the GRIP temperature variations larger, i.e. the resulting calibrated temperature

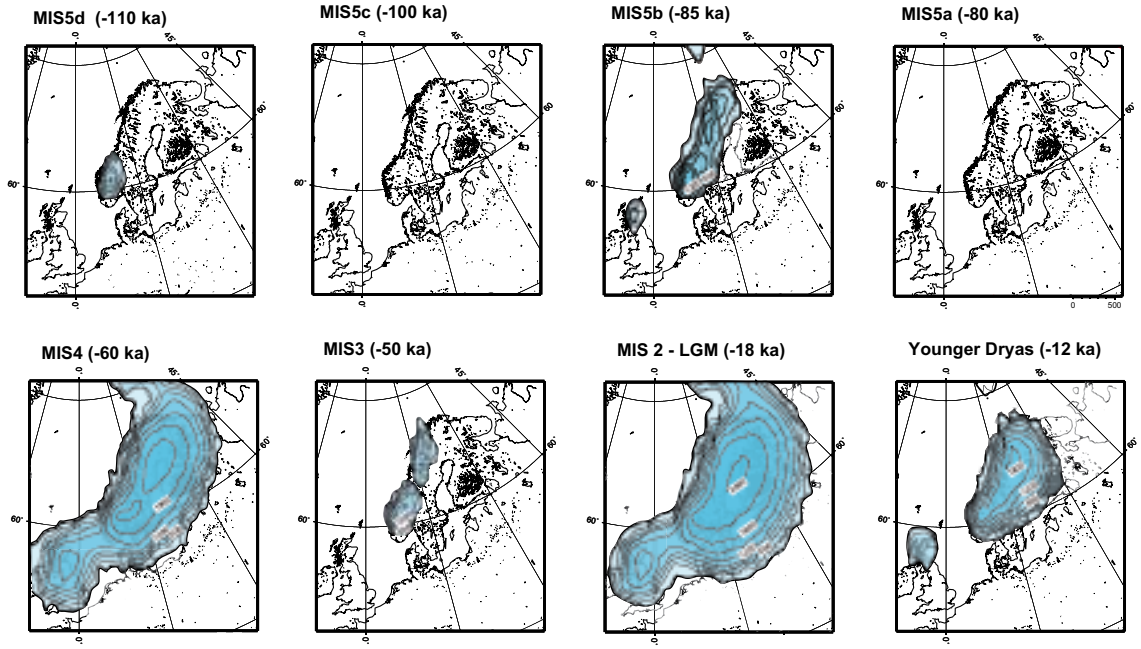

Figure 3-14. *Selected maps of ice thickness during the Weichselian in the reference glacial cycle simulation. The ice sheet grows to its full LGM configuration in progressive phases of increasing maximum extent, with intervening periods of more restricted ice coverage.*

curve has larger amplitude, with colder cold periods than the original, non-calibrated GRIP data set. The calibrated GRIP temp curve of the present project is more similar to the NorthGRIP curve, with temperatures calculated as in /Dansgaard et al. 1993/, than the original GRIP curve. Thus, the NorthGRIP record may be better correlated to Scandinavian conditions than the GRIP record. The similarity between the calibrated GRIP temperature curve and the NorthGRIP curve gives confidence in the way the ice sheet model is calibrated.

The resulting calibrated evolution of the Weichselian ice sheet is seen in Figures 3-12 and 3-14. Ice extends over the model domain during the cold stadials during Marine Isotope Stages (MIS) 5d, 5b, 4, and 2. During warmer interstadials the ice cover is in general more restricted. There is a clear trend of more and more pronounced ice coverage during the stadials through the glacial cycle, with the LGM peak around 18 ka BP.

Different types of output data have been extracted and post-processed from the reference glacial cycle simulation for various purposes, for example 1) basal and surface melt rates for groundwater modelling /Jaquet and Siegel 2006/, 2) Basal and subaerial temperatures for permafrost modelling (Section 3.4), and 3) ice thickness variations for modelling of global isostatic adjustment (Section 3.3) and crustal stresses (Section 3.5).

The UMISM model also has a high-resolution modelling option. The first step is typically to model the entire ice sheet at low resolution, typically 100–50 km resolution as in Figure 3-14. Then, a user defined sub-area is selected for embedded, high-resolution modelling. DEM data with a higher resolution are then used. For the smaller area, the model is then run again for the same period and with the same time step. In the new run, lateral boundary conditions for the smaller area are taken from the initial coarser model run.

The reference glacial cycle simulation was first made for the entire Weichselian area at a 50 km resolution, using the DEM /ETOPO2 2001/ as input. Subsequently various sub-areas have been run at higher resolution (typically 10 km) for different purposes. Examples of results from a 2.5 km resolution model run are seen in Figure 3-15.

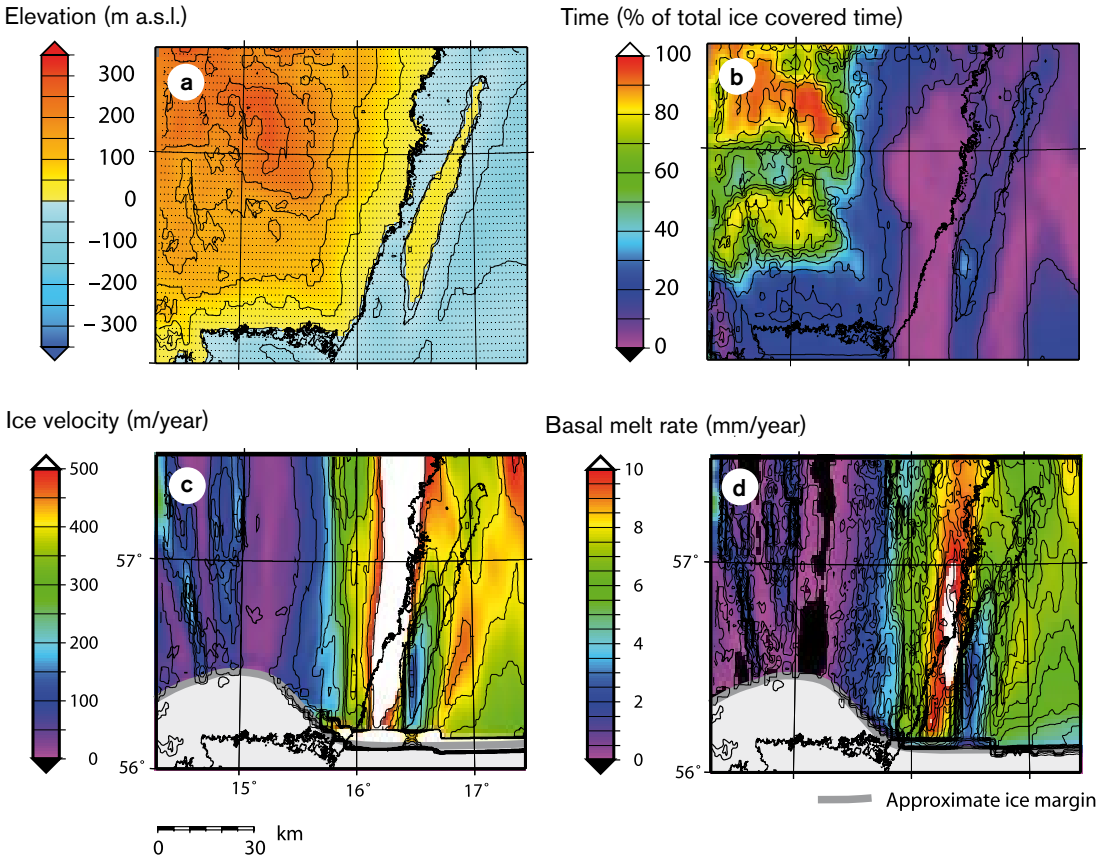

Figure 3-15. *Ice velocities and basal characteristics of the ice sheet in south-eastern Sweden from high-resolution ice sheet modelling. a) Bed elevation, b) time covered by cold-based ice (% of total ice covered time), c) ice surface velocity (m/year), and d) basal melt rate (mm/year). Figure c) and d) show the situation during a dynamic phase of the deglaciation, around 14,300 years before present. An ice free area (grey) is located south of the ice sheet (various colours, incl. black and white). The east-west trending ice margin is denoted with a bold grey line. From /Näslund et al. 2005/.*

3.1.5 Time perspective

It is generally agreed that ice sheets take longer to grow than to decay. However, our knowledge of the deglaciation phase is much better than of the inception phase, reflecting the fact that there are more geological traces from the last deglaciation than for early stages. On glaciers and ice sheets ablation rates are generally 3–4 times higher than accumulation rates, which suggests that the time for decay should be one-third to one quarter of the growth time /Paterson 1994/. In reality, it is often even faster, to a large extent due to efficient ice shelf calving processes for marine parts of ice sheets, for example calving of the Fennoscandian ice sheet in the Gulf of Bothnia. In line with the present modelling results of the Weichselian ice sheet (Figures 3-12 and 3-14) it is generally concluded that ice sheets may build up in a series of glacial build-up periods, peaking in a glacial maximum close to the end of the glacial cycle. Subsequent rapid deglaciation is recorded in rising global sea-levels /e.g. Fairbanks 1989/. The Fennoscandian ice sheet seems to exhibited such dynamic behaviour during the last glacial cycle. This has also been inferred from studies of so called Heinrich events /cf Heinrich 1988/ recorded in North Atlantic marine sediments, suggesting that even large ice sheet systems are dynamic features, responding relatively quickly to rapid changes in climatic forcing.

During the last 700 ka, glacial cycles have typically had a duration of about one hundred thousand years, with interglacials lasting around ten to twenty thousand years /Raymo et al. 1998, McIntyre et al. 2001/. As noted above, the last glacial cycle of the Fennoscandian ice sheet was also characterised by a number of cold growth phases and intervening warmer periods

with less ice, although from the geological record we still do not know how to date or correlate all observed interstadial localities /Lokrantz and Sohlenius 2006/. A typical cold Weichselian stadial seems to have had a duration of 10–30 ka, with the longer periods towards the end of the glacial cycle. The deglaciation of the Weichselian ice sheet from the LGM ice margin to the last ice remnants in the Scandinavian mountain range took about 8,000 years, including a number of temporal halts in the retreat, the most pronounced one occurring during the Younger Dryas (about 13–11.5 ka).

3.1.6 Handling in the safety assessment SR-Can

The evolution of ice sheets is investigated by means of numerical modelling. The base variant of the main scenario in SR-Can is based on a reference ice sheet model reconstruction of the Weichselian glaciation. The thermo-dynamic ice sheet model used is capable of simulating realistic ice sheets which are typically not in balance with the climate. Derived ice temperatures, together with density variations with depth, control ice viscosity and ice flow. The thermo-dynamic calculation accounts for vertical diffusion, vertical advection and heating caused by internal shear. The climate input, forcing ice sheet evolution, is the mean annual air temperature at sea level, and its variation over time. The mass balance is determined from an empirical relationship based on a simple parameterisation of the ice sheet's effect on local climate /Fastook and Prentice 1994/. Distributed temperatures over the model domain are determined from height above sea level and distance from the pole.

The model simulation of the Weichselian ice sheet over Fennoscandia was controlled by the temperature curve from the GRIP ice core, obtained from central Greenland /e.g. Dansgaard et al. 1993/, a typical method used in ice sheet modelling of the Weichselian glacial cycle. The geothermal heat flow and its spatial variation has been shown to be of importance for obtaining realistic modelled basal ice temperatures and basal melt rates /Waddington 1987, Näslund et al. 2005/. Basal temperatures and basal water conditions are in turn important for the overall ice flow and ice dynamics. A detailed dataset of geothermal heat flux values, based on national measurements of gamma emissions in Sweden and Finland has been compiled /Näslund et al. 2005/, and for the first time ever has been used as input to an ice sheet model. This eliminates previous large uncertainties in geothermal heat flow, and associated uncertainties in modelled basal conditions of the ice sheet.

The ice sheet model was calibrated so that modelled ice sheet configurations were in good agreement with dated geological information on ice marginal positions. For this purpose, geological information on the Weichselian glaciation history of Scandinavia have been compiled by /Lokrantz and Sohlenius 2006/. For further, detailed information on the ice sheet modelling, see the preceding parts of Section 3.1.

3.1.7 Handling of uncertainties in SR-Can

Uncertainties in mechanistic understanding

Model simplification uncertainty. The most important simplifications made in the ice sheet modelling in the reference glacial cycle simulation are the following.

The temperature proxy climate curve driving the model is the GRIP Greenland temperature curve. First of all this curve describes the climatic conditions at Greenland, but in the absence of similar palaeoclimate data from Fennoscandia, or other closer areas, these are the best data available. With the applied modelling approach, the Greenland proxy data generate Fennoscandian ice sheets that are in fair agreement with geological information on LGM and Younger Dryas ice margin positions, even *without* model calibration, which is a justification that this approach is valid. There are also uncertainties introduced by the conversion from oxygen isotopes values in the ice core to Greenland palaeo-air temperatures /Johnsen et al. 1995/. The temperature proxy climate curve is probably the biggest assumption made in the modelling experiments, and therefore this parameter has been selected for adjustment in model calibration.

In the model, the amount of basal sliding is coupled to the thickness of the basal water layer of the ice sheet. This is a simplification, but still a reasonable way of handling the difficult topic of prescribing basal sliding in a good way. One thing that is excluded in the model is the possible presence of subglacial deformable sediments, for example in the Baltic depression, which may enhance ice velocities, especially in ice streams. The exclusion of the effects of such sediments could, in some cases, lead to some overestimation of ice thickness.

In the UMISM model, as in most other ice sheet models, the so-called shallow ice approximation is used. This means that the horizontal velocity is only dependant on the local driving stress. Horizontal and longitudinal englacial stresses are neglect, i.e. there are no push and pull effects within the ice sheet, as in nature. This is an appropriate assumption for the major part of the ice sheet, with the possible exception of frontal near parts and ice divides. However, the model has not been used in such a way that this has been a shortcoming. However, for detailed studies of ice stream features associated with warm geothermal anomalies, a higher-order model, including a full treatment of the stress fields /Pattyn 2003/ has been used.

In the UMISM model, horizontal advection of heat is not included in the thermodynamic treatment of the ice. The result is that the model may overestimate basal ice temperatures to some extent. This is likely to be of importance only in fast-flowing situations like ice streams. The model used for detailed ice stream studies /Pattyn 2003/ includes horizontal advection of heat.

The hydrostatically supported elastic plate model included in the UMISM model is a simplification, but sufficient for adjusting bed- and ice sheet surface elevations to obtain a reasonable good surface mass balance.

The UMISM model does not include an ice shelf model. Instead, ice shelves are simulated by adjusting a marine calving rate directly at the dynamic grounding line.

The spatial resolution of model domain is approximately 50×50 km. This resolution may, in some cases, be too coarse to correctly depict smaller features in for example geothermal heat flow pattern.

Input data and data uncertainty

The temperature proxy climate curve. See section on Model simplification and uncertainty above, and Section 3.1.4.

Digital elevation data. The accuracy of the DEM /ETOPO2 2001/ is good enough for the 50×50 km and 10×10 km resolution ice sheet model simulations made.

Geothermal heat flux. The new high-resolution data set on spatially varying geothermal heat flux is of high quality in the context of ice sheet modelling. In the new data set, high resolution geothermal data are available only for Sweden and Finland, not for the entire area covered by the Weichselian ice sheet. However, this does not affect modelled basal conditions in Sweden, since basically all parts of Sweden are located *down-stream* from areas with high-resolution data. There are assumptions made in the calculation of the data set that could be refined improve the data set in the future, for example using a varying lithospheric thickness in the calculation of surface heat flow. Also, denser data on γ-emission measurements from bedrock are available for parts of Sweden, which may be used for future versions of the data set. All in all, this new type of ice sheet model input has improved ice sheet modelling significantly from all previous reconstructions of palaeo-ice sheets by numerical modelling.

Sea-level. The sea-level curve used as input is derived from numerical ice sheet modelling of all Northern Hemisphere ice sheets. The present volume of the Antarctic ice sheet was held constant. The maximum lowering of sea-level in this data set is 100 m, somewhat less than the ~ 120–135 m of global sea-level lowering at LGM deduced from coral-reef data /Yokohama et al. 2000/. However, this is of minor importance since the position of the grounding-line in the

western Atlantic part of the ice sheet is determined by the bed topography (i.e. continental shelf location), and the eastern part is advancing and retreating over the Baltic Sea which do not have contact with the Atlantic during such low global sea levels.

3.2 Ice sheet hydrology

This part of the report summarises the knowledge on water flow in and beneath glaciers and ice sheets. Many concepts in hydrology and hydraulics are applicable to water flow in glaciers. However, the unique situation of having the liquid phase flowing in conduits of the solid phase of the same material is not encountered elsewhere. This situation means that the heat exchange between the phases and the resulting phase changes also have to be accounted for in the analysis. The fact that the solidus in the pressure-temperature dependent phase diagram of water has a negative slope provides further complications. It means that ice can melt or freeze from both temperature and pressure variations.

3.2.1 Overview/general description

The hydrology of glaciers has been reviewed by several authors /Weertman 1972, Lang 1987, Röthlisberger and Lang 1987, Hooke 1989, Hubbard and Nienow 1997, Fountain and Walder 1998, Schneider 2000, Boulton et al. 2001, Jansson et al. 2003, Hock and Jansson 2005, Hock et al. 2005/. However, most reviews concern specific topics and do not provide an overview also no reviews exist in which the current state of knowledge is viewed in the context of ice sheets. The traditional view of the glacier hydrological system is similar to a combination of a groundwater system and a limestone karst system of shafts and tunnels, and consists of supra-, en- and sub-glacial system components. Figure 3-16 shows the situation on a typical glacier in summer.

The surface can be divided into two parts, a lower part where the surface consists of solid ice, referred to as the ablation area since a net loss of mass occurs in this area, and where water will run off by mostly channelised surface flow and an upper part, referred to as the accumulation area because a net mass gain occurs, where the surface consists of permeable snow or firn, snow that has survived one year of melting. The snow and firn pack is porous and allows water to percolate into the glacier and accumulate at depth as firn water bodies, equivalent to groundwater bodies whereas ice effectively is impermeable.

On an ice sheet, the snow-covered area can be further subdivided into zones depending on their thermal conditions, see Figure 3-16. At the centre of ice sheets, an example of which is modern Greenland, the snow pack is cold and no surface melting occurs during any part of the year. This is the *cold snow zone*. At some point at lower elevation, surface melting can occur because of warmer conditions caused by the atmospheric temperature lapse rate. Hence there is a zone where percolation occurs increasingly wetting the upper part of the snow pack at lower altitude since the potential for melt increases at lower altitude. This zone is called the *percolation zone*. At some elevation the melting is strong enough to completely warm the snow pack. The zone of completely temperate snow is called the *wet snow zone*. These zones describe the conditions met during parts of the season. During winter most of the ice sheet will be covered by dry snow and development of the different zones initiate as air temperature rises during spring and summer. This also means that the different zones start to develop at lower altitude and move upglacier as the season progresses to reach their uppermost position at the end of the melt season or when the annual temperature cycle has reached maximum temperature. This also indicates that the surface flow system will develop throughout the entire melt season with accompanying effects on runoff and water input to an en- and subglacial drainage system.

Water is also generated at the base of ice sheets where the basal temperature is at the pressure melting point. The amount of energy available for melting is given by the geothermal heat flux and the deformational energy, so called *strain-heating*, in the ice produced by ice flow.

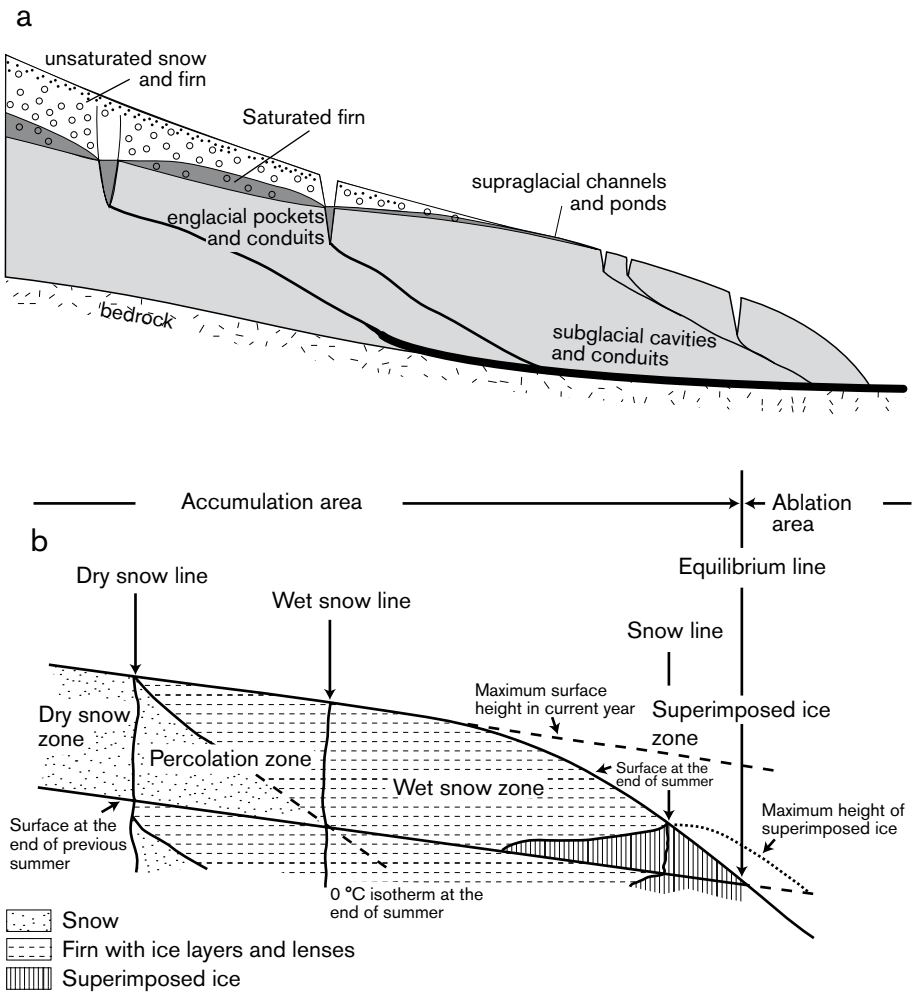

Figure 3-16. *a) The hydrological system of a glacier consist of supra-, en- and subglacial subsystems and interacts with the substrate hydrological systems. After /Röthlisberger and Lang 1987/. b) The glacier surface can be divided into different facies starting with the cold snow zone through the percolation zone to the wet snow zone. After /Benson 1961, Müller 1962/ and /Paterson 1994/.*

The geothermal heat flux varies spatially according to the geologic structure of the Earth's crust /Näslund et al. 2005/ but does not vary significantly in time over the time periods under consideration for a geologic repository for spent nuclear fuel. The energy available from strain heating varies both spatially and temporally with the waxing and waning of the ice sheet as well as with the induction and demise of faster flow features in the ice sheet. There is, therefore, a strong feedback between ice deformation, heat production, and water production available for enhanced sliding beneath temperate-based parts of an ice sheet. The cold-temperate boundary is also affected by the strain heating, which may enlarge the areas subjected to basal melting. Typical basal melt rates may vary from a few to up to 10 mm/year, although even higher melt rates can probably occur under special circumstances where ice flow is very rapid or geothermal heat fluxes are abnormally high /e.g. Hooke 2004, p 34/. Such circumstances do not, however, occur on an ice sheet-wide scale.

Water generated at the surface from melt and liquid precipitation can enter the en- and subglacial system through crevasses and vertical shafts, *moulins*. If the ice is temperate, it may also be slightly permeable. Water that enters the glacier will flow through an englacial system for some time. Commonly water reaches the bed within a couple of ice thicknesses in distance but englacial drainage can occur over longer distances. Most often this is associated with over-deepened basins.

The area over which surface water can penetrate the ice sheet and reach the bed is not well known. Remote sensing of *e.g*. the Greenland ice sheet indicates that surface melting occurs up to very high altitudes but also that the melting zone varies substantially from year to year (O. Humlum, personal communication 2005). Such conditions were surely present on the Weichselian ice sheet, especially during its retreat phase. Hence, water is in ample supply. Mechanisms whereby connections from the surface to the bed may be established through ice below the pressure melting point have been debated. However, /Alley et al. 2005b/ have shown theoretically that water-filled crevasses may penetrate even cold ice and thus constitute a mechanism for establishing hydraulic connection between surface and bed, even on a thick largely cold ice sheet. Although no observations have been made of such crevasse-based linkages, observations of surface drainage patterns on the Greenland ice sheet indicate the presence of an intricate pattern of surface drainage and moulins connecting to the base even tens of kilometres from the terminus. The width of the zone in which water may reach the bed remains elusive but is likely to range between tens and several ten kilometres. It is likely that the zones on the waning Weichselian ice sheet were at least similar in extent. Since the waning ice sheet probably exhibited surface profiles lower in elevation than, say, the modern quasi-steady state Greenland ice sheet, ablation zones were likely larger simply because larger areas of the Weichselian ice sheet were at lower elevation.

Once water enters the bed it can be transported in either fast or slow flow systems. The fast systems are able to transmit large quantities of water at low pressure. They can be thought of as tunnel systems. The slow systems transmit smaller quantities of water while maintaining higher pressure and holding larger volumes of water. One example of such a system is the so-called linked cavity system /Kamb 1987/. The fast systems are self-organising and tend to occur at a spacing that is determined by flow volumes, although the mechanisms are not completely understood. The slow systems are dependent on smaller-scale (O(m)) roughness features.

Because of the seasonal variations in water input from the surface (basal contributions do not vary on a seasonal basis), the en- and subglacial drainage pathways transmitting such water also experience seasonal variations. Conduits in ice adapt to transient hydraulic conditions by creep closure if water pressure is lower than hydrostatic ice pressure in the ice surrounding the conduit. If water fluxes increase, pressure builds to force more water through the conduits. This causes an increase in the viscous dissipation of heat and results in melting of the conduit walls and hence an increase in flow capacity of the system. The enlargement by melting may be faster than the creep closure depending on the transient hydraulic conditions. Hence, glacier conduit systems respond quickly to increases in water fluxes by enlarging the conduits. When water fluxes decrease, pressures in the system may drop drastically until creep closure has equilibrated to the water flux to maintain a balance between closure and conduit wall melting.

Seasonal, as well as shorter term, variations in water influx will affect the basal water pressures, although it is unlikely that diurnal variations in water pressure will significantly affect the pressure variations in an underlying groundwater aquifer because of their high frequency and the need for diffusion of such variations in a porous medium.

The ice sheet hydrology described above may affect a number of geosphere variables of importance for a deep geological repository (Table 3-2).

Groundwater composition is indirectly influenced by ice sheet hydrology since it is the hydrological conditions at the ice/bed interface that control the recharge of glacial melt water into the bed which in turn will affect the composition of the groundwater.

A review of glacial hydrology, within an ice sheet context, is given in /Jansson et al. 2006/.

Table 3-2. Summary of how geosphere variables are influenced by ice sheet hydrology.

Geosphere variable	Influenced by climate issue variable/s	Summary of influence
Groundwater flow	Configuration of sub-glacial system	Groundwater recharge and flow will be determined by the temperature regime, melt water production and thickness of the ice sheet (see Section 3.1). It is the configuration of the basal hydrological system that ultimately determines the distribution of melt water and thus groundwater recharge and distribution of water pressures at the ice/bed interface determining the gradients for groundwater flow.
Groundwater pressure	Configuration of sub-glacial system Melt water supply	The groundwater pressure depends on the pressure of the water at the ice/bed interface, the ice sheet thickness and the ice load compressing the subsurface (see Section 3.1). The pressure of the water at the ice bed interface is determined by the supply of melt water and the conductivity and distribution of conductive features in the sub-glacial system.

3.2.2 Controlling conditions and factors

Climate – melt water supply

The coupling between the climate system and the hydrological system of glaciers and ice sheets is through the energy exchange between the atmosphere and the glacier surface. Energy arriving at the surface will be expended by first warming the surface to the melting point (if below melting to start with) and second to melt snow and ice at the surface. The energy balance at the glacier surface is given by

Equation 3-8 $$M + \Delta G = R + H - L_v E + L_f P'$$

/e.g. Paterson 1994; all terms are in W m^{-2}/ where M is the heat used to melt snow and ice; this term represents a gain in heat and is negative if melt water refreezes in the snow pack; ΔG is the rate of gain of heat in a vertical column from the surface to the depth at which vertical heat transfer is negligible; H is the rate of heat transfer from the air to the surface by turbulence (H is negative if the air is cooler than the surface); L_v is the specific latent heat of vaporisation (2.8×10^6 J kg^{-1}); E is the rate of evaporation from the surface (E is negative if condensation occurs); L_f is the specific latent heat of fusion for ice (3.34×10^5 J kg^{-1}); and P' is the precipitation rate of rain (negligible if the surface is melting but significant for warming up the snow pack from refreezing under cold conditions). R is the net radiation, defined as $R = Q(1-\alpha)+I_i-I_o$, where Q is the rate of incoming solar direct and scattered radiation at the surface; α is the ratio between reflected and incident solar radiation, *albedo*; I_i is the rate of incoming long-wave radiation at the surface; and I_o is the rate of emission of long-wave radiation by the surface.

The surface melting can be calculated by applying Equation 3-8 to measured data from meteorological stations on glaciers and ice sheets. However, for estimating conditions on palaeo-ice sheets simpler solutions must be applied since all parameters in Equation 3-9 cannot be easily estimated. This has led to the development of statistical approaches to melt estimation. The most successful and most widely used is the *degree-day method* approach /e.g. Hock 2005/.

The degree-day method is based on the notion that melting is a function of the time the air is at a positive temperature. Hence degree-day methods use the integrated time of positive temperature as a proxy for the heat exchange and hence melting through empirical correlation between measured melting and integrated time of positive temperature. In its simplest form the sum is of

positive degree-days, hence the name of the method, defined by $S = \Sigma_i \alpha_i T_i$ where T_i is the mean daily temperature and $\alpha_i = 1$ if $T_i \geq 0°C$ and $\alpha_i = 0$ if $T_i < 0°C$. The melting is associated to the degree-day sum by a degree-day factor, λ, as $M = \lambda T$. /Hock 2005/ has summarised degree-day factors which show significant variation depending on local conditions. The degree-day approach has also been refined by /Hock 1998/ to yield a temporally varying sub-daily variation by introducing the potential direct solar radiation as a modulating factor γ_t to the empirical relationship, $M_t = \gamma_t \lambda T$, where subscript t denoted conditions at a specific time t.

Melt water is also generated englacially and at the base of glaciers and ice sheets. The deformation that occurs as ice is flowing generates heat which can melt minute amounts of water. Water production through strain heating requires the ice to be temperate and varies proportionally to the deformation rate. There is a positive feedback between strain heating and melting in that strain heating also warms colder ice to the pressure melting point and thereby allows the ice to melt; water increases velocity which in turn increases the strains. The amounts produced by strain heating are relatively small. Estimates are difficult to make since they depend on the deformation rates which vary spatially. Based on the typical flow regime of an ice sheet strain heating is negligible near the ice divide and is likely to increase towards the margins of the ice sheet.

Water is also generated subglacially through energy supplied by geothermal heat. The resulting melt rates will be directly proportional to the geothermal heat gradient in the bed rock. As with internal heating, geothermal heat may also first warm basal ice to its melting point resulting in subsequent melting. /Näslund et al. 2005/ have shown the importance of geothermal heat on the basal temperature and water production beneath the past Weichselian ice sheet.

3.2.3 Observations in nature and present-day natural analogues

Our knowledge on the hydrology of glaciers and ice sheets is largely based on observations from valley glaciers. There is no reason to believe that other processes would be present in association with an ice sheet, however, the magnitude of the processes will be scaled proportionally to the differences between valley glacier scale (1–100 km^2) and ice sheet scale (1,000–10,000 km^2 and larger).

The conditions experienced by a subterranean repository involve all phases of a glaciation; advance, retreat and possibly periods of quasi-stability. According to the ice sheet models we can expect transient conditions over the two suggested possible repository sites during both advance and retreat and very few, or no, periods of quasi-steady state. This indicates that no close modern analogues can be found. Since the sector of the Scandinavian ice sheet of interest was land based, except for a shallow sea calving front below the highest shoreline, and contained a pronounced ablation zone, the only approximate modern analogue is the Greenland Ice Sheet. We will therefore briefly summarise what is known about ice sheet hydrology on Greenland.

The surface hydrology of the Greenland Ice Sheet has been studied by /Thomsen et al. 1989/ in relation to a proglacial river near Illulissat/Jakobshavn for hydroelectric power production planning. The study showed that the surface of the ice sheet was punctured by numerous moulins, each draining a well-defined area of the ice surface (Figure 3-17). Satellite-based imagery indicates that the surface of the eastern flank of the ice sheet is covered by perennial supraglacial lakes interconnected by streams (Figure 3-18). The low slope and relief is probably the reason why the lakes are long-lived and do not drain catastrophically as is known from other ice-dammed lakes around the world /Richardson and Reynolds 2000/.

Satellite-based radar imagery also provides a good overview of the facies distribution on the Greenland Ice Sheet. Figure 3-19 shows the conditions from the centre of the ice sheet to the margin. The ablation area at this section of the ice sheet is approximately 100–150 km wide and the percolation and wet snow zones combined are 300–400 km wide. Unfortunately, it is impossible to conclude how much of the combined percolation and wet snow zone which contributes

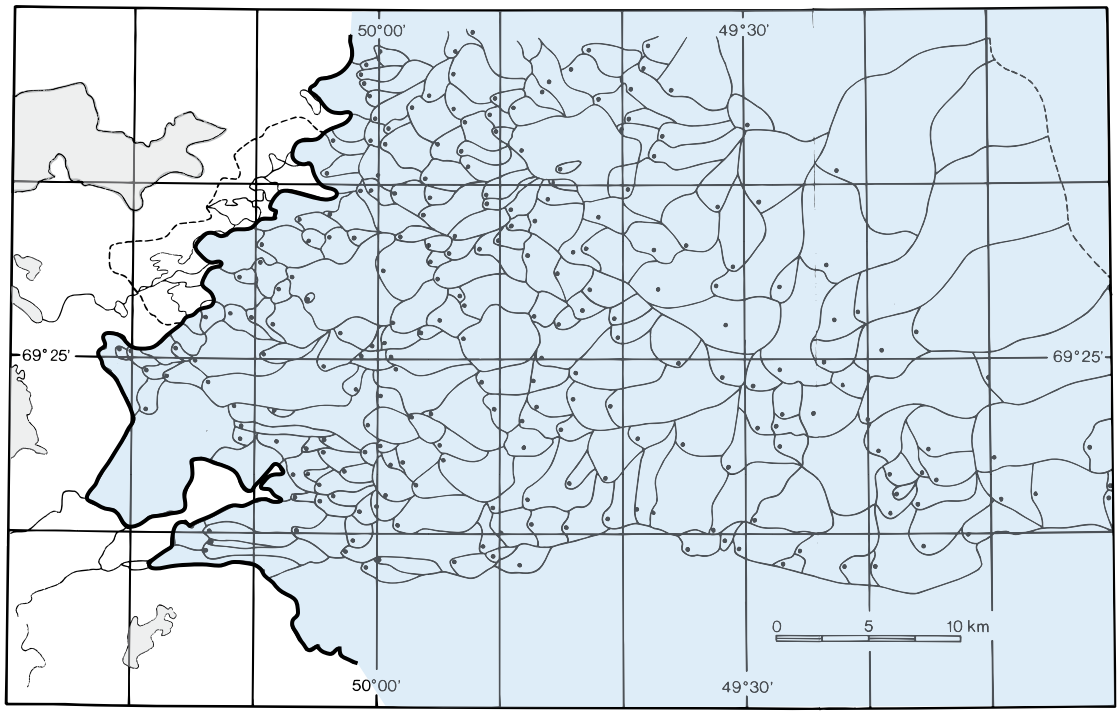

Figure 3-17. *Surface drainage basins on the ablation area of the Greenland Ice Sheet near Illulisat/ Jakobshavn area, redrawn from /Thomsen et al. 1989/. Filled circles mark the location of moulins in each surface drainage basin.*

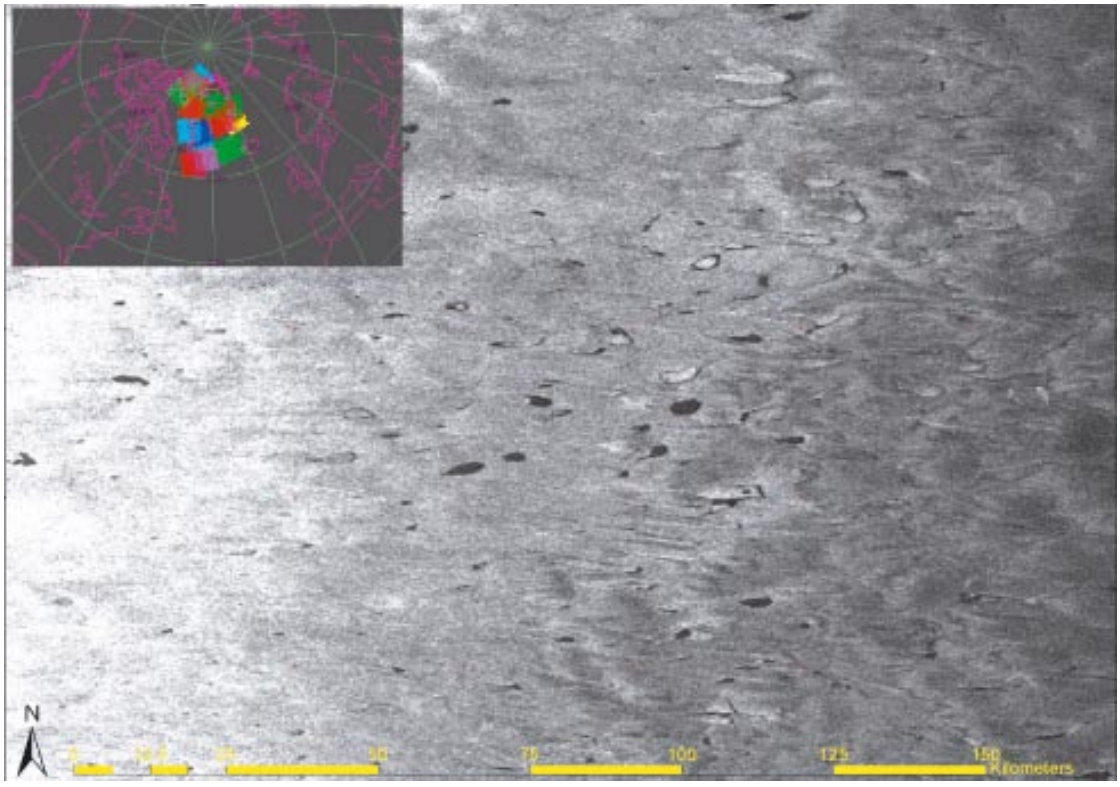

Figure 3-18. *Radarsat-1 ScanSAR image of the ablation zone of the Greenland Ice Sheet near Kangerlussuaq, East Greenland. The background grey scale indicate surface conditions from bare ice (white) through superimposed ice (medium grey) to wet snow (dark grey). The black areas are lakes that absorb the radar waves completely. Some lakes near the right centre have complete or partial lake ice cover, in some cases indicated by a central floe surrounded by a black rim of open water.*

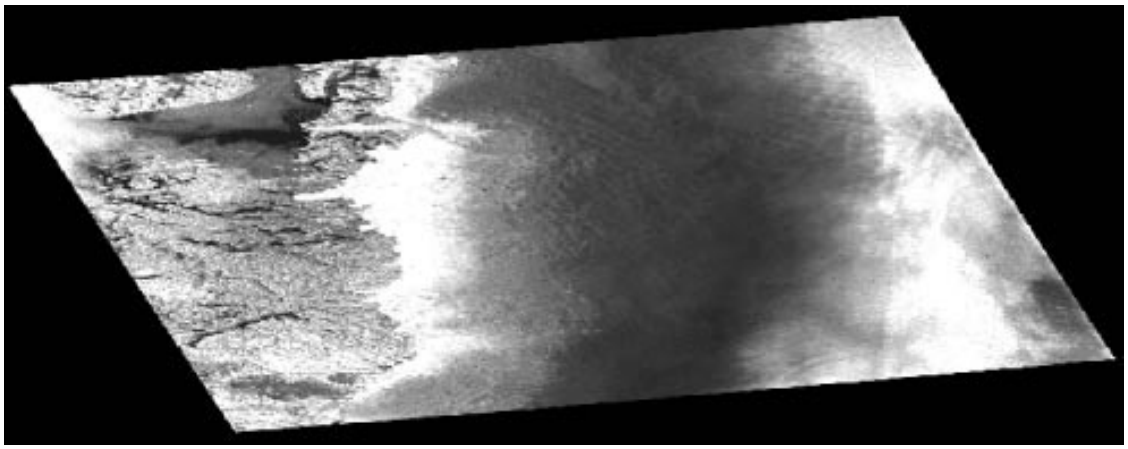

Figure 3-19. *Radarsat-1 ScanSAR image over east Greenland. The dark area at the centre of the image (between approximately –48° W and –44° W) comprises the percolation and wet snow zones that are bounded by the white dry snow zone to the right and the bare ice of the ablation zone to the left. The speckled grey zone to the extreme left (approximately left of –49° W) in the image is bare ground outside of the ice sheet. A part of Disco Island is visible in the upper left corner of the image.*

to runoff. However, it is reasonable to think that half that width may contribute. Furthermore, In /ACIA 2005/ it was shown that the different zones vary substantially in location from year to year. The lack of long-time series of data makes it impossible to draw any conclusions as to what might be a typical situation.

A study of the surface velocity at the equilibrium line of the Greenland Ice Sheet /Zwally et al. 2002/ indicates that the ice sheet experiences seasonal variations in ice velocity. They used their observations to postulate that the hydrology beneath the equilibrium line is fed by the seasonal variation in melt conditions at the surface and hence that direct connections exist even higher up on the ice sheet. This study has been challenged since no actual observations have been made at the bed. A ground penetrating radar profile (Figure 3-20) in the vicinity of the location of Zwally et al.'s observations indicates that temperate basal conditions may prevail far inland from the margin. A study by /Alley et al. 2005b/ shows that it is possible for surface water to connect to a basal drainage system through cold ice by the propagation of water-filled crevasses from the ice surface. It is therefore not unreasonable to think that surface water can enter the basal system far from the ice sheet margin. However, it is also possible that the velocity variations observed by Zwally et al. are caused by longitudinal coupling effects and are due to variations in velocity farther down-stream /e.g. Kamb and Echelmeyer 1986, Jansson 1997/.

Observations of shorter-term variations of subglacial water pressure have been carried out on many glaciers, among them Storglaciären. Figure 3-21 shows the water pressure record from Storglaciären. The hydrological system in this part of the glacier has been inferred to be a distributed tunnel (fast) system. The data shows how water pressures vary very rapidly in response to environmental factors influencing water input, air temperature governing glacier melt and liquid precipitation causing rapid runoff events on the glacier surface. Such fast systems are characterised by rapid flow and pressures that fluctuate rapidly due to the inability of the system to maintain high pressures.

Figure 3-22 shows an example of how a slow system may be configured. The figure is of the linked cavity system proposed by /Kamb 1987/ to explain a drainage type that has large cross-sectional area, high pressure and slow flow velocity. The system is such that small passages constrict flow, but a large volume of water is held in delayed storage throughout time.

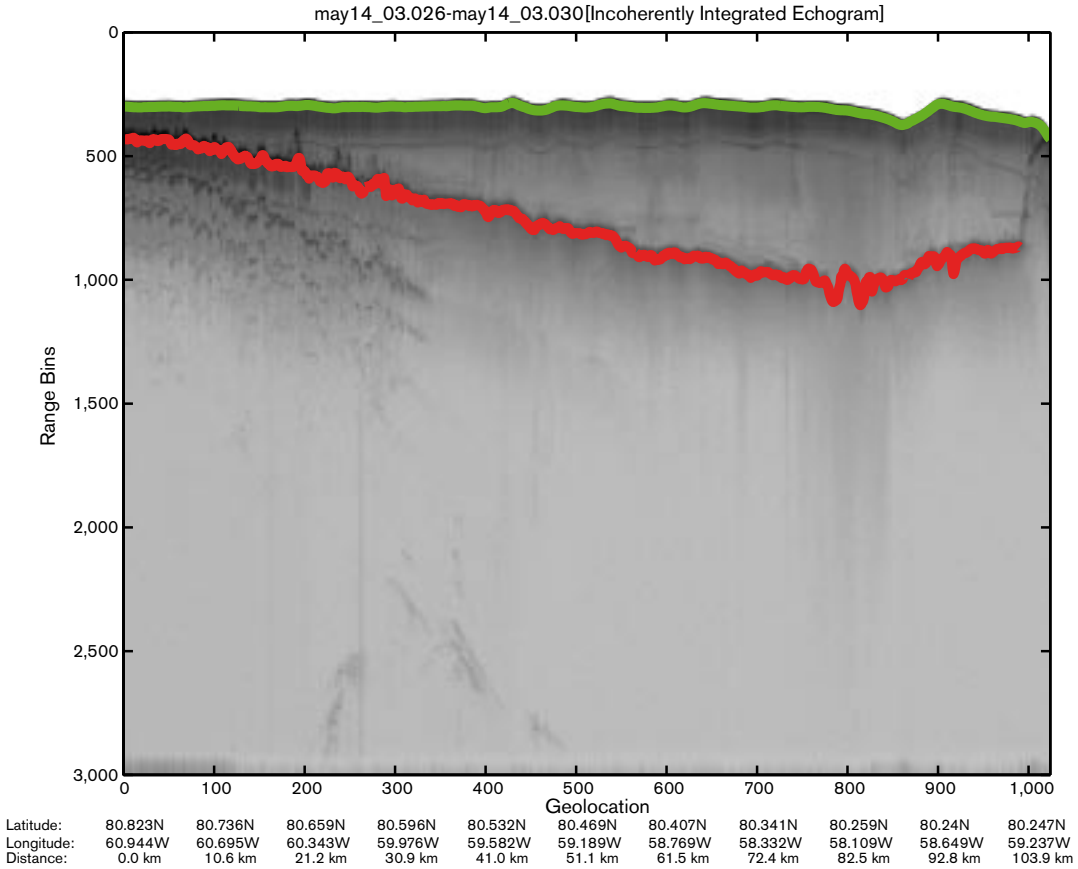

Figure 3-20. *Air-borne ground-penetrating radar image from east Greenland. The image is uncorrected and shows all reflections relative to the air-borne platform. The surface echo is marked by a green line, the bed echo is marked by a red line. Note the stronger echo and multiple reflections from 0–35 km, which may indicate the presence of water and hence greater reflection at the bed. Also note that 0 km is not the ice sheet margin. Image supplied by K. Steffen.*

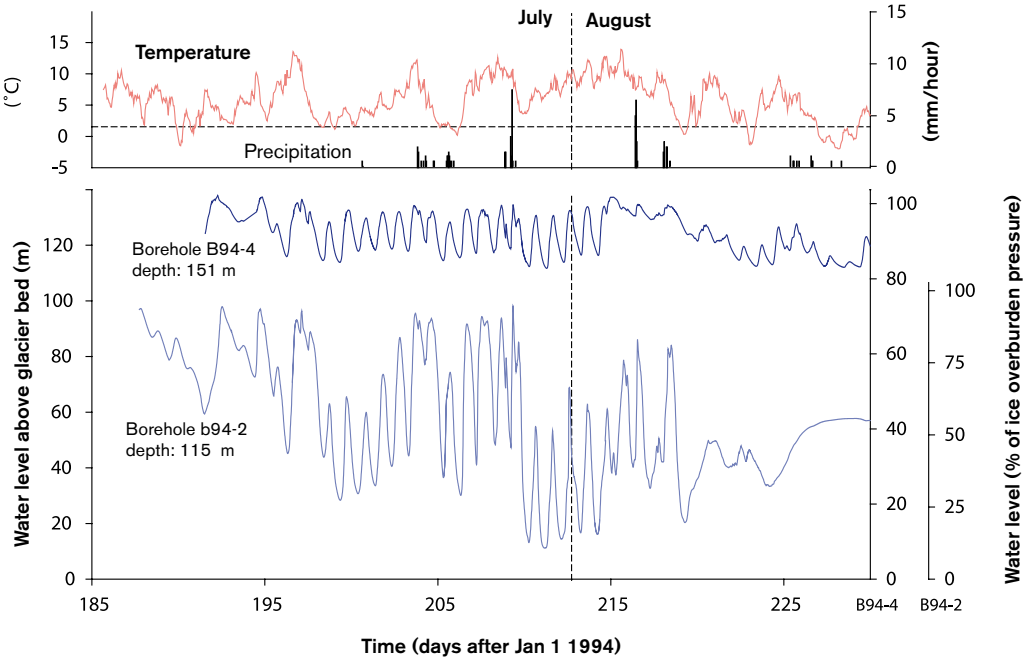

Figure 3-21. *Water pressure record from Storglaciären showing large diurnal variations in water pressure from near zero to near overburden pressure. Longer-term changes in the pattern of the water pressure fluctuations can also be seen.*

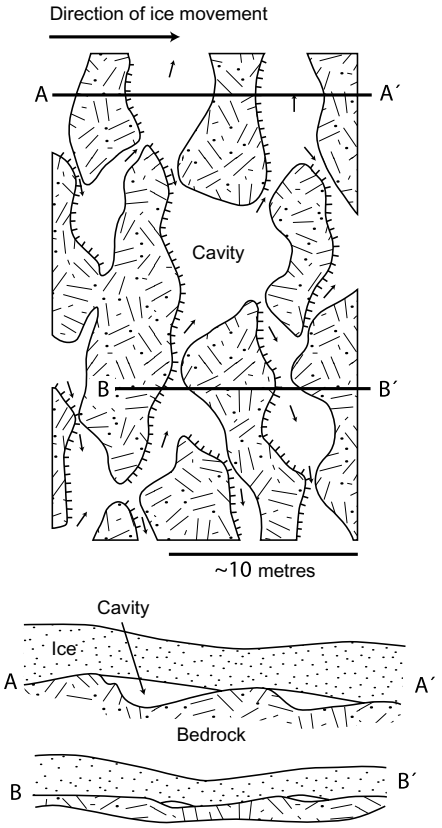

Figure 3-22. *Linked cavity system, an example of a subglacial slow flow system. From /Kamb 1987/.*

3.2.4 Model studies

In a study made for SKB /Boulton et al. 2001b/ developed a theory of sub-glacial drainage beneath ice sheets based on flow in sub-glacial tunnels (R-channels), which are supposed to be the main agents of large-scale longitudinal melt water discharge (see Figure 3-23). The widespread glacial melt water is supplied to the tunnels as groundwater flow. The drawdown of the piezometric pressure by the tunnels provides the mechanism for predominantly transverse groundwater flow towards the tunnels.

The tunnels are supposed to develop from water-filled cavities formed at the ice/bed surface when the groundwater head beneath the glacier exceeds the ice pressure. The groundwater head elevation rises as a result of increased water supply to the bed or if the ice sheet advances over a low-conductive bed. Hence, in the theory of Boulton et al. tunnel spacing is a function of the relation between bed transmissivity and water recharge.

In the summer season the high discharge by surface melting is expected to create short-lived water-filled voids between the large tunnels (Figure 3-24). Many of these voids will form locally beneath the bases of water conducting moulins and crevasses. In the winter seasons such drainage routes will be closed by internal ice flow. /Boulton et al. 2001b/ argued that the relatively long winters and short summers representative of the climate around large ice sheets will inhibit the development of well-integrated summer drainage patterns, except very close to the ice sheet margin.

Commonly glacier hydrology is modelled by empirical models and only three models exist in which the entire hydrological system or parts of it are modelled using a physically based model. The choice of model depends on the purpose of the analysis in question, what geometric scale is to be studied, and available data. Two models describe the complete hydrology of a glacier /Arnold and Sharp 2002, Flowers and Clarke 2002ab/.

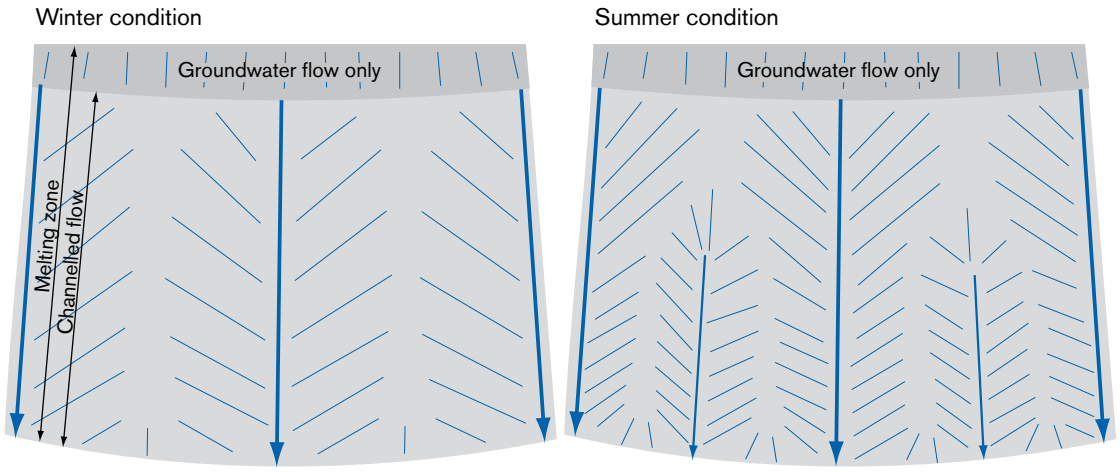

Figure 3-23. *Postulated patterns of groundwater flow in relation to the distribution of subglacial tunnels. From /Boulton et al. 2001b/.*

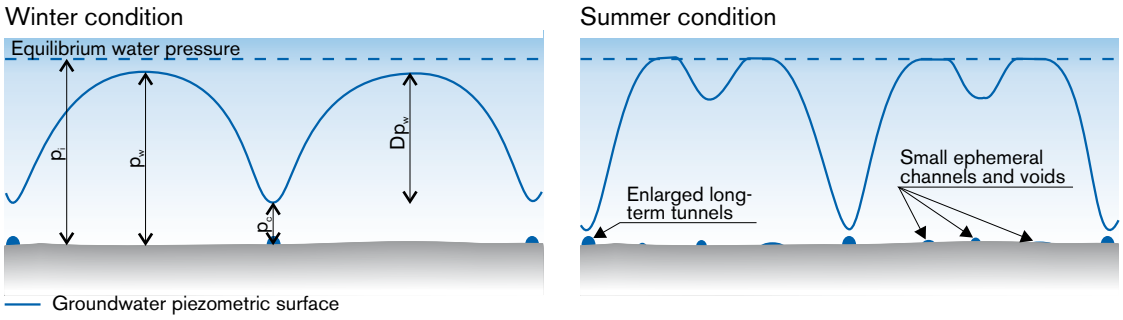

Figure 3-24. *Left: Transverse cross-section of a glacier showing the postulated relationships between groundwater surface and sub-glacial tunnels during the winter period. Right: The situation during the summer period of high discharge. Interfluve zones of high pressure, where effective pressures tend to zero, will tend to create short-lived water filled voids. From /Boulton et al. 2001b/.*

The present state of physically-based models is still crude, in that these models have been tailored to specific glaciers or glacier types and are not necessarily easily and generally transferable. Melt water production and the supra-glacial system are handled comparatively well; it is probably also the simplest part to model since the entire system is easily observable. The en- and sub-glacial systems are more complicated, characterised by large variability in possible drainage system configurations. Much uncertainty yet remains as to the exact geometry of drainage systems and how these systems can co-exist or switch from one state to another, thus limiting the applicability of physically-based modelling.

Modelling the physics of glacier hydrology is complex, since it involves the liquid phase, namely water, moving through the solid phase, namely ice, at the melting temperature. Furthermore, ice is deformable under relatively low stresses, which allows channels and conduits in glaciers to change size and shape much more rapidly than channels eroded in rock or sediment. The glacier system is thus transient on all time scales and over all spatial scales.

The first physically based models in glaciology were made to reproduce simple observable phenomena in glacier hydrology. /Röthlisberger 1972/ and /Shreve 1972/ presented simple numerical models (Röthlisberger: conduit flow; Shreve: water pressure potential flow) for water flow in glaciers. The assumptions made were that the rate of melt enlargement is balanced by creep closure (Röthlisberger) and that water pressure is in balance with ice pressure /Shreve 1972/. /Nye 1976/ and /Spring and Hutter 1981/ presented a physically based theory of unsteady

flow through intraglacial channels. /Hooke 1984/ investigated the effects of non-steady conditions, in particular open channel flow, on the Röthlisberger system. This was elaborated by /Kohler 1995/ who investigated the ratio of open-to-filled channel flow in a subglacial system. Most models have assumed circular cross-section pipe flow and semi-circular tunnels. However, discrepancies between measurements and model calculations led /Hooke et al. 1990/ to propose low broad tunnels in place of semicircular ones in order to be able to apply Glen's flow law of ice deformation with reasonable viscosity parameter values. Conduit flow was found not to reproduce water pressure and fluxes observed during the surge of Variegated Glacier, Alaska. This prompted /Kamb 1987/ to propose the linked cavity system which combined large cross-section with small flow velocities. /Walder and Fowler 1994/ extended Röthlisberger's model to include 'canals' cut into deformable till.

A first approach to producing a complete physically based model for a glacier was reported in /Arnold et al. 1998; henceforth referred to as the Arnold model/. This model has three components. A surface-energy sub-model calculates distributed glacier surface melt water production. A routing sub-model takes rain- and melt-water and either delivers the total water flux to *a priori* prescribed moulins, where it enters the glacier interior, or supraglacially to the ice margin. The third and final component is a subglacial sub-model which involves a conduit system. The englacial drainage is treated as part of the subglacial conduit system and simulated analogous to a sewage pipe system. Subglacial conduits are fed by a network of "drains", which represent moulins where water can enter or overflow from the system. Subglacial conduits can enlarge and contract in response to changes in the rates of wall melting and creep closure associated with changes in water inputs. In addition, the configuration of the system can change between a distributed system and a channelised system represented by different predefined number and geometries of conduits. "Distributed" links were changed to "channelised" flow paths as the modelled snowline passed in the up-glacier direction over each moulin. From this perspective the subglacial model is rigid, since switching between systems does not permit smooth transitions with the bed being partially drained by each system. The model was applied to Haut Glacier d'Arolla, Switzerland, and performed well in comparison with proglacial stream discharge, but limitations are indicated by discrepancies between model outputs and field observations of subglacial water pressure and water velocities, although the substantial features of these records could be reproduced.

/Flowers and Clarke 2002ab; henceforth referred to as the Flowers model/ developed a different approach to a complete physically-based model. The model comprises coupled surface runoff, englacial, subglacial, and groundwater systems. Each of the four components is represented as a two-dimensional, vertically integrated layer that communicates with its neighbours through water exchange. Melt is computed by a distributed temperature index model. Englacial hydrology is represented by describing a variety of bulk storage elements and allowing water transport between them in a system of cracks. Hence, the englacial system is treated as fracture-connected crevasses and pipes. The Flowers model was built to represent conditions at Trapridge Glacier, Canada, which is underlain by thick porous sediments. Their subglacial model, therefore, comprises flow through macroporous glacier sediments at the ice-bed interface and subsurface aquifers of buried sediment layers not directly exposed to the base of the glacier. Hence there are no explicit tunnels as in the Arnold model. The model reproduced well diurnal cycles of subglacial water pressure as measured in boreholes.

A crevasse-like englacial network, as adopted in the Flowers model, has been observed on Storglaciären, Sweden /Fountain et al. 2005ab/, countering previous notions of englacial water flow through few melt-enlarged conduits. If permeable subglacial sediments are present, groundwater flow may be a significant part of the system, as in the Flowers model, or flow may occur in channels eroded into the subglacial sediments. On harder beds or beds of less permeable sediments such as tills, water flow may occur in conduit systems melted into the ice or in linked cavity systems. Hence, a general physically-based model would have to accommodate all these possibilities and even couple different types of systems beneath different parts of a glacier. Such a model would be inherently complex.

Another issue which is not satisfactorily addressed in existing models is the time-transgressive development of subglacial systems. In the Flowers model, this is not necessary since flow through porous sediments does not involve significant time-dependent changes, except possible changes such as development of piping or siltation of the porous media from fines produced through sediment deformation. In the case of the Arnold model, it is widely reported /e.g. Nienow et al. 1998/ that the subglacial drainage system changes both in sizes of conduits and in complexity of the network of channels through the course of a season. The subglacial system is very dynamic and it seems as if a complete and accurate model description of this system may be distant. However, most changes in such a system occur in response to rapid changes, both increases and decreases in water inputs, so a first-order approximation may be to switch between a series of systems prompted by key events in the forcing.

Hence the state of glacier hydrological modelling adequately reproduces the large scale features, such as the regional direction of flow. Finer details, such as the position of individual conduits and the behaviour of the conduits and the water pressure within them is not completely resolved.

3.2.5 Time perspective

The time perspective of glacier hydrology can be divided in two main categories, times scales under which the ice sheet undergoes significant changes in volume and extent and where the associated hydrological conditions change with the ice sheet; and time scales under which the ice sheet can be considered constant in volume and extent and where the variability of the acting processes dominates.

Seen under the perspective of an entire glaciation, the hydrological system varies spatially with the size of the ice sheet. This means that different parts of the bed are either temperate or cold and can be associated with hydrological systems of different overall structure and parameterisation. The distribution of cold and temperate basal conditions changes in time and also in location with the waxing and waning ice sheet. From this perspective, a possible repository site will experience changing conditions of active hydrology under thawed bed conditions or cold frozen bed conditions. The location of large tunnel systems also varies on this time scale. This is because, with changing ice sheet configuration, the basal hydraulic conditions vary so that shifts in location of drainage pathways occur. How much time a specific location is subjected to either kind of condition is determined by the large scale fluctuations of the ice volume and extent.

The processes in the hydrological system of an ice sheet exhibit variations ranging from diurnal (in the case of temperature-dependent melt variations) or possibly shorter duration (in the case of rainfall-induced variations) to seasonal variations that depend on temperature variations on an annual basis. Since all variations in temperature-induced melting and liquid precipitation yield variations in input to the hydrological system, they also yield variations in subglacial water pressure with oscillations on similar time scales. This means that the base of an ice sheet will exhibit variations on a diurnal and subdaily scale superimposed on longer-term variations coupled to weekly variations due to changing air masses of different temperature and lastly variations due to seasonal temperature fluctuations.

3.2.6 Handling in the safety assessment SR-Can

Information from natural analogues and model studies has been used to set up boundary conditions for groundwater flow modelling. Information on drainage areas on the Greenland ice sheet and distances between eskers in Sweden has been used to estimate the spacing between conductive features in the sub-glacial layer. Data on ice sheet thickness, basal- and surface melt rates were generated by the dynamic ice sheet model described in Section 3.1.

3.2.7 Handling of uncertainties in SR-Can

Uncertainties in mechanistic understanding

Although the theories and empirical studies of glacier hydrology are of appropriate quality to reproduce observed phenomena at individual glaciers or sites on glaciers, there are no generally applicable theories for the spatial and temporal variations in hydrology and hydraulic conditions. Perhaps more importantly, the coupling between discrete drainage pathways and the continuum mechanics of ice sheet models is not, thereby preventing integrated modelling. The main obstacle to enhancing our understanding of the dynamics of glacier hydrology is the transient nature of the system and difficulties in observing its structure and behaviour. The division between subglacially derived and surface-derived water emanating from, say, the Greenland ice sheet is also unknown. In essence, very little is known about real conditions in ice sheets. Almost exclusively, process studies have been made on valley glaciers. Although processes are the same regardless of the size of the glacier, the special conditions relevant to an ice sheet, in particular its large thickness compared with valley glaciers make some inferences hard to accept when moved from the valley glacier where they are observed to the ice sheet where they are applied.

3.3 Isostatic adjustment and shoreline migration

3.3.1 Overview/general description

The geoid is the equipotential surface of the Earth's gravitational field which best fits the undisturbed surface of the oceans. Shoreline migration is the result of changes in the height of the geoid relative to the solid surface of the Earth.

Sea level is defined to be zero on land and positive in the oceans, where it corresponds to the depth of the ocean. The surface of the ocean corresponds to the geoid surface (see Figure 3-25). Relative sea level is the vertical height difference between the geoid at an arbitrary time and the present height of the geoid (see Figure 3-25). Relative sea level is defined to be zero at the present day. It is positive during *transgression*, when the intersection of the geoid with the solid surface is higher than present, and negative during *regression*, when the intersection of the geoid with the solid surface is lower than present. The shape of the geoid is governed by the gravitational field of the Earth and varies over time. Over time scales of 100 to 100,000 years, changes in relative sea level throughout Fennoscandia are dominated by the process of glacial isostatic adjustment (GIA). GIA is the response of the solid Earth, by viscous and elastic processes, to surface loading during a glacial cycle. The surface loading arises as water is transported between ice sheets and the oceans.

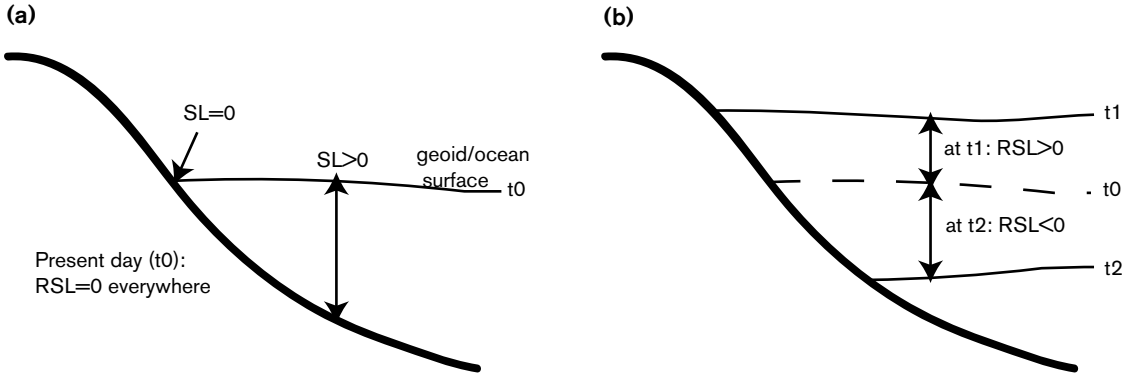

Figure 3-25. *a) Definitions of sea level (SL) and relative sea level (RSL). The present-day surface of the ocean defines the zero level of RSL. b) Changes in relative sea level are the result of solid Earth uplift or depression and/or changes to ocean water volume. Note the change in both the shape and height of the geoid, or ocean surface, at different times.*

Relative sea-level changes associated with GIA are a result of the coupled phenomena *isostasy* and *eustasy*. Isostasy is the response of the solid Earth to loading by ice or water, or unloading due to denudation, whereas eustasy refers to changes in global sea level arising from a change in ocean water volume following a mass exchange between ice reservoirs and the oceans.

Global relative sea-level changes exhibit complex spatial and temporal patterns, and are strongly dependent upon the location relative to major ice sheets. Relative sea-level change at locations far from ice sheets (hereafter referred to as far-field locations) is dominated by the eustatic signal; during deglaciation monotonic sea-level rise causes land inundation and the shift of shorelines inland. At locations close to ice sheets (hereafter referred to as near-field locations) the isostatic signal dominates; rebound of the solid surface from the time of deglaciation onwards causes land emergence and the migration of shorelines oceanwards. These are two end-member cases, and, in general, sea-level change, and hence shoreline migration, is governed by a complex interplay of isostatic and eustatic processes.

GIA-induced sea-level changes depend on the following factors (see Figure 3-26).

- The location and thickness of ice sheets.
- The depth and extent of the oceans.
- The structure and properties of the solid Earth and its response to surface loading.

Changes in surface loading arise due to the exchange of mass between ice sheets and ocean basins throughout a glacial cycle. The presence of ice-dammed lakes and the redistribution of sediments also contribute to changes in surface loading, although, in Fennoscandia, the short-lived nature of ice-dammed lakes, and their shallow depth, means that this perturbation to the pattern of surface loading probably has a negligible effect when considering the solid Earth response. The denudation of bedrock and redistribution of associated sediments persists over a much longer time scale, on the order of millions of years. On a regional scale, over a single glacial cycle, the effect of sediment redistribution upon solid Earth deformation will be negligible in relation to the ice load, but over several glacial cycles, or locally, it may be of significance.

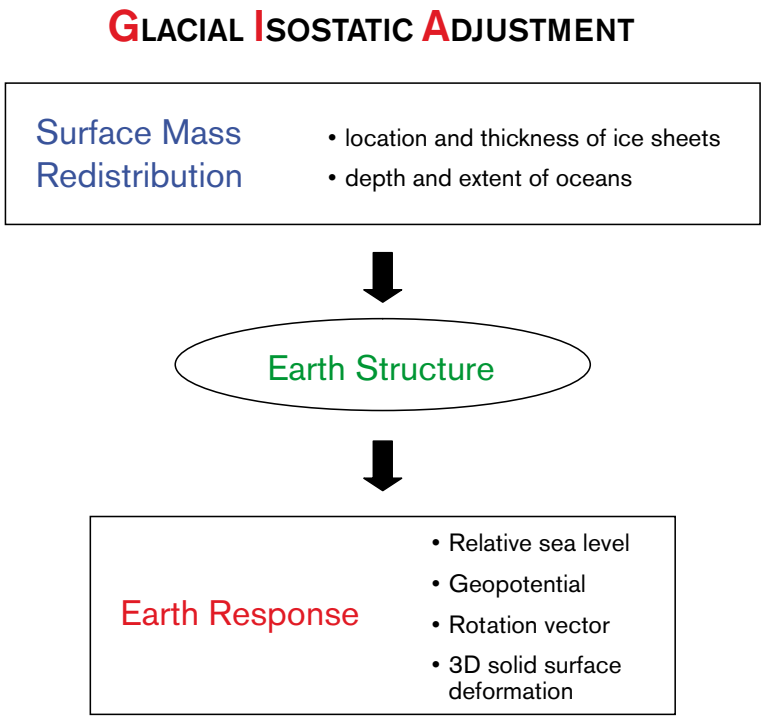

Figure 3-26. *The theory of Glacial Isostatic Adjustment (GIA): inputs and outputs of the system.*

The Earth consists of the lithosphere, the upper and lower mantle, and the outer and inner core. The lithosphere is the outer layer of the Earth. It is less dense than the mantle below and responds approximately elastically to forces applied at the surface. The deformation of this layer is short-lived once the load is removed. The mantle responds viscoelastically to forces applied over a time scale of ~ 100, 000 years. The recovery of this layer to a state of isostatic equilibrium following loading takes several orders of magnitude longer than the recovery of the lithosphere. The rheological properties of the lithosphere and upper and lower mantle determine the precise magnitude and duration of solid Earth deformation during a glacial cycle, and are discussed further in Sections 3.3.2 and 3.3.4. The outer and inner cores are not affected by the processes of GIA.

GIA-induced sea-level changes arise as a result of the gravitationally-consistent redistribution of water between ice sheets and ocean basins, and thus the evolution of surface loading. Any redistribution of surface mass alters the shape of the geoid, which in turn defines the position of the surface of the oceans.

The height of the geoid, or mean ocean surface, is dependent upon *direct* and *indirect* geoid perturbations /Milne et al. 2002/, as well as changes in ocean water volume and capacity of ocean basins. *Direct* effects refer to the deflection of the geoid due to the direct attraction of surface mass loads, such as ice sheets. *Indirect* effects refer to geoid perturbations arising due to the surface load-induced deformation. The volume of the oceans will vary as water is transferred to and from the ice sheets. Also changes in ocean capacity and bathymetry arise as a result of crustal and geoidal perturbations in response to ice and ocean loading. The ice loading solid surface response includes the depression and rebound of the solid surface in the location of ice sheets, and the raising and lowering of glacial forebulges in areas surrounding the ice sheets. The ocean-loading response is similar to the ice-loading response. However, at continental margins ocean loading induces a levering of the continental lithosphere and a subsidence of offshore regions, this is referred to as *continental levering* /Clark et al. 1978/ (see Figure 3-27). The combination of ice and ocean loading leads to a decrease in the volumetric capacity of the ocean basins during glaciation, and an increase during deglaciation, resulting in a globally uniform rise or fall in sea level, respectively. The ongoing fall in sea level following the last deglaciation has been termed equatorial ocean syphoning /Mitrovica and Peltier 1991, Mitrovica and Milne 2002/.

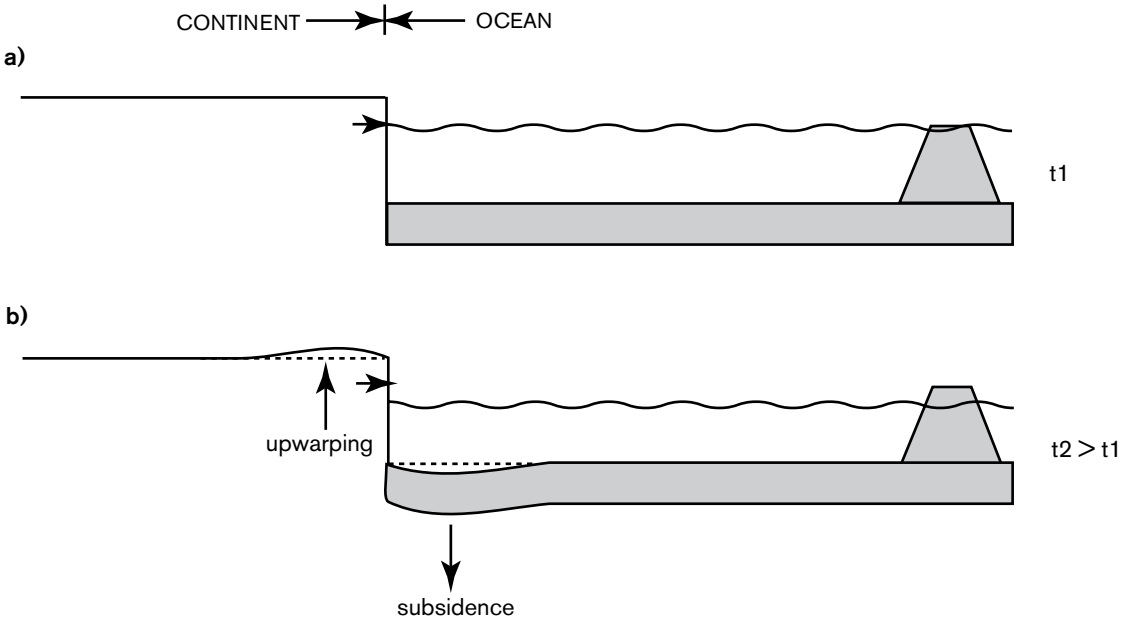

Figure 3-27. *Continental levering: the migration of water into offshore regions following deglaciation results in offshore subsidence and onshore upwarping. Ocean floor subsidence results in sea-level fall at far-field sites.*

Changes in relative sea level result in shoreline migration. A rise in relative sea level and the consequent inland migration of the shore may be due to solid Earth subsidence, an increase in the height of the geoid/ocean surface as a result of ice sheet melting, or a combination of these processes. Similarly, a fall in relative sea level and the consequent migration of the shore towards the ocean may be due to isostatic rebound, a fall in the height of the geoid/ocean surface due to ice sheet build up, or a combination of these processes. In the vicinity of the Fennoscandian ice sheet the effects of isostatic deformation and changes to the height of the geoid/ocean surface occur simultaneously, and may have opposite effects on the position of the shoreline. Further, the surface of the Baltic Sea does not solely depend on the height of the geoid/ocean surface, but also on the elevation of its sills relative to coeval sea level, and ice thicknesses at locations with potential connections to the sea.

The isostatic adjustment and shore-line migration described above may affect a number of geosphere variables of importance for a deep geological repository (Table 3-3).

Indirectly groundwater flow and composition are influenced by shoreline migration. If the site is not subjected to permafrost, and it is not covered by ice, the sea, or a lake, then the groundwater surface follows a subdued version of the topography. Groundwater flow will be driven by topography, assuming precipitation exceeds evaporation. If the site is submerged the situation will be almost stagnant and groundwater flow will be driven by density only /**Geosphere process report**/. Groundwater composition is affected, since relative sea level affects the salinity of the Baltic Sea. Relative sea level and the extent of the ice sheet determine whether there is a connection between the Baltic and the ocean. This together with the runoff to the Baltic basin, determines the salinity in the sea/lake water.

3.3.2 Boundary conditions and internal parameters

The main factors governing the evolution of relative sea level, and hence shoreline migration, throughout Fennoscandia are the loading history – both with regard to ice and ocean water – and the rheological parameters governing the response of the solid Earth to such a load.

Loading

The main factors governing the evolution of relative sea level, and hence shoreline migration, throughout Fennoscandia are the loading history – both with regard to ice and ocean water – and the rheological parameters governing the response of the solid Earth to such a load.

Near-field relative sea levels are very sensitive to variations in the evolution of the near-field ice sheet, /Lambeck et al. 1998, Davis et al. 1999, Tamisiea et al. 2001, Milne et al. 2002, Kaufman and Lambeck 2002, Tamisiea et al. 2003/. There remain uncertainties in the details of ice loading during the last glacial cycle, especially with regard to estimates of ice thickness within Fennoscandia.

Table 3-3. A summary of how geosphere variables are influenced by isostatic adjustment and shoreline migration.

Geosphere variable	Influenced by climate issue variable/s	Summary of influence
Rock stresses	Isostatic depression/rebound	The deformation of the Earth's crust will lead to altered rock stresses, see Section 3.5.
Groundwater pressure	Relative sea level	If the site is not covered by the sea or a lake the groundwater pressures will be determined by topography and groundwater recharge. If the site is submerged the groundwater pressure will be determined by depth of the sea/lake.

The details of far-field ice sheets are irrelevant for the prediction of relative sea-level change in Fennoscandia /Peltier 1998, Mitrovica et al. 2001a, Tamisiea et al. 2003, Bassett et al. 2005/; mass changes in the far field mainly provide an influence on global eustatic sea-level change. However, the overall characteristics of far-field ice sheets may also generate a long wavelength isostatic response in Fennoscandia. This response is likely to be dominated by the signal from a massive North American (Laurentide) ice complex. Due to the position of Fennoscandia on the Laurentide forebulge during the Last Glacial Maximum (LGM) /Mitrovica et al. 1994b/, the presence of the Laurentide ice sheet is predicted to have generated 25–30 m of solid Earth uplift in central Fennoscandia at this time (see Section 3.3.4). The magnitude of this signal does not vary greatly across Fennoscandia (unlike the relative sea-level signal due to local ice loading), and is not dependent upon the local geometry of the Laurentide ice sheet; only its volume.

There is strong evidence that during the last deglaciation an ice-dammed lake prevailed within the Baltic when non ice-covered sills were above sea level and all other potential connections between the Baltic and the North Sea were dammed by ice /Björck 1995, Lambeck 1999/. The surface of the ice-dammed lake was constrained by the height of the ice sheet above sea level and the surrounding topography, i.e. the sill levels, and there is evidence to suggest that immediately prior to the draining of the lake its surface was 25 m above the contemporary relative sea level /Björck 1995/. Due to the relatively small volume of water released to the oceans as the ice lake drained the resulting perturbation of global sea levels was insignificant /Lambeck 1999/. The shallow depth and the short duration of the ice lake mean that its impact on isostasy was negligible in comparison with the ice load. However it is important to be able to predict the formation of any future ice-dammed lake because it will exist at some elevation above sea level, and therefore lake shoreline heights will not correspond to sea level heights at that time. This must also be considered when interpreting palaeo-lake-level data. The local effect upon shoreline migration may be considerable due to low gradient topography within and around the Baltic.

Another process that may impact the loading is erosion and sediment transfer. Erosion and transport of sediment took place beneath warm-based parts of the ice sheet during the last glacial cycle /**Geosphere process report**/, and this mass redistribution affects isostatic loading and topography. However, the average total depth of glacial erosion over all Late Pleistocene glacial cycles in lowland Precambrian parts of Fennoscandia is on the order of a few tens of metres /Lidmar-Bergström 1996/. Therefore, on the time scale of one glacial cycle, the average unloading/loading effect of this process may be neglected. However, any local reshaping of the land will affect the evolution of the shoreline, and this needs to be taken into account.

Rheological parameters and topography

In order to determine the Earth's response to surface loading its internal rheological and density structure must be specified. The characteristic time scale for loading during a glacial cycle will excite both elastic and viscous responses, therefore a viscoelastic (Maxwell) rheology is adopted. Such a system behaves elastically on a short time scale and viscously on a long time scale when placed under stress.

Parameters describing the rheological properties of the Earth's lithosphere and upper and lower mantle define its response to loading during a glacial cycle. The average density and elastic structure of the Earth are taken from /Dziewonski and Anderson 1981/. The average thickness of the lithosphere is approximately 100 km, although this value varies between < 30 km for oceanic lithosphere and up to > 200 km for continental lithosphere /Watts 2001/. Lithospheric thicknesses in Fennoscandia range between ~ 20 km in the north-west and ~ 200 km in the south-east /Pérez-Gussinyé et al. 2004/. The lithosphere is generally regarded as elastic for the purposes of GIA studies, this has been shown to be a good approximation throughout the development of the subject /McConnell 1968/.

The upper mantle lies below the lithosphere, extending to a depth of 660 km, and then the lower mantle extends to 2,900 km below the Earth's surface. The viscosity of the upper and lower mantle have been constrained to lie in the ranges 1×10^{20}–2.6×10^{21} Pa s and 2×10^{21}–1×10^{23} Pa s, respectively, as determined from previous GIA studies /Davis and Mitrovica 1996, Mitrovica and Forte 1997, Simons and Hager 1997, Lambeck et al. 1998, Davis et al. 1999, Milne et al. 2001, 2002, 2004, Mitrovica and Forte 2004/. Lateral variations in radial viscosity structure may be derived from seismic shear-velocity models by converting velocities to temperatures, and then using temperature to estimate viscosity. The seismic model most commonly used is S20RTS /van Heijst et al. 1999, Ritsema and van Heijst 2000, Ritsema et al. 2004/.

Present-day topography is used to constrain palaeotopography. When calculating palaeotopography we assume that all changes to the shape of the land arise from the differential GIA response across the region; however topography is also affected by tectonic, erosional and depositional processes.

3.3.3 Observations in nature and present-day natural analogues

The GIA process may be observed by studying relative sea level markers, both from the geological record and from tide gauge data, Global Positioning System (GPS) observations of the 3D deformation of the solid surface, the time-variation of the gravity field as observed by satellites and land-based gravity surveys, and changes in the orientation of the Earth's rotation vector and length of day.

Geological and tide gauge data complement each other. The tide gauge data consist of monthly or annual observations of mean sea level relative to a local solid Earth marker at coastal sites throughout the world. The data may be accessed through the "Permanent Service for Mean Sea Level" at www.pol.ac.uk/psmsl. The geological data, including palaeoshoreline positions, lake isolation and tilting information, cover a longer time period than the tide gauge data, but the tide gauge data are more accurate, both in terms of their vertical resolution and the dating of the information. A selection of geological relative sea level data for Fennoscandia can be found in /Lambeck et al. 1998, Påsse 2001, Eronen et al. 2001, Kaufmann and Lambeck 2002/, and references therein, but at present there does not exist a complete compilation of such data.

Observations of relative sea level are required in both the near and far field. Far-field data provide constraints on eustatic sea-level change and hence the volume of ice contained in far-field ice sheets. Near-field data exhibit a more complex dependence upon the local distribution of ice and the Earth model.

Care must be exercised when interpreting palaeoshoreline data from the Baltic Sea; it is important to determine whether the data relate to sea level or a lake level. An overriding problem with geological data in Fennoscandia is the lack of relative sea level data prior to the LGM. Most of the evidence of shorelines prior to this time will have been destroyed by the ice sheet. This makes it very difficult to test relative sea level predictions from before 20 kyr before present (BP). It should also be noted that shorelines can only form in ice-free locations. This observation provides an important temporal constraint for the testing of shoreline migration predictions against undated shoreline data.

GPS data provide satellite-measured observations of changes in baseline distances which yield present-day rates of vertical and horizontal motion at a series of discrete positions. The rates are averaged over the period of data collection, which is generally on the order of 10 years at the present, to yield estimates accurate to within ~ 0.1 mm/yr in the horizontal direction, and a few tenths of a mm/yr in the vertical direction.

GPS data from the BIFROST project /Johansson et al. 2002/ provide excellent spatial coverage of present-day solid Earth deformation throughout Fennoscandia to a high degree of accuracy.

The network yields an estimate for the full 3D deformation field, and the horizontal and vertical components of this field have different sensitivities to the ice history and Earth model, opening up the possibility of constraining model parameters more accurately when these data are combined with sea-level observations /Mitrovica et al. 1994ab/. Combining the GPS data with sea-level data is particularly important when one considers that the GPS data are limited by their relatively short time span, and can only yield information about present-day deformation rates. Also, sea-level data are limited by their poor spatial coverage; a factor that is addressed by the distribution of GPS observations throughout the interior of Fennoscandia.

3.3.4 Model studies

The GIA model

The majority of GIA models solve the sea-level equation, which was originally developed by /Farrell and Clark 1976/, and describes the gravitationally-consistent redistribution of water from ice sheets to ocean basins, and thus the evolution of the distribution of water between oceans and land-based ice sheets. Any redistribution of surface mass alters the shape of the geoid, which in turn defines the redistribution of water in the ocean basins; therefore an iterative procedure is required to solve the sea level equation.

There have been many attempts to construct a dynamical model to explain the observed processes of GIA. Following /Farrell and Clark 1976/, early studies neglected the time dependence of ocean shorelines /Wu and Peltier 1983, Nakada and Lambeck 1989, Tushingham and Peltier 1991/, and the ice loading was simply applied as a series of 'finite elements' /Clark et al. 1978, Peltier et al. 1978, Wu and Peltier 1983/. In 1991, Mitrovica and Peltier /Mitrovica and Peltier 1991/ derived a pseudospectral approach to solving the sea level equation, and this method has been widely used throughout the field ever since. Models which take into account the time-varying nature of shorelines began to be developed in the early 1990s /Lambeck and Nakada 1990, Johnston 1993, Peltier 1994, 1998, Milne 1998, Milne et al. 1999, Peltier and Drummond 2002, Kendall et al. 2005/, and the effects of Earth-rotation have also subsequently been considered /Han and Wahr 1989, Bills and James 1996, Milne and Mitrovica 1998, Peltier 1998, Mitrovica et al. 2001b/. Initial investigations into the effect of lateral variations in Earth structure are also in the process of being developed /Kaufmann et al. 2000, Wu et al. 2005, Latychev et al. 2005a, Paulson et al. 2005/.

The GIA model used in this study was developed by Milne /Milne 1998, Milne and Mitrovica 1998, Milne et al. 1999/. Three refinements to the original sea level equation presented by /Farrell and Clark 1976/ have been developed /Mitrovica and Milne 2003/. Firstly, time-dependent shoreline positions are taken into account when calculating the ocean-loading function. Shorelines can change position by several hundreds of kilometres in flat terrains, and this must be accounted for in applying the ocean load. Secondly, the water influx into regions vacated by retreating, marine-based ice is carefully accounted for in the distribution of the load /Milne et al. 1999/. And thirdly, changes to the rotational state of the Earth as a result of both surface and internal mass redistributions are considered. The model used to generate predictions of relative sea-level change in this study is based on a new general theoretical foundation that includes all these recent advances.

The sea-level equation

The sea level equation takes account of changes to the height of the geoid and the Earth's solid surface. Local factors, such as changes to the tidal regime, the consolidation of sediments, and tectonic processes, are neglected in this study.

Equation 3-9 $$\Delta\xi_{rsl}(\tau,\varphi) = \Delta\xi_{eus}(\tau) + \Delta\xi_{isos}(\tau,\varphi) + \Delta\xi_{local}(\tau,\varphi)$$

In the above expression the left-hand side refers to changes in relative sea level at time τ and location φ. The first term on the right-hand side is the time-dependent eustatic signal, the second term relates to the isostatic effects of glacial rebound, including both ice and water load contributions, and the third term refers to local factors, as described above. In order to solve Equation 3-9 in a gravitationally self-consistent manner, a pseudospectral algorithm /Mitrovica and Peltier 1991, Milne and Mitrovica 1998/ is employed. Green's functions are constructed to determine the GIA-induced perturbations to the geopotential and solid surfaces due to loading. The resulting temporal convolutions are evaluated by describing the GIA loading history as a series of discrete Heaviside increments. The spatial convolutions are performed by transforming the problem to the spectral domain and employing the pseudospectral algorithm /Mitrovica and Peltier 1991, Milne and Mitrovica 1998/.

The method by which relative sea level is calculated at a certain position, at a certain time, may be broken down into a series of simplified steps. At the start of the model run, loading is applied to an Earth model that is assumed to be in isostatic equilibrium. Once an ice load is applied at each time step the resulting deformation of the solid Earth and the perturbation to the geoid are calculated. The new shape of the geoid determines the redistribution of water in the oceans and the new extent of the oceans. However, this redistribution of water in turn affects the shape of the geoid and the deformation of the solid Earth in oceanic regions, therefore an iterative procedure is used to ensure the correct treatment of perturbations to the solid and geoid surfaces; Recalculations of the perturbation to the geoid and the redistribution of water are carried out until there are no further changes, at which point loading for the next time step is applied. Loading is applied via forward time stepping.

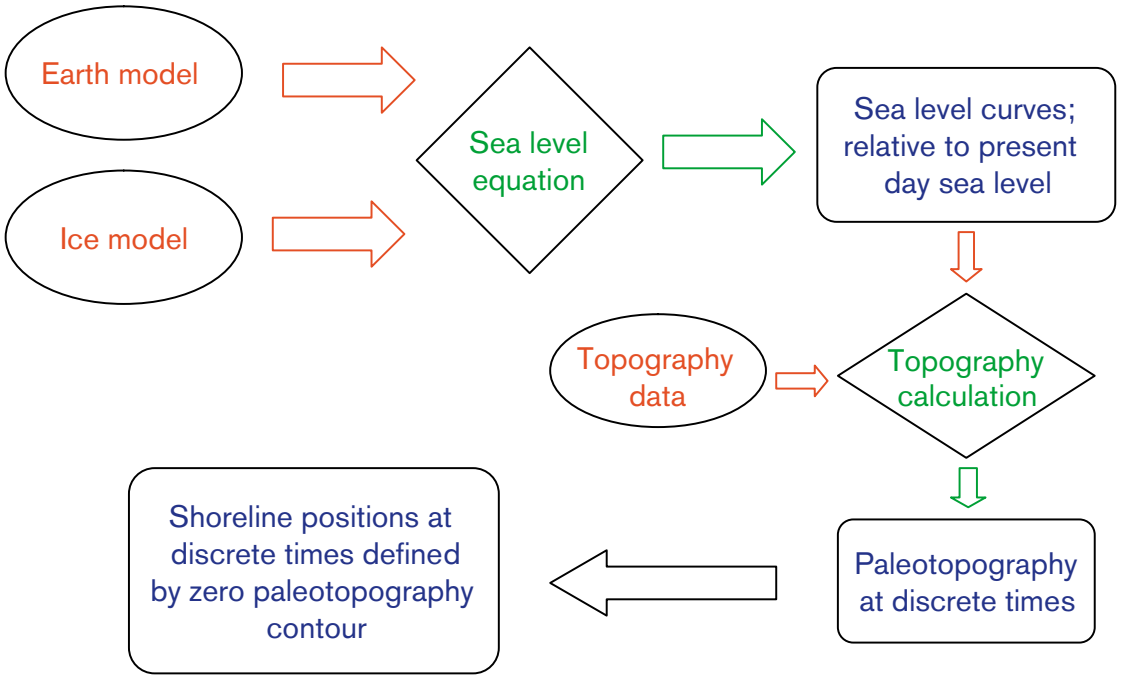

Figure 3-28. *Flow chart outlining the inputs (in red), calculations (in green) and outputs (in blue) required to calculate palaeoshoreline positions due to GIA processes.*

The final output of the GIA model consists of a series of global relative sea level predictions for all time steps used in the model. In the method used here relative sea level is defined to be zero at the present day, and heights are given relative to this 'zero level' at all times in the past (and future). Corrections are applied using present-day topography to determine the height of any point above or below sea level at any given time. Assuming that the underlying topography is unaltered by erosion and sedimentation the evolution of palaeotopography is calculated via the following equation:

Equation 3-10 $$T(\varphi,\tau_p) = T(\varphi,\tau_0) - \xi_{rsl}(\varphi,\tau_p)$$

T is topography, defined to be the height of the solid surface above sea level at time τ, and ξ_{rsl} is relative sea level at time τ. τ_p refers to a time in the past, τ_0 refers to the present day, and φ is the location on the surface of the Earth. Shoreline positions at time τ_p are determined by the zero palaeotopography contour at that time.

Ice loading

The global ice loading model used in this study is modified from the ICE3G deglaciation history /Tushingham and Peltier 1991/, and has been calibrated using far-field relative sea-level data /Radtke et al. 1988, Fairbanks 1989, Bard et al. 1990, 1996, Chappell and Polach 1991, Chappell et al. 1996, Hanebuth et al. 2000, Yokoyama et al. 2000/. A eustatic curve has been used to tune the mass of ice contained within far-field ice sheets. The near-field ice loading for Fennoscandia is discussed in Section 3.1 and has been derived using a thermodynamic ice sheet model employing a proxy data palaeotemperatures curve. From this model, the extent and thickness of the Fennoscandian ice sheet at a series of discrete times from 116 kyr BP to the present day has been derived.

Ice-loading history within Fennoscandia is the principal factor governing relative sea-level change in Fennoscandia. The loading history presented in Section 3.1 is perturbed to investigate the sensitivity of sea-level change to differences in ice thickness, the timing of deglaciation, the pattern of ice build-up, and the time scale over which loading is considered (Table 3-4). The extent of ice at each time step since the LGM has not been perturbed because the geometry of the ice sheet during this period is constrained by geological data. Details of the ice build up prior to the LGM are poorly constrained because the geological evidence has subsequently been destroyed, however, for consistency, the ice extents for this period are also not altered. An Earth model consisting of a 96 km-thick elastic lithosphere, an upper mantle of viscosity 0.5×10^{21} Pa s, and a lower mantle of viscosity 1×10^{22} Pa s is used to investigate the response to the different loading models.

Table 3-4. A summary of the ice loading models used in this study. In all cases the ICE3G global ice model is used to constrain the distribution and thickness of ice outside Fennoscandia.

Model	Description of loading model	Model run time
1	Weichselian glacial cycle as described in Section 3.1	116 kyr
2	Two Weichselian glacial cycles run back-to-back to give a double glacial cycle	232 kyr
3	Weichselian glacial cycle, loading only applied from 40 kyr BP	40 kyr
4	Weichselian glacial cycle with 90% ice thickness in Fennoscandia	116 kyr
5	Weichselian glacial cycle with 80% ice thickness in Fennoscandia	116 kyr
6	Weichselian glacial cycle with the timing of deglaciation advanced by 500 years	116 kyr
7	Weichselian glacial cycle with ice thickness allowed to increase linearly between 60 kyr BP and 20 kyr BP	116 kyr
8	Four relaxation models, as described in the isostatic memory section	Varies
9	Weichselian glacial cycle with all ice removed from Fennoscandia for the duration of the model run, as described in the section on far-field ice sheets	116 kyr

In Figure 3-29a and d the same Fennoscandian surface loading is used, but the model run is initiated at different times. Due to the assumption that the Earth is initially in isostatic equilibrium there will be some discrepancy between relative sea level predictions at early times in a model started at 116 kyr BP and one that has already been running for 100 kyr because the Earth's response is dependent upon loading history as well as the instantaneous load (see the section on Isostatic Memory). Because the Earth has undergone a series of glacial cycles, a loading model which accounts for loading and unloading of the Earth during the previous cycle will give more realistic predictions for relative sea level during the cycle of interest. However, the negligible difference between relative sea level predictions from the single cycle, double cycle and 40 kyr models (models 1, 2, and 3 in Table 3-4), for times between 25 kyr BP and the present day, imply that no long-term error is introduced when a model with a later start time is used. It is important to ensure that the shortest possible time steps are used to ensure that the full loading history is captured; failure to do so will miss short time scale fluctuations in ice distribution, leading to a decrease in the accuracy of the relative sea level predictions.

The effect of altering the thickness of ice in the loading model is illustrated in Figure 3-29b and e. There is little difference in the shape and magnitude of predicted relative sea level curves for the 80%, 90% and 100% loading models during the minor glaciation between ~ 65 kyr BP and ~ 50 kyr BP (models 5, 4 and 1 in Table 3-4), but comparing results from the 80% and 100% models at the LGM yields differences of ~ 75 m at Oskarshamn and ~ 100 m at Forsmark. The larger the range of ice thicknesses used, the greater the range of relative sea level predictions, as illustrated by the range of curves for Forsmark. For all the loading models, a greater relative sea level maximum is predicted for Forsmark; the GIA signal here is greater due to its closer proximity to the centre of the former ice sheet.

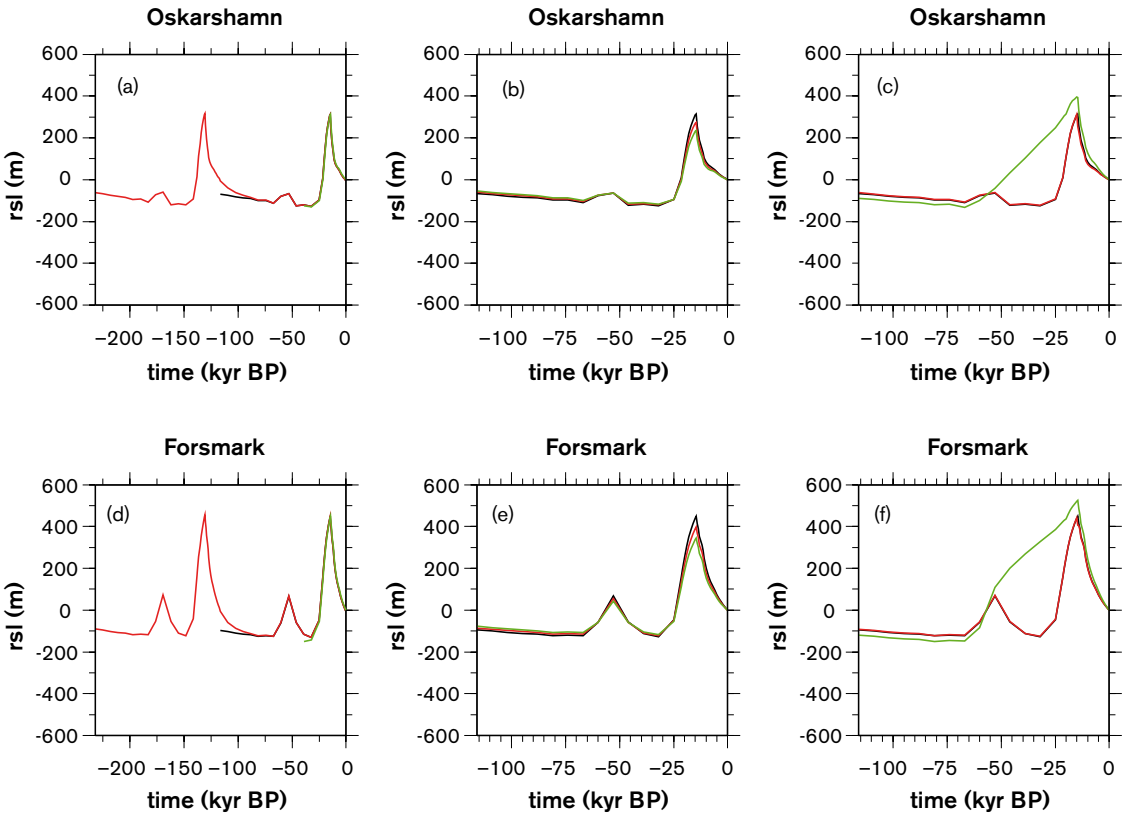

Figure 3-29. *Predicted relative sea level curves for Oskarshamn (including Laxemar) and Forsmark. See Table 3-4 for details of the ice loading models. An Earth model with a thin lithosphere and low upper mantle viscosity has been used in all cases (Model A, Table 3-5). a) and d) black: model 1, red: model 2, green: model 3. b) and e) black: model 1, red: model 4, green: model 5. c) and f) black: model 1, red: model 6, green: model 7.*

The timing of maximum relative sea level is the same for all loading models except that where the timing of deglaciation is brought forwards by 500 years (model 6 in Table 3-4). In this case, maximum relative sea level also occurs 500 years earlier. Apart from this time shift, which decays to zero by the present day, there is otherwise no difference between predictions for this model, and the Weichselian reference glacial cycle simulation. The magnitude of the maximum relative sea level is identical to that predicted by the single cycle, double cycle and 40 kyr loading models (models 1, 2 and 3 in Table 3-4).

In model 7 (Table 3-4), ice thickness is allowed to increase linearly between 60 kyr BP and 20 kyr BP. This model has been developed to test the postulation that there was a continuous ice sheet presence in Fennoscandia during this period /Lundqvist 1992/. The pattern of continuous, linear ice sheet growth is purely an assumption of this model; the maximum thickness of ice in the standard single Weichselian model is never exceeded, but the cumulative effect of loading the Earth for a longer period result in a greater amount of isostatic depression throughout Fennoscandia, and a greater relative sea level maximum. Therefore the GIA signal is not only a function of the thickness and timing of ice loading at a given time, but also the evolution of the loading

The rate of change of relative sea level throughout the glacial cycle is similar for all the loading models except the model where the pattern of ice sheet growth has been markedly altered prior to LGM (model 7 in Table 3-4). However, predictions of present-day uplift rates for the various models do highlight small differences between the models (see Figure 3-30). Uplift rates for the single cycle, double cycle, 40 kyr loading model and the model where the timing of deglaciation is shifted by a small amount are virtually identical. Much lower rates are predicted for the case where only 90% or 80% of the ice thickness is used, although the lateral extent over which rebound occurs is similar to the standard loading models. The final model, where the pattern of ice sheet growth has been altered, yields much greater present-day uplift rates, reflecting the fact that the solid Earth has to rebound from a position of greater isostatic depression at the LGM. In this final case, the area over which rebound is still taking place is greater than that predicted by the other loading models.

Preliminary comparisons between predictions from the GIA model, using the standard Weichselian loading as outlined in Section 3.1 (model 1 in Table 3-4), and observations of relative sea level and present-day uplift rates in Fennoscandia show that the modelling over-predicts the GIA response (see Figures 3-31 and 3-32). One way of making the misfit smaller would be to decrease ice loading, see further below.

Unlike the geological evidence relating to the spatial extent of the Weichselian ice sheet, there exist very few constraints upon the ice sheet thickness, and one explanation for the misfit is that ice thicknesses in the loading model are too large. As pointed out by /Denton and Hughes 1981/, early ice sheet modelling studies of steady-state ice sheets, including their own, produced ice thicknesses that were greater than one would expect from ice sheets during a natural glacial cycle. This has since been confirmed by GIA modelling, showing that those thick ice sheet profiles result in a poor fit to relative sea-level observations. Subsequent dynamical approaches to ice modelling outlined in Section 3.1, including the model used in the present study, produce considerably thinner ice sheets, for example at the LGM. These models yield a closer fit to relative sea level observations when used as an input to GIA models, but there is still a misfit to explain. Some of this difference may be explained by the fact that there are still gaps in our knowledge of basal processes related to, for example, sliding and sediment deformation under ice sheets.

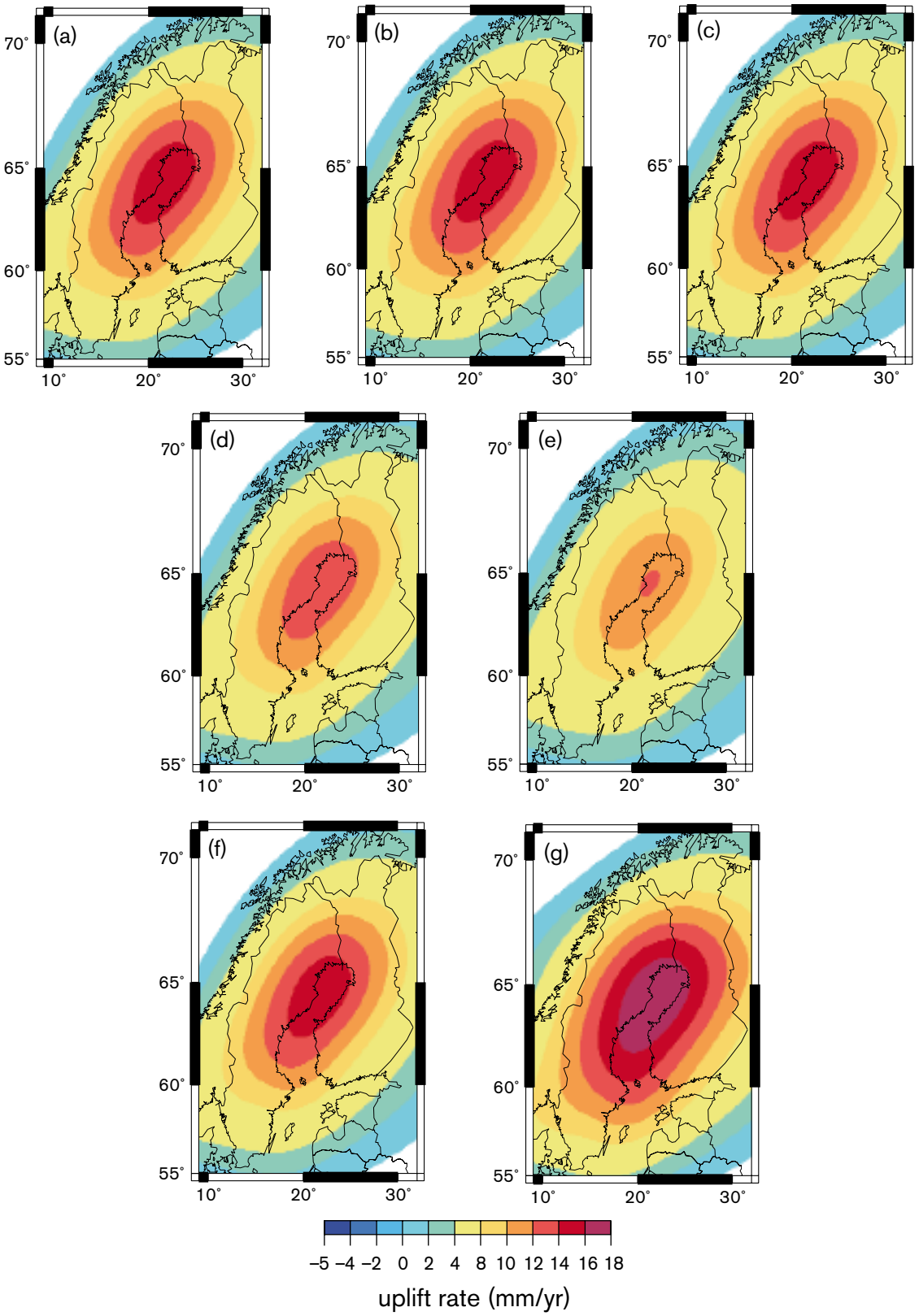

Figure 3-30. *Predicted present-day uplift rates throughout Fennoscandia for the various ice-loading models. See Table 3-4 for details of the loading models. An Earth model with a thin lithosphere and a low upper mantle viscosity has been used in all cases (Model A, Table 3-5). a) Loading model 1. b) Loading model 2. c) Loading model 3. d) Loading model 4. e) Loading model 5. f) Loading model 6. g) Loading model 7.*

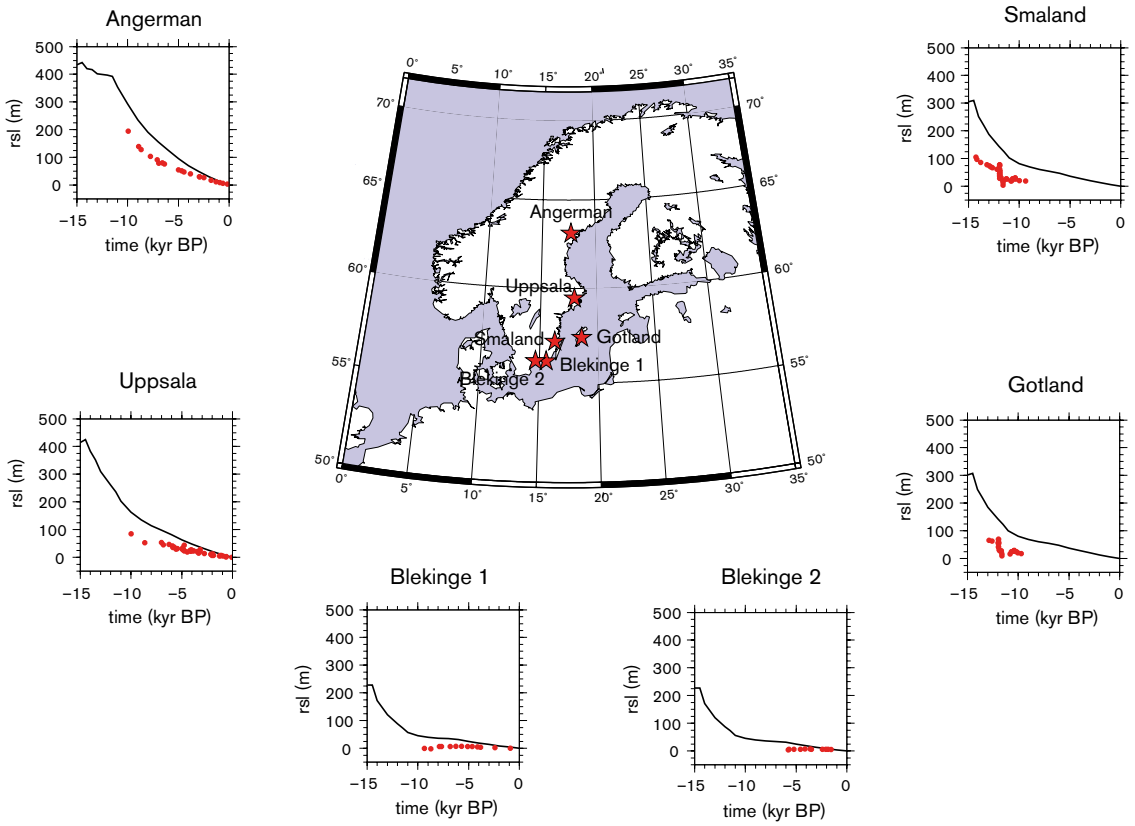

Figure 3-31. *Comparison between predicted relative sea level (black line) and observations from relative sea level markers (red points) at six sites in Fennoscandia for the last 15 kyr. Data compiled from /Lambeck et al. 1998/.*

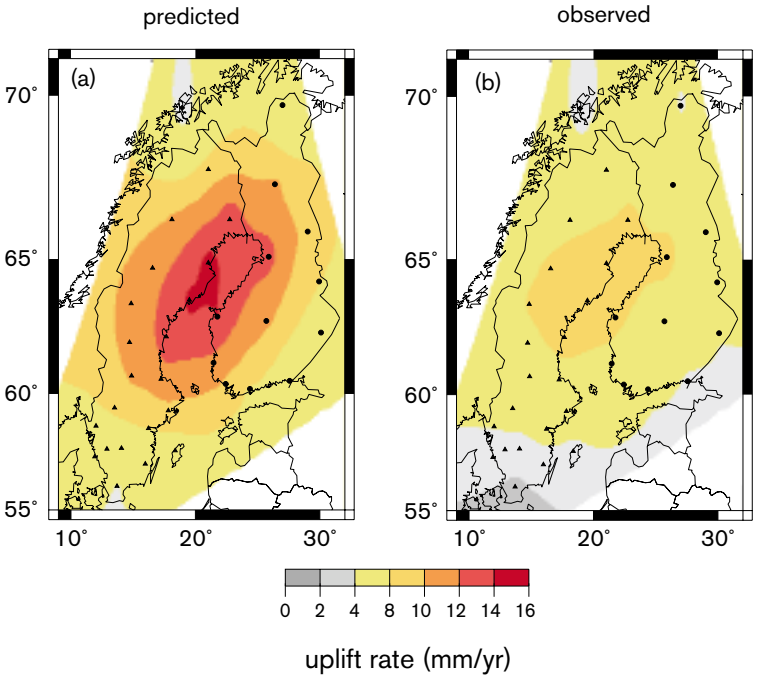

Figure 3-32. *Comparison of predicted and observed present-day uplift rates. a) Predicted present-day uplift rates interpolated at GPS sites (black dots and triangles). Data generated using the standard Weichselian loading model (model 1 in Table 3-4) and an Earth model consisting of a 96 km-thick elastic lithosphere, an upper mantle of viscosity 0.5×10^{21} Pa s, and a lower mantle of viscosity 1×10^{22} Pa s (model A in Table 3-5). b) Observed present-day uplift rates interpolated at GPS sites. Data from the BIFROST project /Johansson et al. 2002/.*

Table 3-5. A summary of the five Earth models considered in this study.

Model	Model description	Lithospheric thickness (km)	Upper mantle viscosity (Pa s)	Lower mantle viscosity (Pa s)
A	Thin lithosphere	96	0.5×10^{21}	1×10^{22}
B	Thin lithosphere, strong lower mantle	96	0.5×10^{21}	4×10^{22}
C	Thick lithosphere	120	0.5×10^{21}	1×10^{22}
D	Thick lithosphere, strong lower mantle	120	0.5×10^{21}	3×10^{22}
E	Thick lithosphere, strong upper mantle	120	0.8×10^{21}	1×10^{22}

Earth rheology

The second main factor governing sea-level change is the Earth model. A three-layer, 1D radial structure is used in these experiments. A discussion of the reasonable joint parameter range for the rheological properties of the lithosphere and mantle can be found in Section 3.3.2. The details of the models used in this investigation are outlined below in Table 3-5.

For all of the loading models considered here, for the majority of the glacial cycle, there is less than ~ 20 m difference in predicted relative sea level across all five Earth models (see Figure 3-33). However during the deglaciation of the Fennoscandian ice sheet, at around 14.5 kyr BP, the difference in predictions for the five Earth models increases to ~ 80 m for Oskarshamn and ~ 100 m for Forsmark. At any one time, differences in geoid height at any fixed point will be negligible if the same loading model is used; any differences in the relative sea level are therefore due to variations in the solid Earth response to loading.

The divergence in the predictions is short-lived, implying that the phenomenon is related to the elastic properties of the lithosphere. In general, an Earth model with a thinner lithosphere will undergo the greatest isostatic deformation, resulting in the greatest relative sea-level prediction. From the results, it also seems that a model with a weaker lower mantle (e.g. models A and C) will undergo greater deformation than one with a stronger, or higher viscosity, lower mantle, while the model with the strongest upper mantle viscosity (model E), exhibits the smallest amount of solid Earth deformation.

Since the differences in relative sea level predictions are short-lived, and very few relative sea-level data are available from this period, we cannot test these predictions against data in order to constrain the Earth parameters, and instead look at present-day uplift rates.

Earth models with a thinner lithosphere (models A and B in Table 3-5) are predicted to experience greater present-day uplift rates, although the extent over which rebound takes place will be slightly smaller than for models with a thicker lithosphere (see Figure 3-34). Earth models with a weaker lower mantle (models A and C in Table 3-5) tend to experience greater present-day uplift rates, over a larger area, than models with the same lithospheric thickness but greater lower mantle viscosity (models B and D respectively in Table 3-5). The existence of a stronger upper mantle (model E in Table 3-5) also increases the predicted rate of uplift.

In reality, the Earth is not laterally homogeneous, and variations in lithospheric thickness and mantle viscosity will perturb the GIA signal. A recent study predicts that for realistic variations in mantle viscosity, present-day uplift rates may be altered by up to 10% /Paulson et al. 2005/. The depth to the Moho varies by a factor of two or more over Fennoscandia /Kinck et al. 1993, Olesen et al. 2002/. The effect of such 3D variations has not yet been quantified.

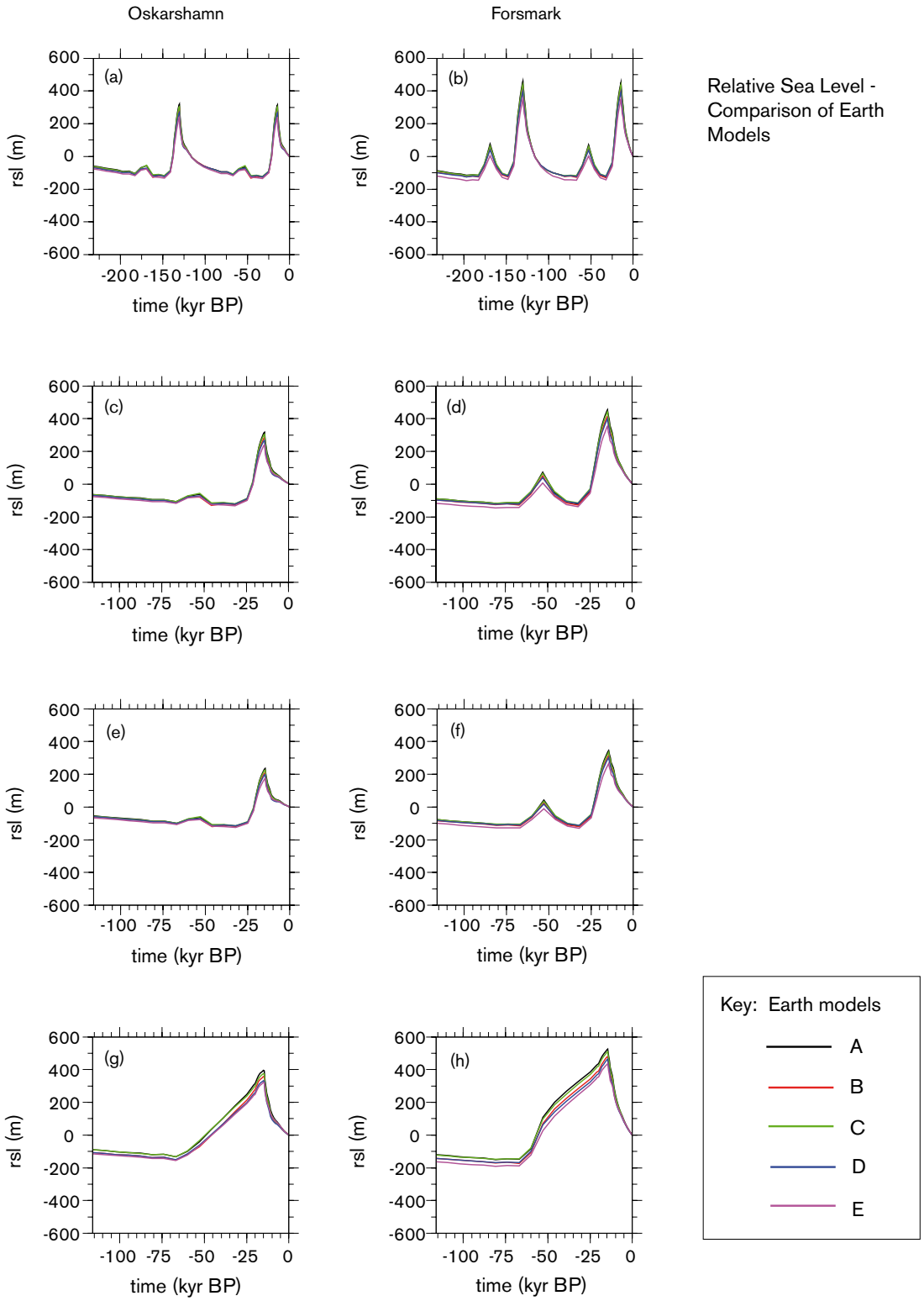

Figure 3-33. *Comparison of Earth models. Predicted relative sea-level curves for Oskarshamn (including Laxemar) and Forsmark for all five Earth models under consideration. See Table 3-4 for details of the loading models. a) and b): Double Weichselian cycle – loading model 2. c) and d): Single Weichselian cycle – loading model 1. e) and f): Single Weichselian cycle with 80% ice thickness in Fennoscandia – loading model 5. g) and h): Single Weichselian cycle with a constant, linear increase in ice thickness in Fennoscandia between 60 kyr BP and 20 kyr BP – loading model 7.*

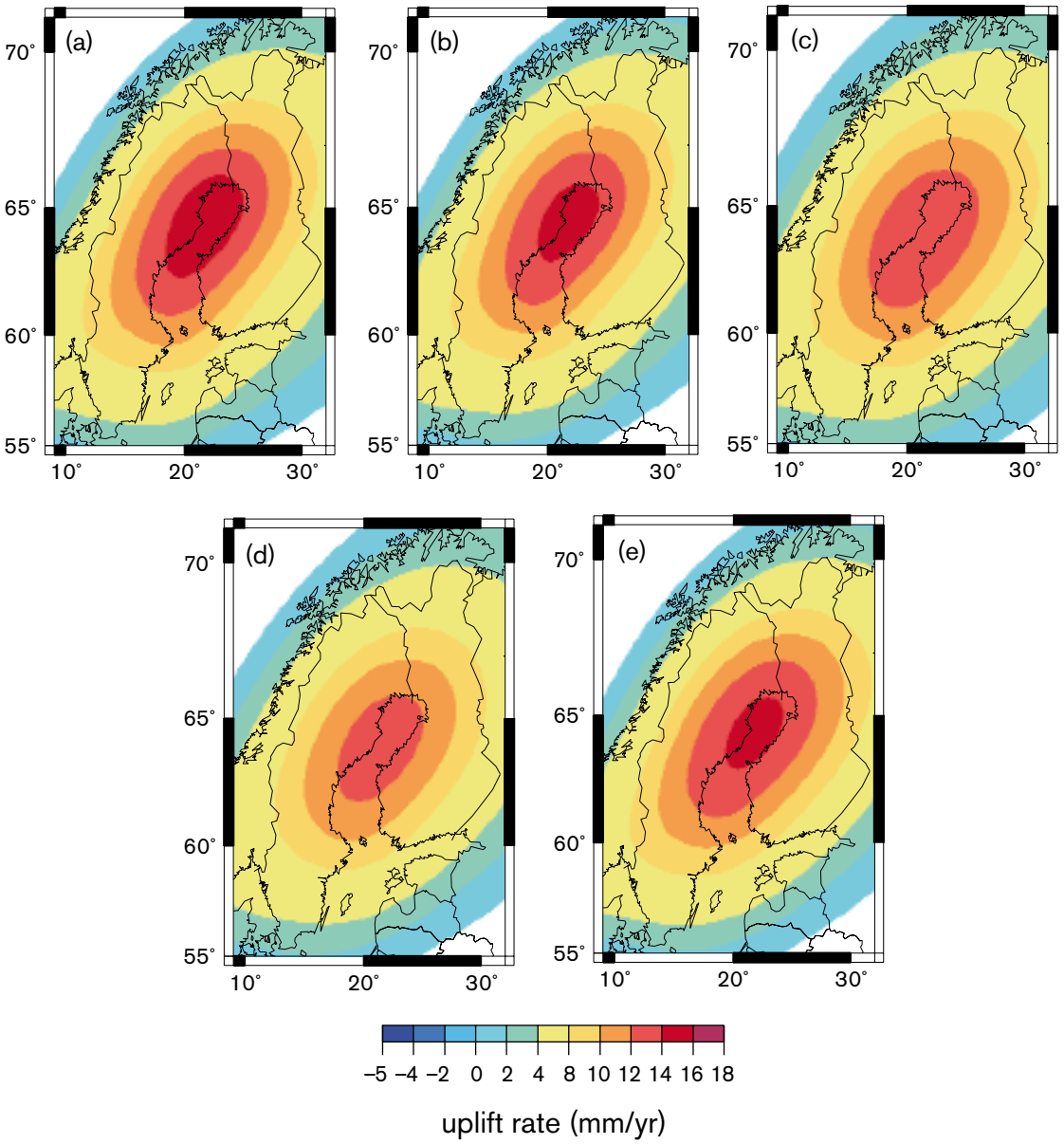

Figure 3-34. *Comparison of Earth models. Predicted present-day uplift rates throughout Fennoscandia for the five Earth models under consideration. The loading model is defined to be a single Weichselian glacial cycle (Model 1) in all cases. a) Earth model A. b) Earth model B. c) Earth model C. d) Earth model D. e) Earth model E.*

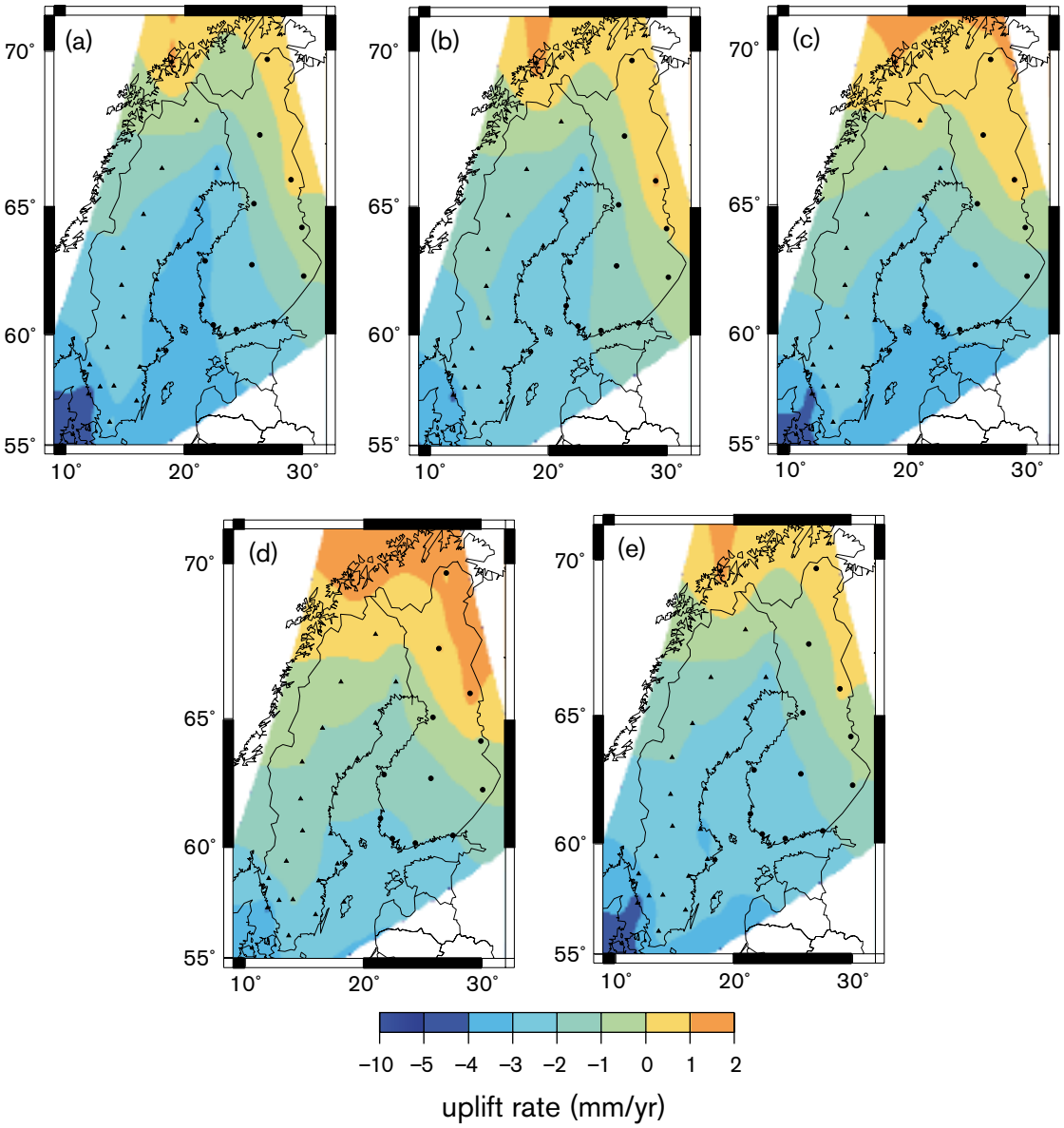

Figure 3-35. *Residual present-day uplift rates throughout Fennoscandia for the five Earth models under consideration. The predictions of Figure 3-34 are interpolated at the BIFROST GPS sites and then subtracted from the observed signal (see Figure 3-36). Loading and earth models as in Figure 3-34.*

Isostatic memory

The time scale over which the GIA model is run has implications for the accuracy of relative sea-level predictions due to the viscous memory of the Earth model. The Earth is assumed to be in isostatic equilibrium at the start of a model run. In reality, the Earth is unlikely to reach such a state if the advance and decay of ice sheets continues with the same periodicity as seen in the past. Therefore, the model must be run for a long enough period that sufficient loading history is considered, and the initial condition of isostatic equilibrium does not affect predictions during the period of interest.

In order to investigate the recovery of the viscoelastic Earth model following unloading four loading models were defined.

- The ‘standard’ model: standard Weichselian loading is applied for a single glacial cycle.
- The ‘double’ model: standard Weichselian loading is applied over two consecutive glacial cycles.

- The ‘40 kyr’ model: standard Weichselian loading is only applied from 40 kyr BP.
- The ‘80%’ model: Weichselian loading with only 80% ice thickness in Fennoscandia is applied for a single glacial cycle.

In all four cases, the loading models were run using three different Earth models (A, C and D in Table 3-5 above), and following the final loading time step at 0 kyr BP the relative sea-level calculations were allowed to run for another 60 kyr into the future without any further change to the distribution of surface loads, thus enabling the system to return to equilibrium.

The vertical solid Earth response was calculated at six sites for each model run. These sites were chosen to lie roughly 250 km apart along a profile running ~ SSE from the present-day centre of isostatic uplift (see Figure 3-36) in order to investigate the solid Earth response at a range of distances from the previous centre of ice loading, and for a range of loading histories.

Deformation at each of the six sites is defined to be zero at the start of the model run. During the experiment, solid Earth deformation at each site is measured relative to the initial position, with negative values indicating a decrease in elevation due to isostatic subsidence. The timing and magnitude of maximum depression is recorded in each case, and when the deflection of the site returns to less than 1% of the maximum deflection, equilibrium is assumed. The isostatic signal at sites 1, 4 and 6 are shown in Figure 3-37, whereas Table 3-6 summarises the results of the model runs.

For a given site and Earth model, there is little variation in the recovery time for the four different loading models. The shortest loading model is initiated only ~ 25 kyr before the timing of maximum deformation, and the difference in solid Earth deformation between this model and the double-cycle loading model is negligible from the timing of maximum deformation onwards (see Figure 3-37). Therefore the isostatic response of the Earth models is not dependent upon loading prior to ~ 25 kyr before the timing of maximum deformation, and a loading model need only contain information from ~ 25 kyr prior to the period of interest to ensure no distortion of the results due to initial conditions.

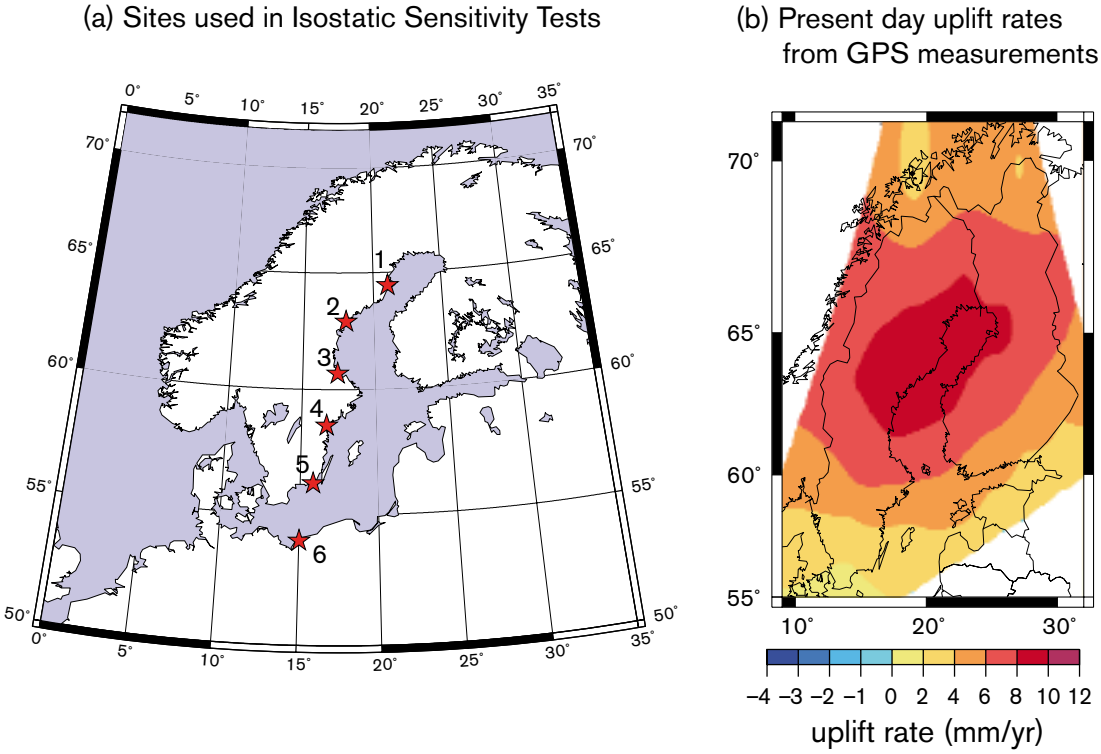

Figure 3-36. *a) Map showing the location of the six sites where the isostatic response is calculated and b) the present-day pattern of uplift in Fennoscandia from BIFROST GPS rates /Johansson et al. 2002/.*

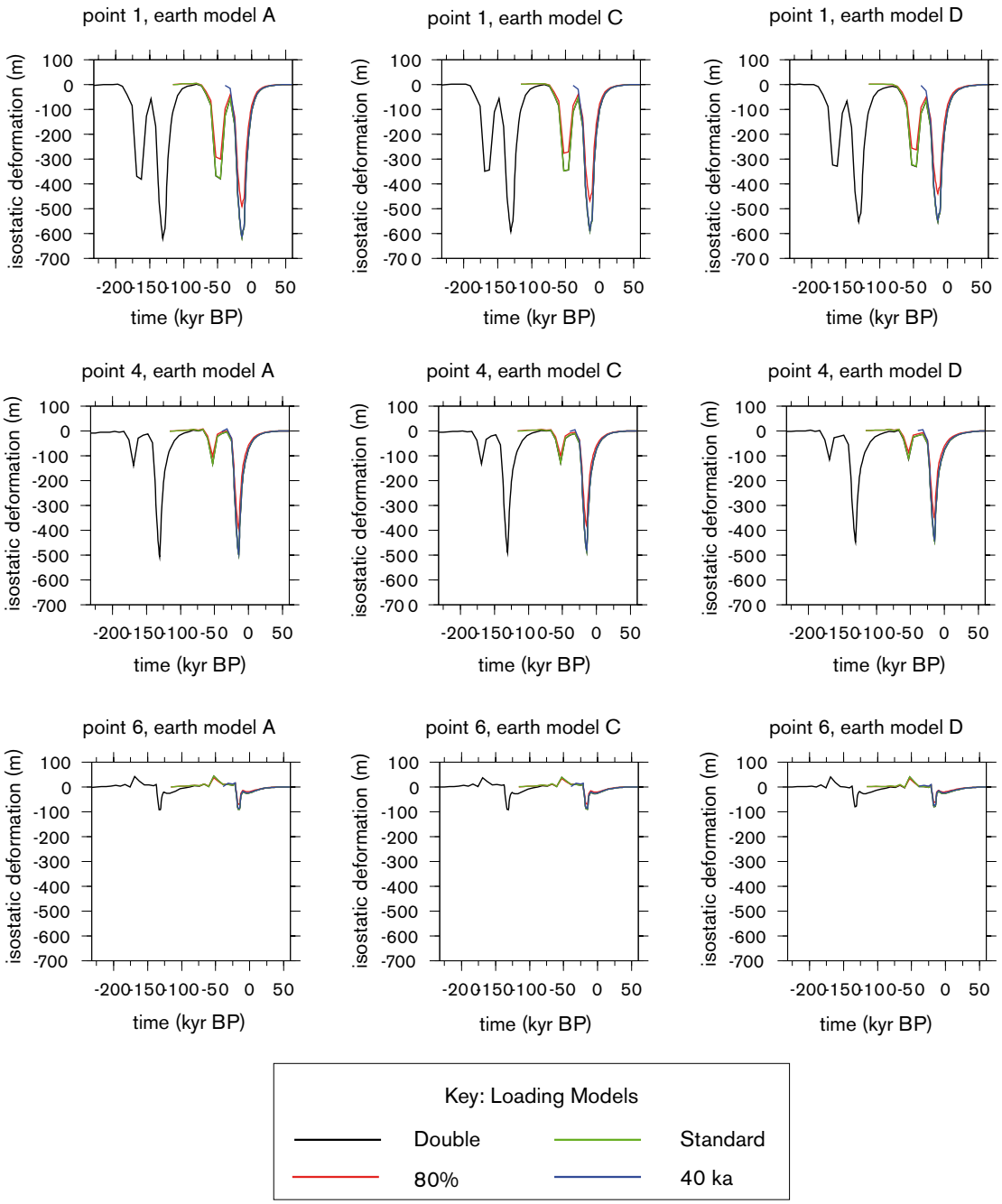

Figure 3-37. *Isostatic recovery sensitivity tests. Solid Earth deformation at sites 1, 4 and 6 (see Figure 3-36) for the four loading models and three Earth models described in the isostatic recovery sensitivity tests.*

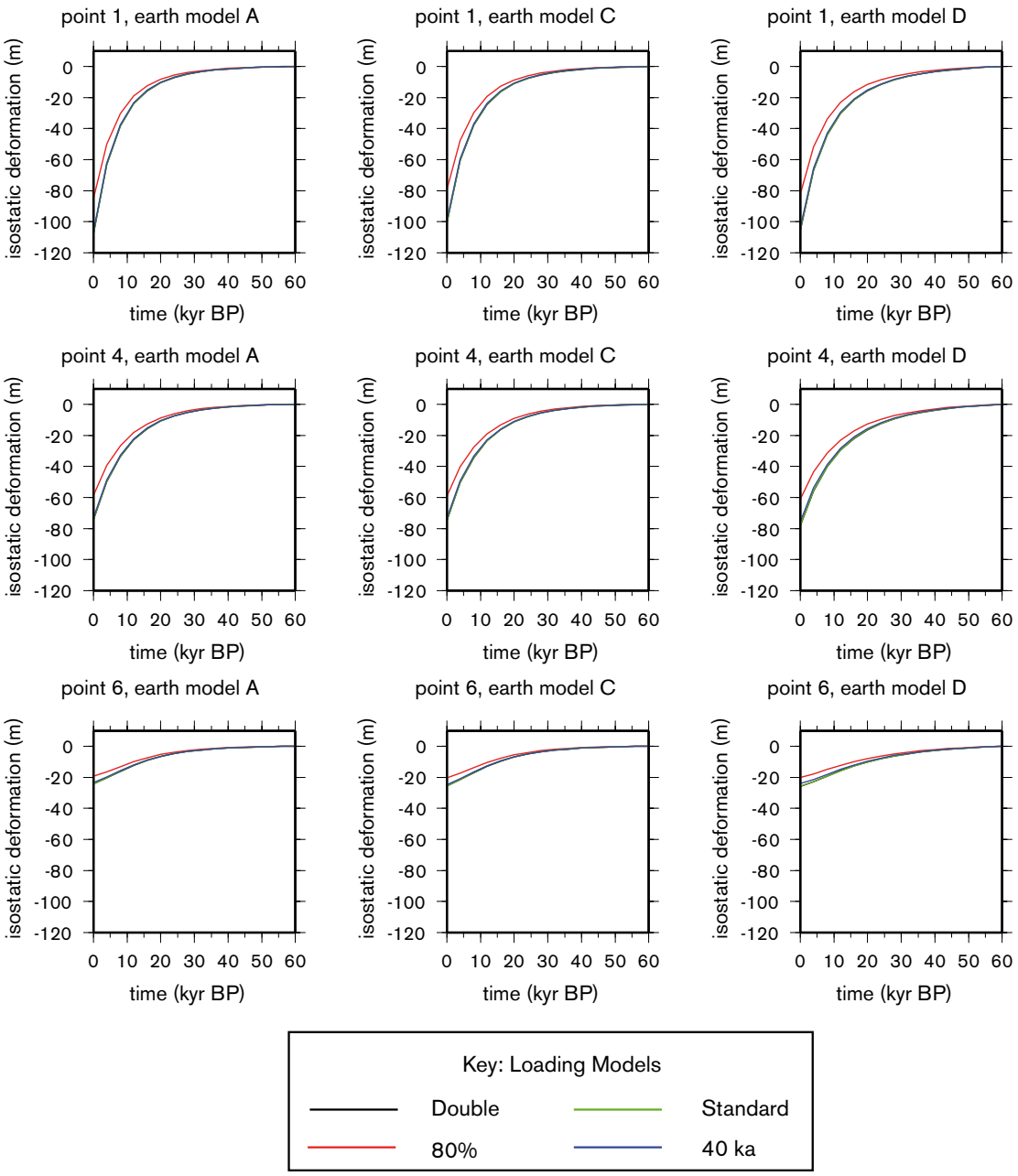

Figure 3-38. *Isostatic recovery sensitivity tests. Predictions of deformation between the present day and 60 kyr in the future. Deformation at the present day may be regarded as the remaining deformation before equilibrium is attained. Other details as for Figure 3-37.*

Table 3-6. Results of the isostatic recovery sensitivity tests. Each triplet of numbers, '(a/b) c', describe the time of maximum depression in kyr BP (a), the time of return to equilibrium in kyr after present (b), and the time take to return to equilibrium in kyr (c = b–a).

Earth model	Loading model	Point 1	Point 2	Point 3	Point 4	Point 5	Point 6
A	40 kyr	(–14.5/28) 42.5	(–14.5/28) 42.5	(–14.5/28) 42.5	(–14.5/32) 46.5	(–14.5/36) 50.5	(–15/44) 59
C	40 kyr	(–14.5/28) 42.5	(–14.5/28) 42.5	(–14.5/28) 42.5	(–14.5/32) 46.5	(–14.5/36) 50.5	(–15/44) 59
D	40 kyr	(–14.5/36) 50.5	(–14.5/36) 50.5	(–14.5/36) 50.5	(–14.5/40) 54.5	(–15/44) 59	(–17/56) 73
A	Standard	(–14.5/28) 42.5	(–14.5/28) 42.5	(–14.5/28) 42.5	(–14.5/32) 46.5	(–14.5/36) 50.5	(–15/44) 59
C	Standard	(–14.5/28) 42.5	(–14.5/28) 42.5	(–14.5/32) 46.5	(–14.5/32) 46.5	(–14.5/36) 50.5	(–15/44) 59
D	Standard	(–14.5/36) 50.5	(–14.5/36) 50.5	(–14.5/36) 50.5	(–14.5/40) 54.5	(–15/44) 59	(–17/52) 69
A	80%	(–14.5/28) 42.5	(–14.5/28) 42.5	(–14.5/28) 42.5	(–14.5/32) 46.5	(–14.5/36) 50.5	(–15/44) 59
C	80%	(–14.5/28) 42.5	(–14.5/28) 42.5	(–14.5/32) 46.5	(–14.5/32) 46.5	(–14.5/36) 50.5	(–15/44) 59
D	80%	(–14.5/36) 50.5	(–14.5/36) 50.5	(–14.5/36) 50.5	(–14.5/40) 54.5	(–15/44) 59	(–17/56) 73
A	Double	(–14.5/28) 42.5	(–14.5/28) 42.5	(–14.5/28) 42.5	(–14.5/32) 46.5	(–14.5/36) 50.5	(–15/44) 59
C	Double	(–14.5/28) 42.5	(–14.5/32) 46.5	(–14.5/32) 46.5	(–14.5/32) 46.5	(–14.5/36) 50.5	(–15/44) 59
D	Double	(–14.5/36) 50.5	(–14.5/36) 50.5	(–14.5/36) 50.5	(–14.5/40) 54.5	(–15/44) 59	(–17/56) 73

Following unloading, the time to reach equilibrium varies between ~ 40 kyr and ~ 75 kyr. This range, and the observation that regions of maximum deformation recover more rapidly, may partly be attributed to the non-linear nature of solid Earth rebound. However, the distribution of relaxation times is principally an artefact of the method by which rebound is calculated: The rebound criterion states that deflection must return to within 1% of the maximum deflection. Therefore regions of greatest deformation seem to recover more rapidly as they only need return to a larger absolute deflection. The positive isostatic deformation at point 6 (Figure 3-37) indicates that this site was uplifted as part of a glacial forebulge prior to being loaded. For all sites, the time for recovery was found to be similar for Earth models A and C, but the model with the stiffer lower mantle (Earth model D) took consistently longer to reach maximum deformation and recover to equilibrium.

The '80%' model was included in this study because it gives the closest fit to present-day uplift rates. However, despite attaining a smaller maximum amount of deformation, the long-term rate of recovery for this loading model is not substantially different from that for models with 100% ice thickness. Therefore, the rate of isostatic recovery is not strongly dependent upon the magnitude of the load, but rather the timing of loading.

Importance of far-field ice sheets

Variations in the far-field Laurentide (North American) and Antarctic ice sheets perturb the shape and height of the global geoid signal, and generate an isostatic solid Earth response. Due to the distance of Fennoscandia from these ice sheets, the geoid signal will effectively be detected as a near-uniform rise or fall in the height of the geoid/ocean surface, dependent upon the surface mass change associated with these far-field ice sheets and distance from these surface masses. The solid surface signal due to far-field ice sheets will only be detectable in Fennoscandia if this region is located upon the forebulge of the deformation, as was the case during the maximum extent of the Laurentide ice sheet during the LGM /Mitrovica et al. 1994b/.

The magnitude of the solid Earth signal due to far-field ice sheet loading was calculated using a standard global ice-loading model for a single glacial cycle /Tushingham and Peltier 1991/ with the ice removed from Fennoscandia during the last glacial cycle. Estimates of horizontal and vertical deformation at the proposed sites of Forsmark and Oskarshamn are shown in Figure 3-39.

The positive sign of the predicted vertical deformation due to far-field ice loading at Oskarshamn and Forsmark (Figure 3-39a and b) indicates that these two sites lay on the deformational forebulge of the Laurentide ice sheet, as predicted by /Mitrovica et al. 1994b/. However, the calculated signal may overpredict reality, due to the neglect of any lateral structure in the Earth model /Latychev et al. 2005b/. The negative sign of the horizontal deformation indicates motion in an easterly direction. The non-zero magnitude of predicted deformation at the present day simply implies that the system has not yet returned to equilibrium following the removal of the far-field ice load.

The vertical deformation peaked at 18kyr BP, coincident with the maximum extent of the Laurentide ice sheet. The steady increase in the signal over time is a result of the gradual growth of the Laurentide ice sheet throughout the last glacial cycle. The magnitude of this deformation reached ~ 25 m for Earth models with a smaller lower mantle viscosity of 1×10^{22} Pa s (models A, C and E), and only ~ 20 m for Earth models with a stronger lower mantle (models B and D). The strong lower mantle models demonstrate a slower, smaller response to loading, and a slower rate of recovery following unloading.

This separation in the style of deformation according to lower mantle viscosity is also seen in the smaller horizontal signal (Figure 3-39c and d). When a stronger lower mantle is assumed, the magnitude of deformation is smaller during the majority of the glacial cycle, except during deglaciation, when the recovery of the solid Earth is delayed by ~ 10 kyr for these models. The reason for this is unclear, but should provide a useful constraint upon lower mantle viscosities when testing predictions against data. In general, horizontal deformation peaks later than vertical deformation; at ~ 14.5 kyr BP for models with a weaker lower mantle, and ~ 4 kyr

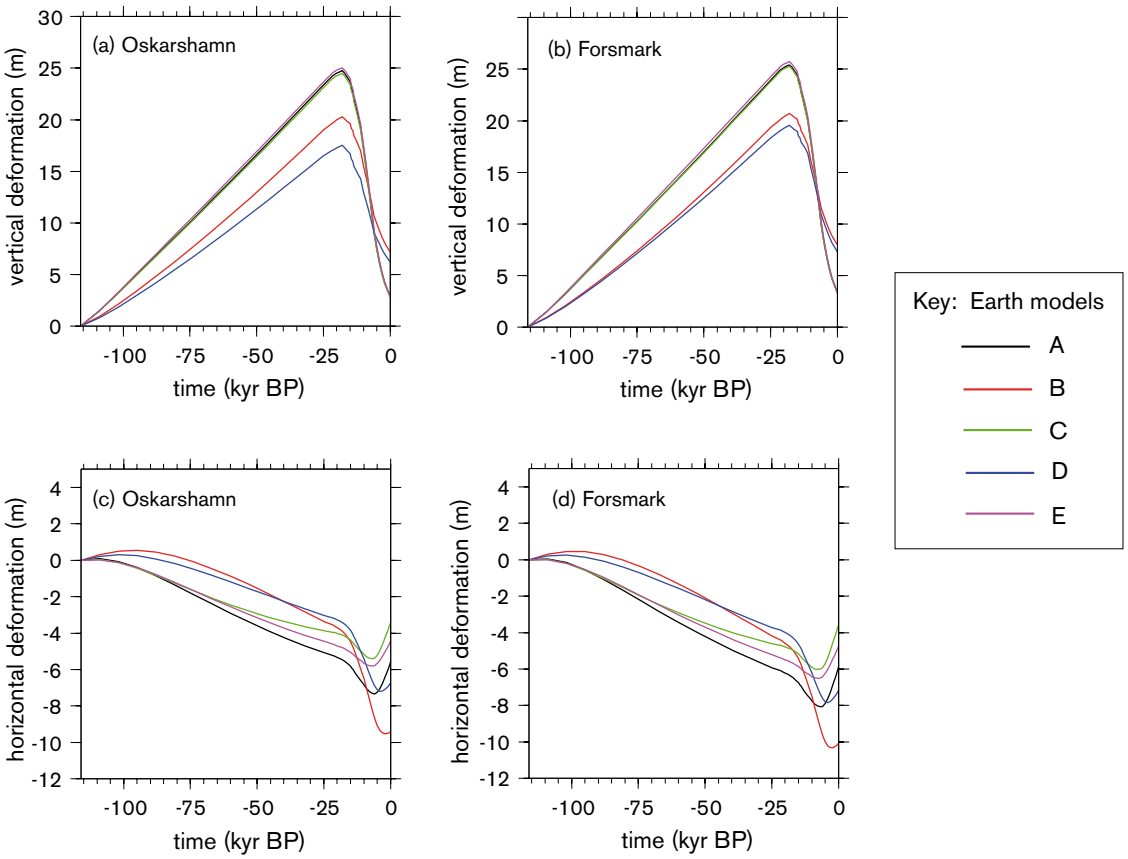

Figure 3-39. *Solid surface deformation due to far-field ice loading. See Table 3-5 for a description of the Earth models used. a) Vertical deformation at Oskarshamn, b) vertical deformation at Forsmark, c) horizontal deformation at Oskarshamn, d) horizontal deformation at Forsmark.*

BP for models with a stronger lower mantle. A greater magnitude of horizontal deformation is predicted for models with a thinner lithospheric thickness of 96 km (as opposed to 120 km), but the absolute magnitude of the difference is small, and this phenomenon is not apparent in the vertical signal.

There is little difference in the deformation predicted at the two sites, indicating that this is truly a far-field signal that will not be dependent upon the small-scale details of ice sheet geometry in the far field. The magnitude of the far-field signal is small in comparison with predictions of near-field isostatic deformation (< 10% of the total signal) during the Weichselian glaciation, but must not be neglected; Even if the Fennoscandian ice sheet does not re-form for many millennia, the presence of a full-scale Laurentide ice sheet could generate a vertical isostatic signal of ~ 25 m throughout Fennoscandia.

The results of these sensitivity tests may be extrapolated to yield predictions for shoreline migration during a glacial cycle. In order to determine the best-fitting ice loading and Earth response models for Fennoscandia, the predictions must be tested against a range of data sets, due to the sensitivity of the parameters to different aspects of the model. There are trade-offs between the different parameters, but differences in the predictions are limited, so it will not be too important to uniquely determine the best-fitting models.

3.3.5 Time perspective

Shoreline migration is an ongoing process. It is strongly coupled to the global distribution of water between the oceans and land-based ice sheets, and the isostatic response of the Earth to loading during a glacial cycle. This isostatic deformation is a slow process in relation to the rate at which ice sheets grow and decay during such a cycle.

As ice sheets grow, water is removed from the oceans and global eustatic sea level falls. During the build-up to the last glaciation, eustatic sea level fell at a mean rate of ~ 1.3 mm/yr between 120 kyr BP and 20 kyr BP /Fleming et al. 1998, Yokoyama et al. 2000, Clark and Mix 2002, Milne et al. 2002, Peltier 2002, Mitrovica 2003/, although there were many departures from this rate during the build-up period, due to higher frequency climatic oscillations /Imbrie et al. 1984, Lambeck et al. 2002, Waelbroeck et al. 2002, Siddall et al. 2003/. During deglaciation, the initial rate of eustatic sea-level rise between ~ 21 kyr BP and 17 kyr BP was only ~ 6 mm/yr, followed by an average rate of ~ 10 mm/yr for the next 10 kyr /Fleming et al. 1998/. Perturbations from this rate occurred during meltwater pulses at ~ 14.5 kyr BP and ~ 11 kyr BP. These are attributed to rapid melting events, during which rates of eustatic sea-level rise reached ~ 15 mm/yr /Fairbanks 1989, Bard et al. 1990, 1996, Clark et al. 1996, Fleming et al. 1998, Lambeck and Chappell 2001, Lambeck et al. 2002, Peltier 2005, Bassett et al. 2005/. Rates of eustatic sea-level change fell to negligible values following the end of deglaciation around 5 kyr BP. However, meltwater is not distributed uniformly throughout the oceans due to the alteration to the shape of the geoid following the redistribution of surface masses. Sea level can actually fall at sites within ~ 20° of a melting ice sheet /Farrell and Clark 1976/, therefore the rate of eustatic sea-level change is a poor indicator of local rates of sea-level change, especially for a local melt source.

The local rate of relative sea-level change incorporates both local changes in sea level and the isostatic deformation of the solid Earth. The balance between rates of isostatic deformation and local sea-level change determine whether a site has advancing or retreating shorelines.

During the final build-up of the Fennoscandian ice sheet from ~ 32 kyr BP, isostatic rates of solid Earth subsidence due to surface loading by ice are estimated to have reached values of 40 mm/yr (see Section 3.3.4). During future glacial cycles, modelling predictions imply that maximum rates will be attained immediately prior to the time of greatest ice thickness. In general, the time of maximum ice thickness is predicted to precede the time of maximum solid Earth deformation, with the latter being delayed by up to ~ 3 kyr. During the period between maximum ice thickness and maximum deformation, the rate of solid Earth subsidence will decrease to zero.

There is usually a delay between the time of maximum deformation and the time at which a location becomes ice-free. Again, modelling predictions imply that as an ice sheet thins, rates of isostatic rebound will be low; < 20 mm/yr for this reconstruction of the Weichselian. Maximum rebound rates occur immediately following the final removal of an ice sheet, with uplift rates reaching ~ 75 mm/yr in this model at sites which had the greatest ice cover. The rate of rebound then decays exponentially with time; maximum rates at the centre of present-day uplift in Fennoscandia are ~ 10 mm/yr, and these are expected to decay to negligible values within the next 30 kyr (see Section 3.3.4).

During a glacial cycle, immediately following the removal of ice, local uplift rates are far greater than the rate of local sea-level changes, consequently a situation of regression dominates, and shorelines migrate oceanwards. The rate of shoreline migration depends upon the local gradient of topography. A typical Swedish Baltic shoreline with a gradient of 2 m of elevation per 1km would experience 35 m/yr of oceanward shoreline migration for an uplift rate of 70 mm/yr, or 5 m/yr of oceanward shoreline migration for an uplift rate of 10 mm/yr (the present maximum in the Baltic), assuming negligible changes in local sea level.

A combination of decreasing rates of isostatic rebound and sea-level rise due to far-field melting slows the rate of regression with time, with a switch to transgression taking place if rates of local sea-level rise exceed the rate of local isostatic rebound. This situation is likely to arise during a global meltwater pulse at sites with low rebound rates, but will not be maintained because melting takes place on a shorter time scale than isostatic rebound. Rebound will once again become the dominant factor governing shoreline migration as sea-level changes become negligible. During the current interglacial period decaying uplift rates persist. These, along with processes related to ocean syphoning (see Section 3.3.1), act to maintain a situation of gradual oceanward shoreline migration throughout the majority of the Baltic for the first few 10 kyr of an interglacial so long as the higher interglacial temperatures do not give rise to a longer-term melting event, such as the destabilization, and subsequent melting, of the Greenland Ice Sheet.

Handling in the safety assessment SR-Can

Isostatic evolution and shoreline displacement have been investigated by means of numerical modelling. In this context, the main question for the safety assessment is whether the studied sites are submerged or not. The salinity in the lake/sea covering the site is also of interest. A Glacial Isostatic Adjustment (GIA) model has been used to simulate shoreline migration. The evolution of the shoreline has been calculated for a glacial-interglacial cycle using a loading function based on the Weichselian reference glacial cycle simulation discussed in Section 3.1. The GIA model used for generating the reference evolution is that developed by Milne /Mitrovica and Milne 2003/. The *global* ice-loading function used in the study is modified from the ICE3G deglaciation history /Tushingham and Peltier 1991/, and has been calibrated using far-field relative sea-level data. An eustatic curve has been used to tune the mass of ice contained within far-field ice sheets. The Earth model is based on Maxwell rheology with a 1D radial three-layer structure. The lithosphere is represented by a 96 km thick layer with a very high viscosity and thus behaves as an elastic medium over GIA time scales, the density and elastic structure are from the preliminary reference Earth model (PREM) which has been determined to a high degree of accuracy by seismic methods /Dziewonski and Anderson 1981/.

At the start of a GIA model run, the Earth is assumed to be in isostatic equilibrium. In reality the Earth is unlikely to reach such a state if glaciations occur with similar periodicity as in the past. To correct for this, the GIA modelling has been initiated by a glacial loading history yielding shorelines comparable to those reported by /Funder et al. 2002/ at the peak of marine inundation in the Early Eemian about 130,000 years ago. This gives shorelines similar to the present at the early phase of the reference glacial cycle. During the first 1,000 years after closure and for the analysis of biosphere and hydrological evolution during the initial temperate domain, the shoreline evolution is extrapolated from shoreline data /Påsse 2001/. For further, detailed information on the Glacial Isostatic Modelling, see the preceding parts of Section 3.3.

3.3.6 Handling of uncertainties in SR-Can

Uncertainties in mechanistic understanding

The processes involved in GIA, and their effect upon shoreline migration, are very well understood. There are no major uncertainties in our understanding of the mechanistic processes which cause shoreline migration.

Model simplification uncertainty

- Discussions of the uncertainty in the calculated shoreline are based on the sensitivity analysis presented above.
- The assumption of a 1D Earth model is a simplification of the situation in Fennoscandia. For example, lithospheric thickness is estimated to range between 80 km in the south-west to > 160 km in the north-east of the region. Preliminary studies indicate that lithospheric and sub-lithospheric lateral variations in Earth structure have a non-negligible effect upon predictions of solid earth deformation in Fennoscandia /Whitehouse et al. 2006/.
- The time discretisation of the basic loading model is fairly coarse (every 7 kyr) between 116 kyr BP and 21 kyr BP, reflecting the lack of constraints upon ice history and sea level prior to the LGM. If long time steps are used the loading function may be under- or over-estimated, leading to inaccuracies in relative sea level, and hence shoreline migration, predictions for this period. A higher time resolution has been investigated, and discrepancies in relative sea-level predictions may vary by up to 50 m between a model which uses a time step of 7 kyr and one which uses a time step of 1 kyr, during periods of rapid change in ice sheet geometry. However, using a coarse time scale during the early stages of a model run has a negligible effect upon predictions of relative sea-level change during the latter stages of a model run. A high resolution time scale has been used for ice loading since the LGM, i.e. for the period when ice history is known reasonably accurately.
- At the beginning of a model run, the Earth is assumed to be in a state of isostatic equilibrium, with no deformation remaining from a previous glacial cycle or any other process which upsets the isostatic balance of the system. In reality, as the Earth enters each glacial cycle it will be pre-stressed, with deformation ongoing as a result of the previous loading event. GIA-induced deformation decays over a few tens of thousands of years, and after this period there will be a negligible difference between predictions from a model which started from equilibrium and one which was pre-stressed. However, in order to reproduce the relative sea-level evolution for the Weichselian as closely as possible the model was run twice in succession, with the second run taken to represent the Weichselian scenario. A small degree of inaccuracy remains at early times in the model since deformation will depend upon the details of the Saalian deglaciation, about which very little is known.

Input data and data uncertainty

As demonstrated by the similarity of the shoreline predictions for a range of rheological parameters in Section 3.3.4, uncertainties in the lithospheric thickness and mantle viscosity parameters are currently significant. The values of such parameters will be more tightly constrained following detailed analysis of the results of the GIA modelling in comparison with relative sea level and GPS data.

3.4 Development of permafrost

3.4.1 Overview/general description

Permafrost is defined as ground which remains at or below 0°C isotherm for at least two years /French 1996/. This definition is based exclusively on temperature, and disregards the texture, degree of compactation, water content, and lithologic character of the material. As a result, the term *permafrost* does not always equate to *perennially frozen ground*, since depending on pressure and composition of groundwater and on adsorptive and capillary properties of ground matter water in ground freezes at temperatures below 0°C. Therefore, permafrost encompasses the perennially frozen ground surrounded by a *cryopeg*, i.e. a ground layer in which water remains unfrozen at sub-zero temperatures. Furthermore, "dry" permafrost results when water is absent.

Permafrost occurs in the permafrost domain as defined in Section 1.3.3, and in cases also beneath an ice sheet as *subglacial permafrost* in the glacial domain. Permafrost originates from the ground surface depending on a complex heat exchange process across the atmosphere/ ground boundary layers and on an almost time-invariant geothermal heat flow from the Earth's interior due largely to radioactive decay of long-lived isotopes of uranium (U), thorium (Th) and potassium (K). The heat exchange between the atmosphere and the Earth's surface can be expressed by the following heat balance equation /Lockwood 1979, Washburn 1979, Lunardini 1981, Williams and Smith 1989, Smith and Riseborough 1996, Yershov 1998/:

Equation 3-11 $$Q^* + Q_H + Q_{LE} + Q_G = 0$$

where Q^* represents the net radiation heat flux due to shortwave solar radiation, and longwave terrestrial and atmospheric radiation, Q_H is the sensible heat flux due to turbulent heat exchange, Q_{LE} the latent heat production/loss due to evaporation/condensation and Q_G the terrestrial heat flux due to conduction and convection. The heat exchange depends on climate conditions and their long-term, annual and diurnal variation, as well as on surface conditions such as snow cover, vegetation, topography, soil characteristics and presence of water bodies, see further Section 3.4.2.

Ground temperature that defines the presence of permafrost is principally controlled by the ground thermal energy balance, which can be presented in the following form:

Equation 3-12 $$\mathrm{div}\,\vec{q} + C\frac{\partial T}{\partial t} + \frac{\partial L}{\partial t} = A$$

where $\vec{q}$ is the general heat transfer vector and C the volumetric heat capacity of the ground, T is the ground temperature, L the volumetric latent heat production/loss of phase change processes of water and A the volumetric internal heat generation due to radioactive decay of U, Th and K-isotopes in the bedrock. The evolution of ground temperature depends mainly on heat conduction properties, specific heat content and geothermal heat production of the ground and on the amount heat generated by the phase change processes which are discussed further in Section 3.4.2.

Freezing of water within permafrost is based on the thermodynamics of interdependent thermal, hydraulic, mechanical, and chemical processes in the ground. In addition, freezing of water influences the thermal, hydraulic, mechanical, and chemical behaviour of the ground. Thermal properties change from those of unfrozen ground to those of frozen ground, affecting the heat transfer process. Ice formation in pores of the ground confines groundwater flow through the almost impermeable frozen ground, therefore altering the overall groundwater circulation. Ice formation can also cause deformations of the ground and changes in the mechanical stress state and lead to break down of the ground at shallow depths. Frost weathering and degradation of the ground surface and patterned ground are further consequences of cyclic freezing and thawing processes. Moreover, exclusion of salts in the freezing of saline groundwater can lead to increases in salinity concentrations in the cryopeg.

Issues associated with permafrost development in the geosphere are comprehensively explained in /Washburn 1979, Williams and Smith 1989, French 1996, Yershov 1998/ and reviewed in /Gascoyne 2000, Ahonen 2001, Vidstrand 2003/. Table 3-7 summarises how geosphere variables are influenced by permafrost development.

3.4.2 Controlling conditions and factors

Climate and surface conditions

The principal factors controlling the heat exchange between the atmosphere and the Earth's surface, and hence the ground surface temperature and development of permafrost, are climate, topography, vegetation and snow covers, soil characteristics and water bodies. These factors are mutually dependent and can vary considerable in time and location.

The main climatic parameters are insolation, air temperature, wind, and precipitation. Insolation is a driving force governing the heat exchange between the atmosphere and the Earth's surface and affecting the other climatic parameters. Air temperature, which is commonly applied to map permafrost distribution, controls the longwave atmospheric radiation, the turbulent heat exchange, and evaporation and condensation. Wind in turn influences mostly the sensible heat

Table 3-7. Influence of permafrost development on geosphere variables.

Geosphere variable	Influenced by climate issue variable/s	Summary of influence
Temperature	Permafrost depth	Permafrost is by definition a thermal condition hence having no influence on temperature.
Groundwater flow	Frozen/unfrozen fraction of groundwater	Freezing occurs at temperatures below the freezing point /**Geosphere process report**/. Groundwater transformed from liquid to solid phase can be regarded as immobile. Filling fractures and pores, ice also affects the groundwater flow through permeability, which decreases exponentially with a reduction in the unfrozen fraction of groundwater.
Groundwater pressure	Frozen/unfrozen fraction of groundwater	The volume increase in the phase change of water from liquid to solid causes an increase in the pressure of water which remains liquid. Moreover, freezing of water in porous ground matter can lead to cryosuction and depression of groundwater pressure in the unfrozen ground.
Groundwater composition	Frozen/unfrozen fraction of groundwater	When saline water is transformed from liquid to solid phase, the solutes present are not incorporated in the crystal lattice of ice but transferred in the liquid phase. Therefore the salinity in the unfrozen fraction increases /see **Geosphere process report**/.
Rock stresses	Frozen fraction of groundwater	Deformations due to ice formation will lead to changes in rock stresses. The effect of the changes is strongest nearest to the surface where the in situ stresses are lowest.
Fracture geometry	Frozen fraction of groundwater	Freezing can have some influence on the fracture geometry at shallow depths due to the frost cracking. Close to the surface frost wedges can be formed to the depth of some metres. Otherwise, there can be widening of fractures due to freezing but the effect is probably reversible as thawing takes place.

exchange, but also latent heat production and loss. Precipitation together with evaporation and condensation determine groundwater recharge affecting the groundwater content and flow and hence the terrestrial heat flux.

Topography has a significant impact on climate conditions. Generally, air temperature decreases with altitude by about 0.4−0.6°C per 100 m /Yershov 1998/. Furthermore, the slope angle and azimuth affect the flux of shortwave radiation, and where topographical differences are large, a more patchy distribution of permafrost can be expected.

Vegetation and snow covers are sensitive to climatic conditions and topography. The characteristic parameters of the surface cover are surface albedo, emissivity, and roughness controlling the incoming shortwave radiation, the longwave terrestrial radiation and the turbulent heat exchange, respectively, as well as the thermal properties and the thickness of the surface cover affecting terrestrial heat transfer. In general, the surface covers moderate the ground temperature and thus the aggradation of permafrost. Vegetation is an insulating cover limiting cooling in winter and warming in summer, hence reducing the annual fluctuation of ground temperature. Vegetation is also important for the creation of snow cover, which protects the ground from heat loss in winter. However, the high albedo of snow can lead to a snow surface temperature ~ 0.5−2°C lower than the mean winter air temperature /Yershov 1998/. As a rule, for a majority of the surface covers, depending on the climatic conditions and topography, permafrost can build from the ground surface if the annual mean air temperature lower than a value ranging between –9 and –1°C /Washburn 1979, Williams and Smith 1989, French 1996, Yershov 1998/. An exception occurs with peat layers, which can insulate the ground from warming in summer more effectively than from cooling in winter, with the resulting effect that permafrost can exist when the mean annual air temperature is actually above 0°C /Williams and Smith 1989/.

Properties and thickness of the soil cover affect the terrestrial heat flow. Of importance are the porosity and water content of the soil, influencing the annual fluctuation of ground temperature and the thickness of the active layer, i.e. the seasonally thawing ground layer. The soil cover acts also as an insulating cover, since the thermal conductivity of the soil cover is lower than that of the underlying bedrock.

Water bodies, i.e. the sea, lakes, and watercourses, because they have a high specific heat content, influence permafrost creation and distribution considerably. A talik, i.e. an unfrozen layer, can exist beneath water bodies that do not freeze to their bottom in winter. Depending on the characteristics of the climatic zone, the critical depth of a water body to remain unfrozen in winter is approximately 0.2−1.6 m /Yershov 1998/. Sea water extensively reduces the development of costal permafrost. On the other hand, when the shoreline of a highly saline sea is rising, submerged permafrost and perennially frozen deposits can survive for a long time beneath a cold seabed /Washburn 1979, Yershov 1998/.

Hydraulic surface conditions are important for the freezing of groundwater. Especially in the glacial domain, a warm-based overlying ice sheet can increase the subglacial groundwater pressure ~ 2 orders of magnitude, in which case the freezing point can decrease to such a degree that the subglacial ground is kept unfrozen. A similar, but minor, effect can occur when cold ground is submerged and submarine freezing is reduced by the pressure of the sea water. Furthermore, groundwater flow, whether carrying fresh glacial meltwater or saline seawater, can influence the freezing process by altering the groundwater composition.

Subsurface and repository

Heat transfer within the ground can occur through conduction, convection and radiation /Sundberg 1988/. In general, only conduction is viewed as important to permafrost evolution, since radiation is of importance only in unsaturated high-porosity ground at high temperatures, and convection is of importance only when groundwater and gas fluxes are large.

Heat conduction depends on the ground temperature gradient, ambient temperature conditions, and thermal properties of the ground matter. Thermal conductivity, describing the ability of

material to transport thermal energy, and heat capacity characterising the capability of material to store heat, depend on a number of variables such as mineralogy, porosity and groundwater content. Having typically 3−4 times higher conductivity than other common rock forming minerals, quartz is the most important mineral for determining thermal characteristics in native rock materials. Freezing of water has a minor effect on heat transfer in water-saturated ground when the porosity is less than 1%. The degree of saturation has relevance to the thermal properties of ground due to the very low thermal conductivity and heat capacity of air, e.g. the thermal conductivity of 1%-porosity granite can decrease by over 10% with decreasing saturation /Clauser and Huenges 1995/. In rocks, heat capacity is not very dependent on ambient temperature and pressure conditions, whereas thermal conductivity is a rather variable function of both temperature and pressure. The thermal conductivity of granite decreases with increasing temperature by approximately 5−20% per 100°C and increases with increasing pressure by about 1−2.5% per 100 MPa /Seipold 1995/. The pressure dependence of thermal conductivity is increased when rocks are unsaturated /Sundberg 1988, Clauser and Huenges 1995/. Moreover, /Allen et al. 1988/ have reported observations of a strong correlation between lithology and permafrost depth, which could be directly explained by differences in thermal conductivity.

The heat flow from the interior towards the Earth surface varies from place to place and combines effects of mantle heat flow and radioactive decay of elements in the crustal rocks. /Näslund et al. 2005/ have made a detailed compilation of heat flow density in the Fennoscandian Shield (see Section 3.1), which has been used in modelling of ice sheet evolution and ice sheet basal conditions.

In addition to the thermal properties above, the geohydro-chemical and mechanical properties of ground important for freezing of groundwater are permeability, porosity, adsorptive capacity of ground matter, chemical composition of groundwater and deformation properties of the ground.

Also, the spent nuclear fuel will generate heat with an exponentially decreasing rate for a considerable amount of time. This heat will warm up the surrounding bedrock /**Geosphere process report/** and act to reduce the thickness of permafrost near the repository.

3.4.3 Observations in nature and present-day natural analogues

Approximately 25% of the total continental land area of the Earth is occupied by permafrost in continuous, discontinuous, sporadic, and subglacial forms. About one fifth of this permafrost is subglacial in Antarctica and Greenland. Permafrost is abundant in Alaska, the northern parts of Canada and Russia, and in parts of China /French 1996/. Along the coast of southern and south-western Greenland both continuous and discontinuous permafrost can be found /Mai and Thomsen 1993/.

Furthermore, permafrost can frequently be observed in mountainous terrain. For example, in the area of Tarfala in the Kebnekaise massif in northern Sweden, the discontinuous permafrost has been reported to be 100−350 m thick at an altitude above 1,500 m /King 1984, Isaksen et al. 2001/. In the Jotunheimen massif, southern Norway, the permafrost depth is between 100 and 200 m at an altitude of 2,200 m.

The deepest known permafrost occurs in the central part of Siberia in Russia, where thicknesses of up to 1,500 m have been reported /Fotiev 1997/. The extensive region of continuous permafrost in central Siberia corresponds to areas that are believed not to have been covered by Quaternary ice sheets and that have experienced cold climate conditions over a very long time.

SKB, together with co-funding parties from Finland (Geological Survey of Finland and Posiva), Great Britain (UK Nirex Ltd) and Canada (Ontario Power Generation and University of Waterloo), has carried out a research project on permafrost at the Lupin gold mine in northern Canada /Ruskeeniemi et al. 2002, 2004/. In this area, the depth of the permafrost extends to ~ 500−600 m. The main objective of the project is to provide data describing the subsurface conditions in a permafrost area with crystalline bedrock. Permafrost depth, temperatures, groundwater composition and hydraulic properties have been measured.

The mean annual air temperature at this site is −11°C and the annual mean precipitation is low; ~ 270 mm /Ruskeeniemi et al. 2002/. Based on a seismic refraction survey, the depth of the active layer has been interpreted to be ~ 1.5 m, varying between 1.2 and 1.8 m. The present permafrost depth is believed to have been developed over the last 5,000 years.

In the Lupin area, all shallow lakes freeze down to the bottom during winter. Lakes deeper than 2–3 m are expected to have unfrozen bottoms all year. The latter lakes may have the potential to support closed taliks. The large Lake Contwoyto, located about 1,300 m from the mine at surface, provides the most significant talik structure which may extend through the deep permafrost. However, direct observations beneath this lake are lacking.

In order to investigate the distribution of permafrost and locate salinity differences in the deep groundwaters, a number of electromagnetic soundings were conducted in the Lupin mine area. Furthermore, drillings were made from the deeper parts of the mine through the base of the permafrost, in order to sample groundwaters and to study the distribution of open fractures and hydraulic conditions.

The main result of the electromagnetic sounding surveys were anomalies forming a sub-horizontal layer at the depths between 400 and 700 m. /Paananen and Ruskeeniemi 2003/ made the interpretation that this conducting layer represents saline or brackish water at the base of the permafrost. According to the temperature measurements made in the mine, the base of permafrost occurs at a depth of 540 m. The drillings revealed the existence of a ~ 100 m thick unsaturated or dewatered zone below the permafrost. An alternative interpretation of the subhorizontal conductor at ~ 650 m depth could be that it represents the groundwater table /Ruskeeniemi et al. 2004/. The dry zone below the permafrost could either be a natural result of very limited recharge through the permafrost or an effect of mine drainage. No pressurised water or gas flow was observed in the boreholes. The available data from water sampling does not provide any evidence of highly saline water below the permafrost /Ruskeeniemi et al. 2004/.

3.4.4 Model studies

The purpose of the model studies is to analyse the main factors of importance for the development of permafrost and perennially frozen ground.

The permafrost model includes mathematical expression for freezing and thawing of saline groundwater-saturated bedrock. The bedrock is considered as an elastic porous medium and the groundwater as an ideal solution of water and ionic solvents. The model is based on the principles of continuum mechanics, macroscopic thermodynamics and the theory of mixtures being capable of describing heat transfer, freezing of saline water, groundwater flow and deformations of bedrock. The transport of solutes, however, is excluded from the model at the moment. A description of the model can be found in /Hartikainen 2004/. A detailed account of the numerical permafrost modelling is presented in /Hartikainen, in prep./.

To capture the most important factors and parameters affecting the development of permafrost, sensitivity analyses have been performed considering the following issues:

- Surface conditions.
- Subsurface conditions.
- Presence of the repository.

Surface temperatures, together with the influence of surface covers such as snow, vegetation and water bodies, have been included as factors of importance in the surface conditions. The investigated subsurface conditions are thermal properties of the bedrock and interior Earth conditions affecting geothermal heat flow. The heat generated by the spent fuel has been considered in the presence of repository case. The calculations were carried out in two steps; 1) by using constant surface temperatures, and subsequently 2) using surface temperatures based on site-specific climate scenarios.

The first task in the sensitivity analysis of surface conditions was to investigate the ground surface temperatures required to reach different permafrost depths. A set of constant mean annual ground surface temperatures were assumed and applied to a 1-D subsurface model based on present-day reference data for Forsmark and Laxemar (Table 3-8 and 3-9, Figure 3-40). The subsurface temperatures at depths outside the range of site investigations (Figure 3-40) were modelled as glaciation cycle-mean temperatures for individual subsurface conditions /Hartikainen 2006/. In addition, the surface geothermal heat flow data have been corrected for palaeoclimatic impacts, mainly due to the warm period of Holocene, according to /Balling 1995/.

Table 3-8. Site-specific reference physical properties and conditions of rock mass and groundwater at Forsmark, mainly from site description model Forsmark 1.2 /SKB 2005a/.

Rock mass							
Thermal properties							
Parameter	**Unit**	**Reference**	**Min**	**Max**	**Temperature dependency**		
Thermal conductivity	W/(m·K)	3.6	3.2	4.0	11.0% decrease/100°C increase		
Heat capacity	MJ/(m^3·K)	2.3	2.1	2.5	27.5% increase/100°C increase		
Thermal diffusivity	mm^2/s	1.57	1.28	1.9	38.6% decrease/100°C increase		
Interior earth conditions by depth							
		0 m			**10,000 m**		
Parameter	**Unit**	**Reference**	**Min**	**Max**	**Reference**	**Min**	**Max**
Geothermal heat flow	mW/m^2	59.0	48.0	65.0	43.2	41.7	46.0
Radiogenic heat prod.	µW/m^3	2.5	1.0	3.0	0.92	0.37	1.1
Reference temperature conditions by depth							
Parameter	**Unit**	**400 m**	**500 m**	**600 m**			
Temperature	°C	10.6	11.7	12.8			
Temperature gradient	°C/km		11.0				
Reference hydro-mechanical properties by depth							
Parameter	**Unit**	**100 m**	**200 m**	**300 m**	**≥ 400 m**		
Bulk density	kg/m^3	2,700	2,700	2,700	2,700		
Young's modulus	GPa	74	74	74	74		
Poisson's ratio	–	0.26	0.26	0.26	0.26		
Kinematic porosity	–	0.00001	0.00001	0.00001	0.00001		
Total porosity	–	0.0001	0.0001	0.0001	0.0001		
Permeability	m^2	$1.0\cdot10^{-13}$	$1.0\cdot10^{-15}$	$1.0\cdot10^{-17}$	$1.0\cdot10^{-18}$		
Groundwater							
Reference salinity concentrations by depth							
Ionic solvent	**Unit**	**10 m**	**100 m**	**300 m**	**500 m**	**≥ 1,000 m**	
Na^+	g/m^3	65	500	2,000	2,000	2,000	
Ca^{2+}	g/m^3	60	250	1,200	1,000	3,500	
Cl^-	g/m^3	15	1,300	5,500	5,500	10,000	
SO_4^{2-}	g/m^3	20	170	500	400	50	

Table 3-9. Site-specific reference physical properties and conditions of rock mass and groundwater at Laxemar, mainly from site description model Laxemar 1.2 /SKB 2006ab/.

Rock mass

Thermal properties

Parameter	**Unit**	**Reference**	**Min**	**Max**	**Temperature dependency**
Thermal conductivity	W/(m·K)	2.75	2.4	3.1	2.6% decrease/100°C increase
Heat capacity	MJ/(m^3·K)	2.2	2.0	2.4	28% increase/100°C increase
Thermal diffusivity	mm^2/s	1.25	1.0	1.55	30.6% decrease/100°C increase

Interior earth conditions by depth

		0 m			**10,000 m**		
Parameter	**Unit**	**Reference**	**Min**	**Max**	**Reference**	**Min**	**Max**
Geothermal heat flow	mW/m^2	63.0	52.0	68.0	44.0	39.4	45.9
Radiogenic heat prod.	µW/m^3	3.0	2.0	3.5	1.10	0.74	1.29

Reference temperature conditions by depth

Parameter	Unit	400 m	500 m	600 m
Temperature	°C	12.1	13.8	15.5
Temperature gradient	°C/km		15.0	

Reference hydro-mechanical properties by depth

Parameter	**Unit**	**100 m**	**300 m**	**500 m**	**700 m**	**≥ 900 m**
Bulk density	kg/m^3	2,700	2,700	2,700	2,700	2,700
Young's modulus	GPa	80	80	80	80	80
Poisson's ratio	–	0.27	0.27	0.27	0.27	0.27
Kinematic porosity	–	0.00001	0.00001	0.00001	0.00001	0.00001
Total porosity	–	0.005	0.005	0.005	0.005	0.005
Permeability	m^2	$1.62 \cdot 10^{-14}$	$8.23 \cdot 10^{-15}$	$8.82 \cdot 10^{-16}$	$2.21 \cdot 10^{-16}$	$1.16 \cdot 10^{-16}$

Groundwater

Reference salinity concentrations by depth

Ionic solvent	**Unit**	**20 m**	**100 m**	**300 m**	**500 m**	**1,000 m**	**≥ 1,500 m**
Na^+	g/m^3	30	100	150	400	3,400	7,500
Ca^{2+}	g/m^3	20	50	50	100	4,500	17,000
Cl^-	g/m^3	10	120	150	150	13,000	42,000
SO_4^{2-}	g/m^3	10	30	50	100	600	1,000

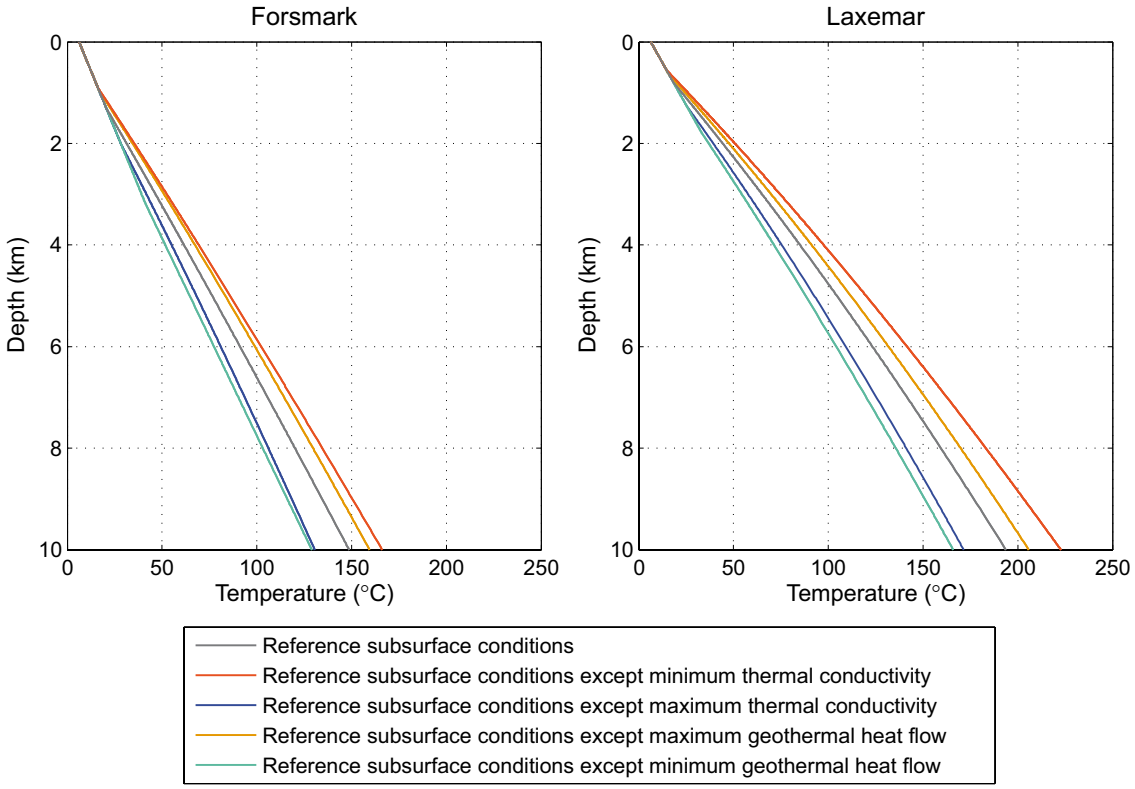

Figure 3-40. *Present-day subsurface temperatures for site-specific reference subsurface conditions at Forsmark and Laxemar.*

The intention was to find steady state permafrost depths. The modelling, however, showed that no steady state could be reached in a time frame of two glaciation cycles. The results from this modelling effort for the time period of 120,000 years are shown in Figure 3-41. The modelling indicates that reaching a permafrost depth of 400 m at Forsmark without a heat contribution from spent fuel requires a mean annual surface temperature lower than −7°C and that temperatures of −8, −10 and −12°C must prevail for longer than 26,000, 8,800 and 5,300 years, respectively. For permafrost to reach a repository depth of 500 m at Laxemar, the mean annual surface temperature must be lower than −13°C and temperatures of −14, −16 and −18°C must persist for longer than 56,000, 23,000 and 14,000 years, respectively. The thickness of the cryopeg varies from some metres to over 70 m at Forsmark and 30 m at Laxemar (Figure 3-41). The results of permafrost development rates (aggradation rates) shown in Figure 3-42 indicate that permafrost can develop (aggradate) 1.2–1.9 times faster at Forsmark than at Laxemar.

In the modelling of surface conditions, the objective was to define a correlation between air and surface temperatures in consideration of the insulating effects of surface covers. The so-called *n*-factor concept /Lunardini 1978/ yields an empirical relationship between the mean annual surface temperature $\overline{T}_s$ and the mean annual air temperature $\overline{T}_a$ as

Equation 3-13 $$\overline{T}_s = f\left(\overline{T}_a, A_a; n_{fr}, n_{th}\right)$$

where A_a is the amplitude of annual air temperature variations, which can be defined as the half of the temperature difference between the monthly mean summer maximum and monthly mean winter minimum. n_{fr} and n_{th} are so-called freezing and thawing *n*-factors. These factors are ratios between the surface and air freezing indexes, i.e. annual time integrals of associated temperatures below the freezing point, and the surface and air thawing indexes, i.e. annual time integrals of associated temperatures above the freezing point, respectively. Depending on the type of surface cover, freezing *n*-factors can vary between 0.1 and 1 whereas thawing *n*-factors can have values in the range from 0.3 to 1.5 /Lunardini 1978, Shur and Slavin-Borovskiy 1993,

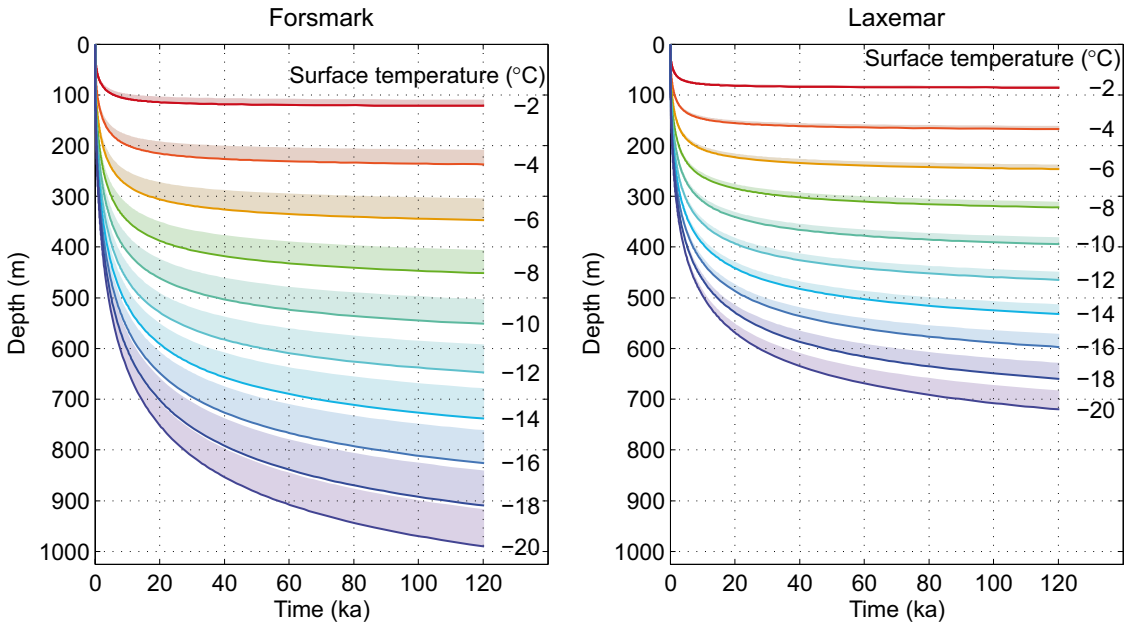

Figure 3-41. *Evolution of permafrost depth (thick lines) and related cryopegs (shadowed areas) for constant ground surface temperatures of –2, –4, …, –20°C at Forsmark and Laxemar when reference subsurface properties are assigned.*

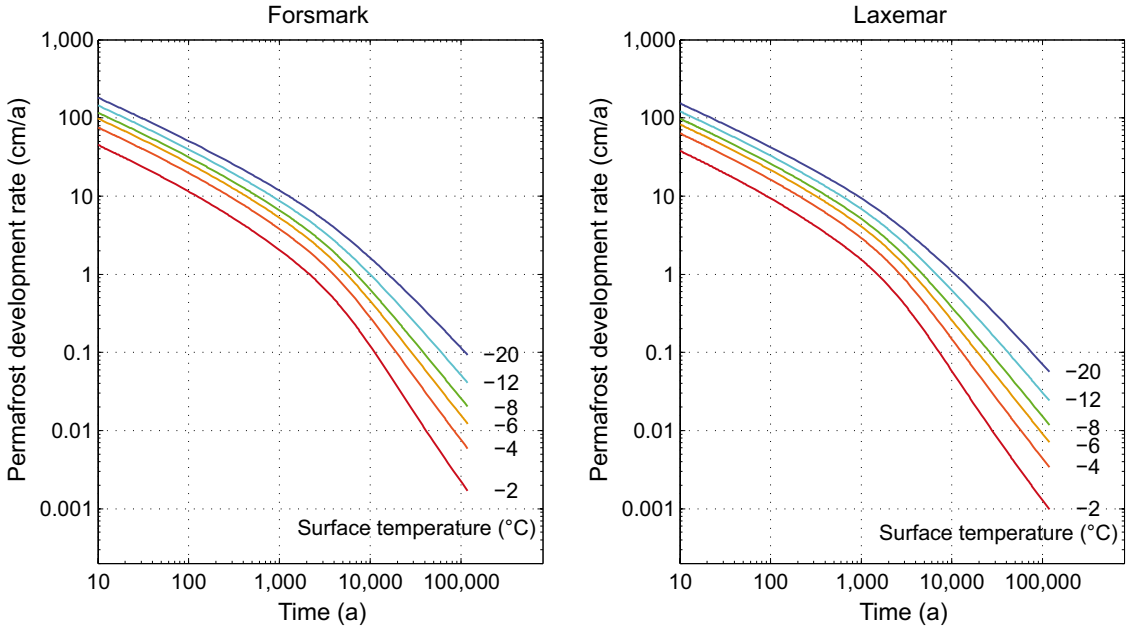

Figure 3-42. *Evolution of permafrost development rate for constant ground surface temperatures of –2, –4, –6, –8, –12 and –20°C at Forsmark and Laxemar when site-specific subsurface properties are assigned.*

Taylor 1995, 2001, Klene et al. 2001, Karunaratne and Burn 2004/. Figure 3-43 shows the relation of the mean annual air temperature to the mean annual surface temperature obtained for a reference surface cover when vegetation and snow are considered and for a bare surface when no vegetation and snow exist.

Large water bodies will affect permafrost depth and the presence of taliks. A talik can exist beneath a water body when the water bottom temperature remains above the freezing point.

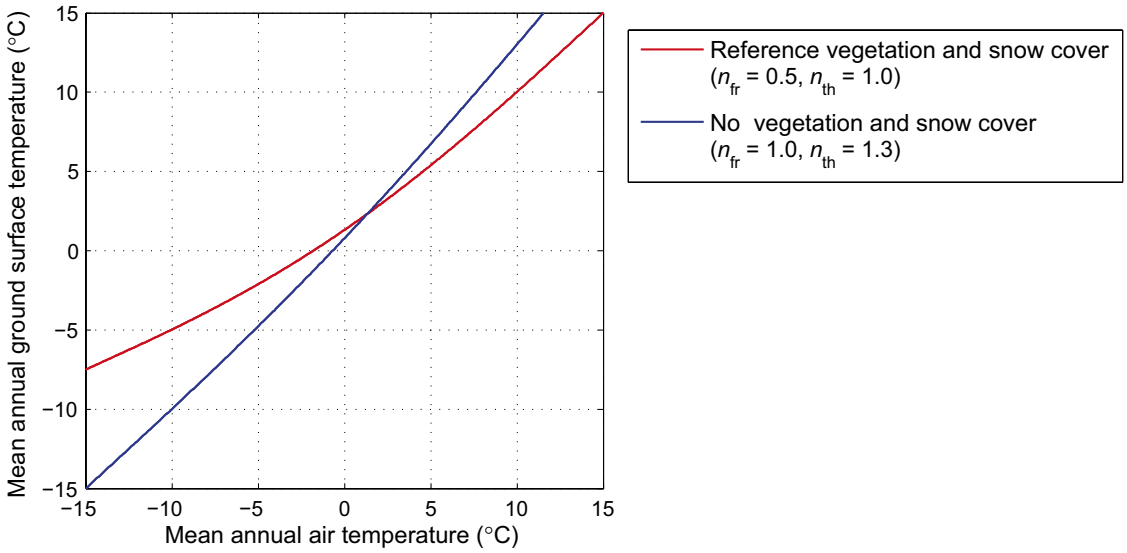

Figure 3-43. *Relationship between the mean annual air temperature and the mean annual surface temperature considering reference vegetation and snow cover, and no vegetation and snow cover.*

It was determined that a two metres deep water body maintains its bottom temperature above 0°C and that a water body deeper than 8 m has a bottom temperature around +4°C. The size of the water body required to retain a talik was investigated by permafrost modelling. To this end, permafrost development was simulated in the vicinity of circular lakes with constant positive lake bottom temperatures and constant negative lake bottom level subsurface temperatures. The results shown in Figure 3-44 indicate that an open talik can survive beneath a circular shallow lake, if its radius is greater than the thickness of surrounding undisturbed permafrost thickness. Furthermore, the results in Figure 3-45 demonstrate that a radius greater than 0.6 times the thickness of surrounding undisturbed permafrost is big enough for a deep circular lake to maintain an open talik. It is remarkable that these results seem to be independent of the site. Moreover, the results apply for different lake bottom level subsurface temperatures.

Since the factors of major importance of the subsurface conditions are the bedrock thermal properties and the conditions affecting the geothermal heat flow, the development of permafrost was investigated for extreme thermal diffusivities and geothermal heat flows as shown in Tables 3-8 and 3-9. The minimum thermal diffusivity results from the minimum thermal conductivity and maximum heat capacity, whereas the maximum thermal diffusivity results from the maximum thermal conductivity and minimum heat capacity. The results calculated for a set of constant surface temperatures (Figures 3-46 and 3-47) indicate a rather large impact of the investigated factors on the development of permafrost. The range between the minimum and maximum permafrost depth can vary approximately from some metres to 200 m at Forsmark and 150 m at Laxemar. Furthermore, the thermal diffusivity seems to have a larger effect on the permafrost development rate than the geothermal heat flow. It is noteworthy that simultaneous maximisation of thermal diffusivity and minimisation of geothermal heat flow with relevant subsurface temperatures do not result in deeper permafrost depths than those obtained from varying these factors individually.

To investigate the impact of the heat generated by the spent fuel on the evolution of permafrost thickness, it was assumed that 6,000 canisters, with individual initial power of 1,700 watts and normalized time-decaying rate of heat production as shown in Figure 3-48, are spread evenly over a repository area of 2.58 km^2 and at a depth of 400 m at Forsmark, and over an area of 3.41 km^2 and at a depth of 500 m at Laxemar. The areas were taken from the envelope of the respective repository layouts /Brantberger et al. 2006, SKB 2006c/. The results shown in Figure 3-49 demonstrate that the influence of heat from the spent fuel on the development of permafrost exceeds the time period of a glaciation cycle. The influence is largest during the first 20,000 years when the reduction of permafrost thickness can be more than 100 m for both sites.

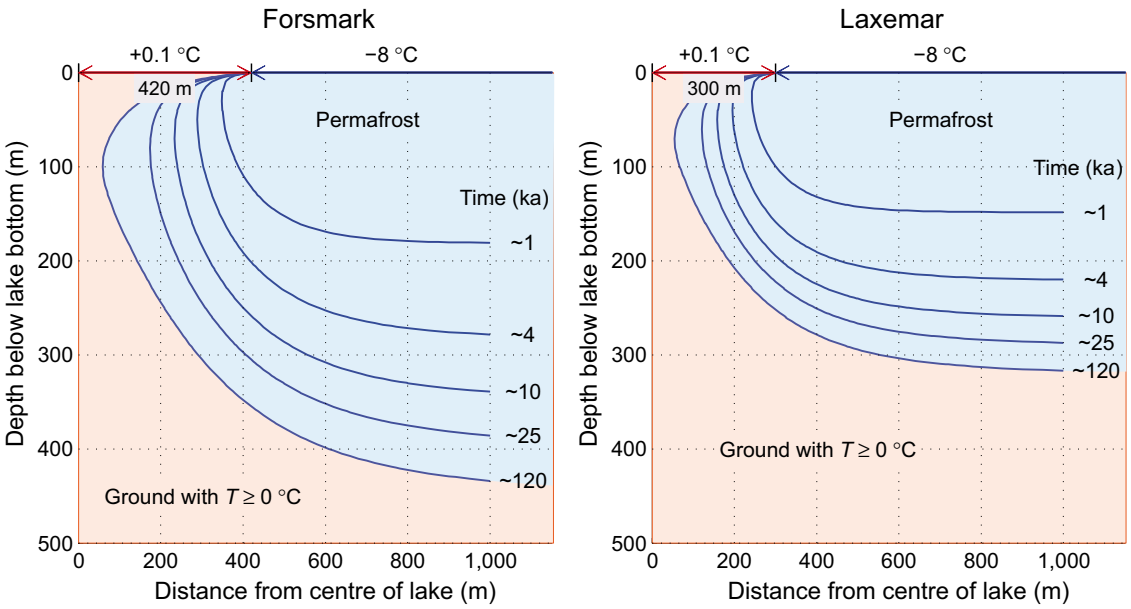

Figure 3-44. *Evolution of permafrost in the vicinity of a circular lake (red colour) of radius of 420 m at Forsmark and 300 m at Laxemar when a constant lake bottom temperature of +0.1°C, and a constant subsurface temperature of –8°C at lake bottom level and reference subsurface properties are assigned.*

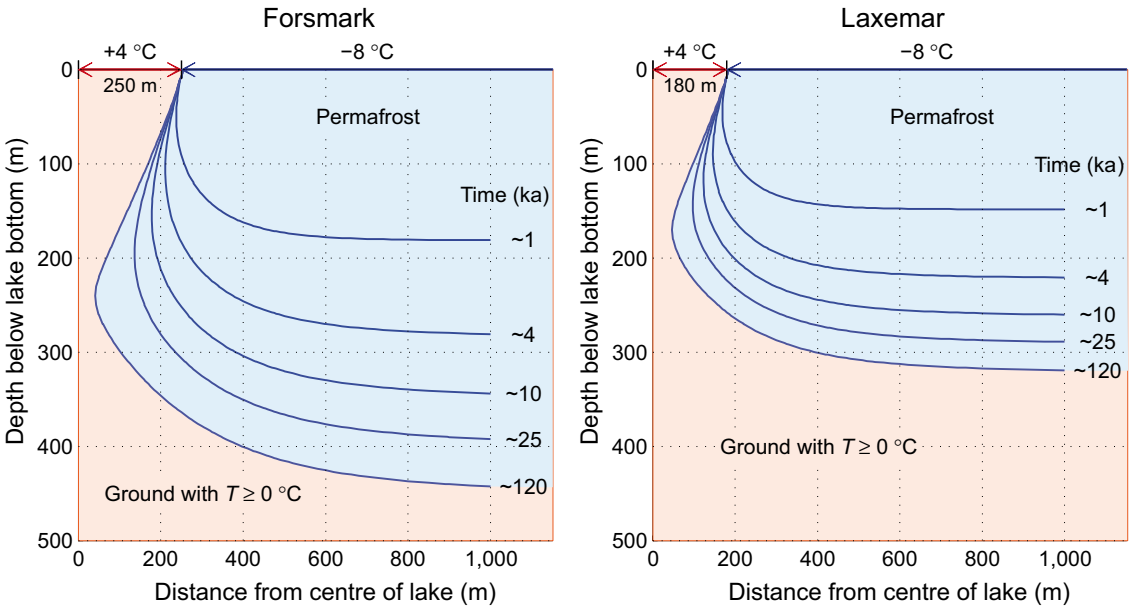

Figure 3-45. *Evolution of permafrost in the vicinity of a circular lake (red colour) of radius of 250 m at Forsmark and 180 m at Laxemar when a constant lake bottom temperature of +4°C, and a constant subsurface temperature of –8°C at lake bottom level prevail and reference subsurface properties are assigned.*

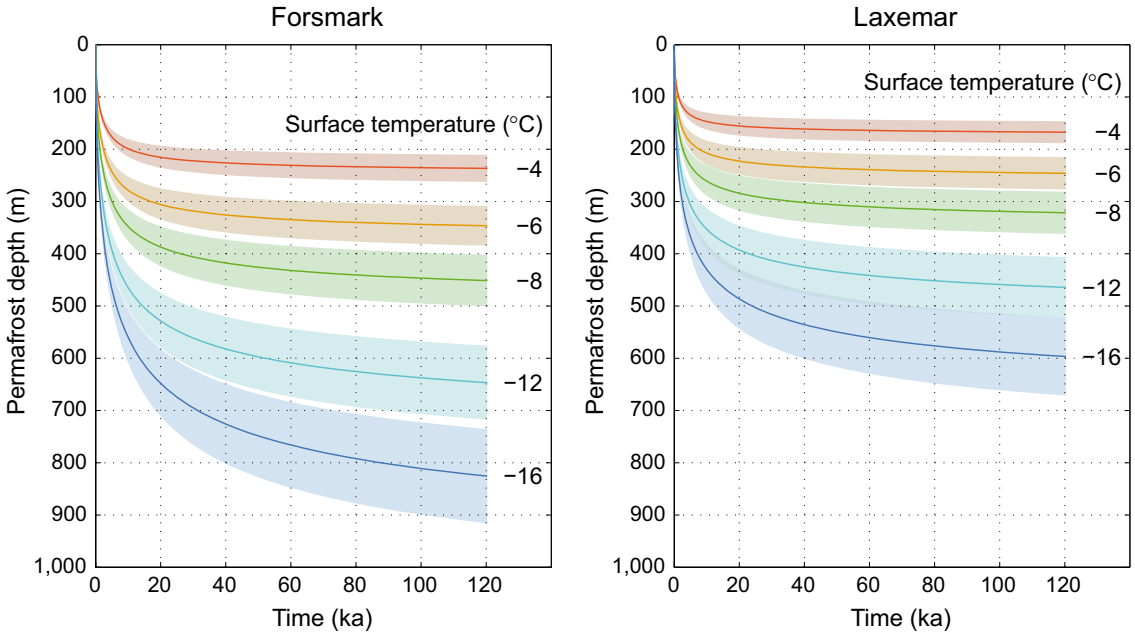

Figure 3-46. *Evolution of permafrost depth for constant ground surface temperatures of –4, –6, –8, –12 and –16°C at Forsmark and Laxemar under various values of thermal diffusivity: the upper edge of the shadowed area is associated with the minimum and the lower edge with the maximum thermal diffusivity; the solid lines apply for the reference thermal diffusivity. The investigated range and reference thermal diffusivity values are found in Tables 3-8 and 3-9.*

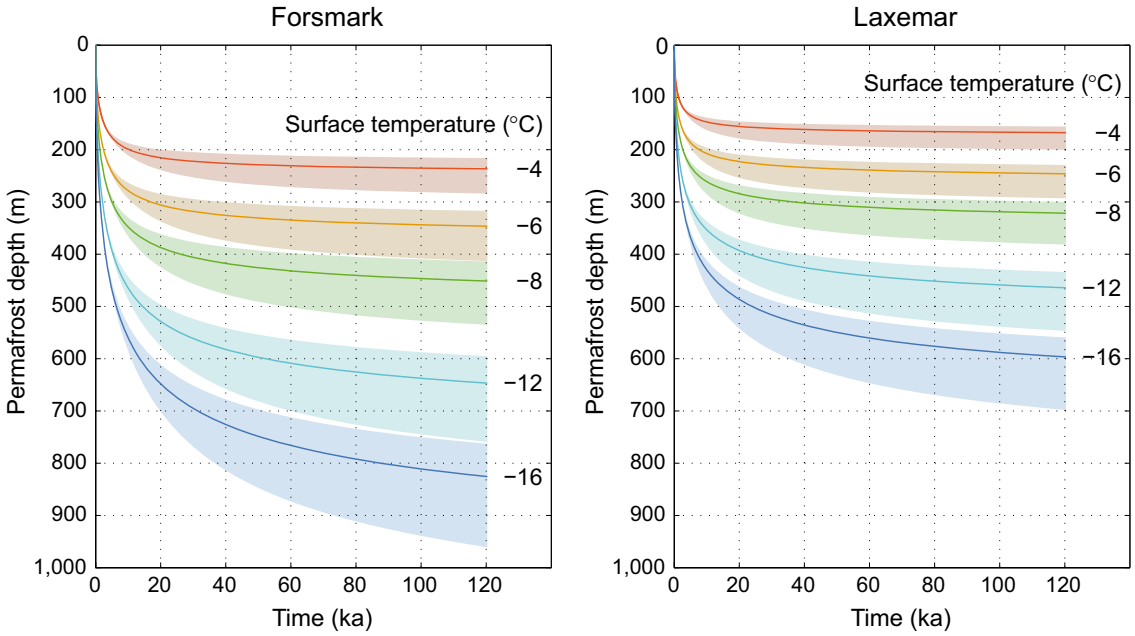

Figure 3-47. *Evolution of permafrost depth for constant ground surface temperatures of –4, –6, –8, –12 and –16°C at Forsmark and Laxemar under various values of geothermal heat flow: the upper edge of the shadowed area is associated with the maximum and the lower edge with the minimum geothermal heat flow; the solid lines apply for the reference geothermal heat flow. The investigated range and reference geothermal heat flow values are found in Tables 3-8 and 3-9.*

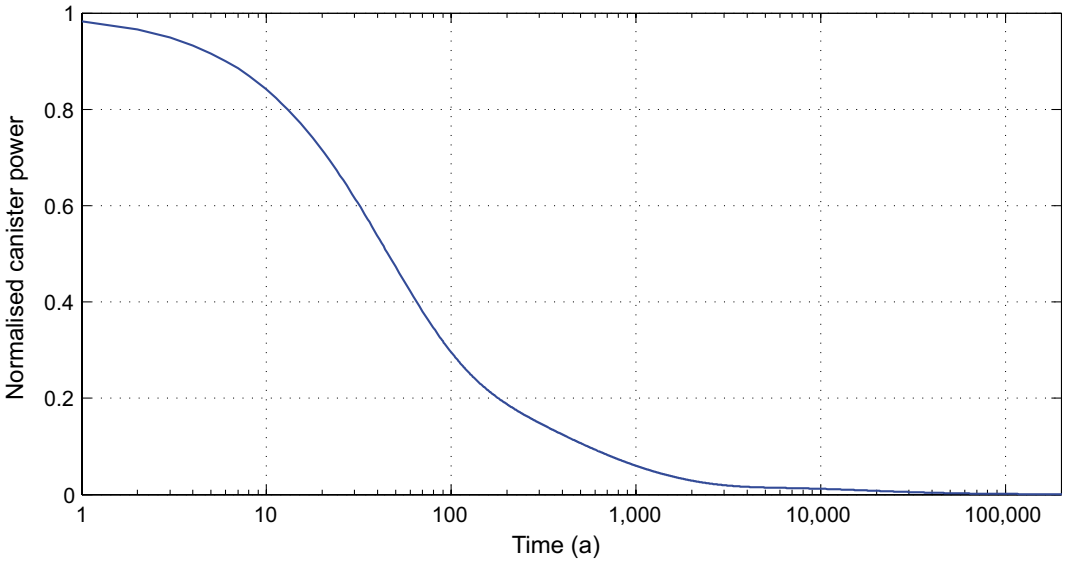

Figure 3-48. *Evolution of normalized heat power from a spent fuel canister. After /Håkansson 2000/.*

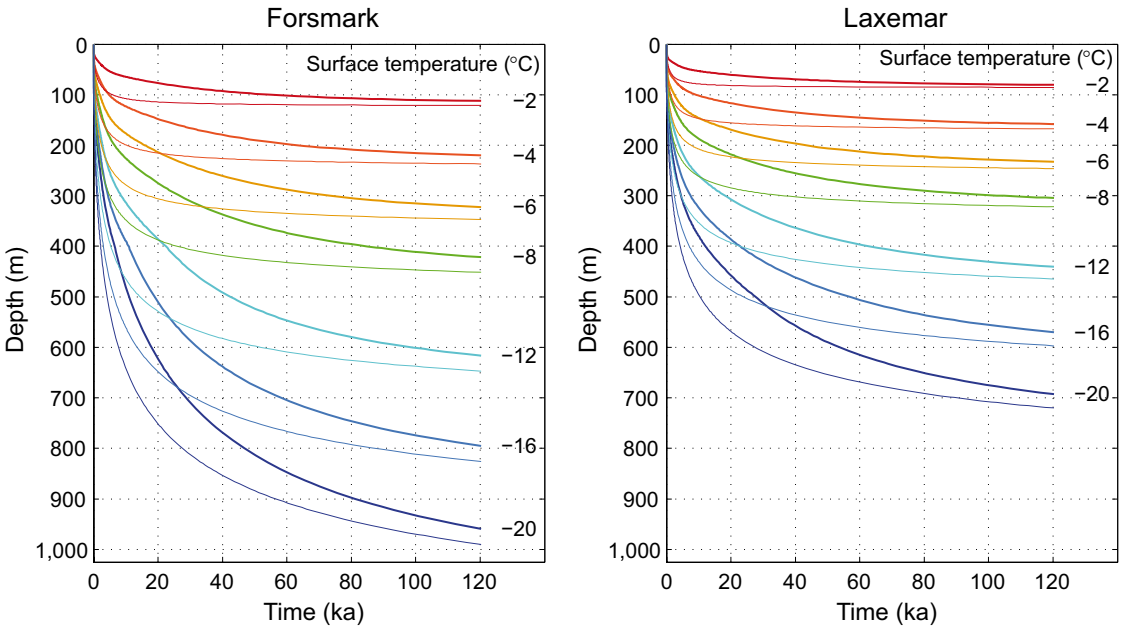

Figure 3-49. *The effect of considering heat from the spent fuel (thick lines) in comparison to no heat from the spent fuel (thin lines) on the evolution of permafrost depth for constant ground surface temperatures of –2, –4, –6, –8, –12, –16 and –20°C at Forsmark and Laxemar with reference subsurface properties.*

After the sensitivity analysis using constant surface temperatures, permafrost development was modelled for time-varying site-specific surface conditions. For this purpose, the ice sheet model in Section 3.1 was used to extract site-specific time series of ground-level annual air temperatures and basal ice sheet temperatures, as well as information on site-specific ice thickness variations. The GIA model in Section 3.3 was used to produce data on shoreline migration. The following two cases were analyzed:

- Reference surface conditions.
- Extreme surface conditions favouring permafrost development.

The reference surface conditions case (Figure 3-50), applies when ice sheet development and shoreline migration occurs as described in the base variant of the SR-Can main scenario, i.e. a repetition of the conditions reconstructed for the last glacial cycle. The extreme surface conditions case favouring permafrost development (Figure 3-51) is the consequence of a cooling glacial cycle, but in an extremely dry climate with no ice sheet formation and the sites remaining above sea level. When sites are ice covered, surface temperatures equal the basal temperatures from the ice sheet model. When the sites are submerged, the surface temperature is set to +4°C. In the extreme case, the site-specific air temperatures (Figure 3-51) were calculated from ice sheet model data on air temperatures (Figure 3-50) by making a correction for the difference in elevation between the height of the ice sheet and that of the ground surface.

The results of the development of permafrost, perennially frozen subsurface and cryopeg for reference surface conditions with vegetation and snow cover, and considering heat from the spent fuel are shown in Figure 3-52. Figure 3-53 shows the same information for the extreme surface condition case without an ice sheet and without vegetation and snow cover. The associated rates of permafrost aggradation and degradation are shown in Figures 3-54 and 3-55. The rather thick cryopeg layers during glaciations are due to large water pressures created by warm-based ice sheets keeping the subglacial bed unfrozen down to a temperature about –2°C.

From sensitivity tests, differences in permafrost depth for reference surface conditions at Forsmark and Laxemar due to the effects of vegetation and snow cover, and variations in thermal diffusivity, geothermal heat flow and heat from the spent fuel are shown in Figures 3-56, 3-57, 3-58 and 3-59. Differences in permafrost depth for extreme surface conditions at Forsmark and Laxemar due to variations in thermal diffusivity, geothermal heat flow and heat from the spent fuel are shown in Figures 3-60, 3-61 and 3-62. The maximum permafrost depths and related perennially frozen subsurface depths including the time of occurrence are summarised in Tables 3-10 and 3-11.

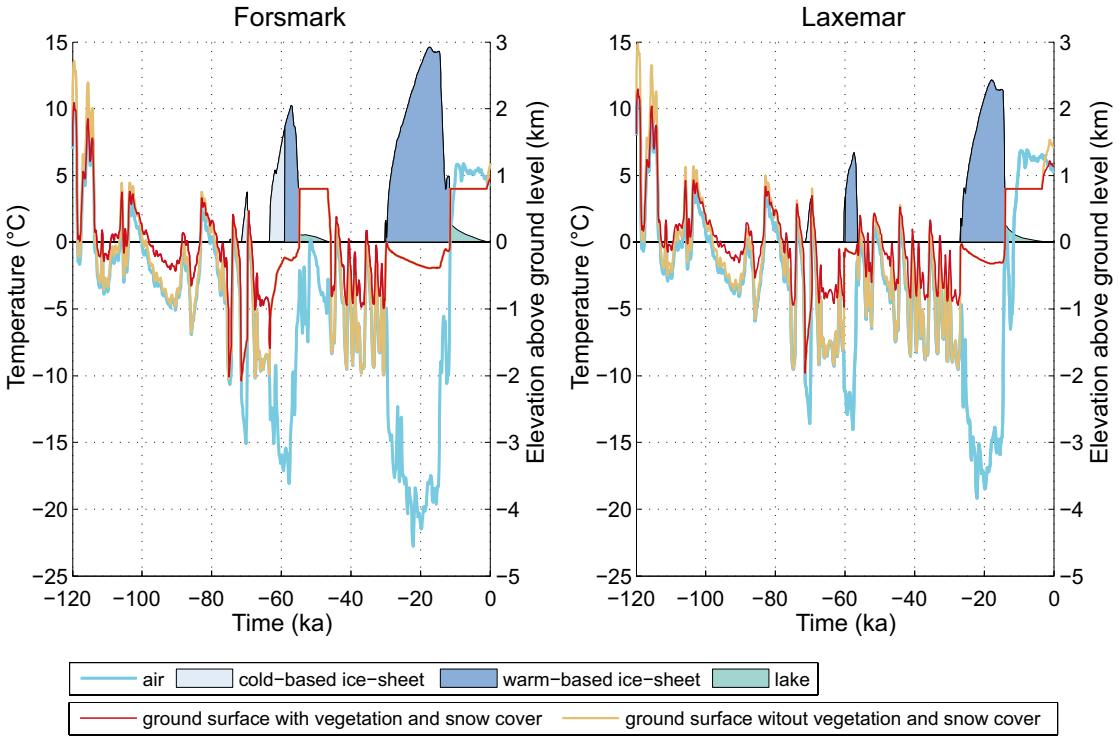

Figure 3-50. *Evolution of air temperature, ice sheet thickness, lake depth and modelled ground surface temperature with and without vegetation and snow cover for the reference surface conditions, i.e. ice sheet development and shoreline migration occurs as described in the base variant of the SR-Can main scenario.*

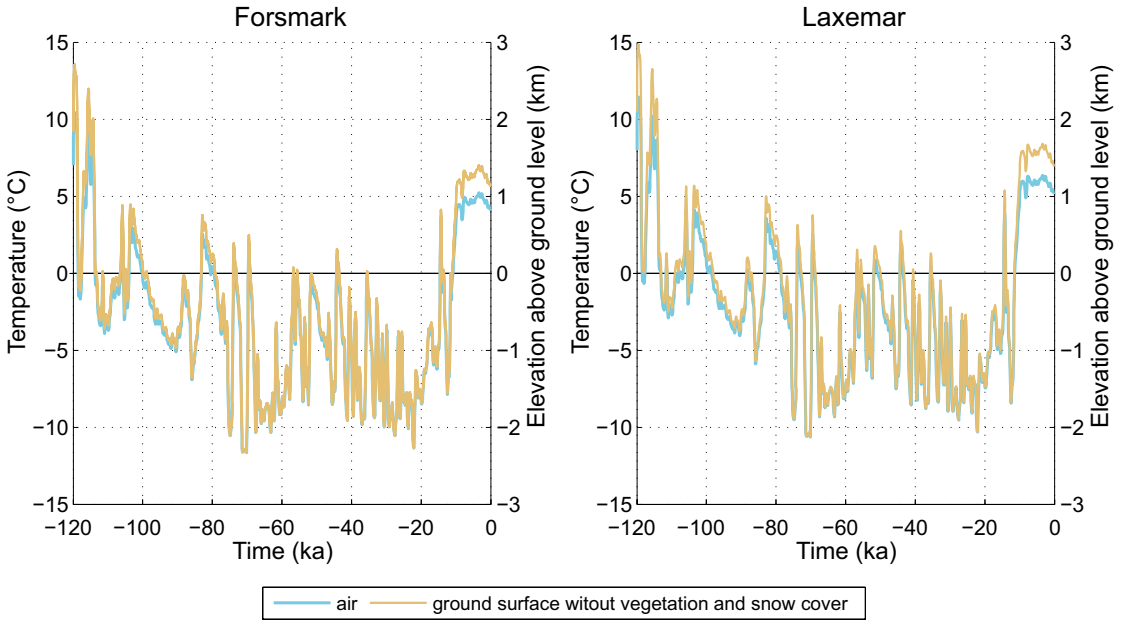

Figure 3-51. *Evolution of air temperature and modelled ground surface temperature without vegetation and snow cover at Forsmark and Laxemar for the extreme surface conditions when temperatures drop as during the last glacial cycle, but no ice sheet development takes place and the site remains above sea level.*

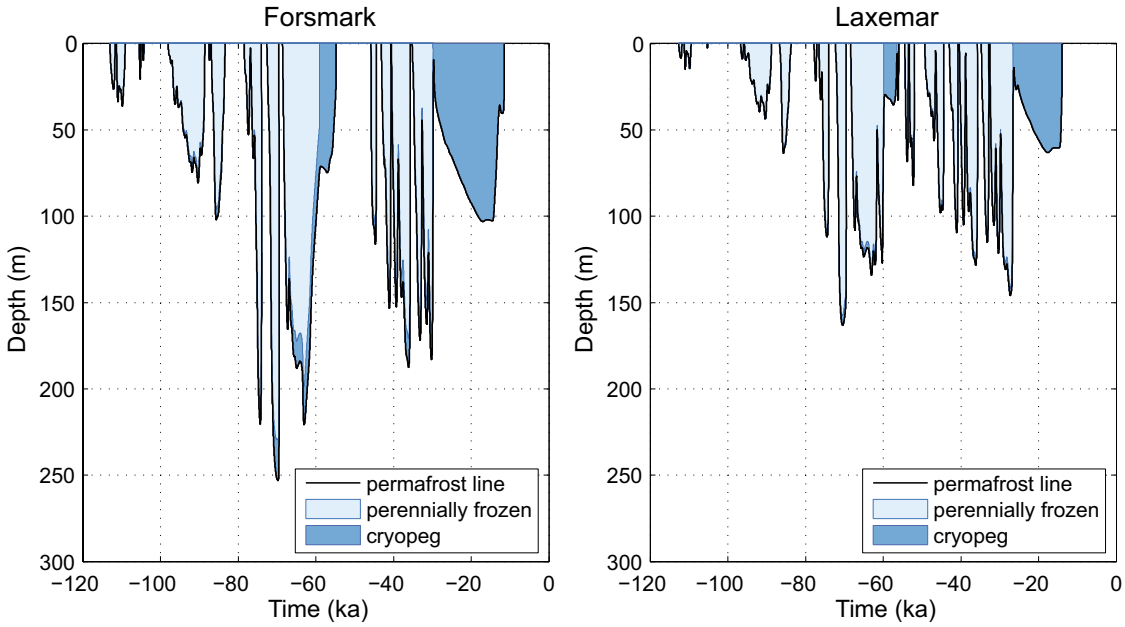

Figure 3-52. *Evolution of permafrost, perennially frozen subsurface and cryopeg at Forsmark and Laxemar considering reference surface conditions, reference subsurface properties and heat from the spent fuel.*

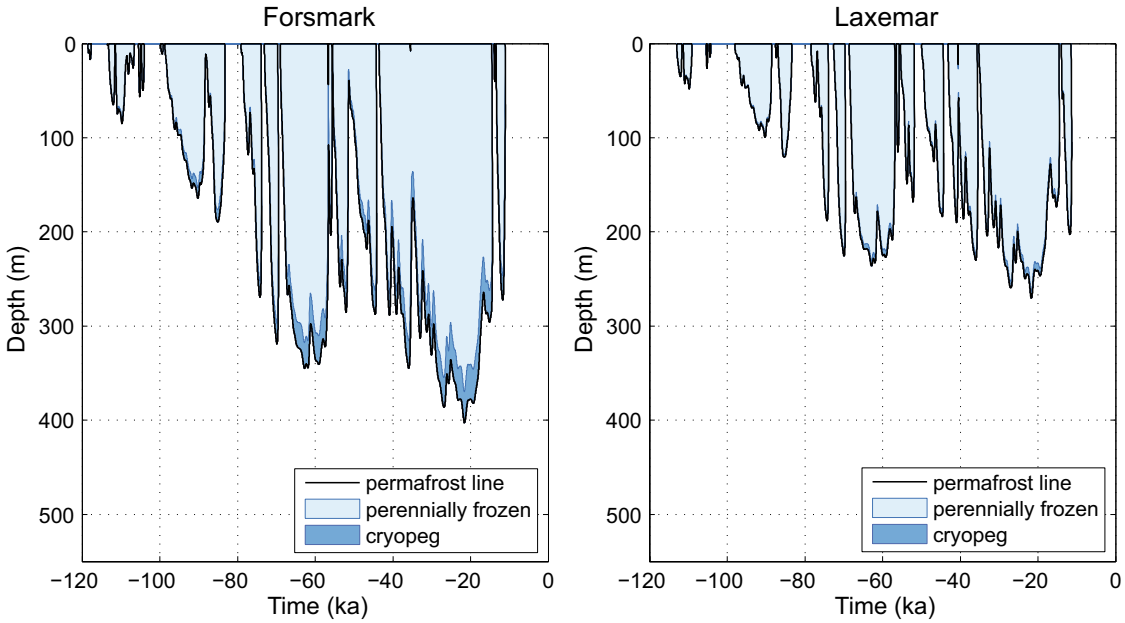

Figure 3-53. *Evolution of permafrost, perennially frozen subsurface and cryopeg at Forsmark and Laxemar considering cold and extremely dry surface conditions (without any ice sheet development), reference subsurface properties and heat from the spent fuel.*

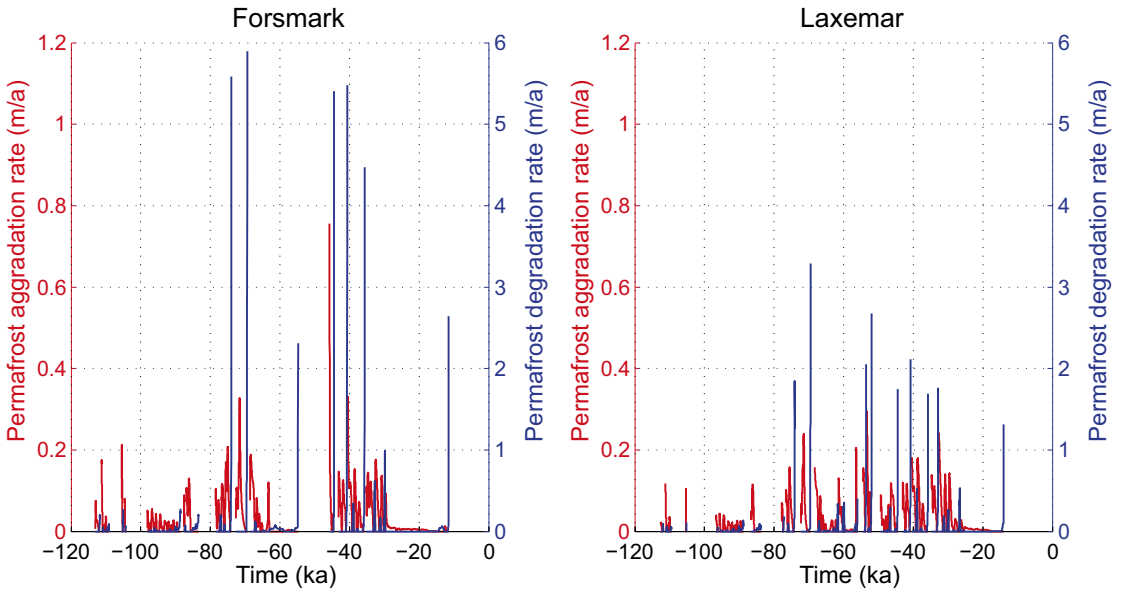

Figure 3-54. *Evolution of permafrost aggradation and degradation rates at Forsmark and Laxemar considering reference surface conditions with vegetation and snow cover, reference subsurface properties and heat from the spent fuel.*

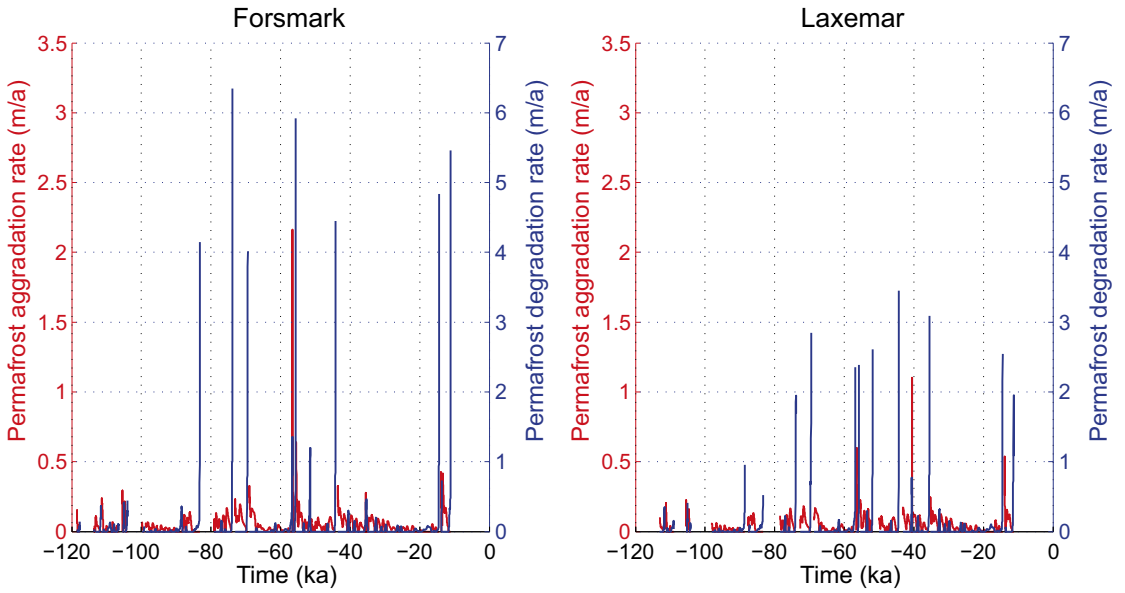

Figure 3-55. *Evolution of permafrost aggradation and degradation rates at Forsmark and Laxemar considering cold and extremely dry surface conditions (without any ice sheet development), reference subsurface properties and heat from the spent fuel.*

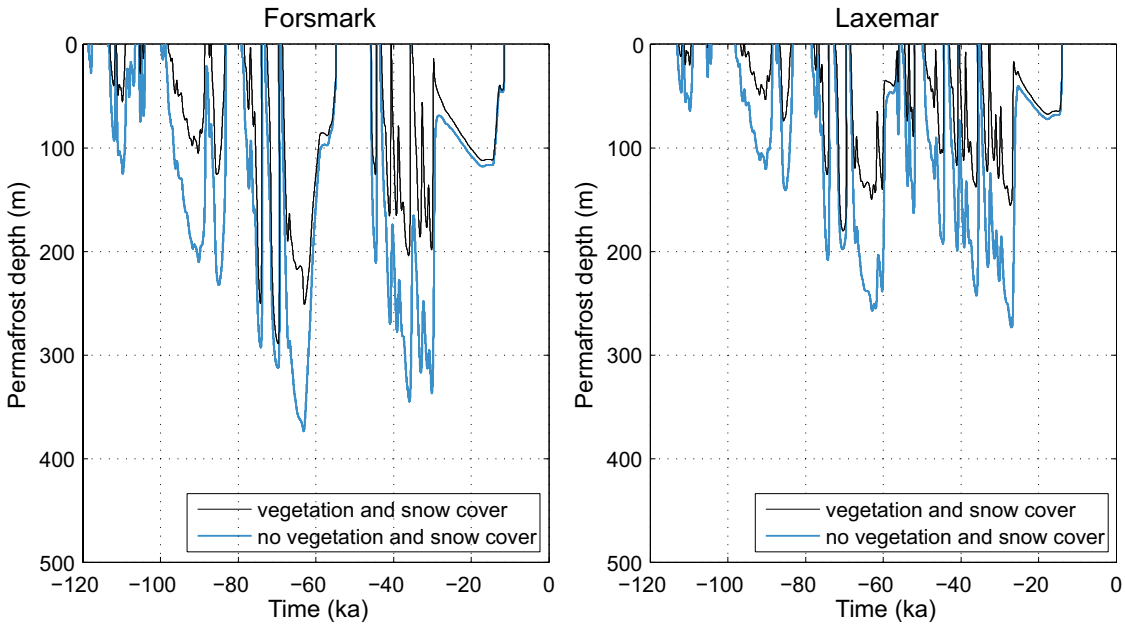

Figure 3-56. *Evolution of permafrost depth at Forsmark and Laxemar considering reference surface conditions with and without vegetation and snow cover, reference subsurface properties and no heat from the spent fuel.*

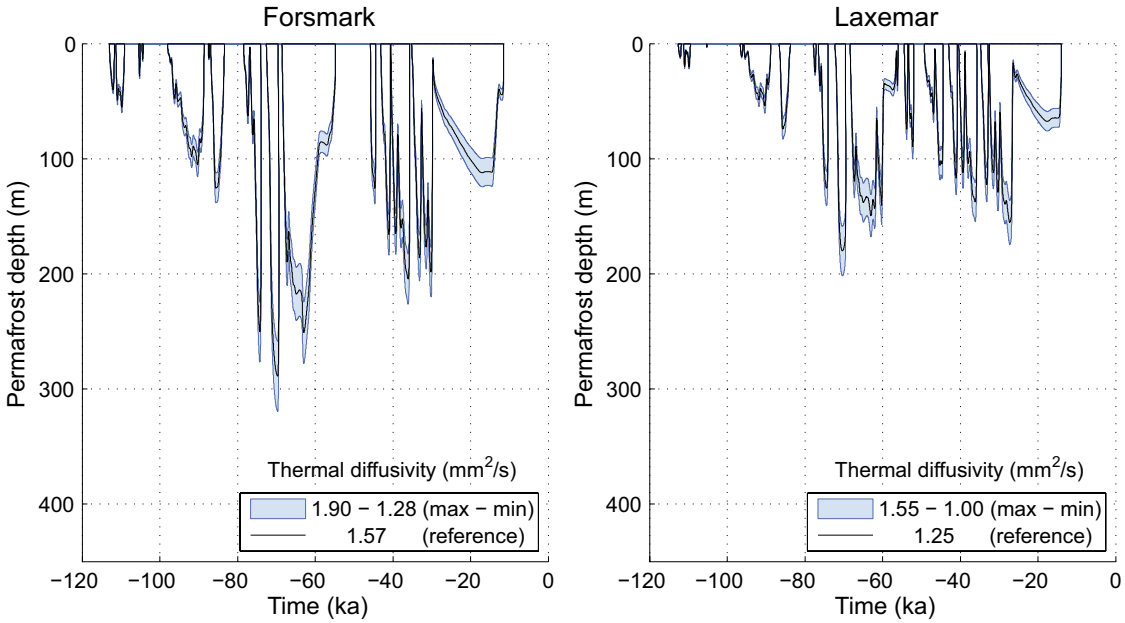

Figure 3-57. *Evolution of permafrost depth at Forsmark and Laxemar considering reference surface conditions, variable thermal diffusivities (the upper edge of the shadowed area is associated with the minimum and the lower edge with the maximum) and no heat from the spent fuel.*

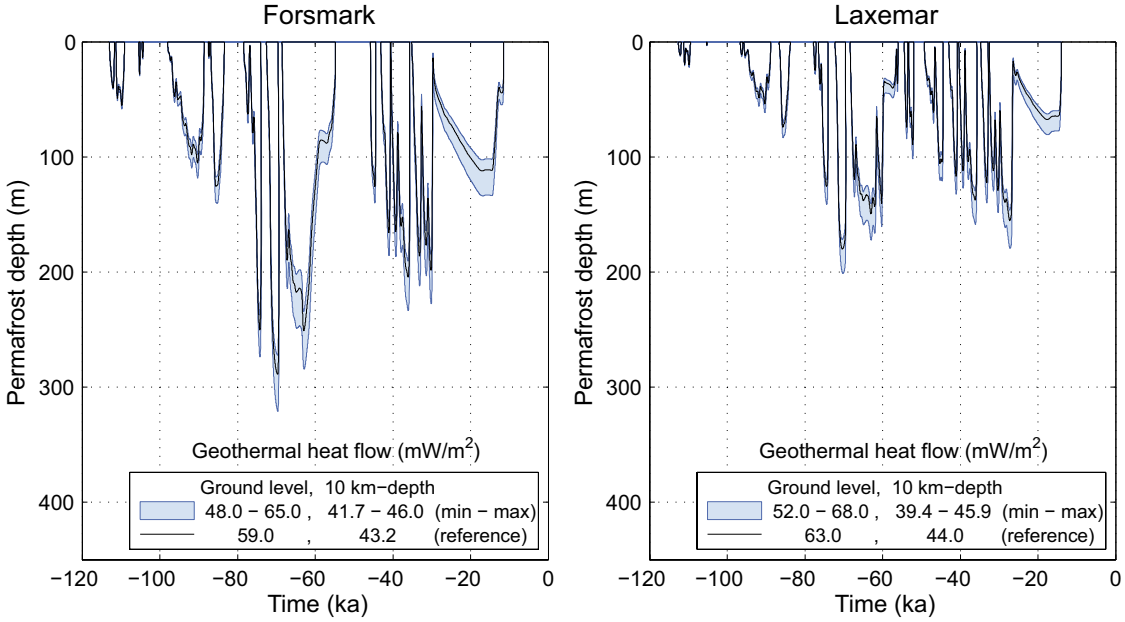

Figure 3-58. *Evolution of permafrost depth at Forsmark and Laxemar considering reference surface conditions, variable geothermal heat flows (the upper edge of the shadowed area is associated with the maximum and the lower edge with the minimum) and no heat from the spent fuel.*

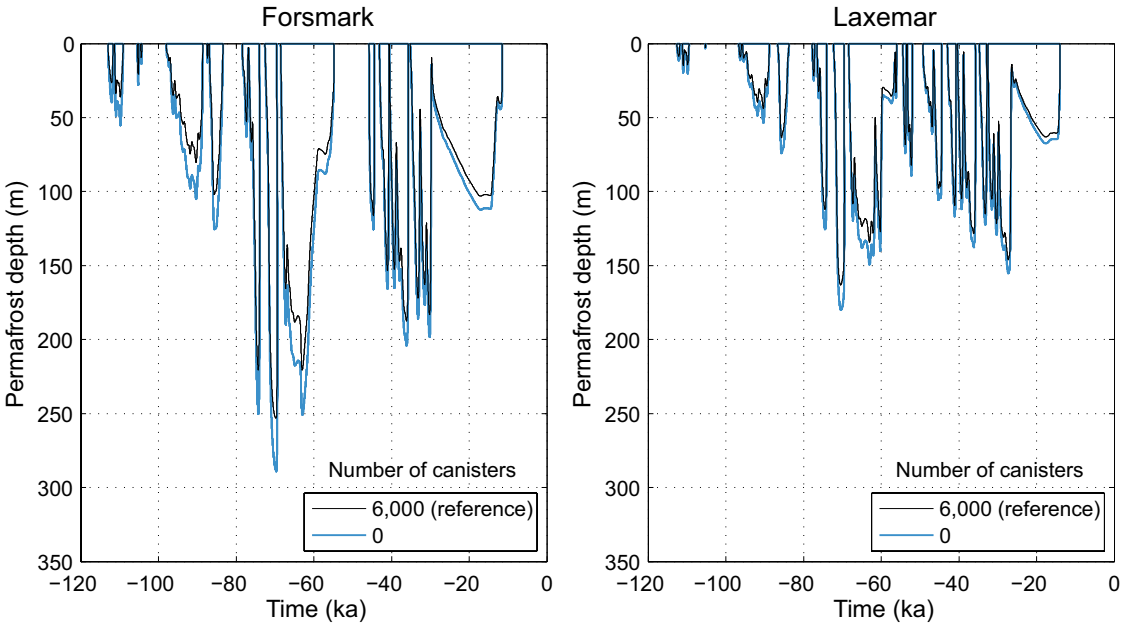

Figure 3-59. *Evolution of permafrost depth at Forsmark and Laxemar considering reference surface conditions, reference subsurface properties and heat or no heat from the spent fuel.*

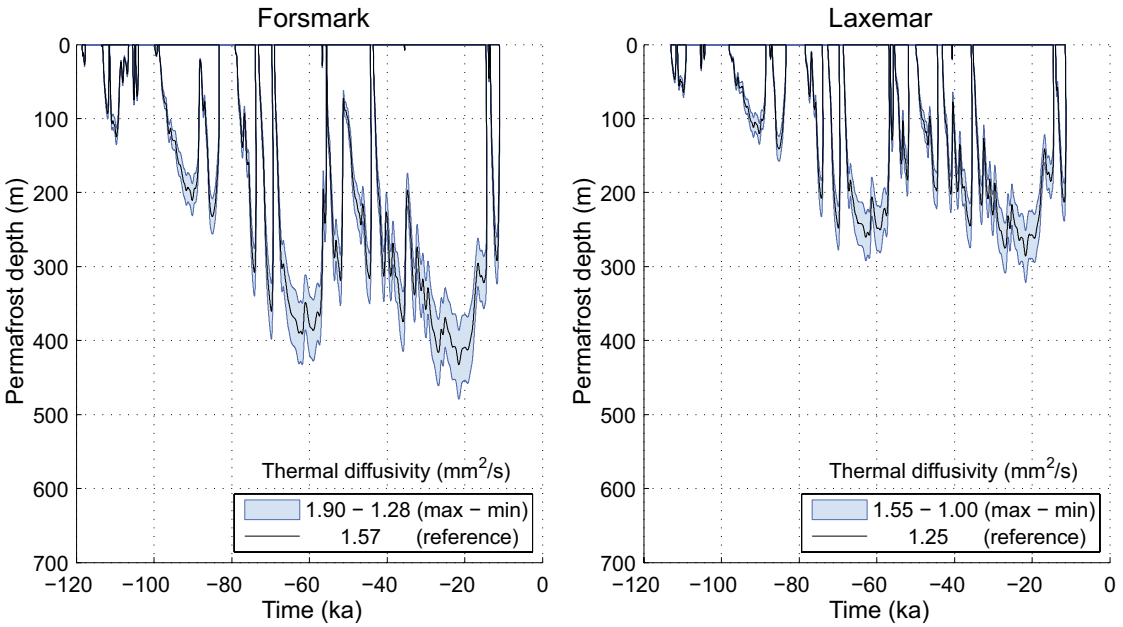

Figure 3-60. *Evolution of permafrost depth at Forsmark and Laxemar considering extreme surface conditions, variable thermal diffusivities (the upper edge of the shadowed area is associated with the minimum and the lower edge with the maximum) and no heat from the spent fuel.*

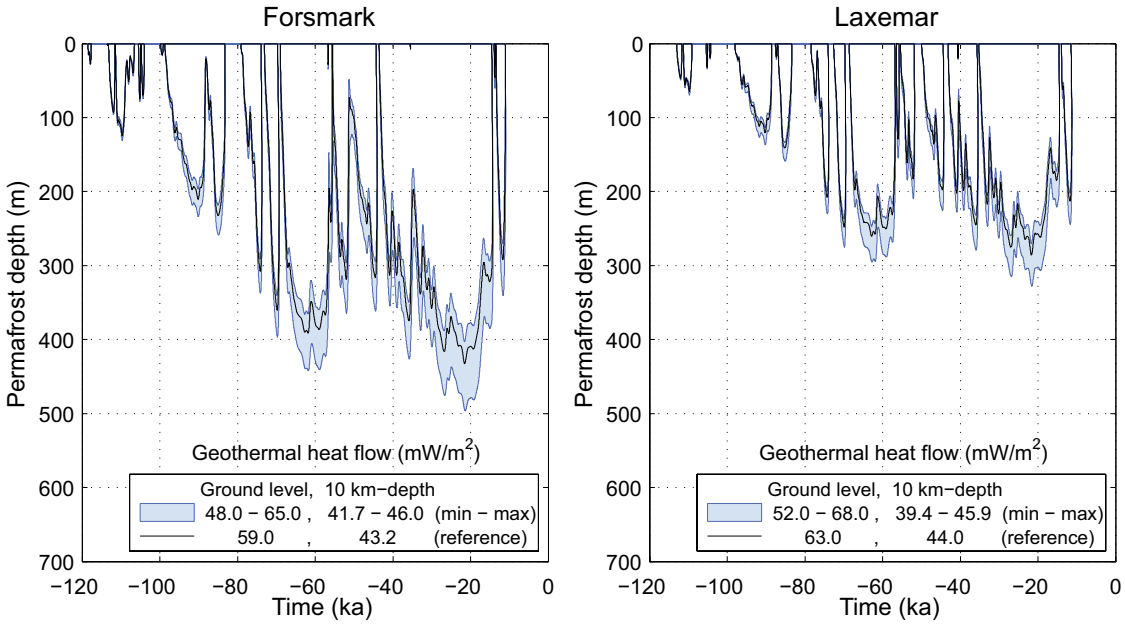

Figure 3-61. *Evolution of permafrost depth at Forsmark and Laxemar considering extreme surface conditions, variable geothermal heat flows (the upper edge of the shadowed area is associated with the maximum and the lower edge with the minimum) and no heat from the spent fuel.*

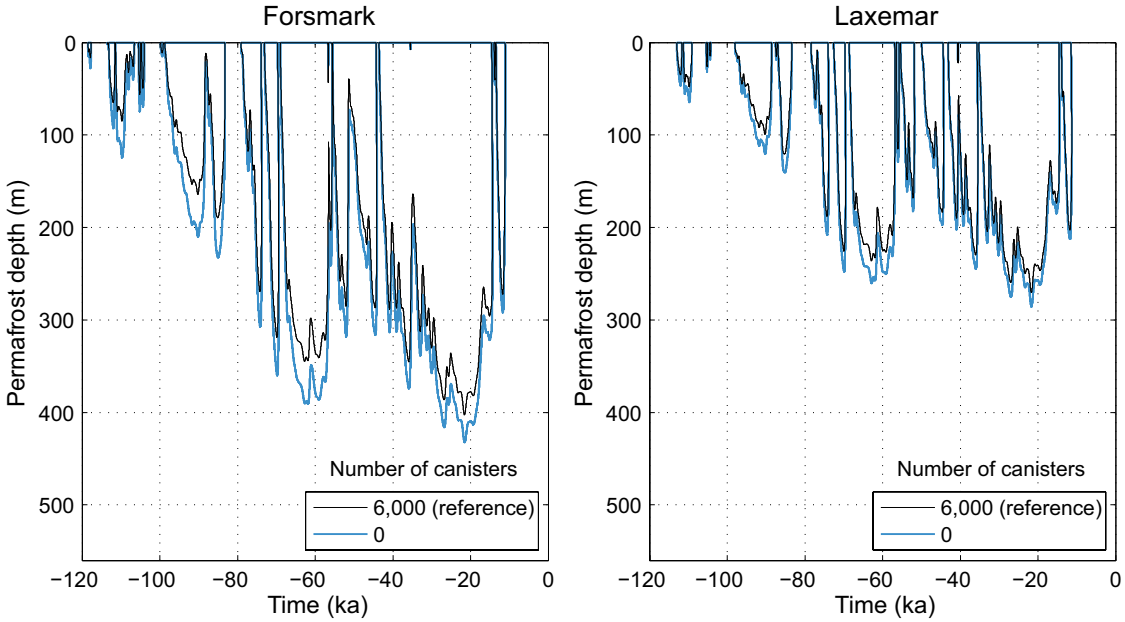

Figure 3-62. *Evolution of permafrost depth at Forsmark and Laxemar considering extreme surface conditions, reference subsurface properties and heat or no heat from the spent fuel.*

Table 3-10. Maximum permafrost depths and associated perennial frozen depths for reference surface conditions at Forsmark and Laxemar. The table also shows the time of occurrence.

	Forsmark Permafrost depth (m)	Perennial frost depth (m)	Time (a)	Laxemar Permafrost depth (m)	Perennial frost depth (m)	Time (a)
Vegetation and snow cover *(reference subsurface, no heat from the spent fuel)*						
Reference cover	289	261	−69,650	180	173	−70,330
No cover	374	336	−63,120	273	265	−26,940
Thermal diffusivity *(reference vegetation and snow cover, no heat from the spent fuel)*						
Minimum	259	236	−69,650	159	153	−70,350
Reference	289	261	−69,650	180	173	−70,330
Maximum	320	286	−69,650	202	193	−70,320
Geothermal heat flow *(reference vegetation and snow cover, no heat from the spent fuel)*						
Maximum	272	247	−69,670	172	165	−70,380
Reference	289	261	−69,650	180	173	−70,330
Minimum	321	288	−69,610	201	192	−70,190
Number of canisters *(reference vegetation and snow cover, reference subsurface)*						
6,000	253	230	−69,720	163	157	−70,430
0	289	261	−69,650	180	173	−70,330

Table 3-11. Maximum permafrost depths and associated perennial frozen depths modelled for extreme surface conditions at Forsmark and Laxemar. The table also shows the time of occurrence.

	Forsmark Permafrost depth (m)	Perennial frost depth (m)	Time (a)	Laxemar Permafrost depth (m)	Perennial frost depth (m)	Time (a)
Thermal diffusivity *(no vegetation and snow cover, no heat from the spent fuel)*						
Minimum	386	354	−21,510	251	245	−21,670
Reference	433	396	−21,510	286	277	−21,660
Maximum	479	437	−21,510	321	310	−21,660
Geothermal heat flow *(no vegetation and snow cover, no heat from the spent fuel)*						
Maximum	403	370	−21,560	270	263	−21,690
Reference	433	396	−21,510	286	277	−21,660
Minimum	497	451	−213,90	328	317	−21,590
Number of canisters *(no vegetation and snow cover, reference subsurface)*						
6,000	403	370	−21,560	270	263	−21,690
0	433	396	−21,510	286	277	−21,660

The evolution of subsurface temperatures and residual pore water pressures at the repository depth of 400 m at Forsmark and 500 m at Laxemar for reference surface conditions, with vegetation and snow cover, considering heat and no heat from the spent fuel are shown in Figure 3-63. Corresponding information for extreme surface conditions, without vegetation and snow cover, are shown in Figure 3-64. The negative residual pore water pressures result from the cryogenic suction due to freezing of adsorbed pore water. The weaker impact of the cryogenic suction at Laxemar than at Forsmark (Figure 3-64) is a consequence of more reduced permeability due to freezing, which in turn is a result from the fact that groundwater at permafrost depths is more dilute at Laxemar than at Forsmark. The minimum subsurface temperatures with the time of occurrence at the repository depths with and without vegetation and snow cover, and considering variations in thermal diffusivity, geothermal heat flow and heat from the spent fuel are presented in Tables 3-12 and 3-13.

Table 3-12. Minimum subsurface temperatures at repository depth (400 m at Forsmark, 500 m at Laxemar) for reference surface conditions. The table also shows the time of occurrence.

	Forsmark Temperature (°C)	Time (a)	Laxemar Temperature (°C)	Time (a)
Vegetation and snow cover *(reference subsurface, no heat from the spent fuel)*				
Reference cover	2.7	−69,520	9.2	−26,500
No cover	0.6	−63,090	6.7	−26,530
Thermal diffusivity *(reference vegetation and snow cover, no heat from the spent fuel)*				
Minimum	3.9	−69,470	11.1	−26,370
Reference	2.7	−69,520	9.2	−26,500
Maximum	1.8	−69,570	7.8	−26,600
Geothermal heat flow *(reference vegetation and snow cover, no heat from the spent fuel)*				
Maximum	3.4	−69,520	10.1	−26,500
Reference	2.7	−69,520	9.2	−26,500
Minimum	1.7	−69,520	7.3	−26,490
Number of canisters *(reference vegetation and snow cover, no heat from the spent fuel)*				
6,000	4.2	−69,520	10.2	−26,490
0	2.7	−69,520	9.2	−26,500

Table 3-13. Minimum subsurface temperatures for extreme surface conditions at repository depth (Forsmark 400 m and Laxemar 500 m). The table also shows the time of occurrence.

	Forsmark Temperature (°C)	Time (a)	Laxemar Temperature (°C)	Time (a)
Thermal diffusivity *(no vegetation and snow cover, no heat from the spent fuel)*				
Minimum	0.34	−21,490	8.1	−21,020
Reference	−0.71	−21,560	6.1	−21,200
Maximum	−1.6	−21,630	4.6	−21,330
Geothermal heat flow *(no vegetation and snow cover, no heat from the spent fuel)*				
Maximum	−0.07	−21,560	7.0	−21,200
Reference	−0.71	−21,560	6.1	−21,200
Minimum	−1.8	−21,560	4.2	−21,200
Number of canisters *(no vegetation and snow cover, reference subsurface)*				
6,000	−0.06	−21,560	7.0	−21,190
0	−0.71	−21,560	6.1	−21,200

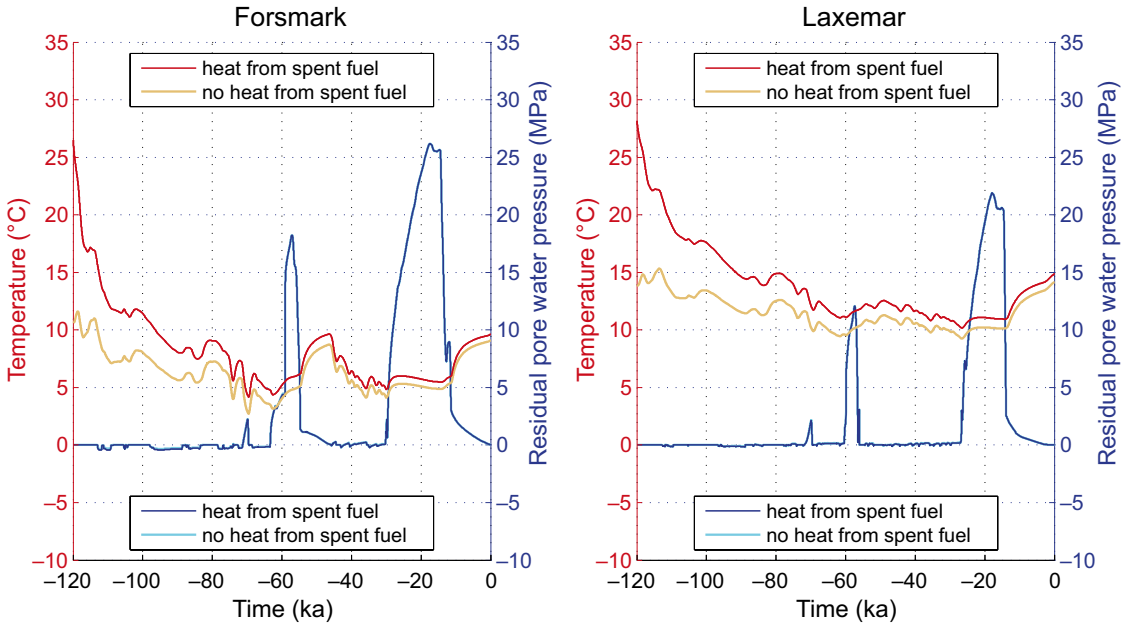

Figure 3-63. *Evolution of subsurface temperature and residual pore water pressure at the repository depth of 400 m at Forsmark and 500 m at Laxemar considering reference surface conditions with vegetation and snow cover, reference subsurface properties and heat or no heat from the spent fuel.*

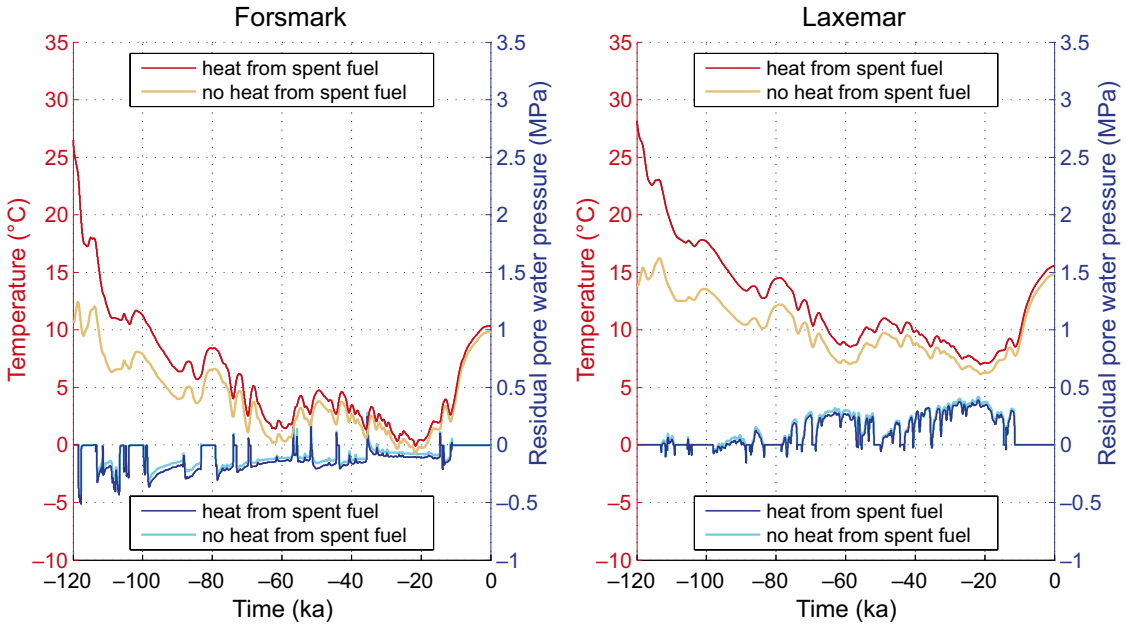

Figure 3-64. *Evolution of subsurface temperature and residual pore water pressure at the repository depth of 400 m at Forsmark and 500 m at Laxemar considering extreme surface conditions without vegetation and snow cover, reference subsurface properties and heat or no heat from the spent fuel.*

The surface conditions can be seen as the driving force for the development of permafrost, with the subsurface conditions and the heat from the spent fuel acting as either reducing or enhancing factors. The results indicate that permafrost (0°C isotherm) can advance to repository depth at Forsmark in a time frame of 100,000 years, when the extreme surface conditions favouring permafrost development prevail and can develop to near repository depth under the reference

surface conditions when the insulating effects of vegetation and snow cover are excluded. The repository at Laxemar, on the contrary, seems to remain well outside the range of permafrost (0°C isotherm) development in every investigated case. Results of simulations of additional colder climate variants are presented in Section 4.4.

3.4.5 Time perspective

Changes in annual ground surface temperature due to climate change can lead to development of permafrost and freezing of ground. If the mean annual ground surface temperature decreases constantly from the present day value to approximately –8°C, permafrost can develop to the depth of 400 m in a period of 26,000 years at Forsmark. At Laxemar, a temperature of −14°C must prevail for over 56,000 years to create permafrost to the depth of 500 m (Figure 3-41). Under periglacial conditions, permafrost can aggregate from some centimetres to some decimetres in a year whereas its degradation can take place several times faster than that, especially when the surface temperature is increased above 0°C and permafrost decays simultaneously from the bottom upwards and from the top downwards (Figure 3-55). Large degradation rates can occur also at the onset of glaciation when the surface temperature rises sharply to the freezing point beneath an advancing ice sheet (Figure 3-54).

3.4.6 Handling in the safety assessment SR-Can

The evolution of permafrost is investigated by means of numerical modelling. The base variant of the main scenario in SR-Can is based on a reference permafrost model reconstruction of the Weichselian glacial cycle. Additional scenarios, describing colder and dryer climate variants are also investigated. The permafrost model includes a mathematical expression for freezing and thawing of saline-groundwater-saturated bedrock. The bedrock is considered as an elastic porous medium and the groundwater as an ideal solution of water and ionic solvents. The model is based on the principles of continuum mechanics, macroscopic thermodynamics and the theory of mixtures, and is capable of describing heat transfer, freezing of saline water, groundwater flow and deformations of bedrock. To capture the most important factors and parameters affecting the development of permafrost, sensitivity analyses have been performed considering the following issues:

- Surface conditions.
- Subsurface conditions.
- Presence of the repository.

Surface temperatures, together with the influence of surface covers such as snow, vegetation and water bodies, have been included as factors of importance in the surface conditions. The investigated subsurface conditions are thermal properties of the bedrock and interior Earth conditions affecting geothermal heat flow. The heat generated by the spent fuel has been considered in the presence of repository case. The calculations were carried out in two steps; 1) by using constant surface temperatures, and subsequently 2) using surface temperatures based on site-specific climate scenarios. For further, detailed information on the permafrost modelling, see the preceding parts of Section 3.4.

3.4.7 Handling of uncertainties in SR-Can

Uncertainties in mechanistic understanding

There are no major uncertainties in understanding of mechanistic processes regarding permafrost development. Minor uncertainties are associated with the fact that the exclusion of salts in freezing of groundwater and the geochemical weathering of the geosphere due to freezing and thawing processes are not yet well-founded.

Model simplification uncertainty

The major model simplification is to carry out the studies in 1-D excluding implications from lateral variations in physical properties, boundary conditions and geometry. For example, full consideration of the anisotropy of thermal conductivity and heat capacity and the features of water bodies and topography, as well as the heat generation from the spent fuel, requires 3-D modelling. The 1-D modelling approach could, in certain situations, result in somewhat higher temperatures than would be calculated using a full 3-D approach. Lateral groundwater flow, cooling down the bedrock, is the most important factor that would need 3-D modelling instead of 1-D in the context of permafrost development. However, groundwater flow, as mentioned above, only has a minor role in permafrost development, compared to heat conduction. Furthermore, the anisotropy of thermal properties is not a problem in 1-D, since one can choose a combination of thermal properties that would give lowest temperatures, or at least very close to the lowest temperatures. Therefore, it is not likely that 3-D simulations would yield notably lower temperatures than the range obtained by the full series of 1-D sensitivity modelling simulations that have been performed.

Additional model simplifications are the continuum approach for the modelling of groundwater flow and neglect of salinity transport. However, both the Forsmark and Laxemar sites are largely composed of relatively low-porosity and low-permeability bedrock, in which case the groundwater flow and salinity of groundwater have minor effects on permafrost development. If salt transport would have been included, some calculated permafrost depths would have been slightly shallower.

Input data and data uncertainty

Some data uncertainty exists when it comes to effective thermal conductivity and heat capacity of rock at the two candidate repository sites. In the calculation of ground temperature and the rate of freezing, thermal conductivity is the most important input parameter in terms of physical properties of the ground. The predominant rock type in Forsmark has a mean thermal conductivity of 3.56–3.71 W/(m·K), depending on the method used for the determination /SKB 2005a/, whereas subordinate rock types have values between 2.96 and 3.54 W/(m·K).

Some uncertainty also exists in determination of hydraulic and mechanical properties of bedrock and salinity concentrations of groundwater versus depth at the suggested repository sites /SKB 2005a, 2006ab/.

The in situ ground temperature has been measured in boreholes to a depth between 500 and 1,400 m. Between different boreholes the temperature deviates in a range of 2°C /SKB 2005a, 2006ab/. A considerable uncertainty is associated with determination of the ground surface temperature from the air temperature as well as with estimation of the in situ temperature and geothermal heat flow in the depth range of 1,000–10,000 m for the thermal boundary and initial conditions of the model.

3.5 Glacially induced faulting

3.5.1 Overview/general description

In this section, we will use the term “glacially induced faulting” or “glacially induced fault” (GIF) for all earthquake activity related to the emplacement or removal of large ice sheets. Other common terms are end-glacial and post-glacial faults, which in our context would be sub-classes of GIFs occurring at the end of, or any time after, a glaciation, respectively. The existence of large, kilometre scale, GIFs have until now only been confirmed in northern Scandinavia /Kujansuu 1964, Lagerbäck 1979, Olesen 1988, Munier and Fenton 2004/. These faults ruptured

as very large, reverse faulting earthquakes just as the ice withdrew from the affected areas at the end of the last glaciation. The strike of the faults is well known, but fault geometry at depth is virtually unknown.

Due to uncertainties in fault geometries, the tectonic state of stress, crustal pore pressures and ice histories, the mechanics of faulting of the GIFs is not well understood. The temporal evolution of an ice sheet (see Section 3.1) will cause time varying deformation and stress in the Earth, a process referred to as glacial-isostatic adjustment (GIA) /e.g. Peltier 1974, Johnston et al. 1998, Lund 2005/. As the ice sheet advances and the ice load increases, the elastic lithosphere will bend and the viscoelastic mantle flow laterally. This will produce a depression below the ice and a corresponding bulge outside the ice margin (Figure 3-65). The horizontal stresses induced by lithospheric bending are larger in magnitude than the increase in vertical stress due to the ice load and are compressional in the depression under the ice and tensional in the fore-bulge (Figure 3-66). The horizontal stresses will be larger than the vertical stress all through the glacial cycle, and especially so towards the end of deglaciation. The isostatic rebound of the depressed elastic lithosphere is a much slower process than the retreat of the ice sheet and corresponding removal of the ice load, leaving remanently high horizontal stresses in the lithosphere after the vertical stress induced by the ice sheet is gone. The shape of the depression and, therefore, the magnitude and distribution of induced stresses, depend critically on the shape (e.g. spatial extent and slope) and thickness of the ice.

Generally, the emplacement of a large ice sheet stabilizes faults in the crust since the mean stress, approximately equivalent to the normal stress on faults, increases more rapidly than the deviatoric stresses. Towards the end of glaciation, however, the rapid decrease in vertical stress, caused by the deglaciation and removal of the ice load, tends to destabilise the crust /e.g. Wu and Hasegawa 1996a, Lund 2005/. The tectonic stress state is very important in the assessment of glacially induced faulting /e.g. Wu and Hasegawa 1996ab, Lund 2005/. The glacially induced shear stresses, superimposed on an isotropic, lithostatic stress, are not large enough at seismogenic depths to induce faulting. A further source of deviatoric stress, such as tectonic stress, is necessary. The tectonic stress state largely determines which faults will be reactivated, how and when they will slip and where, in relation to the ice sheet, instabilities will occur.

As discussed in /**Geosphere process report**/, pore pressure is a vital component in all faulting related processes. Increased pore pressure decreases the normal stress on a fault and, thus, decreases the shear stress needed to cause movement. The ice sheet is expected to increase pore pressure in the crust below, both through the increase in mean stress by the load itself and through high water pressures at the base of the ice sheet (see Section 3.1 and 3.2). The increased pore pressure will tend to lower fault stability all through the glacial cycle, the effect will, however, be largest at the end of glaciation when fault stability is generally decreasing.

Groundwater pressure and groundwater flow will be affected by glacially induced faulting. As the rock mass and fractures are compressed or dilated during rupture and passing of elastic waves, large fluid pressure transients are expected which will change groundwater flow. The permanent plastic and elastic deformation due to the earthquake will also influence fluid pressure since fractures and pore volumes may be altered. The pressure gradients induced due to this volume alteration will remain as long as it takes for the groundwater to flow out of or into to the fractures or pores. Further, glacially induced faults also cause permanent elastic deformation of the repository which may alter flow patterns.

Glacially induced faulting may affect a number of geosphere variables of importance for a deep geological repository (Table 3-14).

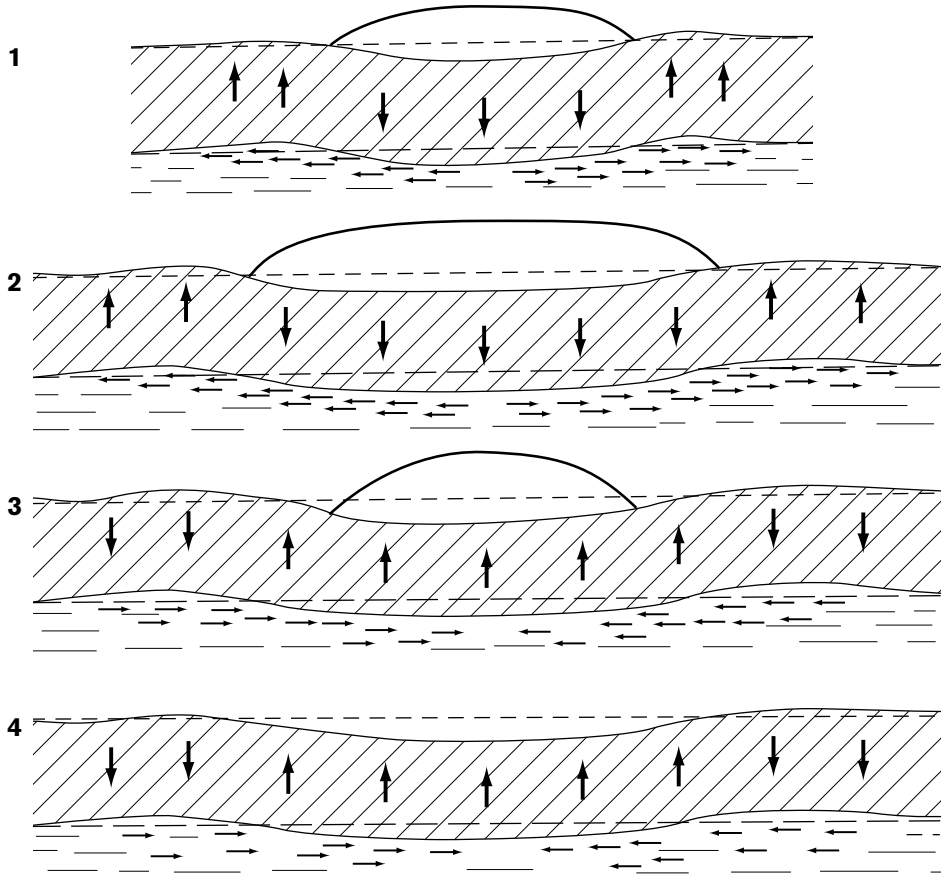

Figure 3-65. *Sketch of the glacial isostatic adjustment process during glacial loading and unloading/. Arrows denote motion of the medium. The ice load on the lithosphere creates a depression under the ice and a bulge outside the ice margin. The bulge moves outward as the ice grows and inwards when the ice retreats. The rebound of the lithosphere is not finished when the ice disappears but takes considerably longer. Figure based on /Nansen 1922/.*

Table 3-14. Summary of how geosphere variables are influenced by glacially induced faulting.

Geosphere variable	Influenced by climate issue variable/s	Summary of influence
Repository geometry	Location Magnitude Focal mechanism	An glacially induced fault will alter the geometry of the repository tunnels and deposition holes if the fault occurs close to or within the repository and the magnitude is large enough.
Fracture geometry	Magnitude Location	Rupture, primary or secondary, will reopen sealed fractures, perhaps link previously separate fractures and, possibly, create new fractures. Stress and pore fluid pressure changes from an earthquake will also affect fracture aperture.
Rock stresses	Magnitude Location Focal mechanism	Rock stresses will be strongly influenced in the vicinity of a rupture. Shear stresses will be relaxed around the centre of the rupturing fault and the stress state in the vicinity of the fault will be modified, temporarily by the elastic wave field but permanently by the static elastic stress field from the fault rupture, coupled with plastic deformations. In addition, secondary fault motion, due to stress and pore fluid disturbances from the earthquake, will influence the stress field at some distance from the rupture.

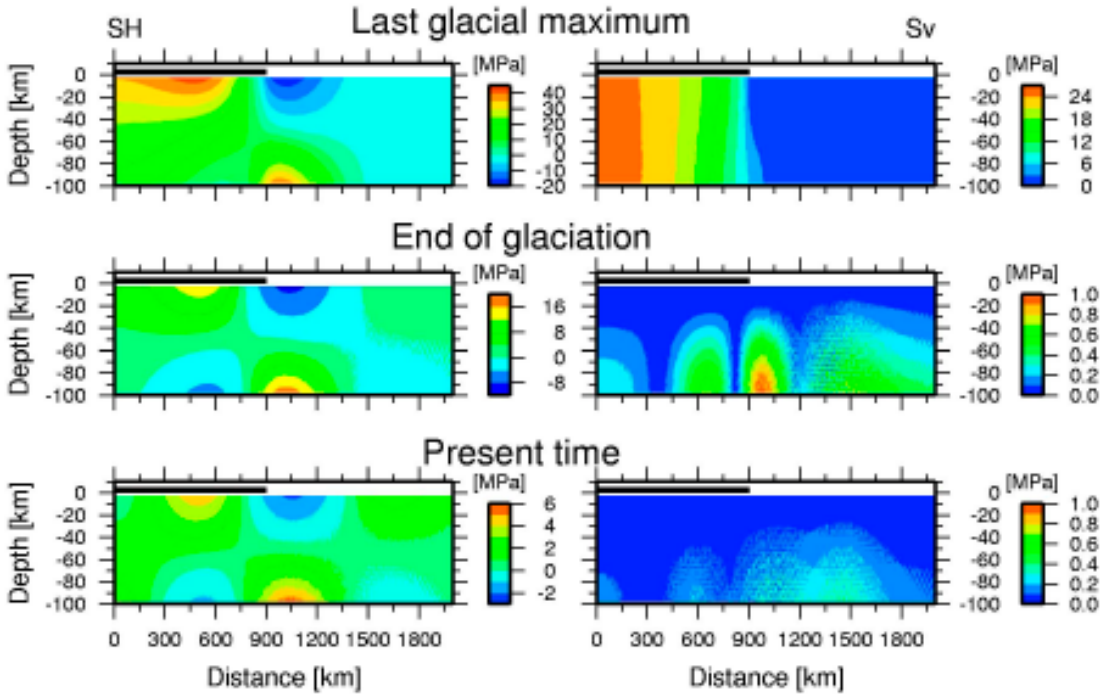

Figure 3-66. *Maximum horizontal (left) and vertical (right) induced glacial stresses at three different times: the last glacial maximum, the end of glaciation and present. The Earth model is a simple 2D model with a 100 km elastic lithosphere overlying a viscoelastic half-space subject to an elliptic cross-section ice load with 900 km lateral extent and 25 MPa central pressure at the last glacial maximum.*

3.5.2 Controlling conditions and factors

Evolution and properties of the ice sheet

The ice sheet evolution controls the deformation of the lithosphere, and therefore also the amount of stress induced in the crust. A thorough understanding of the process of glacially induced faulting, therefore, requires thorough knowledge about the ice sheet. The areal extent of the ice sheet controls the location of eventual GIFs, the thickness of the ice determines the magnitudes of the induced stresses and the slope of the ice edge determines the bending of the lithosphere and, therefore, the amount of induced deviatoric stress. All of these factors evolve though time as the ice sheet evolves and the longer (in relation to the time constants of the viscoelastic parts of the Earth) an area is ice covered, the larger are the induced stresses.

The basal conditions of the ice sheet, the ice sheet thickness and the characteristics of the hydrological system of the ice sheet determine how the fluid pressure at the base of the ice develops, see Section 3.1 and 3.2. The incremental pore fluid pressure induced in the crust by the ice sheet is very important for fault stability assessment and variations in this pressure will significantly affect the stability of the crust.

Rheological parameters, Baltic shield and deformation zones

The response of the Earth to an applied ice load is determined by its rheological structure. Due to the long time spans involved in a glacial cycle both elastic and viscous deformation will occur. The lithosphere is generally regarded as a purely elastic plate overlying a viscoelastic mantle.

The induced GIA stresses are significantly more sensitive to variations in the rheological parameters (i.e. elastic moduli, density, viscosity) than the corresponding surface deformations /e.g. Klemann and Wolf 1998, Lund 2005/. Estimates of the elastic moduli are readily available from seismic surveys and densities from gravity measurements and modelling. Lateral

variations in layer thicknesses, such as the thinning of the crust and lithosphere from the central Baltic shield westward to the oceanic crust and lithosphere off the coast of Norway, should be included in studies of induced stresses and GIF. Care must be taken, however, when considering the inclusion of Earth layers defined by seismic investigations into GIA models. The vastly different time scale of observation usually translate into different layer definitions. Studies such as /Pérez-Gussinayé et al. 2004/, which use gravity data to define the effective elastic thickness of Fennoscandia, are probably better suited for GIA modelling. The viscosity structure, and the relative strengths, of the lithosphere and upper mantle is a debated topic. Direct observational data on viscosities are scarce and any inferred refinement of the viscosity structure has to be carefully evaluated by modelling of available deformation data, such as GIA measurements, due to the large impact the viscosity distribution has on both stress magnitudes and the temporal evolution of the stress field.

The stability of faults in a particular stress field depends to a large extent on their orientation with respect to the principal stress axes. Since there is observational evidence that the GIFs frequently occur along pre-existing zones of weakness, such as old shear zones, /e.g. Lagerbäck 1979/ it is important to identify such zones and their orientation when analysing glacially induced faulting. Not only is the strike of weak zones important, dip information is crucial when assessing fault stability.

Initial state of stress

As discussed above, the initial state of stress, before the onset of glaciation, is very important for the stability of faults. Due to the slow time variations (1–10 Myr) in tectonic plate configuration, the tectonic stress field prior to glaciation can be assumed to be very similar to the current stress field, albeit there may be a small contribution left from the Weichselian GIA stresses in the current stress field. The current stress field in the Baltic Shield is, however, not very well determined at seismogenic depths. Earthquake studies show predominantly strike-slip faulting conditions in south-central Sweden, with a larger component of reverse faulting in the north /Slunga 1991/. Analysis of the 6.5 km deep boreholes in Siljan, central Sweden, indicates strike-slip faulting conditions at approximately 5 km depth /Lund and Zoback 1999/.

3.5.3 Observations in nature and present-day natural analogues

Almost all of the large faults (kilometre scale) that are currently generally accepted as being glacially induced are located in northern Scandinavia /Kujansuu 1964, Lagerbäck 1979, Olesen 1988, Munier and Fenton 2004/. Most of the GIFs strike north to northeast with dip to the east and downthrow to the west. They are almost exclusively reverse faults. The longest GIF is approximately 150 km long, with maximum displacement of 10–15 m. The GIFs are inferred to have ruptured as one-step earthquakes, reaching magnitude 7–8, just as the ice was retreating from the respective areas /Lagerbäck 1979, 1990, Olesen 1988/. The GIFs mostly ruptured through old zones of weakness (shear zones), not necessarily following one zone but instead jumping to another to comply with the restraints set by the causative stress state /Lagerbäck 1979, papers in Bäckblom and Stanfors 1989/. Although much effort has been spent on investigating the faults with both geological and geophysical methods /e.g. Bäckblom and Stanfors 1989, Lagerbäck 1990, Olesen et al. 1992, Kuivamäki et al. 1998/, key questions concerning the formation and current status of the faults are still unresolved. These include fault geometry at depth, fault strength and current deformation rates. Large GIFs have, for the time being, been identified exclusively in northernmost Scandinavia /review in Munier and Fenton 2004/ although much of Scandinavia was subject to a substantial ice load. This is an intriguing problem which poses a difficult challenge to models of GIF formation. Other observations /e.g. Mörner 2004, Kotilainen and Hutri 2004, Anda et al. 2002/ suggest that GIF was widespread throughout Fennoscandia. However, when actual faults have been observed, they are significantly smaller than those in northern Scandinavia.

The influence of a large ice sheet on seismicity can be studied today in Greenland and Antarctica /e.g. Johnston 1987, 1989/. The absence of high seismic activity and large earthquakes, at least over the time span of modern seismic instrumentation (approximately 100 years), in these areas confirms results from GIA modelling and fault mechanics analyses.

3.5.4 Model studies

Models of GIF mechanics need to consider both an ice sheet model /e.g. Lambeck et al. 1998/, and Section 3.1 in the present report and an Earth model. In addition, considerations such as a fault stability criterion, the initial stress state and pore pressure have to be taken into account.

Fault stability during a glacial cycle has been modelled with varying degrees of model complexity during the last decades. Early models /Walcott 1970, Stein et al. 1979, Quinlan 1984, Johnston 1987/ did not consider a viscous mantle and, therefore, did not capture stress relaxation effects. The models generally agree on increased fault stability during the loading phase of the ice sheet and then decreased fault stability during deglaciation. Wu and co-workers estimated the onset in time and space of fault instability, using sophisticated viscoelastic Earth models and a variety of simple /Wu and Hasegawa 1996a, Johnston et al. 1998/ as well as globally and regionally consistent ice models /Canada: Wu and Hasegawa 1996b, Wu 1997, Wu and Johnston 2000, Fennoscandia: Johnston et al. 1998, Wu et al. 1999, Antarctica: Kaufmann et al. 2005/. These models use the difference in Fault Stability Margin, dFSM, /Quinlan 1984, Wu and Hasegawa 1996a/ to infer increased/decreased fault stability. The dFSM stability criterion is based on Mohr-Coulomb frictional theory, which describes the amount of shear stress necessary to overcome frictional resistance and cause slip on a fault. dFSM assesses whether or not a change in the state of stress will make fault slip more, or less, likely. dFSM was also used by /Klemann and Wolf 1999/ as one of a number of parameters in their study of the implications of a ductile layer in the crust for the deformation caused by the Fennoscandian ice sheet and by /Lambeck and Purcell 2003/ in their recent assessment of fault stability in Finland. /Lund 2005/, using various viscoelastic Earth models and simple ice models, compared the dFSM measure with an absolute stability measure, also based on the Mohr-Coulomb criterion. All these studies generally find that earthquake activity is suppressed by the emplacement of the ice sheet, but greatly enhanced at the end of deglaciation. The onset and location of increased fault instability, however, varies with ice sheet dimension and temporal evolution, lithospheric and mantle structure and the initial state of stress. The models are very large scale and predict large areas of fault instability, not necessarily in agreement with the observations.

Current numerical modelling procedures have been thoroughly tested against a variety of simple problems where analytical solutions are available /e.g. Johnston et al. 1998, Wu 2004, Lund 2005/. Different numerical implementations, such as finite element analysis and spherical harmonic spectral analysis, have been tested against each other, so that the current models are thought to be correct within their limitations. Verification and validation of the GIA models can be made with surface deformation data. There are, however, very few stress data to compare the model predictions with, which is a problem in the context of fault stability analysis. Stress orientations and some measures of relative magnitudes of stress can be obtained from earthquake data /Slunga 1991/. There are also borehole data available at some locations in Fennoscandia, notably the North Sea oil fields, the SKB site investigations at Forsmark and Oskarshamn /SKB 2005a, 2006b/ and the Siljan deep boreholes /Lund and Zoback 1999/ where the model predictions can be tested /e.g. Grollimund and Zoback 2000/.

Observations of postglacial rebound can to first order /e.g. Milne et al. 2004/ be modelled using very simple models of the Earth with a single layered elastic lithosphere and a two layered viscoelastic mantle characterised by linear Maxwell rheology. The Earth models used in most GIA modelling to date have been rather simple, horizontally layered models. Elastic properties are derived from seismic studies and viscoelastic properties are inferred from the fit of the GIA

models to observations such as sea-level data, GPS data and geological records, see discussion in Section 3.3. Observations at different time and length scales can be difficult to reconcile, e.g. there is evidence of a ductile lower crust from laboratory measurements but such a ductile layer is not required by GIA modelling, which implies that the values of the rheological parameters needs further consideration. /Lund 2005/ tested how variations in various rheological parameters affected induced shear stress and vertical deformation in simple Earth models. A general conclusion of the study was that induced stresses are significantly more sensitive to variations in the rheological structure of the Earth model than the corresponding vertical deformations. Models with laterally varying layer thicknesses have been tested, mostly with respect to surface deformations as recorded in relative sea-level data /Kaufmann et al. 1997, 2000/. The results of /Lund 2005/ also showed that induced GIA stresses are much more sensitive to lateral rheological variations than are the resulting surface deformations, implying that such variations, e.g. the thinning of crust and lithosphere from the central Baltic shield to the Norwegian margin, must be included when assessing the stress field. Recently, fully three-dimensional, spherical Earth models have been developed where lateral variations in viscosity and elasticity can be generally studied /e.g. Martinec 2000, Wu and van der Wal 2003, Latychev et al. 2005/.

Models of the Weichselian glaciation are steadily improving and come in a variety of modelling approaches. In Section 3.1 the model uses glacial dynamics and climate data to develop an ice sheet, whereas Lambeck and co-workers /Lambeck et al. 1998, Lambeck and Purcell 2003/ have built a model based on sea-level, lake-level and geological data. Although the general features of these models are similar, they display enough differences in their details to warrant careful examination in the fault stability context, due to the sensitivity of the GIA induced stresses to the shape of the ice load. Ice sheet hydrology and basal fluid pressure conditions are areas of active research (see Section 3.1 and 3.2) the outcome of which are of great importance for the modelling of pore pressure effects on fault stability.

The initial tectonic stress field in the models can either be taken straight from the available data, as discussed above, or the available data can be used as a basis for assumptions regarding the initial field. There is much evidence for an intraplate brittle crust in frictional-failure equilibrium on pre-existing faults, using laboratory derived coefficients of friction /e.g. Zoback and Townend 2001/. Such an initial state provides a consistent background, which will clearly indicate when the applied GIA stresses cause fault instability. It is imperative to analyse various initial stress fields as they determine which areas, with respect to the ice sheet, and faults of which orientation will become most unstable. Also, the timing of onset of fault instability is governed by the initial stress field and the ice evolution.

A specific example of the type of modelling discussed here is shown in Figure 3-67 and is based on the procedures discussed in /Lund 2005/. The figure shows the estimated stability of faults at various times along a 2D profile that crosses northern Scandinavia at the latitude of the large glacially induced faults. The Earth model is a very simple, 100 km thick elastic plate on a viscoelastic half-space with viscosity $1 \cdot 10^{21}$ Pa s. The ice model is the SCAN-2 model of /Lambeck et al. 1998/, projected along the 2D profile. The initial state of stress is a reverse faulting regime in frictional equilibrium on optimally oriented faults with a coefficient of friction of 0.6. Pore pressure is not taken into account in the model. We see in Figure 3-67 that fault instability is developed in the model during two time periods, the first at around 30 kyr BP and the second after deglaciation, ~ 12 kyr BP to present. Both time periods are periods of rapid deglaciation. Instability develops under the central parts of the ice sheet, higher in magnitude to the west where the slope at the ice edge is the largest. The 2D profile cuts through the Pärvie fault at kilometre 260 km and the Lansjärv fault at 460 km, both in the central section of the developed instability field. The example shows that quantitative models can predict fault instability at the approximately correct locations at the right time. There are, however, still many unresolved questions in going from model response to earthquake generation.

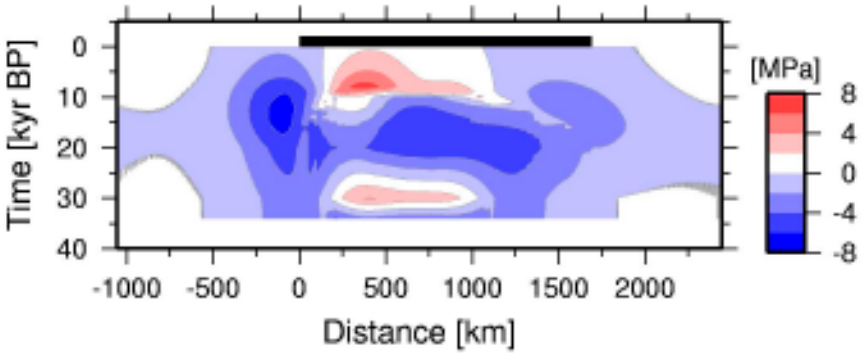

Figure 3-67. *Stability of optimally oriented faults at different times along a 2D profile across northern Scandinavia at the latitude of the large glacially induced faults. Zero along the profile corresponds to the westernmost extent of the ice sheet, off the coast of Lofoten, Norway. To the east, the profile extends well into Russia. Positive, red colours, indicate unstable faults and negative, blue colours, indicate stable faults. The black bar across the top shows the maximum lateral extent of the ice along the profile. See the text for information about the Earth and ice models.*

Most models of the kind discussed above do not include the effect of slow tectonic strain accumulation during glaciation. The strain rates due to plate tectonics in Scandinavia have been considered small in comparison to the glacially induced strain rates /e.g. Muir-Wood 1995/ and, therefore, negligible in the context of glacially induced faulting. Recently, however, /Adams 2005/ argued that the accumulated effect of tectonic strain rate would be sufficient to generate all the observed glacially induced faults of northern Scandinavia. That study uses an estimate of the long-term seismicity rate of Stable Craton Cores (SCC) /Fenton et al. 2006/ and a variety of earthquake data sets from Fennoscandia, including current seismicity, the mapped glacially induced faults of northern Scandinavia and the palaeo-earthquakes of /Mörner 2004/. The approach of /Adams 2005/ does not allow any inferences to be made about the location, orientation or type of faulting events.

Current models of the process of glacially induced faulting are still not mature enough that they can accurately predict the location and magnitude of GIFs. Efforts are, however, underway to include more complex processes in the models, such as poroelastic effects, permafrost effects, strain release effects and local geological conditions. As discussed above, fully three-dimensional Earth models have just recently become feasible and recent ice models are detailed enough to produce the necessary loading resolution. There is, within the next couple of years, potential for a large increase in the understanding of the mechanics of glacially induced faulting.

3.5.5 Time perspective

Glacially induced faulting is a process strongly correlated with the emplacement or withdrawal of an ice sheet from a region. It is, however, not necessarily limited in time to the actual end of a glacial cycle, but may well occur at any rapid increase or decrease in ice volume and/or areal extent during the glacial cycle. The evolution of the ice sheet, therefore, determines the likelihood of glacially induced faulting at any specific period in time.

3.5.6 Handling in the safety assessment SR-Can

Glacially induced faulting is investigated by means of numerical finite element modelling. The evolution in time of a reconstructed Weichselian glaciation is used to calculate the resulting deformations and rock stresses. The Earth model used consists of an elastic lithosphere on top of a viscoelastic mantle. The modelling requires that the initial state of stress is specified. The effects of varying rheological parameters (i.e. elastic moduli, density and viscosity), as well as different shapes of the ice sheet, have been investigated in a previous parametric study by /Lund 2005/.

Two different ice models, the SCAN-2 model by /Lambeck et al. 1998/ and the UMISM model (see Section 3.1) are used as input along a 2-D profile in order to calculate the time-varying stress field in the Earth's crust. The latter modelling work has not yet been finished. The results are used to estimate the stability/instability of faults at different times based on assumptions of fault strength.

Stress output from the numerical model is also used as boundary conditions for 3DEC modelling of induced shear displacements and estimates of the potential for canister damage /Hökmark and Fälth 2003/.

For further, detailed information on the modelling of glacially induced faulting, see the preceding parts of Section 3.5.

3.5.7 Handling of uncertainties in SR-Can

Uncertainties in mechanistic understanding

Uncertainties in the understanding of the phenomenon of glacially induced faulting can be divided into two broad categories. The first is associated with the general understanding of the processes involved in glacially induced faulting, such as the characteristics of the ice load, the necessity of high fluid pressures, the role of pre-existing zones of crustal weakness, the tectonic stress field, the geometry of the faults. These factors determine where and when fault instability can occur in a region and they are currently not well understood, although modelling efforts are underway to address these issues. A major problem with current models is that they indicate widespread, in time and space, crustal instability whenever the ice sheet is rapidly decreasing. This is not in agreement with current field observations of glacially induced faulting.

The second category of uncertainties derives from limitations in the general understanding of the mechanics of faulting. Although large efforts have been directed toward the understanding of earthquake nucleation and the rupture process, there is not yet a generally accepted model for how earthquakes nucleate, how they grow from small to large earthquakes and, eventually, how rupture propagation terminates. It is therefore difficult to deterministically model the size of an earthquake based on indications of fault instability in a specific area.

Model simplification uncertainty

GIA models used to assess fault stability have, so far, only been 1D Earth models. This is likely to be oversimplified for realistic models of the glacially induced crustal stresses. Efforts are underway to incorporate both 2D and 3D Earth models. Consideration of pore pressure is usually not incorporated in the GIA models although the pore pressure effect is likely to be important. The conversion of modelled crustal instabilities to assessments of seismicity is an issue which is currently not well understood and needs significant further work /Hora and Jensen 2005/.

Input data and data uncertainty

The data input to models assessing glacially induced crustal instability is rather large since we require an ice model, an Earth model and the current state of stress in the crust. For refinements of the models, the ice and Earth models also need to include information such as pore fluid pressures and permeabilities, data on structures of weakness in the crust etc. All these models rely on numerous observations in their development and verification. In the models of /Lund 2005/, Earth and ice models were varied so that the effects of variations in a specific parameter could be assessed. Such repeated modelling using available ice models and geophysically sound variations of Earth models, as well as upper and lower bounds on pore pressures and hydrological parameters for the Earth, is a straight-forward albeit time consuming approach to an estimate of the variability in the results.

4 Evolution of climate-related conditions for the safety assessment

4.1 Rationale and general approach

The evolution of climate-related conditions accounted for below are the external conditions in the main scenario of SR-Can (Figure 1-2). Since it is impossible to describe an expected evolution of climate conditions the next million years or 100,000 years, the two variants of the main scenario should not be seen as prognoses or attempts to predict future evolutions. Instead, they are *examples* of future evolutions that in a realistic way cover all relevant climate-related changes that can be expected in a 100,000-year time perspective.

As the reference evolution, used in the base variant of the main scenario, a model reconstruction of the Weichselian is selected. Despite remaining uncertainties regarding the Weichselian history, especially regarding the earlier phases of the period /Lokrantz and Sohlenius 2006/, it is the best known glacial cycle. This yields possibilities to use geological information for testing and constraining the adopted models. In line with the discussion above, the purpose is not to produce a "best estimate" of the Weichselian evolution, but rather to define a scientifically reasonable starting point for the analysis of potential climate impacts on repository safety.

The scenario extend over 120,000 years. Three models are used to yield boundary conditions for the safety assessment:

1. A dynamic ice sheet model.
2. A Glacial Isostatic Adjustment (GIA) model.
3. A permafrost model.

The ice sheet model is the University of Maine Ice Sheet Model (UMISM) (see Section 3.1.4). The GIA model was developed at the University of Durham (see Section 3.3.4) and the permafrost model at Helsinki University of Technology (see Section 3.4.4). The basis for the reference evolution of climate-related conditions is a reconstruction of the evolution of the Fennoscandian ice sheet during the Weichselian employing the ice sheet model. The generated ice sheet evolution has been used as input to the global isostatic adjustment (GIA) model. The third main component in modelling the reference evolution is the permafrost model, yielding permafrost depths given the evolution of ice sheet, shoreline, and vegetation. The main data flows between the ice sheet, GIA and permafrost models are shown in Figure 4-1.

The base variant of the main scenario is one example of a conceivable evolution and covers climate-related conditions and sequences that could be expected in a 100,000 year time perspective. Possible alternative evolutions are handled as additional scenarios. The basis for selecting additional scenarios (Figure 1-2) is the analysis of safety under the main scenario. The conditions and sequences that give the largest impact on the safety form the basis for the selection of additional scenarios. Alternatives to the base variant are also selected on the basis of identified concerns of scientists and the public. Therefore, the main scenario also includes a variant depicting an evolution with a warming climate due to an increased human induced greenhouse effect (Figure 1-2). The consequences of additional greenhouse warming are analysed as a very long period of the initial temperate domain.

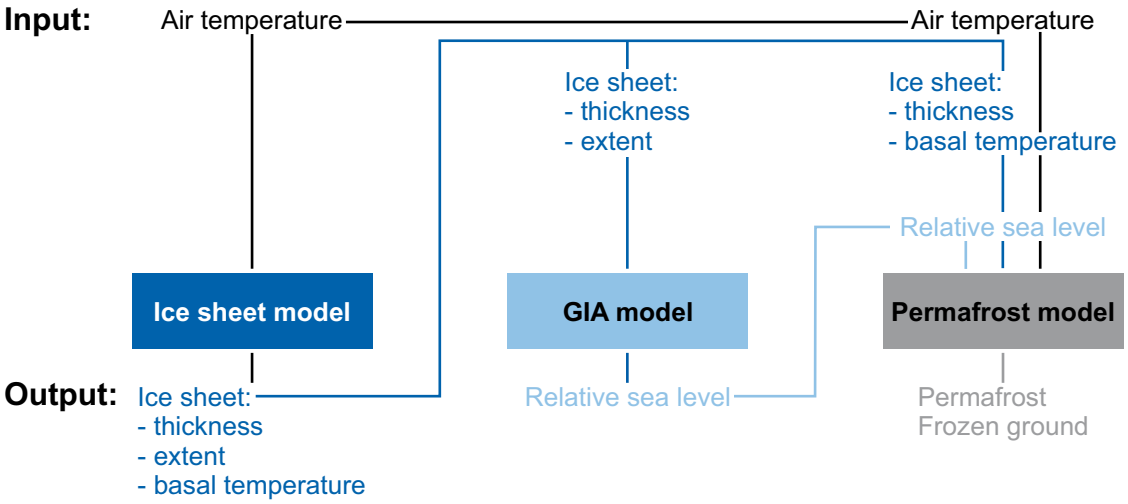

Figure 4-1. *Models used to provide boundary conditions for analysis of the impact of climate-related changes on the repository. Only input and output data shared between the models used to generate the boundary conditions are shown.*

4.2 Main scenario – base variant

The evolution of the repository is affected by shoreline migration and the development of permafrost and ice sheets, whereas the climate at the ground surface is of much less direct importance.

4.2.1 Ice sheet evolution

The dynamic ice sheet model is described in Section 3-1. The modelled ice sheet evolution for the base variant of the main scenario starts in a warm interglacial climate, in a situation in which there is no Fennoscandian ice sheet and the shore level is assumed to be similar to the present. The evolution of ice covered area and ice volume for the base variant of the main scenario are shown in Figure 4-2. The ice configurations for selected times, depicting stadial and interstadial configurations, are shown in Figure 4-3. During the glacial cycle, the ice sheet grows progressively larger in a number of distinct growth phases, with intervening phases of more restricted ice coverage. The Glacial Maximum (corresponding to the Last Glacial Maximum of the Weichselian glaciation), is reached about 100,000 years into the scenario. The overall behaviour of the ice sheet can be characterised as being distinctly dynamic throughout the glacial cycle.

Ice sheet evolution at the candidate sites

The dynamic behaviour of the ice sheet during the glacial cycle is seen also at the two candidate sites. Both sites are covered by ice during the cold stadials about 60 and 100 ka into the scenario (Figure 4-4). Between these stadials, both sites experience ice-free warmer interstadial conditions (corresponding to Marine Isotope Stage 3 in the reconstructed Weichselian glacial cycle) (Figure 4-4). Advances of the Fennoscandian ice sheet during earlier stadials (corresponding to Marine Isotope Stage 5d and 5b) do not reach the candidate sites (Figure 4-3), although the ice sheet margin is close to Forsmark during Marine Isotope Stage 5b. It is worth noting that, even though an ice sheet is present in Fennoscandia during most of the glacial cycle (Figure 4-2), the two specific sites of Forsmark and Laxemar, located in south-central and southern Sweden, are not covered by the ice sheet for the majority of the time.

The Forsmark region is covered by the ice sheet for a total time of ~ 30,000 years and the Laxemar region for ~ 19,000 years. The difference in ice-covered time, 11,000 years, reflects the difference in latitude between the sites. For most of the ice-covered time, both sites are

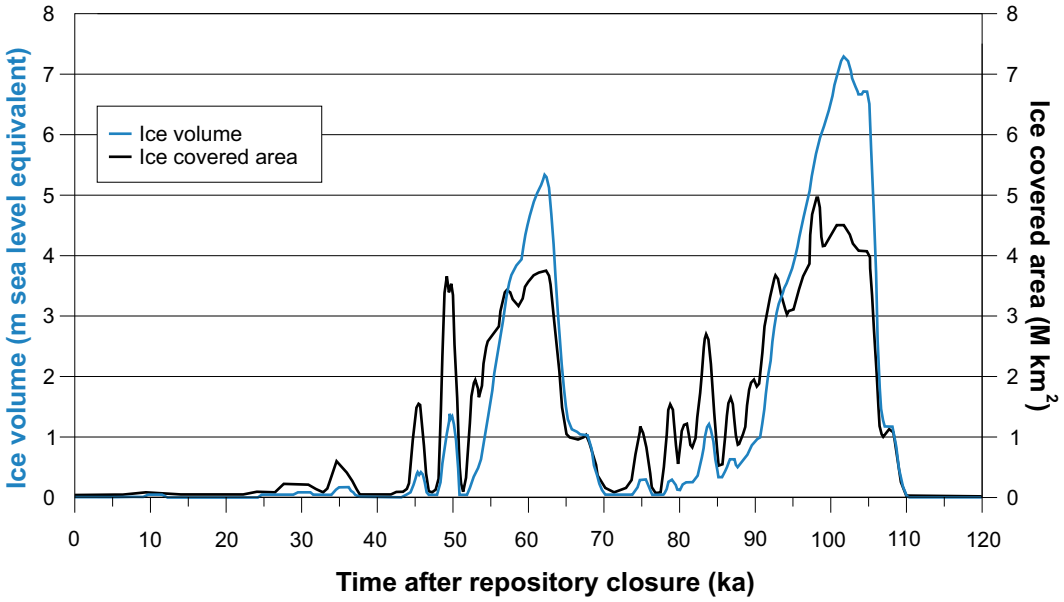

Figure 4-2. *Ice sheet volume and ice covered area for the base variant of the main scenario.*

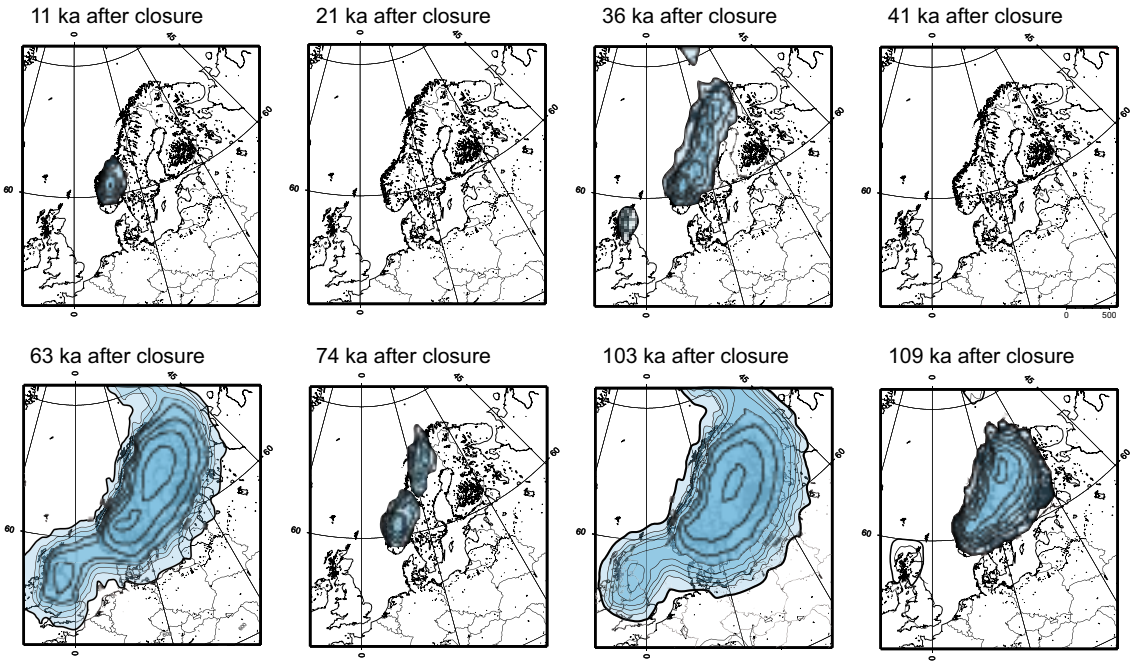

Figure 4-3. *Ice sheet configurations at major stadials and interstadials for the base variant of the main scenario. Contour lines show ice surface elevation with a 300 m contour interval. All maps show present day shoreline position. Ages are expressed as years after repository closure.*

covered by warm-based ice with free water present at the ice-bed interface. Forsmark is covered by wet-based ice for ~ 23,000 years and Laxemar for ~ 16,000 years, corresponding to about 75% and 88% of the ice covered time respectively. This means that during most of the time that the ice sheet covers the sites in the base variant of the main scenario, meltwater is present at the ice sheet bed, typically produced at rates of a few mm/year, up to ~ 10 mm/year. During this time, this melt water is available for groundwater recharge in soil and bedrock.

The short periods of cold-based conditions, with no basal water production, always follow immediately after each time the sites become ice covered (Figure 4-4). During these periods, as well as during deglaciation periods when the sites are close to becoming ice free, water from *surface* melting may still reach the bed in the two regions. However, in cases when the ice sheet margin is located over permafrost ground, this melt water would not contribute significantly to groundwater recharge.

Naturally, the ice sheet over Forsmark and Laxemar was at its thickest during the glacial maximum (corresponding to the Last Glacial Maximum during Marine Isotope Stage 2). The largest ice thickness at this time, about 100,000 years into the scenario, is ~ 2,900 m for the Forsmark region and ~ 2,400 m for Laxemar (Figure 4-4). The difference between the sites is due to the fact that Forsmark is located further to the north, and therefore, at the glacial maximum, further away from the ice margin. It is worth noting that the modelled ice sheet reached significant thickness over both sites not only during the glacial maximum, but also during the cold stadial around 60,000 years into the scenario. At that time, the modelled maximum ice thicknesses at Forsmark and Laxemar are ~ 2,000 and ~ 1,300 m, respectively.

The groundwater pressure at repository depth is, for non-glacial conditions, determined by the depth of the repository, and for glacial conditions by the repository depth as well as an additional pressure induced by the ice load. The ice sheet thickness sets a limit to the maximum hydrostatic pressure that may occur at the ice sheet/bed interface. The additional hydrostatic pressure related to the maximum thickness in the reference glacial case (Figure 4-4) is 26 MPa for Forsmark and 22 MPa for Laxemar. These values are listed in Table 4-2 together with other estimates of *maximum* possible ice loads and associated *maximum* hydrostatic pressures (see Section 4.4.2).

4.2.2 Shoreline evolution

The GIA model used for generating the reference evolution is described in Section 3.3. At the start of a GIA model run, the Earth is assumed to be in isostatic equilibrium. In reality, the Earth is unlikely to reach such a state if glaciations occur with similar periodicity as in the past.

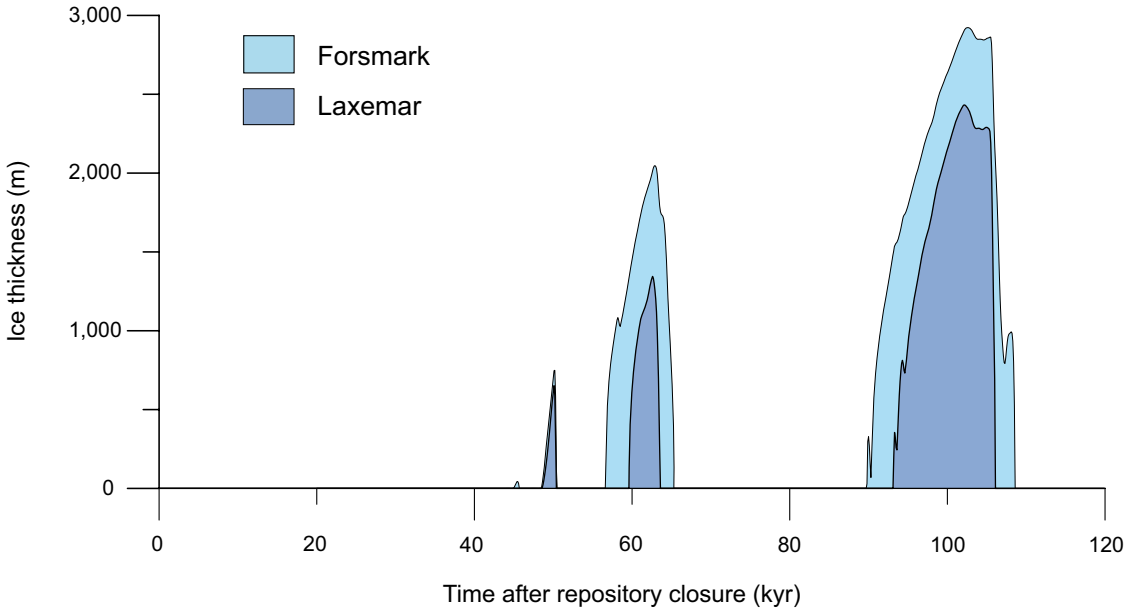

Figure 4-4. *Development of ice sheet thickness at Forsmark and Laxemar during the simulated reference glacial cycle. It is worth noting that, even though an ice sheet is present in Fennoscandia during most of the glacial cycle (Figure 4-2), the two specific sites of Forsmark and Laxemar, located in south-central and southern Sweden, are not covered by the ice sheet for the majority of the time.*

To correct for this, the GIA-modelling has been initiated by a glacial loading history yielding shorelines comparable to those reported by /Funder et al. 2002/ at the peak of marine inundation in the Early Eemian about 130,000 years ago. This gives shorelines similar to the present at the early phase of the reference glacial cycle. During the first 1,000 years after closure, and for the analysis of biosphere and hydrological evolution during the initial temperate domain, the shoreline evolution is extrapolated from shoreline data /Påsse 2001/. From about 8,000 years after closure to the end of the reference glacial cycle, the shoreline evolution is based on GIA modelling.

The evolution of the Baltic

During the initial phase of the glacial cycle, when climate is getting colder and ice sheets expand globally, sea levels fall. At the same time, the rate of isostatic rebound from the previous glaciation decreases. However, even if the rate is low, the amount of remaining uplift until the Earth reaches a relaxed state is significant. In the central part of the Fennoscandian ice sheet it has been estimated to ~ 100 m, and in the distal parts to ~ 25 m. As long as the Baltic is connected to the Atlantic, the relative shoreline along the Baltic coast is determined by isostatic rebound and global sea level change. If and when the relative sea level at Darss sill, south of Denmark, fall below the sill depth (today 18 m below mean sea level), the Baltic Sea is transformed into a lake. The surface level of this lake is determined by the altitude of the contemporary Darss sill. In the reference evolution, the global sea level falls below the Darss sill level after about 9,000 years. Due to the uncertainties in the GIA modelling relating to ice load input, 2-D Earth structure, and Earth rheology, it is likely that this result underestimates the time of isolation of the Baltic.

In the scenario, the Baltic thus constitutes a freshwater lake during a large part of the reference glacial cycle. In connection with the first major ice advance and the following retreat, after about 60,000 years into the scenario (corresponding to Marine Isotope Stage 4), isostatic depression put the candidate sites below water. The Baltic regain contact with the Atlantic after the final glacial advance to the Last Glacial Maximum. At this stage, large parts of southern Sweden again are submerged, this time by a saline Baltic sea. As the ice sheet retreats, also the two candidate sites are submerged. At the end of the scenario, and as isostatic rebound proceeds, the Baltic is transformed to an inland brackish sea.

During interstadials following major glacial advances, it is possible that a connection to the Atlantic can be established over Kilsbergen (Lake Mälaren and Vänern). This connection is probably of relatively short duration due to ice damming and rebound.

Shoreline evolution at the candidate sites

Due to larger ice thicknesses over Forsmark, this site experiences a larger isostatic depression than Laxemar. In connection with the first major deglaciation following the ice advance at around 60 ka in the scenario (corresponding to Marine Isotope Stage 4), isostatic depression puts the Forsmark site below water, whereas Laxemar remain un-submerged (Figure 4-5). During part of the ice free period between the two periods of ice coverage (corresponding to Marine Isotope Stage 3) the Forsmark site rises above the lake level due to isostatic unloading. At this time in the main scenario, Forsmark is situated above sea-level, and free of ice, for approximately 15,000 years. Laxemar is situated above the lake level during all of this ice free period, for about 30,000 years.

When the Baltic regains contact with the Atlantic during the deglaciation following the last and most severe ice covered period, both sites are submerged. The candidate sites again rise above the sea during the brackish phase of the Baltic following the final deglaciation.

The most important factor affecting modelled shoreline migration is the ice loading history, primarily the near-field history, and Earth structure. The uncertainty in modelled shore level mainly manifests itself in that reported relative sea-level values could be too high, resulting

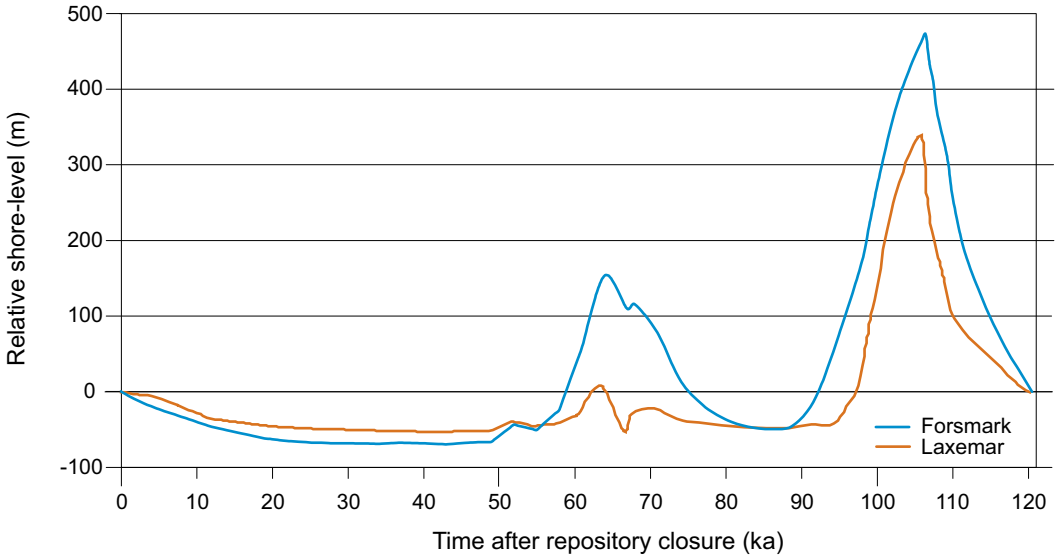

Figure 4-5. *Evolution of the shoreline at the candidate sites in the base variant of the main scenario. Positive numbers on the relative shore level indicate that the sites are submerged and vice versa. Note that for most of the time that the figure show submerged conditions, the sites are covered by an ice sheet.*

from a possible overestimation of isostatic depression. The size of the uncertainty varies over the modelled glacial cycle. Postulating that the ice sheet evolution is correct, the *mean* overestimation of relative sea-level, over the whole glacial cycle, may be up to 45 m for Forsmark and 27 m for Laxemar. At the time of deglaciation after the period of maximum ice sheet thickness, the overestimation of relative sea-level may be up to 50 m at Forsmark and 70 m at Laxemar.

Saline phases occur in the Baltic after major glacial advances, such as the ones occurring around 60,000 and 100,000 year into the scenario (Figure 4-4). During such periods of maximum salinity in the Baltic, both candidate sites are submerged (Figure 4-5).

4.2.3 Permafrost evolution

The permafrost model is described in Section 3.4. The input data of geological, hydrogeological, geothermal, geochemical and geomechanical properties are based on site-specific descriptions and are summarised in Tables 3-8 and 3-9. In the base variant of the main scenario, permafrost develops during the progressively colder phases of the glacial cycle. When the ice sheet comes to covers an area of permafrost, the permafrost typically stops developing and starts to slowly diminish. When the ground is re-exposed to a cold climate, such as during MIS 3, permafrost starts to grow again.

Evolution of permafrost at the candidate sites

The presence of permafrost and frozen ground may, if clay material freezes, impact the safety functions of the buffer and backfill. Freezing of the buffer takes place at a temperature of −5°C or lower /**Buffer and backfill process report**/. Adopting a pessimistic approach in the safety assessment for evaluating the safety function of the buffer, the evolution of the −5°C isotherm, as well as the permafrost depth (0°C isotherm) and frozen depth, were investigated. The evolution of the permafrost, −5°C isotherm, −10°C isotherm and frozen depth at the two candidate sites are shown in Figure 4-6.

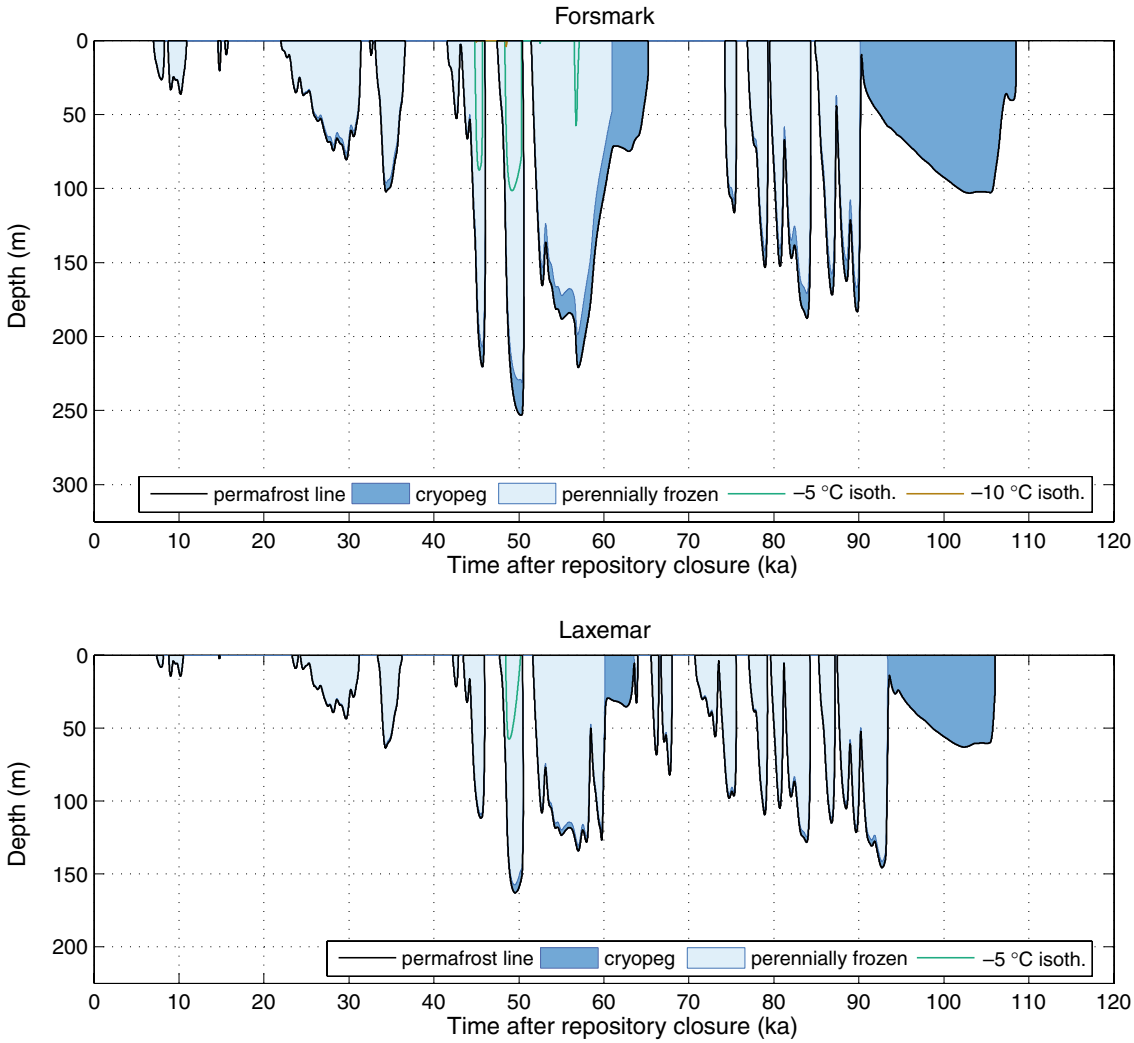

Figure 4-6. *Calculated permafrost depth, perennially frozen depth and the depths of the −5 and −10°C isotherms at Forsmark and Laxemar for the base variant of the main scenario. Note that the −10°C isotherm reach a depth of only 4 m at Forsmark, while it is absent at Laxemar. The greater permafrost depths at Forsmark are mainly due to different thermal bedrock characteristics.*

In the main scenario base variant, the development of permafrost starts about 8,000 years after repository closure at Forsmark, and after about 8,300 years at Laxemar. The permafrost and frozen ground depth reach a maximum at Forsmark and Laxemar prior to the first major glacial advance, at about 50 ka (Figure 4-6). At this time the modelled permafrost depth reaches ~ 250 m at Forsmark. The frozen depth is, at the same time, a few tens of metres shallower. At the same time, the maximum permafrost depth at Laxemar reach a depth of ~ 160 m (Figure 4-6), with the frozen depth being a few metres shallower. Because of more dilute groundwater, the unfrozen cryopeg is thinner at Laxemar than at Forsmark. When the ice sheet advances over the sites, the permafrost stops developing and instead starts to diminish, for example around 60,000 years into the scenario. Subsequently, permafrost again develops at both sites during the ice-free period between the two major ice advances, but at this time to a somewhat shallower depth. At Forsmark, it reaches about 180 m and at Laxemar about 140 m (Figure 4-6). During the major phase of ice coverage, including the ice sheet maximum at more than 100,000 years into the scenario, the maximum permafrost depth is around 100 m at Forsmark and 60 m at Laxemar. Note that, at this time, the frozen depth is zero due to the high pressure induced by ice load, and hence all bedrock is at this time at the pressure melting point temperature (Figure 4-6).

The −5°C isotherm also reaches a maximum depth at both sites prior to the first major ice advance, around 50,000 years into the scenario, reaching a depth of 100 m at Forsmark and 60 m at Laxemar. Just as in the case of the permafrost (i.e. 0°C isotherm), the −5°C isotherm is at a shallower depth at times of thick ice sheet coverage due to the insulating effect of the ice sheet. Furthermore, in this base variant, the −10°C isotherm reaches a depth of only 4 m at Forsmark, whereas no portion of the bedrock profile at Laxemar is at a temperature of −10°C.

Despite some uncertainties introduced in the permafrost modelling, such as the 1-D approach and treatment of vegetation and water bodies (in terms of lakes and shallow sea), some general conclusions about the site specific evolutions can be drawn. In the base variant of the SR-Can main scenario, Forsmark is more exposed to permafrost than Laxemar, mainly because it has different thermal properties of the bedrock which influence permafrost growth. In addition, the two sites have a different climate/ice sheet evolution caused by their different geographical locations, which further affects permafrost development. The maximum depth of permafrost (0°C isotherm), as well as the maximum depth of the −5°C isotherm, is in the base variant of the main scenario far from reaching repository depth at either of the sites. For a description of the uncertainties associated with the conducted permafrost modelling, see Section 3.4.7.

4.2.4 Evolution of climate domains

Based on the above evolutions of ice sheet, shoreline and permafrost, the climate development at the two candidate sites for the base variant of the main scenario can be described as successions of climate domains and submerged periods (Figure 4-7). The evolution of all relevant climate-related variables in the base variant of the main scenario is presented in Figure 4-8 and 4-9.

At Laxemar, the total times of occurrence of the temperate domain, permafrost domain, and combined glacial and submerged domain each occupies about one third of the total time of the scenario (Figure 4-7). At Forsmark the total time of permafrost domain is equal to that at Laxemar, whereas the temperate domain is shorter, with a correspondingly longer combined glacial/submerged domain.

The climate succession bars in Figure 4-7 show that both sites are dominated by temperate conditions for the first ~ 25,000 years, although shorter periods of permafrost domain occur around 10,000 years after repository closure. Then, through the periods free of ice sheets, temperate conditions are gradually replaced by permafrost conditions. The ice-free period around 80–90 ka into the scenario at Forsmark, and 70–90 ka at Laxemar is clearly dominated by permafrost conditions. The trend with gradually more dominating permafrost conditions is a natural result of the progressively colder climate during the glacial cycle. An exception to this trend is the short period after the submerged phase that follows the final deglaciation, at the very end of the scenario. At that time, ice free conditions again are dominated by temperate conditions in a warm interglacial climate. Yet another effect of the progressively colder climate during the glacial cycle is the increasing length of the periods with glacial domain at both sites.

Periods of temperate domain occupy about 31,000 years of the reference evolution at Forsmark and 41,000 years at Laxemar. It occurs in the early phase of the reference evolution glacial cycle, during the interstadial between the two major ice advances, and during the interglacial period following the glacial maximum. The periods of temperate domain in the starting interglacial and early phases of the reference glacial cycle are generally warmer and longer than those occurring during interstadials in the later part of the glacial.

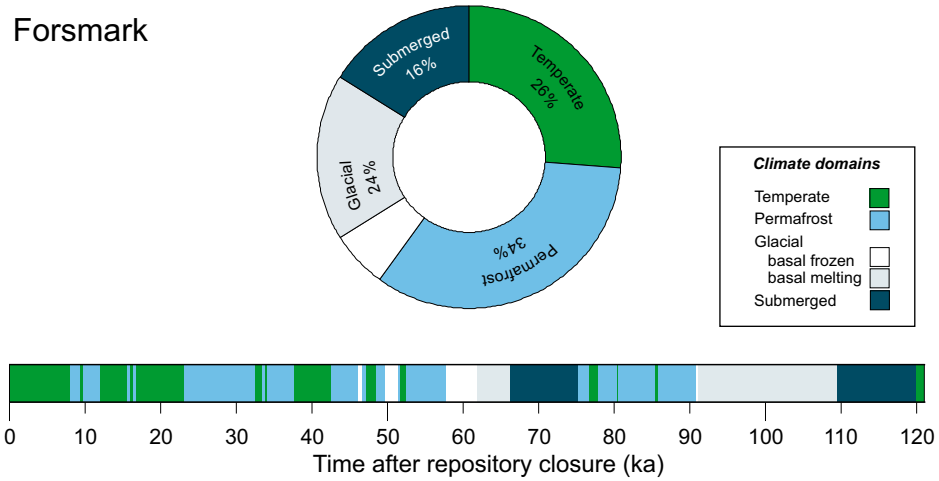

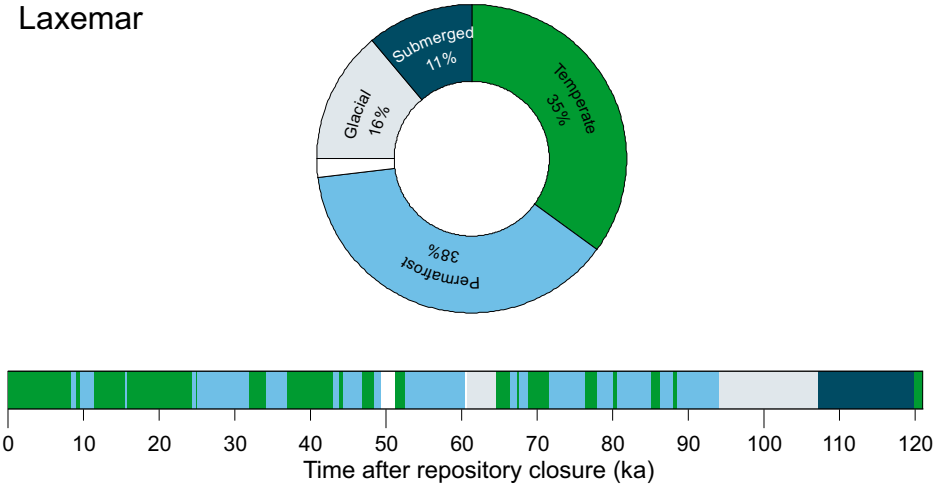

Figure 4-7. *Duration of climate domains at Forsmark and Laxemar, expressed as percentage of the total time of the base variant of the SR-Can main scenario. The bars below the pie charts show the development of climate-related conditions at each site for the base variant as a time series of climate domains and submerged periods.*

During the first 50,000 years of the reference evolution, and in the period between the two ice advances, the increasingly colder climate results in progressively longer periods of permafrost. The total duration of the permafrost domain is about 41,000 years at Forsmark and 46,000 years at Laxemar. In this reference evolution, the permafrost develops to quite great depths during the most severe permafrost periods. The maximum calculated permafrost depth is ~ 250 m in Forsmark and ~ 160 m at Laxemar (Figure 4-8 and 4-9).

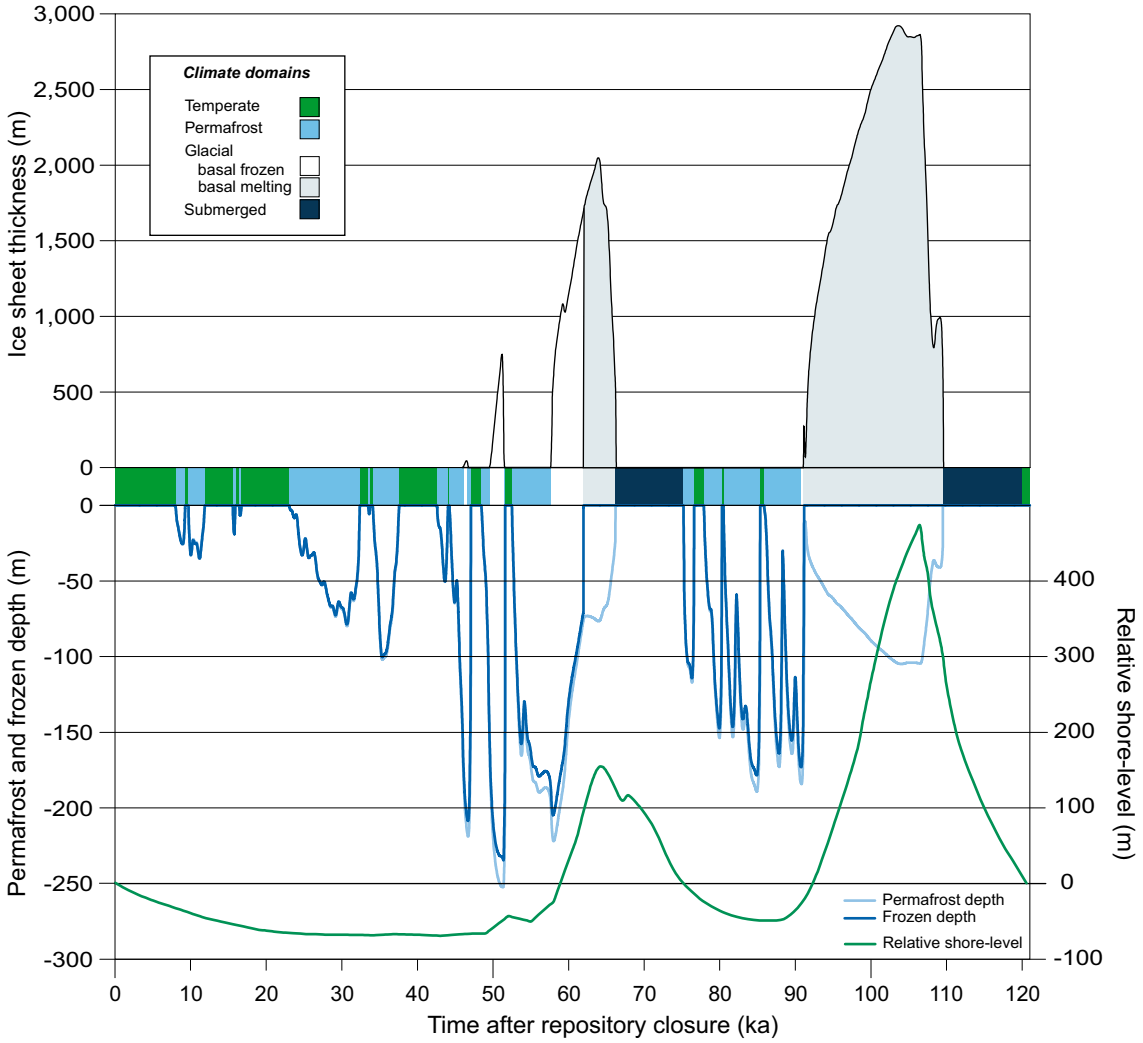

Figure 4-8. *Evolution of important climate-related variables at Forsmark for the base variant of the main scenario.*

Forsmark and Laxemar are exposed to two major ice advances and retreats during the reference glacial cycle, the first around 60,000 years into the scenario and the second after about 90,000 years (Figure 4-8 and 4-9). Prior to both of these glaciated periods, both Forsmark and Laxemar are situated above sea level with prevailing permafrost conditions when the ice sheet advances towards and over the sites.

A period of basal frozen conditions initiates the first major stadial of glacial domain at both sites. At Forsmark, the period of basal frozen conditions is ~ 4,000 years long and at Laxemar a few hundred years. During this period the permafrost, which is now sub-glacial, reaches its maximum depth of about 250 m at Forsmark (Figure 4-8). At Laxemar the maximum permafrost depth of 160 m is reached prior to this time, during a short period of cold-based ice sheet coverage at ~ 50,000 years into the scenario (Figure 4-9).

When the ice sheet grows over the sites, it insulates the subsurface from the cold climate and in time induces ice sheet basal melting conditions. During periods of ice sheet coverage, the development of subglacial permafrost is much more restricted than permafrost development during ice free conditions prior to ice sheet coverage (Figure 4-8 and 4-9). The total length of periods of glacial domain in the base variant of the main scenario is ~ 30,000 years at Forsmark and 19,000 years at Laxemar. During this time, basal melting conditions dominate.

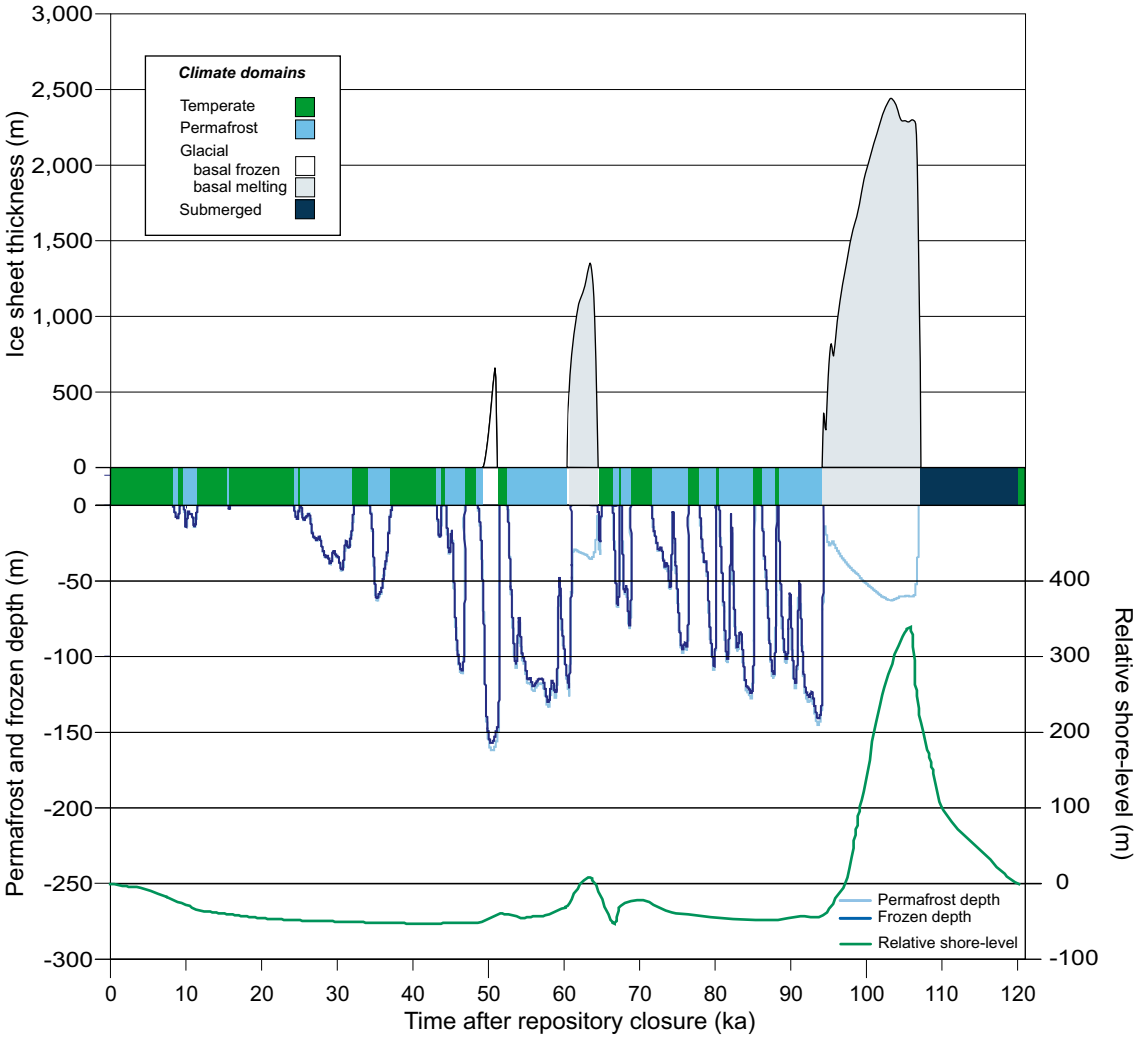

Figure 4-9. *Evolution of important climate-related variables at Laxemar for the base variant of the main scenario.*

A comparison of the climate evolution at Forsmark and Laxemar in the base variant of the main scenario is seen in Figure 4-10. Due to the geographical location, periods of permafrost and glacial domain are in general longer at Forsmark, with correspondingly longer periods of temperate domain at Laxemar. In addition, Forsmark is submerged during a period around 70 ka after repository closure, an event that is not present in the climate-related evolution at Laxemar.

Figure 4-10 also shows the second repetition of the Weichselian glacial cycle, illustrating how several glacial cycles are envisaged to follow each other during a 1 Ma time perspective /see **SR-Can Main Report**/. The first full warm interglacial period for Forsmark and Laxemar is indicated in the figure. The onset and ending of this warm interglacial period is here defined from the development in each region; the onset is determined by the timing of the final deglaciation of the areas, while the ending is determined by the first occurrence of permafrost. The timing and duration of the interglacial period is thus determined from the scenario development, which for this part of the scenario is based on site specific observations and modelling. The resulting, *regionally defined*, interglacial period has a length of around 20,000 years (Figure 4-10). The defined interglacial period is used to calculate accumulated doses during the longest and warmest ice free phase of the safety assessment period /Avila 2006, SKB 2006de/.

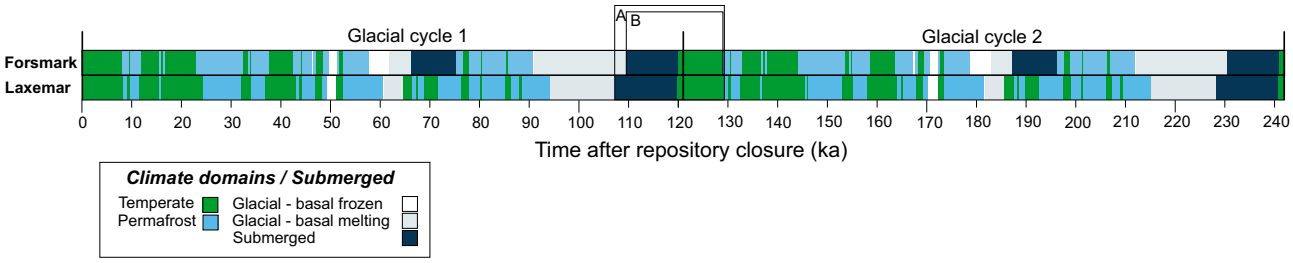

Figure 4-10. *Comparison of climate evolution at Forsmark and Laxemar in the base variant of the main scenario. The figure also shows the second repetition of the last glacial cycle, illustrating the first part of how glacial cycles are envisaged to follow each other during a 1 Ma time perspective /see SR-Can Main Report/. A and B denote the timing and duration of the first full warm interglacial period, regionally defined for Laxemar and Forsmark respectively.*

The uncertainties in the *actual* length of the present and future interglacial periods are of course large. Given this uncertainty, it is again emphasized that the evolution of climate domains as described in the base variant of the main scenario is not an expected future climate evolution. It is one relevant example of an evolution covering the climate-related conditions that can be met in a 100,000 year time perspective. Another possibility for the length of the present interglacial period is handled in the greenhouse variant of the main scenario.

During periods of temperate domain, the main factor of importance for repository safety is shoreline migration. From previous safety assessments it has been concluded that peak doses occur during periods of temperate domain when the sites are emerged from the sea. When the sites are submerged groundwater flow conditions will be stagnant and the dispersion in the biosphere much greater than under terrestrial conditions.

Periods of temperate domain occur in the early phase of the reference evolution, during the warmer interstadial between the two major ice advances and during the interglacial period following the glacial maximum (Figure 4-8 and 4-9). The periods of temperate domain in the interglacial and early phases of the glacial are generally warmer and longer than those occurring during interstadials in the later part of the glacial. At Forsmark the temperate domain prevails 26% of the time of the base variant, and in Laxemar for 35% of the time. The climate conditions during periods of temperate conditions can be expected to be slightly colder at Forsmark than at Laxemar.

Gradually colder periods of permafrost domain occur in the reference evolution. During the initial long period of temperate domain vegetation including forests will establish. It is plausible that this vegetation will remain, with a succession in type, in spite of the transition to colder and drier conditions. The vegetation will to some extent act to reduce the development of permafrost. During this initial phase the heat generated by the spent fuel also has a significant effect on the development of permafrost in the repository area, see Section 4.4.1.

Periods of permafrost domain also occur between the two major ice advances when the land surface is above sea level. During this period vegetation is most probably not established in the same way as in the early phases of the glacial cycle, and the heat from the spent fuel has decayed. In spite of this, the calculated maximum permafrost depth at Forsmark, 250 m, and at Laxemar, 160 m, occurs during the first short phase of ice sheet coverage (Figures 4-6, 4-8, 4-9). As previously mentioned, permafrost is defined as existing if temperatures are at or lower than the 0°C isotherm. The actual transitions from frozen to thawed bedrock conditions at Forsmark and Laxemar occur at a somewhat shallower depth than indicated by the permafrost depth (Figure 4-6), which makes the reported permafrost depths conservative for assessment purposes. Even more important, the freezing temperature of the clay buffer is −5°C or lower /**Buffer and backfill process report,** Section 2.2.2/. In Figure 4-6 it can be seen that the −5°C isotherm reaches a depth of ~ 100 m at Forsmark, and ~ 60 m at Laxemar. The difference in maximum

depths of permafrost and −5°C isotherm between Forsmark and Laxemar is partly explained by the slightly warmer climate conditions at Laxemar but the main reason for the difference is the contrasting thermal properties of the bedrock at the two sites (Table 3-8 and 3-9).

Evolution of hydrological conditions and groundwater

A schematic section through an arbitrary south-western sector of a Fennoscandian ice sheet large enough to cover both candidate sites is shown in the upper panel of Figure 4-11. A zone of basal melting reaches some hundreds of kilometres from the ice margin in the southeast.

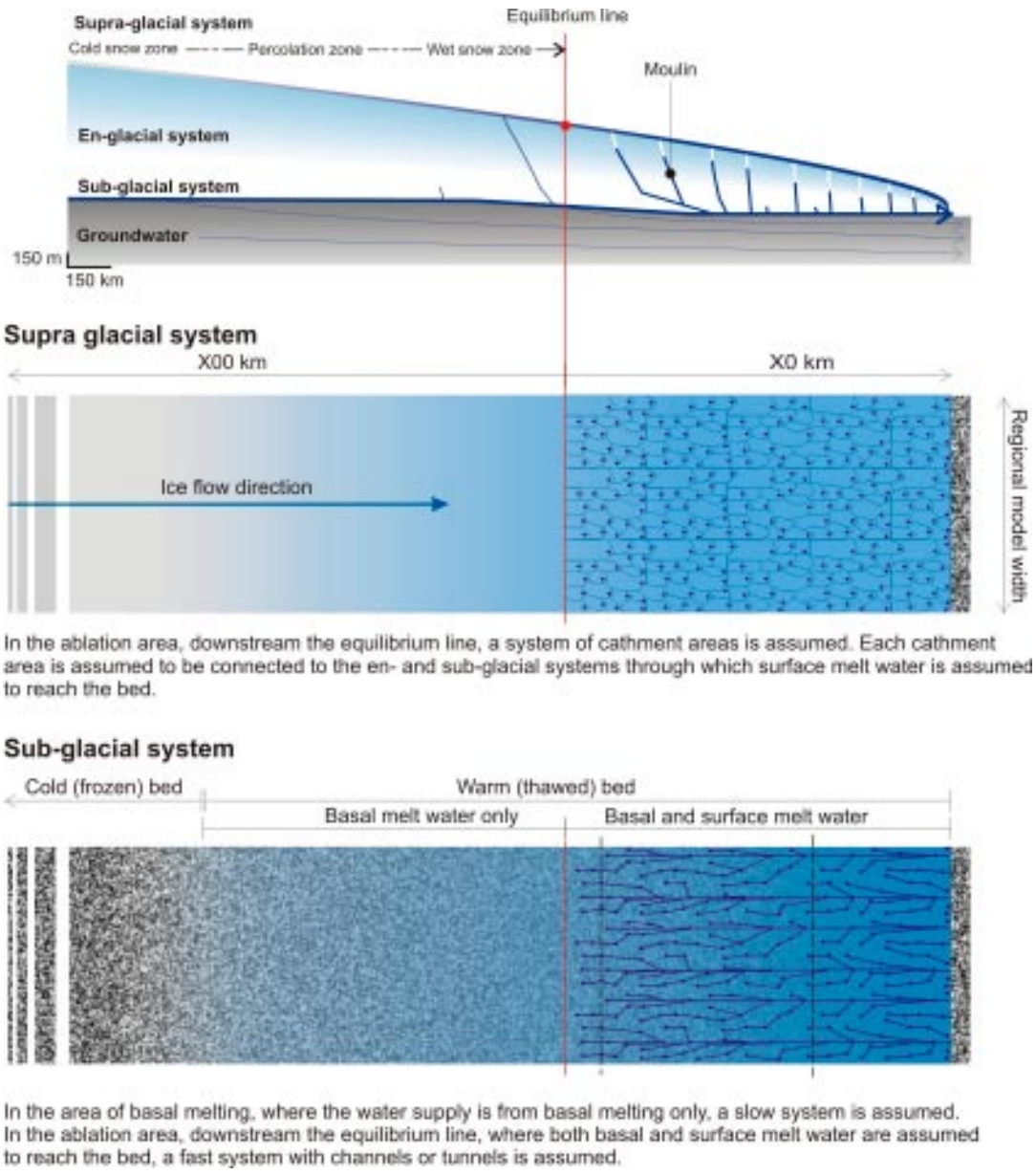

Figure 4-11. *Conceptual model of the ice sheet hydrological system. Upper panel: arbitrary south-western section through a Fennoscandian ice sheet. Middle and lower panels: possible configurations of the supra- and sub-glacial hydrological systems. The depicted model was used for conceptualisation of the upper boundary conditions in regional ground water modelling /Jaquet and Siegel 2006/.*

The production of basal melt water here varies between 1 and 10 mm/year and can be regarded as constant over the year. In the ablation area below the equilibrium line, rain and melt water from the ice surface is brought to the bed through crevasses and moulins. In the base variant of the main scenario (Figures 4-2 and 4-3) surface melt water production in the ablation area typically varies up to 4–8 m of water per year. More ice melts in lower parts of the ice sheet, and less ice closer to the equilibrium line. During the final deglaciation of the ice sheet in this scenario, a maximum surface melt rate of 14 m/year occurs. In the model simulation, the typical surface melt rate values of 4–8 m/year can be compared to observed present average ablation rates of the Greenland ice sheet of a few metres/year /Krabill et al. 2000/ up to ~ 10 m/year /Bøggild et al. 2004/. During the deglaciation of the Weichselian ice sheet, melt rates of more than 10 m/year may have occurred /Humlum and Houmark-Nielsen 1994/.

During periods of temperate domain, the groundwater flow pattern is similar to the present ice free situation, with a mixture of local areas of groundwater recharge, typically at topographically high positions, and discharge, typically in low positions. The groundwater flow is at this time driven by topographic gradients in the landscape.

During the initial periods of permafrost domain, the permafrost distribution is assumed to be sporadic or discontinuous. This results in a modified pattern of groundwater flow, but still with groundwater recharge and discharge taking place. When climate gradually gets colder, permafrost grows progressively thicker and more widespread. The very flat topography at both sites, is favourable for the formation of more or less continuous permafrost once climate is cold enough. When continuous permafrost occurs, the precipitation recharge of groundwater is strongly reduced or stopped, since permafrost influences subsurface hydrology by reducing the hydraulic conductivity of the frozen unit /Burt and Williams 1976/.

During the first period of glacial domain, the ice sheet overrides ground with permafrost at both sites (Figures 4-8 and 4-9). Subglacial permafrost under the ice sheet margin acts as a hydrological barrier for groundwater flow /Piotrovsky 1997/. Therefore, this phase is characterised by a period with no groundwater recharge. Even though the ice sheet is cold-based at this time, water from surface melting may still reach the glacier bed or forefield. However, since permafrost is present, this water does not contribute to groundwater recharge. Proglacial lakes can inhibit permafrost growth, see Section 3.4.4 and /Cutler et al. 2000/. If permafrost formation in front of the advancing ice sheet is reduced because of presence of lakes, the initial period of cold-based ice coverage would be shortened, giving a longer period of wet-based conditions and groundwater recharge, probably also from frontal-near surface melting.

After the initial cold-based period, subglacial groundwater recharge again takes place, at both sites, due to ice sheet basal melting and less permafrost (Figure 4-8 and 4-9). In local areas of former groundwater discharge, a general reversal of the groundwater flow would typically occur under glacial conditions /Breemer et al. 2002, Hoaglund III et al. 2004, Jaquet and Siegel 2006/. This results in a dominant subglacial groundwater flow directed downwards under the major part of the warm-based ice sheet, recharging the groundwater aquifer. Subglacial groundwater discharge may possibly occur close to the ice margin /Breemer et al. 2002/. Even if the hydraulic permeability of the bedrock were to decrease under the load of an ice sheet, the increased physical and hydraulic gradient, especially associated with passages of the ice sheet margin, would likely increase groundwater flow in bedrock compared to temperate domain conditions /e.g. Jaquet and Siegel 2006/.

After the first period of glacial domain, the Forsmark site is submerged for up to 9,000 years (Figure 4-8), whereas Laxemar is situated above the contemporary sea-level directly after this deglaciation (Figure 4-9). When the sites are situated above sea level during this interstadial, climate is generally cold, which induces new long periods of deep permafrost, and associated reduced conductivity in the upper 100–150 m of the bedrock. During the short temperate conditions during this interstadial, groundwater flow may again be characterized by local areas of recharge and discharge.

During the second and most severe glacial phase, starting 90,000 years into the scenario at Forsmark and some thousand years later at Laxemar, the ice sheet is cold-based for a considerably shorter initial time than during the first major glacial phase (Figure 4-8 and 4-9). This makes water from surface and basal melting available for groundwater recharge during most of this period of ice sheet coverage. As in the case of the first ice covered period, steeper physical and hydraulic gradients, especially associated with the passage of the ice sheet front, may, for a limited period, induce more rapid and substantial groundwater flow than under present ice-free conditions.

Thereafter, at the very end of the base variant, an evolution corresponding to the Holocene occurs in the scenario, with Forsmark and Laxemar first being submerged after deglaciation for 10,000 and 12,000 years respectively. When the sites emerge above sea level, the climate is much warmer than during the non-submerged period between the two major glacial advances. Both sites are dominated by temperate domain conditions, with groundwater flow and chemical composition similar to present day conditions. For a description of the geochemical evolution in this scenario, see Section 9.4.7 in /**SR-Can Main Report/.**

4.2.5 Evolution of mechanical conditions

The temporal evolution of an ice sheet will cause time-varying stress and deformation in the Earth. Due to the long time spans both elastic and viscous deformation occurs. Properties of the ice sheet controlling the deformation and stress change are areal extent, thickness and slope of the ice margin /Lund 2005/. As the ice sheet advances and the load from the ice increases, the elastic lithosphere will bend and the viscoelastic mantle will flow laterally. This will, on a large scale, result in a depression beneath the load and an upwarping bulge outside the ice sheet margin. The thicker the ice sheet and the longer that an area is covered by ice, the larger bending stresses are induced. At great depths in the crust, where elastic properties are very high, horizontal stresses induced by the bending will be much larger than the corresponding increase in vertical stress due to the load of the ice. This is of importance for the potential of glacially induced faulting. However, the upper part of the crust is considerably softer and hence, the horizontal stresses generated from the ice loading at repository depths are smaller than the increase in vertical stress.

The evolution of stresses in the crust during a glacial cycle has been studied by means of numerical finite element modelling by /Lund 2006/ using Lambeck's SCAN-2 model of the Weichselian glaciation.

As the ice sheet retreats, the depressed elastic lithosphere will experience an isostatic rebound. This rebound is a much slower process than the removal of the ice load, and consequently, high horizontal stresses are left in the lithosphere for a long time after the vertical stress induced by the ice sheet is gone.

The pore pressures in the crust are increased during glaciation, as a result of the consolidation of the bedrock as well as the recharge of meltwater available at the base of the ice sheet. This means that the effective rock stress (i.e. the total stress reduced by the water pressure) is affected by a glacier advancing over a site, through the interaction of load and pore pressure. The evolution of effective stress will dictate the mechanical behaviour and properties of rock fractures, and hence, also their water-conducting ability, see /Hökmark et al. 2006/.

At shallow depths, both horizontal principal stresses are larger than the vertical stress in a non-glacial stage. As the ice sheet advances over the site, the increase in vertical stress is much larger than the increase in horizontal stress. This means that the stress axes may rotate so that the vertical stress will be the intermediate or even largest principal stress within the upper part of the bedrock. In general, the increase in stress will act to reduce the transmissivity of fractures and fracture zones. However, these stress changes, together with the increase in pore pressure as compared with non-glacial hydrostatic conditions, may result in changed transmissivity anisotropy.

Outside the edge of the ice sheet, initial horizontal stresses may be reduced by the bending stresses /Lund 2006/. This will give rise to a decreased normal stress acting across steeply dipping fractures leading to an increase in transmissivity. Calculations by /Hökmark et al. 2006/ indicate, however, that the increase will be very modest.

Deviatoric stresses may also give rise to shearing of critically oriented fractures, which in turn can yield larger fracture apertures. The same effect may also result from hydraulic shearing, in which the enhanced pore pressure acts to reduce the shear strength. As described by /Hökmark et al. 2006/, hydraulic jacking of fractures is also possible, but most likely not much deeper than a couple of tens of metres.

The general consequence of a large ice sheet covering an area is that faults in the crust are stabilised and seismic activity is suppressed. On deglaciation, the rapid decrease in vertical stress tends to destabilise the crust. The pore pressure in the crust is of great significance in the faulting process, since an increased pore pressure decreases the effective normal stresses on faults, and hence, reduces their shear strength. If the pore pressure is still enhanced at the end of glaciation, when the vertical load from the ice disappears, fault stability will be further reduced. There exists evidence that intense seismic activity, with end-glacial or post-glacial faulting, took place in northern Scandinavia at the end of the last glaciation (see Section 3.5). The fault displacements are considered to have occurred as reactivation of existing structures.

As described in /**Geosphere Process report**/, there are two different views concerning the mechanism of this faulting; release of tectonically generated stresses accumulated under the influence of the stabilising ice sheet or an asymmetrical unloading of the ice sheet. This is further discussed in Section 3.5.

4.3 Main scenario – greenhouse variant

As one variant of the main scenario, a variant with an increased greenhouse effect has been investigated (Figure 1-2). There are two main reasons for doing this; 1) modelling studies of the climate response to increased greenhouse gas emissions, mainly CO_2, indicate that global temperatures will rise in the future under such CO_2 scenarios /e.g. Cubasch and Meehl 2001/, and 2) climate cycles are believed be driven by changes in insolation. The coming 100,000 year period is initially characterised by exceptionally small amplitudes of insolation variations /Berger 1978/, possibly making the present interglacial exceptionally long. /Berger and Loutre 2002/ and others suggest it may end ~ 50,000 years from now, while other suggest an even longer interglacial /BIOCLIM 2003/.

The main process of importance for repository safety in the temperate domain is shoreline migration. The purpose of the SR-Can greenhouse variant is to give a picture of the possible impact of greenhouse warming on the repository and also to cover extremes of warm conditions with respect to repository safety. In general, temperate conditions are beneficial for safety, as the conceivable conditions occurring within the temperate domain have very limited impact on repository safety functions. However, if for some reason, a release from the repository does occur, previous safety analyses have shown that peak doses occur in the temperate domain. Peak doses are related to periods when the area above the repository lies above sea level, and areas of discharge are located within that area. In addition, long periods of temperate conditions above sea-level may result in lower groundwater salinity.

The impact of greenhouse warming on climate-related conditions in Sweden can be regarded as a long and, at least part of the time, very warm period of temperate domain. In the greenhouse variant it is assumed that the temperate domain will prevail for another 50,000 years until the first, restricted, ice advance in Fennoscandia takes place. After that, the first 70,000 years of

the base variant evolution is assumed to follow. The first major ice advance will thus occur after ~ 100,000 years in the greenhouse variant of the main scenario. This scenario is in broad agreement with results of the BIOCLIM project. For two greenhouse warming cases, a warm Eurasian climate and restricted ice coverage were simulated for up to about 100,000 years into the future /BIOCLIM 2003/.

Due to the coastal near location of Forsmark and Laxemar, one question related to increased future greenhouse warming is the response of the present ice sheets, and associated changes in shoreline position. The Greenland ice sheet is much more sensitive to increases in temperature than the Antarctic ice sheet /Huybrechts and de Wolde 1999/. An annual average warming of ~ 3° or more in Greenland may result in a decreasing ice sheet and raising sea-level /Huybrechts et al. 1991/. Excluding complex processes that could counterbalance a simple warming-melting situation, such as changes in oceanic circulation including a strong reduction of the Gulf Stream, many studies suggest that the Greenland ice sheet gets drastically reduced in size and contributes considerably to global sea-level rise under various future greenhouse gas scenarios. In a worst-case IPCC scenario of 8 degree climate warming by the year of 2100 /Cubasch and Meehl 2001/, the warming would lead to a complete and irreversible collapse of the Greenland ice sheet over the next 1,000 years /Huybrechts and de Wolde 1999, Gregory et al. 2004, Alley et al. 2005a/.

The present volume of the Greenland ice sheet corresponds to a global sea-level rise of 7 m. The decay of the Greenland ice sheet under a warming climate is expected to be a smooth function of the temperature rise /Huybrechts and de Wolde 1999/. In the SR-Can greenhouse variant, it is assumed that the Greenland ice sheet completely melts away at a linear rate during the coming 1,000 years, resulting in a 7 m sea-level rise. The effect of this sea-level rise on the development of the Baltic shoreline is investigated by means of GIA modelling (see Section 3.3).

The discrepancy between the GIA results on modelled present-day uplift rates and present uplift rates as observed by GPS measurements (see Section 3.3) could be caused by too large ice load provided to the GIA model from the ice sheet model (Section 3.1), or by the model simplification made in adopting a laterally homogeneous description of the Earth. From sensitivity tests made using the GIA model it was found that a reduction in ice thickness to 80% of the value in the reference glacial cycle would yield a result in accordance with GPS data on present-day uplift. Awaiting results of studies investigating the other possible causes of the misfit between the GIA results and observed uplift rates, such as including a 3-D lateral Earth structure in the GIA model, in the greenhouse variant the GIA model was run with an 80% ice thickness relative to the base variant of the main scenario.

In line with the approach used in the GIA modelling of the base variant, the model was initiated by running one full glacial cycle, but this time with 80% thickness from the base variant, in order to obtain realistic initial uplift rates for the greenhouse scenario. This was followed by linear melting of the Greenland ice sheet over 1,000 years, inducing corresponding changes in global sea levels. This was followed by a 50 ka long period of no change to the loading model, simulating a warm greenhouse climate without a Fennoscandian ice sheet forming. Finally a second full glacial cycle, again with 80% thickness from the base variant, was simulated. The resulting evolution of relative shore level at the two candidate sites is shown in Figure 4-12. The relative shore levels reported for the sites are corrected for the formation of a Baltic lake when all Baltic sills are situated above contemporary sea level.

As seen in Figure 4-12 both sites are situated above sea-level basically for the entire scenario in the greenhouse variant. This is due to the fact that the modelled remaining isostatic uplift is large enough to compensate for the global sea level rise. In this context, the melting of the Greenland ice sheet is of minor importance for the development of the shoreline at Forsmark and Laxemar.

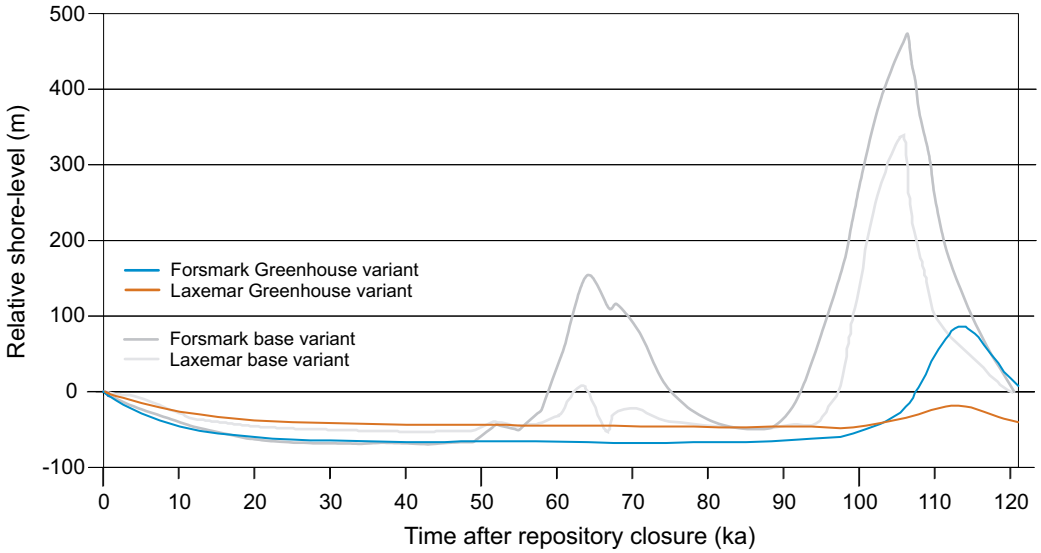

Figure 4-12. *Evolution of relative shore level at Forsmark and Laxemar for the greenhouse variant of the main scenario.*

One factor that has not been included in the analysis is the thermal expansion of oceans in a warming climate. Because of the large heat capacity of the ocean, thermal expansion would continue for many centuries after a warmer climate had been stabilised /IPCC 2001/. The final contribution to sea-level change from thermal expansion would thus be much larger than at the time of climate stabilisation. The IPCC estimates the total sea-level increase due to thermal expansion in the next 1,000 years to be between 1 and 4 m, depending on the chosen CO_2 emission scenario /IPCC 2001/. There is general agreement that the rate of global sea-level rise from thermal expansion of ocean water would initially be low and then increase later in the 1,000 year period.

In the early phase of the greenhouse variant, after an initial period of slow thermal expansion of the oceans, inclusion of this effect could possibly also contribute to a constant or slightly increasing relative sea-level. Another factor that also could contribute to this would be a contribution from collapse of the West Antarctic Ice Sheet /e.g. Nicholls and Lowe 2006/. Although this is a very uncertain event, it could, if it were to occur, give a contribution to global sea level of about 5 m. Nevertheless, after an early phase in the greenhouse variant with these uncertainties, the results of the isostatic modelling suggest that in the long run both sites will be situated above sea level.

Figure 4-13 presents the duration of climate domains at Forsmark and Laxemar as well as the development of climate-related conditions at each site for the greenhouse variant. Naturally, the temperate domain dominates in this scenario, with temperate conditions prevailing for 65% of the time (78,000 years) at Forsmark, and for 72% of the time (86,000 years) at Laxemar. Permafrost conditions prevail for 23% of the time (28,000 years) at both sites, whereas glacial conditions are met with for 9% of the time (11,000 years) at Forsmark and 5% of the time (6,000 years) at Laxemar.

The resulting evolution of important climate-related variables at Laxemar and Forsmark for the greenhouse variant of the main scenario is shown in Figures 4-14 and 4-15.

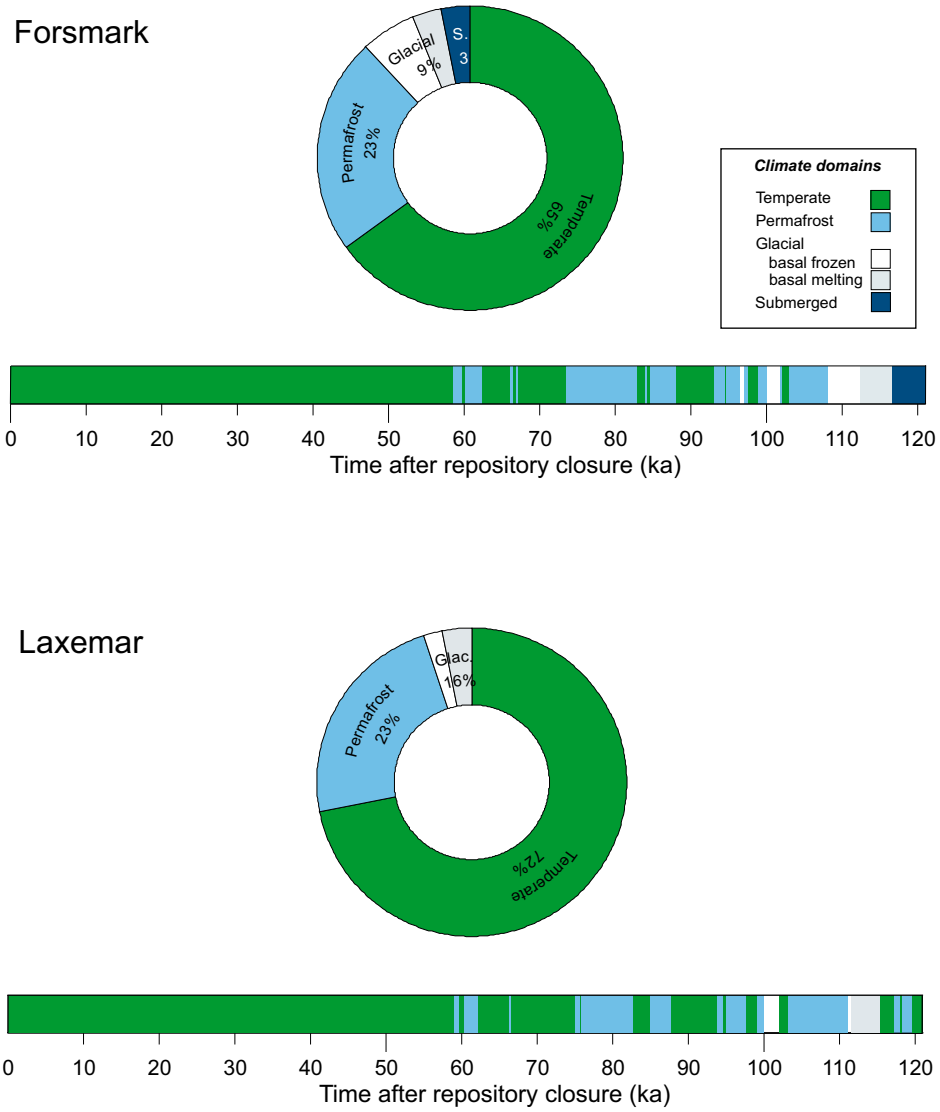

Figure 4-13. *Duration of climate domains at Forsmark and Laxemar, expressed as percentage of the total time of the main scenario greenhouse variant. The bars below the pie charts show the development of climate-related conditions at each site for the greenhouse variant as a time series of climate domains and submerged periods.*

4.3.1 Climate conditions

The greenhouse variant of the SR-Can main scenario (Figure 4-14 and 4-15) constitutes a climate evolution in which the temperate domain dominates at the sites. It persists for 65% of the time at Forsmark and for 72% of the time at Laxemar (Figure 4-13). The climate after the initial temperate period follows that of the first half of the base variant of the main scenario.

For both candidate sites, the climate is dominated by an initial ~ 100,000 year long warm period without ice sheet coverage, a period that gets colder towards the end. During a large part of this warm period, mean annual air temperatures at the candidate sites may be as warm as, or warmer than, at present. During this initial long warm period, it is likely that climate within the temperate domain may vary significantly, with a range that may be larger than that during the Holocene.

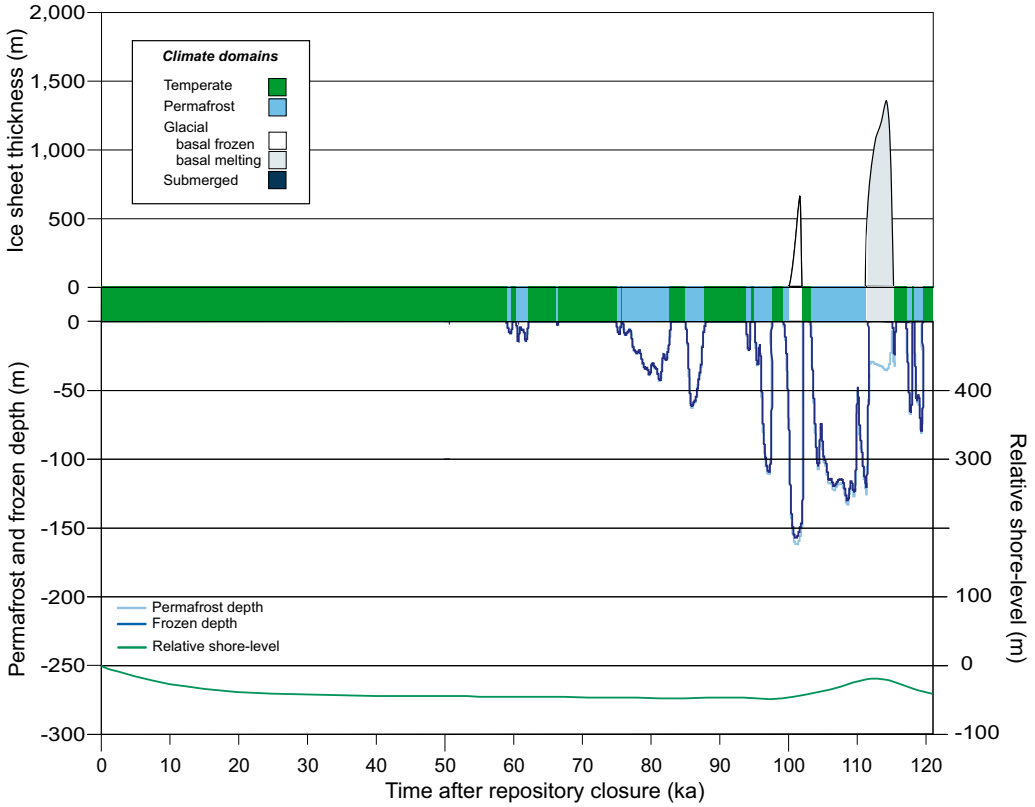

Figure 4-14. *Evolution of important climate-related variables at Laxemar for the greenhouse variant of the main scenario.*

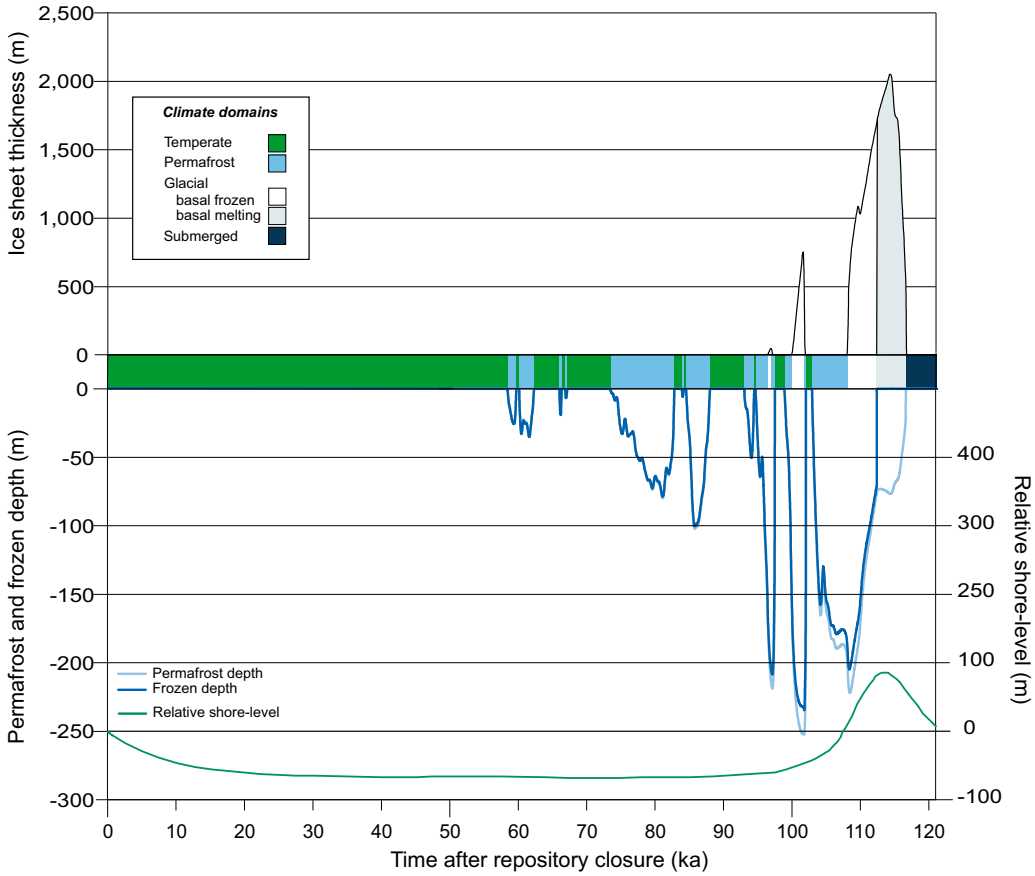

Figure 4-15. *Evolution of important climate-related variables at Forsmark for the greenhouse variant of the main scenario.*

The length of the initial period of temperate domain in the SR-Can greenhouse variant should not be taken as a prediction or statement on a future greenhouse climate change. Under a future warming climate, this period could be shorter or longer than that described in the scenario. In the BIOCLIM project /BIOCLIM 2003/ climate simulations were made with a global coupled ocean-atmosphere model for orbital conditions representative for a period 67,000 years into the future, with a melted Greenland ice sheet, and an increased CO_2 level of 550 ppmv. Even though the timing of this warm period does not match the maximum warm situation in the SR-Can greenhouse variant, results from this climate simulation can be used to estimate climate change in Fennoscandia under increased greenhouse gas emissions and changing orbital parameters. The result suggests that summer climate over Fennoscandia would warm significantly, with June–August temperatures being 2–3° warmer than at present in the regions of interest in south-central Sweden. Winter temperatures are predicted to be less than one degree warmer than at present. In these climate simulations, precipitation is also predicted to increase, especially in summer.

The SWECLIM project /Rummukainen 2003, Tjernström et al. 2003/, used a regional climate model to simulate the climate responses to increased emissions of greenhouse gases over Fennoscandia. The simulations were made with the Greenland ice sheet present, and with IPCC greenhouse gas emission scenario B2 (SRES). For the regions of interest in south-central Sweden, the results suggest an increase in temperature by year 2100 of ~ 2–3° in summer and 4° in winter. Annual mean temperatures in the coastal regions of interest are predicted to increase by 3–4°C, and the annual mean precipitation is predicted to increase by 10–20%, with the larger change taking place in the northern part of south-central Sweden. Using several GCM (Global Climate Models) simulations and various emission scenarios, IPCC report a change in annual temperature over Fennoscandia by year 2100 of 1–5° /IPCC 2001/. The IPCC B2 emission scenario, same as used in SWECLIM project, gave a Fennoscandian annual mean temperature change of 3–4°.

Given the uncertainties and assumptions used in the climate modelling, and the emission scenarios chosen, the results described above suggest that the climate in the regions of Forsmark and Laxemar will be characterised by summer temperatures 2–3° higher than today, and probably also increased winter temperatures. Precipitation is also predicted to increase, especially in summer. These results assume that the thermohaline circulation is not changed in such a way that considerably less heat is transported to Fennoscandia.

In a warming climate due to an increased greenhouse effect, the warmer temperatures at the ground surface would not affect repository safety functions at either of the sites. If precipitation increases, this would not affect groundwater formation significantly, since, on a regional scale, the major part of the groundwater aquifer is fully sustained by present-day precipitation rates. It is possible that the increased precipitation would lead mainly to increased surface runoff. Due to persistent infiltration of meteoric water during the prolonged temperate periods in the greenhouse variant it is possible that groundwater salinity may decrease /see **SR-Can Main Report**/.

One climate-related process that is affected by a warming climate is shore level changes, both from melting of ice sheets and glaciers, and from thermal expansion of ocean water. If sea-level were to rise faster than the remaining isostatic rebound, in contrast to what is shown from the GIA modelling for the SR-Can greenhouse variant, the sites could be submerged for a longer time than suggested in the scenario. For the biosphere, the warmer temperatures would lead to shorter period of seasonal snow cover, which in turn would make the vegetation period longer.

As mentioned in Chapter 2, one possibility within the inferred generally warmer warming climate due to an increased greenhouse effect /IPCC 2001/, is that the thermohaline circulation of the North Atlantic would get reduced or shut-down /e.g. Wu et al. 2004, Schlesinger et al. 2006, Yin et al. 2006/. This would result in less heat being transported towards Fennoscandia by the North Atlantic Drift, which in turn would lead to a regional cooling over Fennoscandia.

If a regional cooling was to take place, the effect could be that permafrost and glacial conditions could occur earlier than in the greenhouse scenario presented here. However, the effects of extreme permafrost and glaciation on repository safety are covered within the Additional scenarios (Section 4.4), Therefore, yet another scenario or variant covering permafrost and ice sheet conditions in a specific case from regional cooling within a greenhouse scenario, is not needed.

During the second half of the greenhouse variant, climate varies within the same range as the first part of the base variant, and consequently the climate-related processes will act in the same way as in the base variant. The first periods of permafrost domain appears at both sites ~ 60,000 years into the greenhouse variant (Figures 4-14 and 4-15). The maximum permafrost depth is the same as in the base variant of the main scenario, i.e. 250 m at Forsmark and 160 m at Laxemar, but occurs much later in the scenario, after ~ 100,000 years (Figure 4-14 and 4-15). The first and only major ice advance during the 120,000 years of the greenhouse variant occurs after more than 110,000 years. The maximum ice thickness at this time is just over 2,000 m at Forsmark and about 1,400 m at Laxemar. After the glacial advance, Forsmark is submerged for about 4,000 years before the ending of the scenario. Due to the thinner ice coverage over Laxemar, this site is not submerged at any time in the greenhouse variant of the main scenario.

The greenhouse scenario reduces the effects of most climate-related processes of importance for repository safety, such as the duration of glacial domain conditions, with the possible exception of changes in groundwater salinity /see further **SR-Can Main Report**/.

4.4 Additional scenarios

The time series of climate domains and the identification of the main processes and conditions of importance for repository safety is the main basis for identifying scenarios additional to the main scenario (see Figure 1-2). The climate-related issues having the greatest impact on repository safety functions are:

- Maximum permafrost depth and duration.
- Maximum hydrostatic pressure.
- Penetration of oxygen to deep groundwater.
- Occurrence of dilute or extremely saline groundwater.
- Reduction of retardation in the geosphere due to high groundwater fluxes and/or mechanical influences on permeability.

All these issues are related to cold conditions and the extremes within the permafrost and glacial domains.

4.4.1 Extremes within the permafrost domain

The main factors of importance for repository safety in the permafrost domain are the permafrost- and frozen depths, the depth of the isotherm at which the buffer freezes, the duration of permafrost or frozen conditions, and the possible freezing out of salt that may result in a zone with high salinity beneath the freeze front. The prevailing climate conditions are the main factor determining the evolution of permafrost. A mean annual temperature well below 0°C for long periods is a prerequisite for the development of permafrost to greater depth.

To investigate the climate conditions required to develop permafrost to repository depth, sensitivity tests on the evolution of permafrost for different constant temperatures were undertaken. The site-specific input of sub-surface parameters were the same as in the modelling of the base variant (Tables 3-8 and 3-9). The calculations were made for two cases, with and without

consideration of the heat from the spent fuel distributed on 6,000 canisters. The results for Forsmark and Laxemar are shown in Figure 4-16. The intention was to obtain steady permafrost depths, but it turned out that no steady state was reached in 200,000 years. The calculations show that, in cases of no heat from spent fuel, at Forsmark the ground temperature must be below −7°C for permafrost to reach the repository depth of 400 m. If the ground temperature is −8°C it takes 26,000 years for the permafrost to develop to repository depth. If heat from spent fuel is present it would take 80,000 years. At Laxemar the ground temperature must be below −13°C to reach the repository depth of 500 m, if no heat from spent fuel is considered. With a ground temperature of −16°C it takes 20,000 years for permafrost to reach repository depth. Including heat from the repository it would take ~ 60,000 years for permafrost to reach repository depth for a ground temperature of −16°C.

In addition to the sensitivity tests, the possibilities for permafrost to develop to repository depth was further investigated by the following model studies of extreme cold conditions:

- To investigate how low temperatures have to be for permafrost and the −5°C isotherm to reach repository depth in a variable climate, the local temperature curve extracted from the ice sheet model and used in the reference permafrost scenario was uniformly decreased in temperature until permafrost or the −5°C isotherm develop to, or just below, repository depth at both sites.
- To investigate the development of permafrost under exceptionally favourable conditions, air temperatures were assumed to fall according to the glacial cycle temperature curve of the reference evolution, but in an extremely dry climate not supporting any ice sheet growth. To favour permafrost growth further, the mitigated effects of snow cover and vegetation were excluded, and the sites were assumed to always remain above sea level.

Results from the first type of calculations are illustrated in Figure 4-17 and 4-18. The results of the second type of calculations are shown in Figure 4-19.

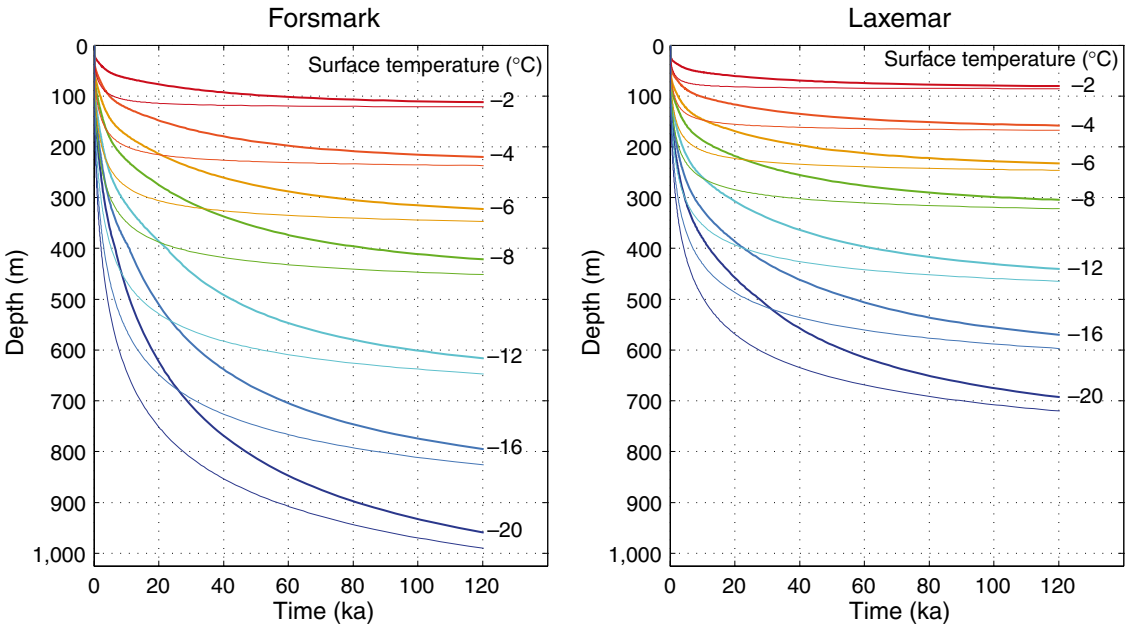

Figure 4-16. *The effect of considering heat from the spent fuel (thick lines) in comparison to no heat from the spent fuel (thin lines) on the evolution of permafrost depth for constant ground surface temperatures of –2, –4, –6, –8, –12, –16 and –20°C at Forsmark and Laxemar with reference subsurface properties.*

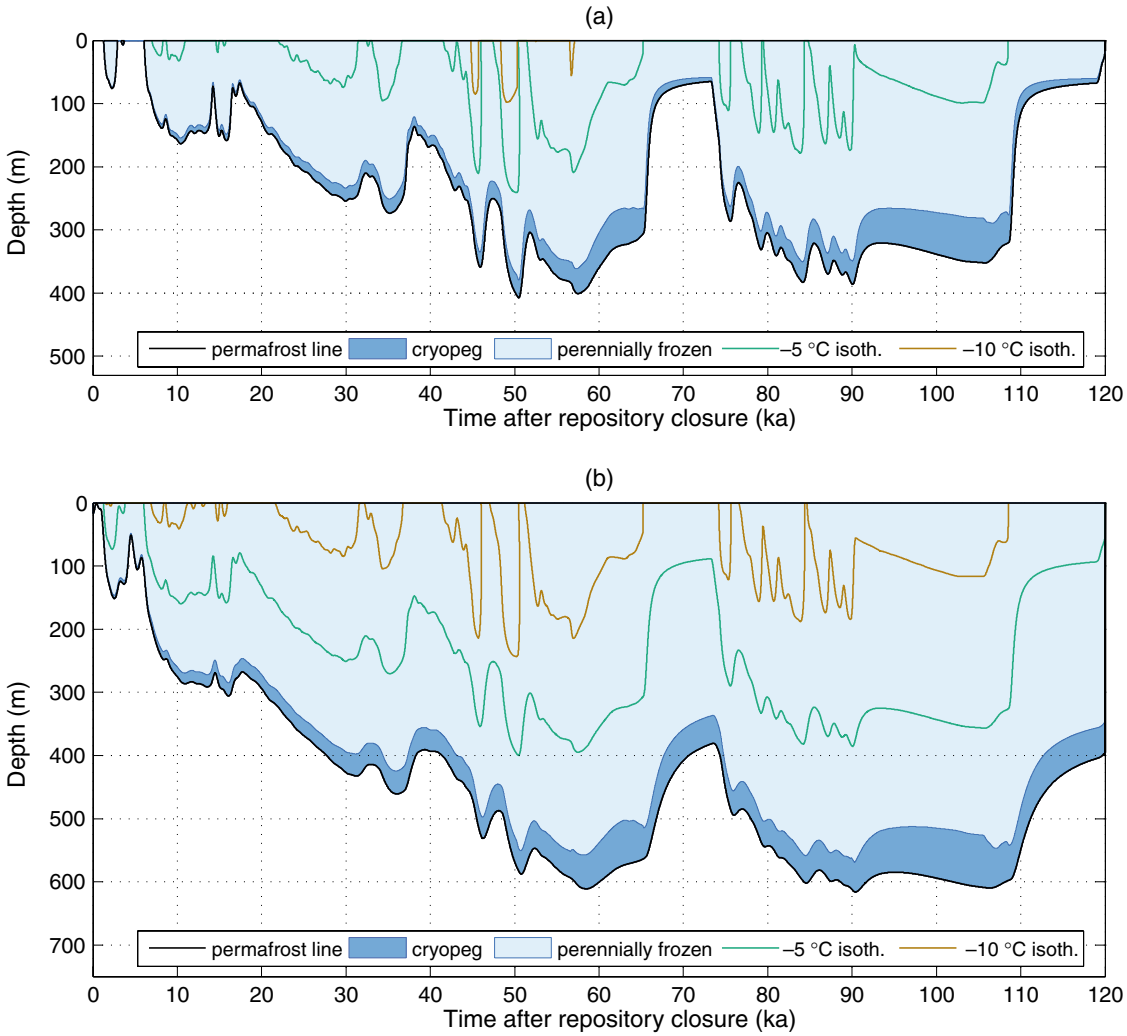

Figure 4-17. *Modelled evolution of permafrost (0°C isotherm) depth, perennially frozen ground, and depths of the −5 and −10°C isotherms at Forsmark for climate conditions with; a) reference scenario surface temperatures decreased by 5°C; and b): reference scenario surface temperatures decreased by 10.5°C.*

At Forsmark, the surface temperature curve of the last glacial cycle needs to be lowered by almost 5°C in order for the permafrost (0°C isotherm) to reach repository depth (Figure 4-17a). The −5°C isotherm reaches repository depth at Forsmark if the temperature curve is lowered by more than 10° (Figure 4-17b). At Laxemar, the surface temperature curve of the last glacial cycle needs to be lowered by 12° for permafrost to reach repository depth (Figure 4-18a). The corresponding temperature lowering for the −5°C isotherm to reach repository depth should be greater than 17° (Figure 4-18b).

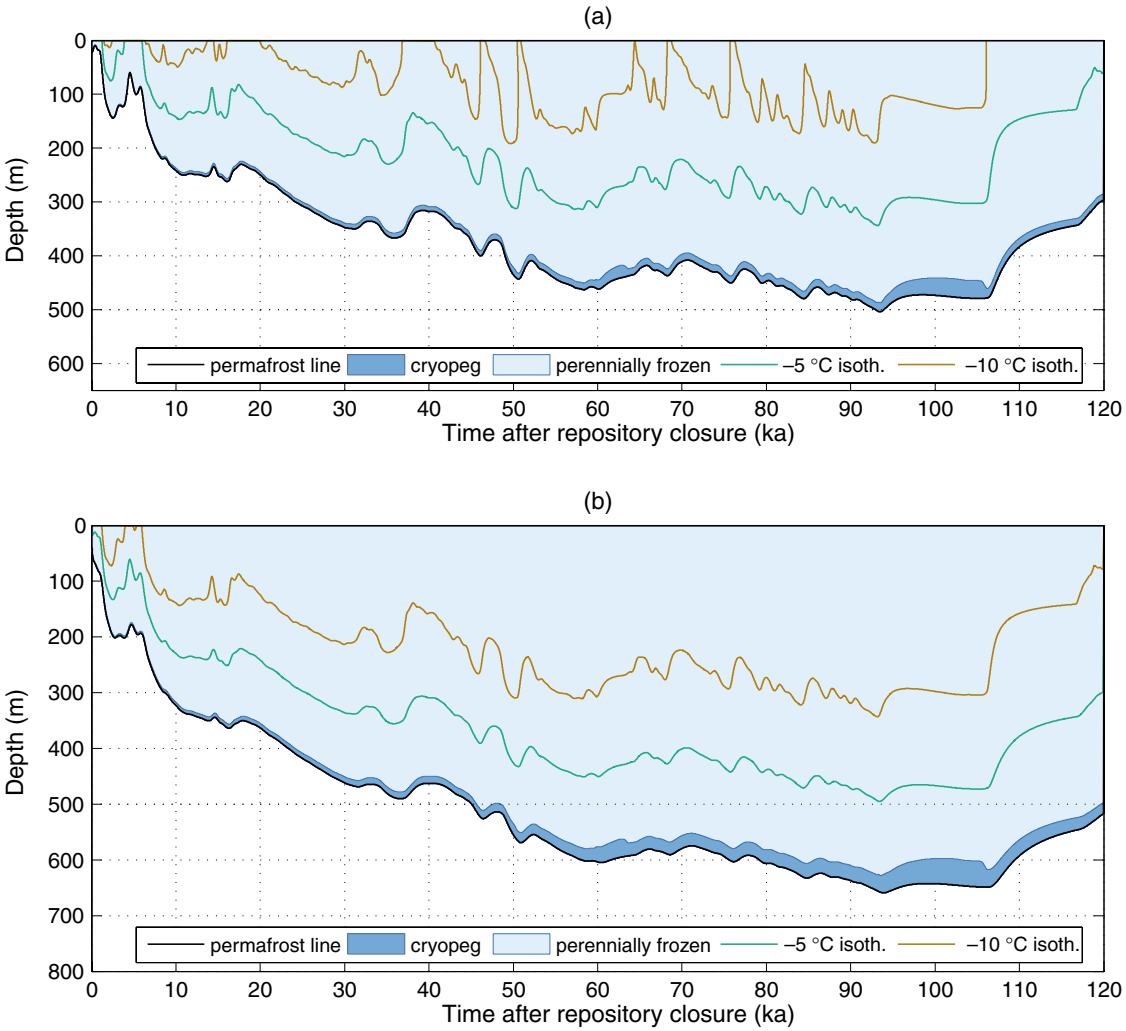

Figure 4-18. *Modelled evolution of permafrost (0°C isotherm) depth, perennially frozen ground, and depths of the −5 and −10°C isotherms at Laxemar for climate conditions with; (a) reference scenario surface temperatures decreased by 12°C; and (b): reference scenario surface temperatures decreased by 17.5°C.*

In the case of development of permafrost under exceptionally favourable conditions, without an ice sheet forming during cooling of the glacial cycle and without snow and vegetation cover, the maximum permafrost depth at Forsmark is 400 m. The −5 and −10°C isotherms reach maximum depths of 200 m and 40 m, respectively (Figure 4-19). For the corresponding case, the maximum permafrost depth at Laxemar is 270 m. Here the −5 and −10°C isotherms reach maximum depths of 130 m and 12 m, respectively (Figure 4-19).

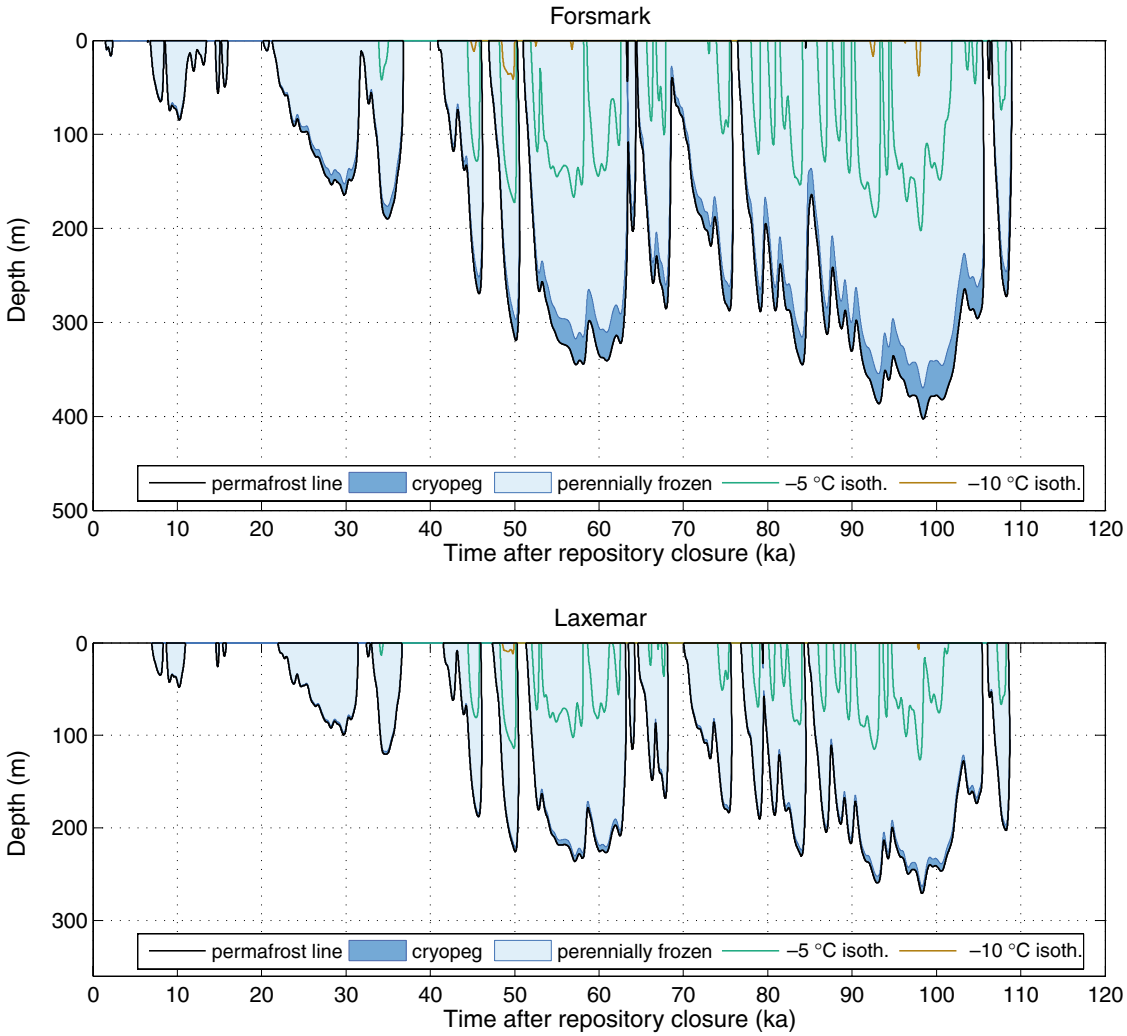

Figure 4-19. *Calculated permafrost depth, perennially frozen depth and the depths of the −5 and −10°C isotherms at Forsmark and Laxemar for the cold and extremely dry case (without ice sheet formation, and in the absence of vegetation, snow cover and sea) favouring permafrost growth. The greater permafrost depths at Forsmark are mainly due to different thermal bedrock characteristics.*

Figure 4-20 and 4-21 show development of bedrock temperature at repository depth for the extreme cases in Figure 4-17 and 4-18, as well as ground surface temperature data used as model input the for these cases.

The development of permafrost under exceptionally favourable conditions (Figures 4-19), with corresponding evolution of bedrock temperature at repository depth (Figure 4-20 and 4-21), is chosen as an extreme variant to the reference evolution concerning the development of permafrost.

Reconstructed late glacial climatic conditions for southern Sweden indicate that continental arctic conditions prevailed prior to ~ 15,000 years before present. At this time, mean July temperatures were around 10–12°C /Lemdahl 1988, Coope et al. 1998, Hohl 2005/, i.e. about 5 ± 2° colder than at present. The difference between the present warm interglacial temperatures and the *coldest* temperatures during the last glacial cycle as recorded in the GRIP ice core is in the order of 12°C (Figure 3-13). Using an alternative way of interpreting ^{18}O values from the ice core in terms of air temperature, /Lang et al. 1999/ suggested that this cold event reflects a temperature change of 16°C, which several degrees more than proposed in /Dansgaard et al. 1993/. However, according to all interpretations, this was a very short-lived climate event /cf Lang et al. 1999/. This exemplifies a typical feature of temperature climate archives namely

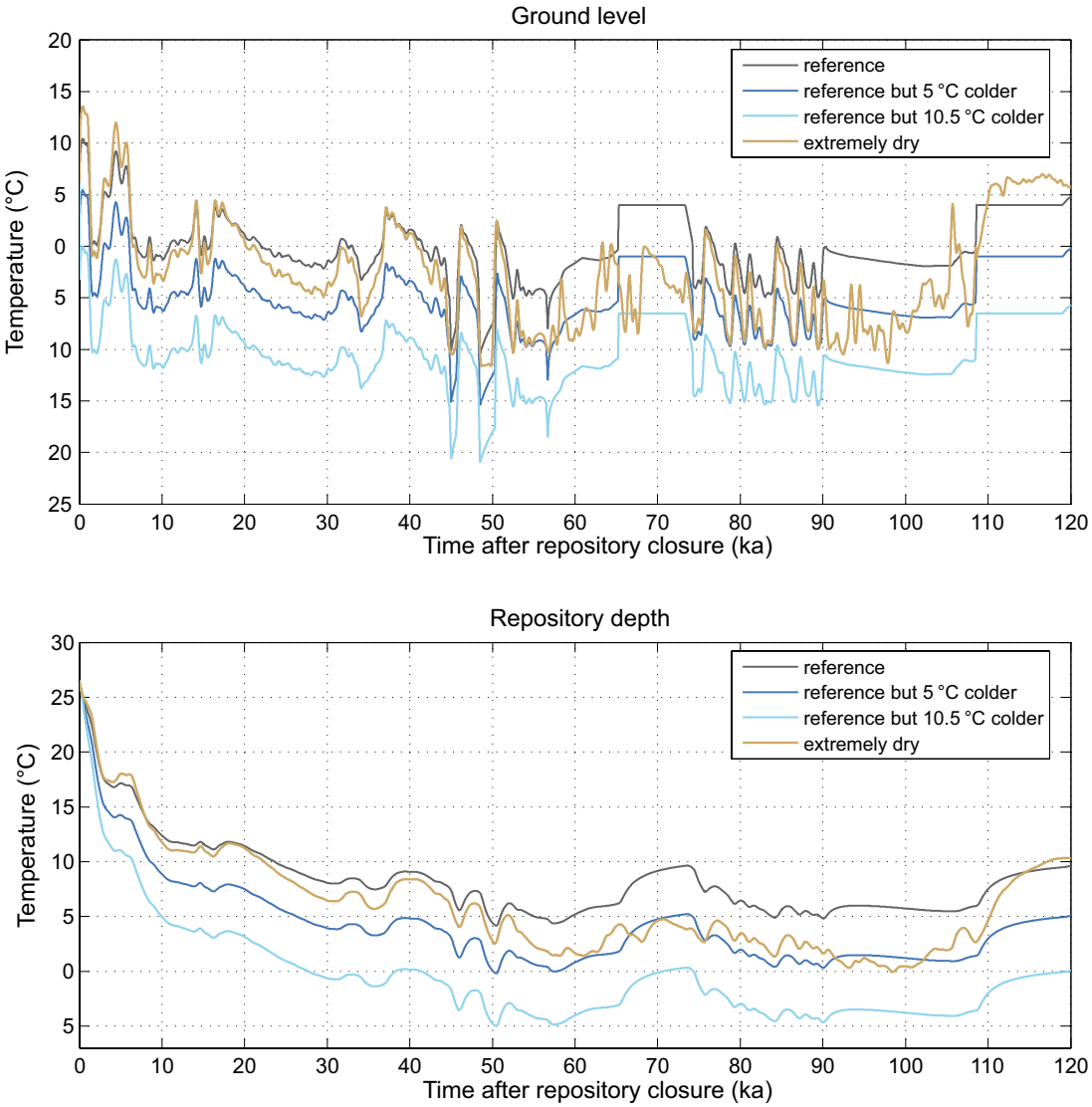

Figure 4-20. *Evolution of temperatures at ground level and repository depth at Forsmark from the extreme cases favouring development of permafrost shown in Figure 4-18.*

that they show that climate is highly variable on both long and short time scales /IPCC 2001 chapter 2/, variability for example seen in the GRIP proxy temperature data (Figure 3-13). When severe cold conditions occur, these conditions do not persist for long periods of time. Such climate variability is observed also in frequency analysis of climate records /Moberg et al. 2005, Witt and Schumann 2005/.

How low could temperatures have been at Forsmark and Laxemar during the last glacial cycle? Current annual mean air temperature is ~ 5.5°C at Forsmark and ~ 6.5°C at Laxemar. Albeit transferred from Greenland conditions to regional conditions in Sweden in a rather simplistic way, air temperatures produced for the sites suggest that annual mean air temperatures during the coldest phases of the last glacial cycle may well have been around −11 to −12°C in the Forsmark and Laxemar regions (Figure 3-51). However, considering the uncertainties in the transfer functions between ^{18}O and temperature, temperatures could have been several degrees lower. These values relate to air temperatures at ground level, whereas the mean annual temperature in the uppermost part of ground is 2–4°C higher, see Section 3.4.2. During the last glacial cycle, really low air temperatures only prevailed for restricted periods of time (Figure 3-13). This prevented permafrost to develop to great depths (Figure 4-6), and would do so also under even more extreme glacial cycle conditions (Figure 4-19).

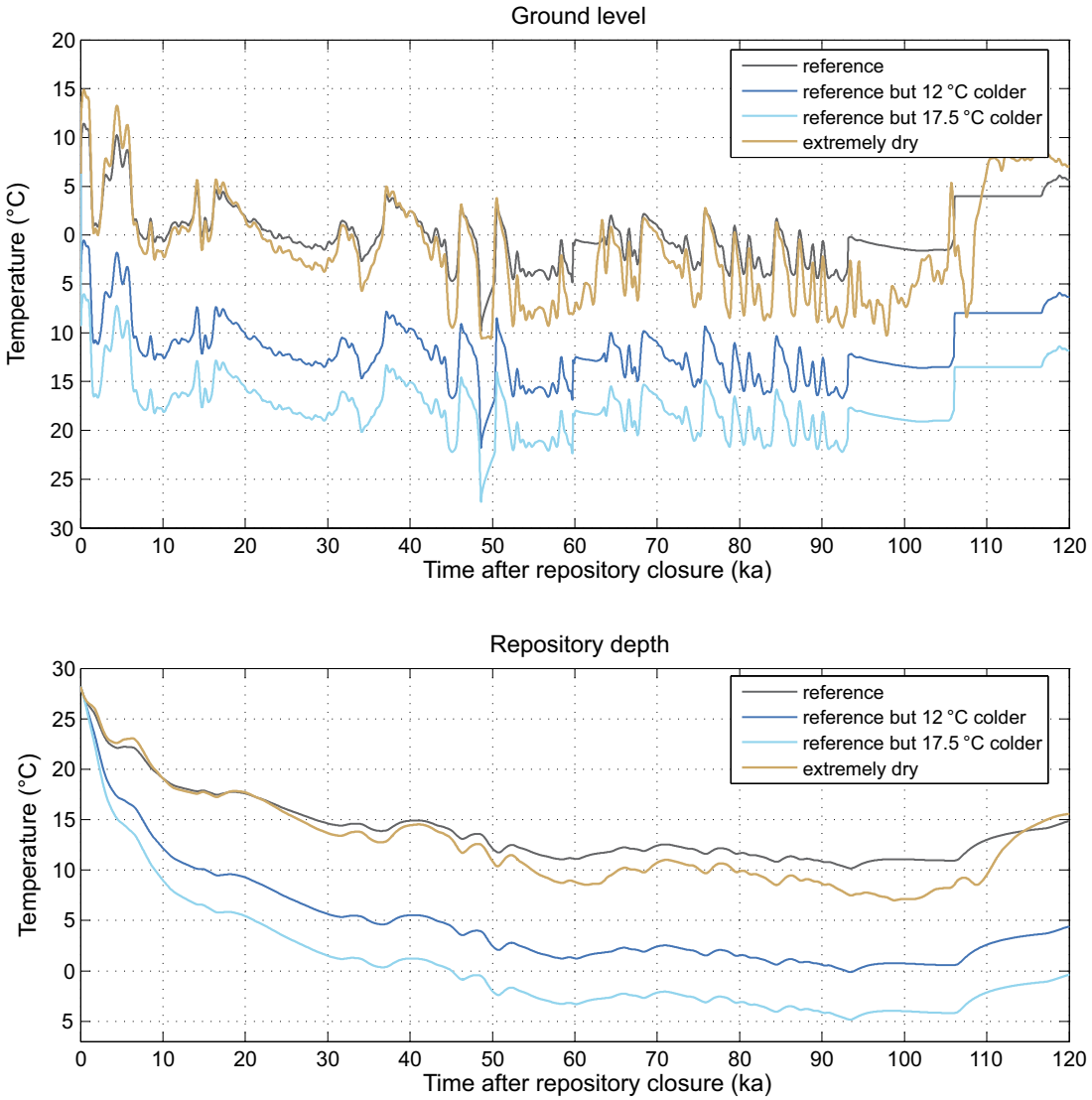

Figure 4-21. *Evolution of temperatures at ground level and repository depth at Laxemar from the extreme cases favouring development of permafrost, shown in Figure 4-19.*

Very cold periods have been relatively short lived in the past, and it is, therefore, very unlikely that they would prevail for considerably longer times during a future glacial cycle. Furthermore, during the coldest phases of a glacial cycle Fennoscandia is covered by an ice sheet, and the glacial domain prevails at the candidate sites. Preliminary calculations using the ice sheet model indicate that if the temperature falls by 9° an ice sheet will develop that covers the Forsmark region, and if temperatures fall by 10° an ice sheet covering both candidate sites will develop. When this happens, permafrost develops at a much lover rate or decreases (Figure 4-8 and 4-9). In association with major ice sheet advances over the sites, these areas are also submerged for some time after deglaciation, which further prevents permafrost development.

Based on the performed model studies and what is known about past climate conditions and climate variability, as well as climate and ice sheet interactions, the possibility that permafrost (0°C isotherm) reaches repository depth at Laxemar is ruled out. At Forsmark there is a small possibility that the 0°C isotherm reaches repository depth when adopting a pessimistic variant on permafrost development and heat generated from the spent fuel has declined (Figure 4-19). However, for buffer safety functions, the 0°C isotherm is not relevant, since the clay buffer material freezes at a lower temperature. Results indicate that the clay does not freeze at −5°C

/**Buffer and backfill process report,** Section 2.2.2/. The study of the development of the −5°C and −10°C isotherms shows that the probability for these isotherms to reach repository depth is ruled out at both sites (Figure 4-19).

Combination of buffer erosion and freezing

If groundwater were to freeze in cavities formed by buffer erosion, the associated volume expansion of the water would induce an additional pressure that possibly could affect the canister safety barrier. The following general approach was adopted to investigate the effects of this combined case:

- Calculations of freezing-induced pressures and freezing point temperatures in buffer erosion cavities were performed using various assumptions on compressibilities of any remaining buffer, shape of the erosion cavity, and surrounding ambient pressure (i.e. surrounding groundwater pressure plus clay swelling pressure).
- The lowest temperature at repository depth for the two sites, resulting from the climate scenario exceptionally favourable for permafrost growth, was used to quantify relevant combinations of freezing-point temperatures and freezing-induced pressures. Considering the uncertainty range in geothermal heat flow, and from that assuming a low heat flow value, the lowest repository depth temperatures are −1.8°C and +4.2°C for the Forsmark and Laxemar sites, respectively (Table 3-13) This pessimistically also assumed no heat contribution from the spent fuel. Thus, the lowest temperature that needs to be considered can be approximated by −2°C.

A simple model was used to estimate the freezing point and pressure increase in a ring-shaped erosion cavity surrounding the canister (Figure 4-22). In the calculations the compressibility of remaining clay was estimated from the swelling pressure of bentonite. It was also assumed that the erosion cavity was completely filled with ordinary compressible water, free from solutes and impurities. The effect of including these compressibilities is that they allow the freezing-induced expansion to occur at considerably higher temperatures than if the surroundings would have been incompressible. The compressibility of ice was also included, whereas the canister and the rock were assumed to be incompressible. Moreover, mean freezing temperatures for the erosion cavity as well as mean pressures for the erosion cavity and bentonite were assumed.

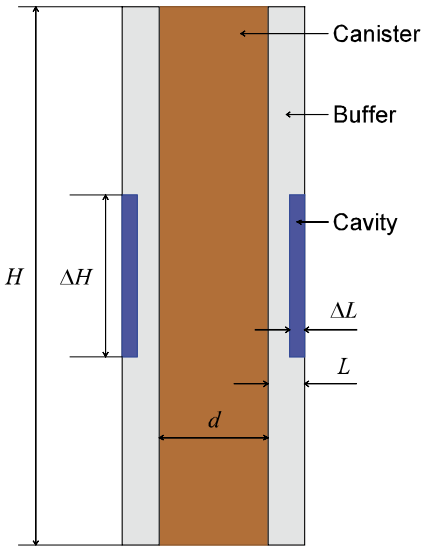

Figure 4-22. *Geometry for calculations of freezing temperatures and freezing-induced pressures in buffer erosion cavities.*

The surrounding groundwater pressure may vary between the hydrostatic pressure, for completely unfrozen conditions, to a value up to the maximum freezing pressure for partially or fully frozen groundwater conditions. The swelling pressure for an intact buffer with average reference density is 7.5–8 MPa for both MX-80 and Deponit CA-N /**Buffer and backfill process report**/. 400 m of overlying rock mass at Forsmark contributes with a hydrostatic pressure of 4 MPa, resulting in a total ambient pressure of around 12 MPa. The full reference density interval for the clay corresponds to a swelling pressure up to 13 MPa, which would yield an ambient pressure of 17 MPa. However, for a certain freezing temperature and for ambient pressures lower than the maximum freezing pressure, the pressure increase from freezing is affected by the ambient pressure, including the swelling pressure, in such a way that the resulting total pressure is constant, see below.

Calculations of freezing temperatures and associated pressure increases were made for ambient pressures between 4 and 100 MPa. Given the mean ambient pressure P_0 (groundwater pressure + swelling pressure) the mean pressure increase ΔP due to freezing can be calculated from

Equation 4-1
$$(1-\xi)\varepsilon_b^v + \xi\varepsilon_c^v = 0,$$

where

Equation 4-2
$$\xi \equiv \frac{V_{c,0}}{V_{c,0}+V_{b,0}} = \frac{\left(\frac{d}{2L}+\frac{\Delta L}{L}\right)^2}{\left(\frac{d}{2L}+1\right)^2}\frac{\Delta H}{H},$$

Equation 4-3
$$\varepsilon_b^v \equiv \frac{V_b - V_{b,0}}{V_b} = \frac{e_0+1}{e_0\left(\frac{P_0}{p_0}\right)^\beta+1} - \frac{e_0+1}{e_0\left(\frac{P_0+\Delta P}{p_0}\right)^\beta+1},$$

Equation 4-4
$$\varepsilon_c^v \equiv \frac{V_c - V_{c,0}}{V_c} = 1 - \frac{\rho_i}{\rho_w}\frac{1+\kappa_i(P_0+\Delta P)}{1+\kappa_w P_0}.$$

Above ε_b^v and ε_c^v are the volumetric strains of buffer clay and erosion cavity, respectively. Moreover, $\Delta L/L$ and $\Delta H/H$ are the relative cavity thickness and height and

d = diameter of canister (1.05 m)

L = thickness of buffer (0.35 m)

e_0 = reference void ratio (1.1)

p_0 = reference swelling pressure (1,000 kPa)

β = –0.19

ρ_i = density of ice (917 kg/m^3)

ρ_w = density of water (999.84 kg/m^3)

κ_i = compressibility of ice ($1.1784\cdot10^{-10}$ 1/Pa)

κ_w = compressibility of water ($5.089\cdot10^{-10}$ 1/Pa)

The mean freezing point T_f in °C can be obtained from /Wagner et al. 1994/

Equation 4-5
$$\frac{P_0+\Delta P+p_k}{p_n} = 1 - 0.626\cdot10^6\left(1-\left(\frac{T_f+T_0}{T_n}\right)^{-3}\right) + 0.197135\cdot10^6\left(1-\left(\frac{T_f+T_0}{T_n}\right)^{21.2}\right),$$

where p_k = 136213.717 Pa, p_n = 611.657 Pa, T_0 = 273.15°C and T_n = 273.16°C.

The mean freezing point and the corresponding pressure increase in erosion cavity as a function of relative cavity thickness and height for ambient pressures of 4, 5, 10, 20, 50 and 100 MPa are shown in Figures 4-23 to 4-28. The mean freezing point and the corresponding total pressure, $P_0 + \Delta P$, in erosion cavity as a function of relative cavity height and ambient pressure for the relative cavity thickness $\Delta L/L = 1$ is shown in Figure 4-29. The mean freezing point and the corresponding total pressure, $P_0 + \Delta P$, in erosion cavity as a function of relative cavity thickness and ambient pressure for the relative cavity height $\Delta H/H = 1$ is shown in Figure 4-30. In the figures, the shaded area represents the region outside the temperature range from 0.01 to –21.985°C of Equation (4-5). Examples of pressure increase and total pressure after freezing for various ambient pressures is presented in Table 4-1.

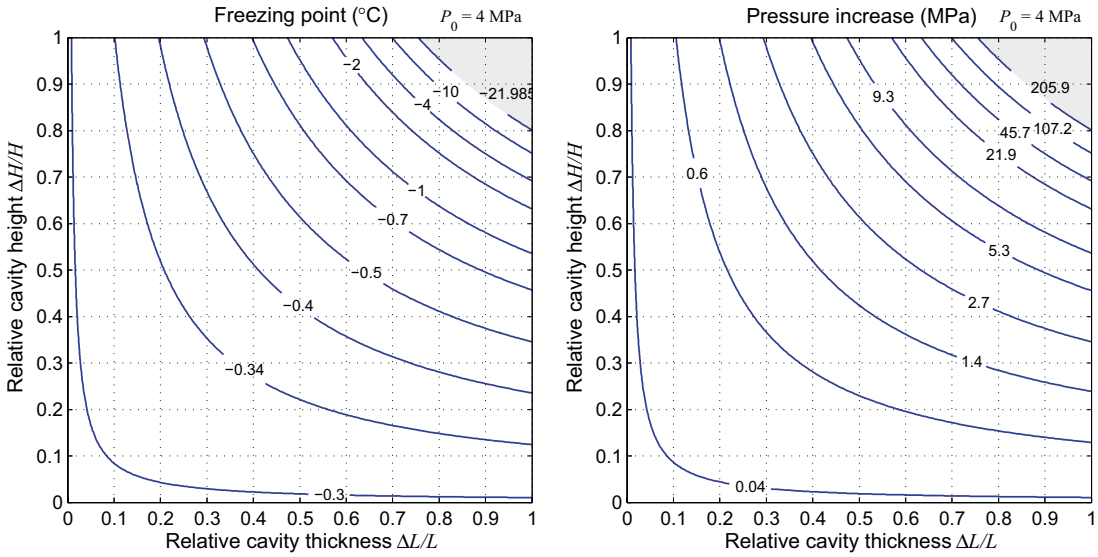

Figure 4-23. *Mean freezing point and pressure increase in erosion cavity for ambient pressure of 4 MPa.*

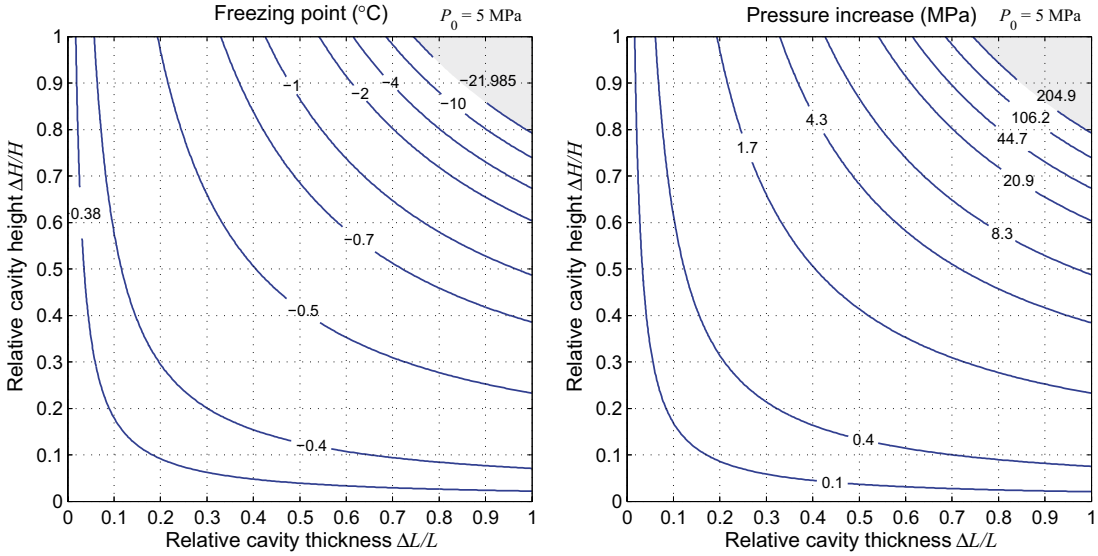

Figure 4-24. *Mean freezing point and pressure increase in erosion cavity for ambient pressure of 5 MPa.*

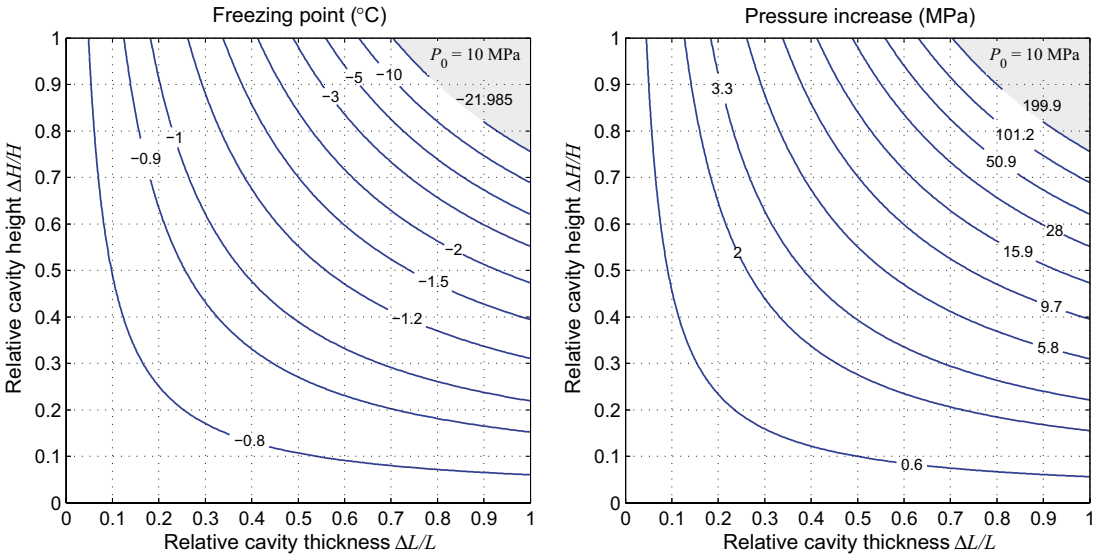

Figure 4-25. *Mean freezing point and pressure increase in erosion cavity for ambient pressure of 10 MPa.*

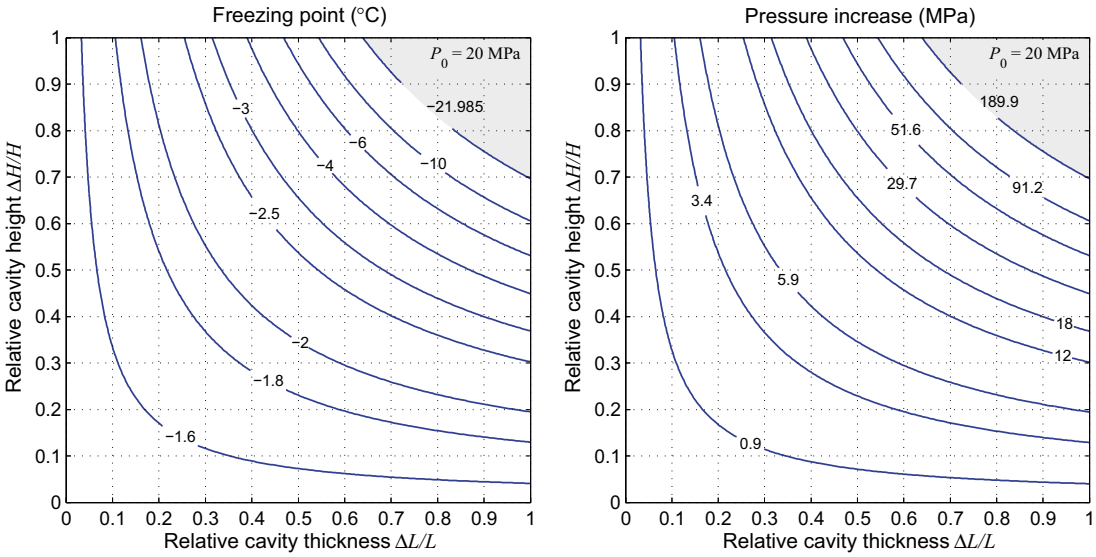

Figure 4-26. *Mean freezing point and pressure increase in erosion cavity for ambient pressure of 20 MPa.*

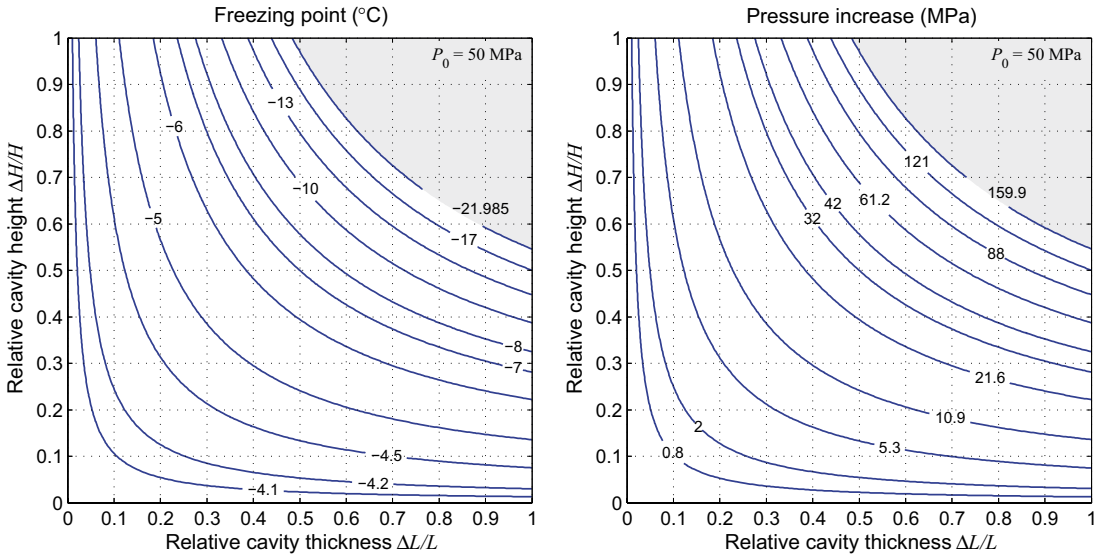

Figure 4-27. *Mean freezing point and pressure increase in erosion cavity for ambient pressure of 50 MPa.*

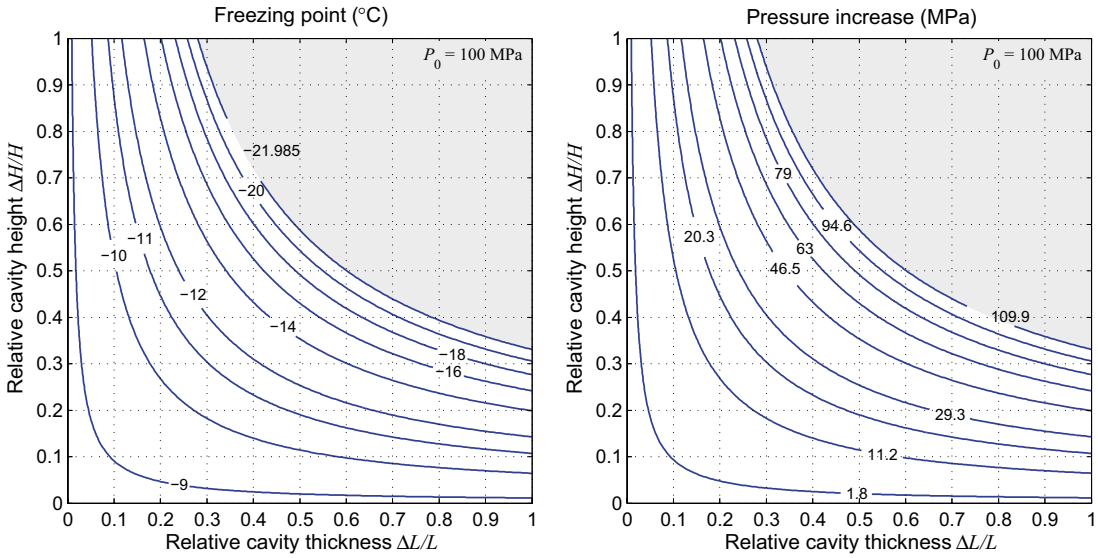

Figure 4-28. *Mean freezing point and pressure increase in erosion cavity for ambient pressure of 100 MPa.*

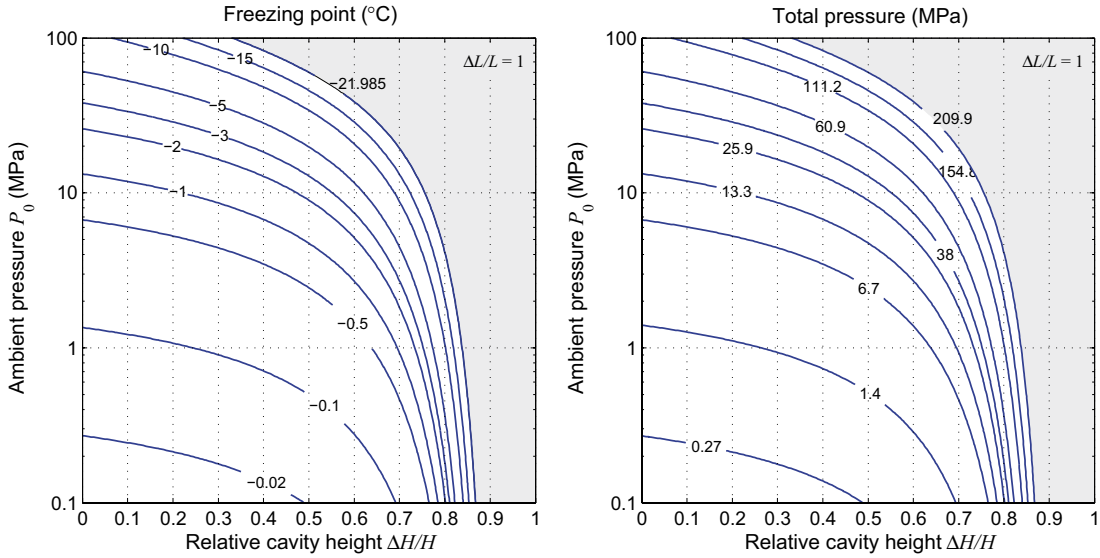

Figure 4-29. *Mean freezing point and total pressure $P_0+\Delta P$ in erosion cavity for relative cavity thickness $\Delta L/L = 1$.*

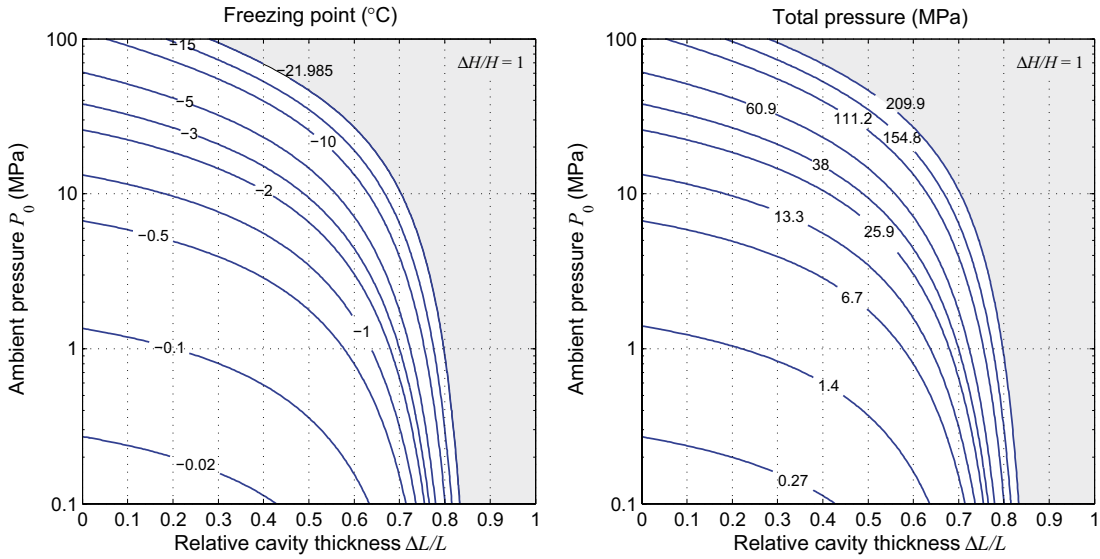

Figure 4-30. *Mean freezing point and total pressure $P_0+\Delta P$ in erosion cavity for relative cavity height $\Delta H/H = 1$.*

Table 4-1. Examples of pressure increase and total pressure after freezing in an erosion cavity for various ambient pressures at a freezing temperature of −2°C. The total pressure after freezing is independent of erosion cavity geometry and size.

Ambient pressure (sum of groundwater pressure and clay swelling pressure) (MPa)	Pressure increase from freezing (MPa)	Total pressure after freezing (maximum freezing pressure) (MPa)
4	22	26
5	21	26
10	16	26
20	6	26
26	0	26
50	0 (no freezing occurs)	50
100	0 (no freezing occurs)	100

The theoretical knowledge and results of the modelling can be summarised as follows:

- Freezing of water in an erosion cavity at a given freezing temperature can increase the pressure from the ambient pressure to the maximum freezing pressure, i.e. the maximum pressure at which freezing can occur at that temperature. For a freezing temperature of −2°C, the maximum freezing pressure is about 26 MPa. For a freezing temperature of −2°C, the total pressure after freezing in the erosion cavity thus is between the ambient pressure and 26 MPa, depending on the size of the erosion cavity.
- The maximum freezing pressure for a certain freezing temperature is independent of the geometry and size of the erosion cavity.
- The pressure increase from freezing depends on the freezing temperature, the ambient pressure and the size or geometry of the erosion cavity. For certain combinations of freezing temperature and ambient pressure, complete freezing takes place and the resulting pressure increase grows with the size of the cavity. This occurs up to a certain point, at which the sum of the ambient pressure and the pressure increase equals the maximum freezing pressure. After that point, the freezing pressure is at its maximum and complete freezing can no longer take place.
- If the ambient pressure exceeds the maximum freezing pressure of 26 MPa, no freezing can occur at a temperature of −2°C, see also Table 4-1.

4.4.2 Extremes within the glacial domain

The advance and retreat of an ice sheet over the repository site brings about the largest climate-related change the repository will experience during a glacial cycle. The main factors of importance for repository safety in the glacial domain are the maximum hydrostatic pressure, the penetration of oxygen rich and/or dilute glacial melt waters to great depth, the up-coning of saline waters from greater depth, the alteration of rock stresses and the occurrence of end-glacial faulting and the alteration of flow properties of the bedrock. Since the presence of fluid water is a prerequisite for most of these effects the basal conditions of the ice sheet are of major importance for its impact on the subsurface.

To find the extremes regarding ice sheet thickness additional simulations were performed with the ice sheet model used in the base variant of the main scenario. The extremes regarding hydrostatic pressure in the glacial domain depend on the ice sheet configuration and on its hydraulic systems. Under the Antarctic ice sheet, sub-glacial lakes have been observed. The hydrostatic pressure in these lakes is assumed to correspond to the ice overburden pressure. A hydro-thermo-mechanical balance is assumed where supply of basal melt water, re-freezing and ice deformation result in a hydrostatic equilibrium where the ice sheet rests, or floats,

on the water surface /e.g. Pattyn et al. 2004/. As further justified below, it is reasonable to assume that also for the Fennoscandian ice sheet, the maximum ice sheet thickness sets a limit to the maximum hydrostatic pressure that may occur at the bed.

Colder climate sensitivity test

To investigate the maximum ice sheet thickness that may occur in Fennoscandia, the ice sheet model was run using a set of temperature evolutions in which local annual air temperatures decreased linearly by 1° per 2,000 years, from present-day temperatures down to various constant levels. In these sensitivity tests, temperatures were lowered between 4 and 16° (Figure 4-31). Ice sheet growth started at a temperature lowering of 6 to 7°. Warmer cases did not produce an ice sheet. In all cases of ice sheet growth, the model simulated a total period of 100,000 years, after which approximately steady-state conditions were obtained with little further change in ice volume and area (Figure 4-31).

The results indicate that with the present model setup, cold climate conditions with annual mean temperatures lowered by 10°C are required for the ice sheet to advance to and over both candidate sites. At both sites the ice is warm-based. A lowering of the annual mean air temperature of 9° generated an ice sheet that covered Forsmark but not Laxemar. The difference is due to the more northerly location of Forsmark. The resulting maximum ice sheet thicknesses from the sensitivity simulations are shown in Figure 4-32.

As expected, the maximum ice sheet thickness increases with colder climates (Figure 4-32 (black line)). However, the rates of increase in thickness with temperature lowering declines as colder cases are considered. From a temperature lowering of approximately 13°, colder climates do not generate thicker ice sheets. These model results is in line with what is known on Antarctic ice sheet variations and on ice sheet climate interactions, see below.

These simulated temperature cases are extreme regarding their prolonged duration. Variations of this magnitude have occurred in the past /Dansgaard et al. 1993/, but never with this extremely long duration without interruptions. The extreme nature of these sensitivity cases is reflected also in the resulting ice sheet configurations for the colder cases. Here, the ice sheet covers all of northern and central Europe, and extends southward all the way to the Alps and beyond. Geological observations of traces from Fennoscandian ice sheets show that such large ice configurations have never occurred, and can thus be considered unrealistic.

The maximum ice thickness for Forsmark and Laxemar in the Weichselian base variant of the main scenario is 2,920 and 2,430 m, respectively (Figure 4-4 and 4-32). In the sensitivity tests, the maximum ice sheet thicknesses developed at Forsmark and Laxemar are 3,670 and 3,640 m, respectively (Figure 4-32). The uniform and high values at both sites reflect that they both have an interior location within these unrealistically large ice sheets.

Estimate of maximum ice thickness during the past 2 million years at the sites

From geological information it is known that the maximum ice extent of Pleistocene Fennoscandian ice sheets (i.e. those occurring the past ~ 2 million years) is larger than that of the Weichselian, typically reaching 100–200 km further south and 300–500 km further to the east /Svendsen et al. 1999/. Modelling results of this so called Saalian ice sheet show that the maximum thickness of the largest ice sheet configuration during the past 2 Ma, supported by geological observations, is 3,130 m for the Forsmark region and 2,540 m for Laxemar. Based on these results, the maximum expected ice sheet thickness is set to 3,200 m for Forsmark and 2,600 m for Laxemar.

From the results of the extreme cases in the sensitivity test, it is unlikely that the ice thickness at Forsmark and Laxemar could under any circumstance exceed 3,700 m. Also, the results of the sensitivity tests can be considered as conservative since it is unlikely that Fennoscandian ice sheets would, in reality, ever reach equilibrium size.

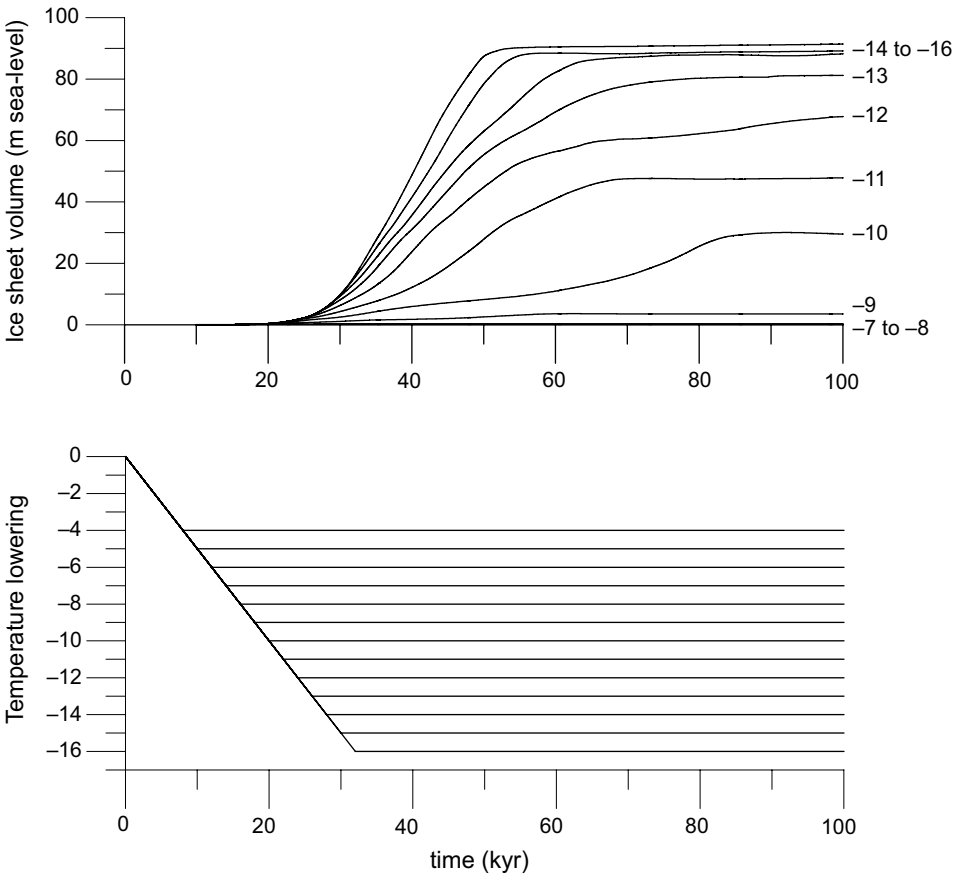

Figure 4-31. *Temperature lowering schemes and resulting development of ice sheet volumes in the additional cold scenario. The volume of the ice sheets is expressed as metres sea-level contribution.*

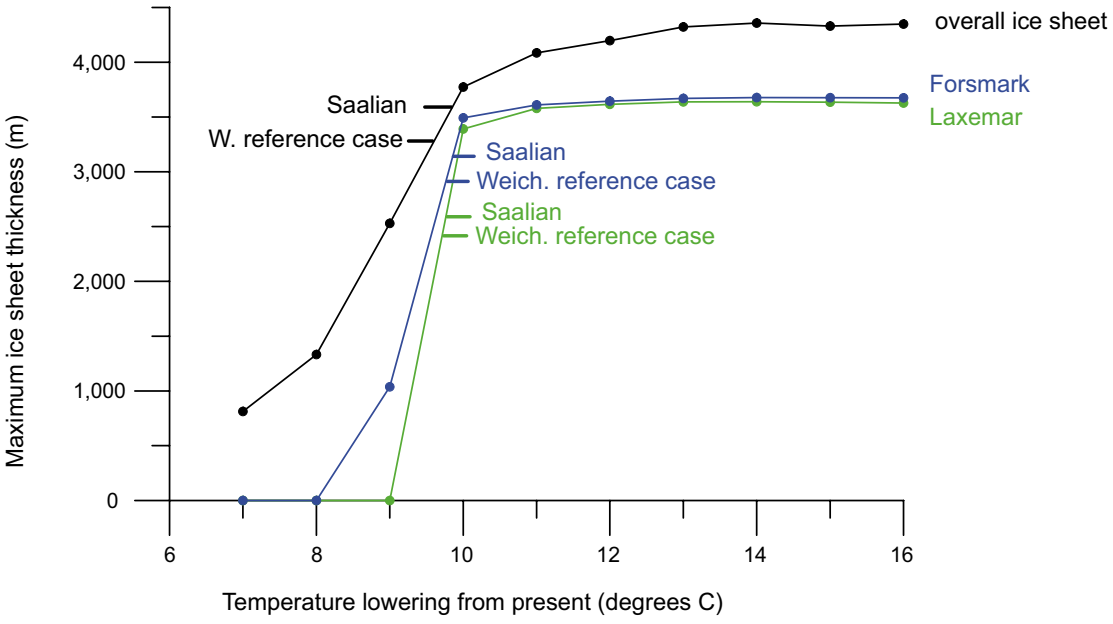

Figure 4-32. *Developed maximum ice sheet thicknesses for the schematic climate evolutions in Figure 4-22. The three curves represent extracted maximum ice thicknesses for the Forsmark region (blue), Laxemar region (green), and overall largest ice sheet thickness (black). Lines marked Weich. reference case show the maximum Weichselian ice thickness in the base variant of the SR-Can main scenario. Lines marked Saalian show the maximum ice thickness for the largest Fennoscandian ice sheet configuration supported by geological observations.*

Estimate of overall maximum ice sheet thicknesses during the past 2 million years

In the climate cooling sensitivity tests, the maximum simulated *overall* thickness of the ice sheets is 4,360 m (Figure 4-32). This thickness occurs for the unrealistic ice configurations derived in the 13° cooling case and colder cases. This is 1,000 m more than the maximum overall ice thickness in the Weichselian base scenario which is 3,300 m (Figure 4-32). The maximum thickness of the largest Pleistocene ice sheet supported by geological interpretations yields a maximum overall Saalian ice thickness of 3,600 m. The maximum expected overall ice thickness of the Fennoscandian ice sheet is therefore set to 3,600 m.

For comparison, the maximum ice sheet thickness occurring on Earth today is about 4,500 m for parts of the East Antarctic ice sheet /Lythe et al. 2001/. The Greenland ice sheet has a maximum thickness of about 3,400 m /Bamber et al. 2001/. In a colder glacial climate, the maximum ice thickness of the Antarctic ice sheet will probably not change significantly. In such a climate, the marginal parts of the Antarctic ice sheet grow significantly, while, at the same time, more interior parts keep the same thickness or even gets thinner due to moisture starvation /Huybrechts 1990, Näslund et al. 2000/. It is, therefore, likely that the maximum thickness of the Antarctic ice sheet seen also over an entire glacial cycle is around 4,500 m. This value is close to the largest overall ice thickness obtained in the sensitivity test, 4,360 m (Figure 4-32). The values are also in line with a largest inferred thickness of the Laurentide ice sheet of about 4,300 m /Tarasof and Peltier 2004/. These observations and results suggest that Pleistocene ice sheets up to date have not grown thicker than approximately 4,500 m, which gives a *hypothetical* upper limit for ice sheet thickness.

Hydrostatic pressures exceeding ice overburden

Hydrostatic pressures exceeding ice overburden can occur in some situations, for example in relation to jökulhlaups, i.e. large sudden outburst floods of glacial melt water from subglacial or supraglacial ice-dammed water reservoirs /Roberts et al. 2000/. In a few cases, higher pressures of non-jökulhlaup origin have been registered also in the ablation area of smaller glaciers (e.g. /Kamb and Engelhardt 1987/, Peter Jansson, personal comm.). These high pressures are of artesian character, with the amount of pressure being ultimately determined by up-glacier ice thickness and presence of meltwater. This could possibly also occur in frontal-near parts of ice sheets /Roberts 2005/. However, during times of maximum ice thickness over Forsmark and Laxemar, during the Last Glacial Maximum, these two sites are located well within the ice sheet interior, far from the ablation area and the margin. For this ice sheet configuration, surface melting is thus absent or negligible above and upstream of these sites due to the high ice surface elevation and associated low air temperatures. In addition, climate is at its coldest at this time during the glacial cycle, also prohibiting surface melt in these high-polar regions of the ice sheet. It is, therefore, reasonable to assume that hydrostatic pressures are dependent only on the *local* ice thickness during periods of maximum ice thickness, and not on ice thickness and surface melting upstream of the sites.

Conclusions on extremes within the glacial domain

For the Weichselian base variant, the additional hydrostatic pressure related to the maximum ice thicknesses at the sites is 26 MPa for Forsmark and 22 MPa for Laxemar, Table 4-2. The *maximum expected* additional hydrostatic pressure, conservatively derived from the largest ice sheet configuration during the past 2 million years supported by geological observations, is 28 MPa for Forsmark and 23 MPa for Laxemar. Maximum ice thicknesses of the more extreme and unrealistic ice sheet configurations discussed above, with associated additional hydrostatic pressures, are also listed in Table 4-2.

Table 4-2. Maximum ice thickness and associated additional hydrostatic pressure for various Fennoscandian ice sheet configurations.

	Maximum ice thickness (m)	Hydrostatic pressure contribution (MPa)
Weichselian base variant ice sheet		
Forsmark	2,920	26
Laxemar	2,430	22
Ice sheet overall	3,300	29
Largest Fennoscandian ice sheet during past 2 Ma supported by geological observations (Saalian)		
Forsmark	3,200	28
Laxemar	2,600	23
Ice sheet overall	3,600	32
Extreme ice sheets from climate sensitivity test		
Forsmark	3,670	32
Laxemar	3,640	32
Ice sheet overall	4,360	39
Maximum hypothetical		
	4,500	40

References

ACIA, 2005. Arctic Climate Impact Assessment. Cambridge University Press, Cambridge. 1042 p.

Adams J, 2005. On the probable rate of magnitude = 6 earthquakes close to a Swedish site during a glacial cycle, in S. Hora and M. Jensen, Expert panel elicitation of seismicity following glaciation in Sweden, Tech. Report 2005:20, Swedish Radiation Protection Authority (SSI), Stockholm, Sweden.

Ahonen L, 2001. Permafrost: occurrence and physicochemical processes. Posiva 2001-05, Posiva Oy.

Ahrens C D, 1994. Meteorology today – An introduction to Weather, Climate and the Environment, West Publishing Company.

Allen D, Michel F, Judge A, 1988. Paleoclimate and permafrost in the Mackenzie Delta. In: Fifth international conference proceedings on permafrost (Vol 1). Tapir publishers.

Alley C R, 1992. Flow-law hypotheses for ice sheet modeling. Journal of Glaciology 38(129): 245–256.

Alley R B, Clark P U, Huybrechts P, Joughin I, 2005a. Ice-sheet and sea-level changes. Science 310: 456–460.

Alley R B, Dupont T K, Parizek B R, Anandakrishnan S, 2005b. Access of surface meltwater to beds of subfreezing glaciers: Preliminary insights. Ann. Glaciol. 40, in press.

Anda E, Blikra L H, Braathen A, 2002. The Berill Fault – first evidence of neotectonic faulting in southern Norway, Norsk geologisk tidsskrift, 82, 175–182.

Andersen B G, Mangerud J, 1989. The last interglacial-glacial cycle in Fennoscandia. Quaternary International 3/4: 21–29.

Andersen K, Azuma N, Barnola J-M, Bigler M, Biscaye P, Caillon N, Chappellaz J, Clausen H.B, Dahl-Jensen D, Fischer H, Flückiger J, Fritzsche D, Fujii Y, Goto-Azuma K, Grønvold K, Gundestrup N S, Hansson M, Huber C, Hvidberg C S, Johnsen S J, Jonsell U, Jouzel J, Kipfstuhl J, Landais A, Leuenberger M, Lorrain R, Masson-Delmotte V, Miller H, Motoyama H, Narita H, Popp T, Rasmussen S O, Raynaud D, Röthlisberger R, Ruth U, Samyn D, Schwander J, Shoji H, Siggaard-Andersen M-L, Steffensen J P, Stocker T, Sveinbjörnsdottir A E, Svensson A, Takata M, Tison J L, Thortseinsson T, Watanabe O, Wilhelms F, White J W C, 2004. High-resolution record of Northern Hemisphere climate extending into the last interglacial period: Nature 431: 147–151.

Andrews J T, Barber D C, 2002. Dansgaard-Oeschger events: is there a signal of the Hudson Strait Ice Stream? Quaternary Science Reviews 21: 443–454.

Archer D, Kheshgi H, Maier-Reimer E, 1997. Multiple timescales for neutralization of fossil fuel CO_2, Geophysical Research Letters, 24(4), 405–408.

Archer D, Kheshgi H, Maier-Reimer E, 1998. Dynamics of fossil fuel CO_2 neutralization by marine $CaCO_3$, Global Biogeochemical Cycles, 12(2), 259–276.

Arnold N, Richards K, Willis I, Sharp M, 1998. Initial results from a distributed, physically based model of glacier hydrology. Hydrol. Proc. 12 (2), 191–219.

Arnold N, Sharp M, 2002. Flow variability in the Scandinavian ice sheet: modelling the coupling between ice sheet flow and hydrology. Quaternary Science Review 21:485–502.

Artemieva I M, Mooney W D, 2001. Thermal thickness and evolution of Precambrian lithosphere: A global study. Journal of geophysical research 106(B8): 16387–16414.

Avila R, 2006. Development of Land scape dose conversion factors for dose-assessments in SR-Can. SKB TR-06-XX (in prep), Svensk Kärnbränslehantering AB.

Balling N, 1984. Gravity and isostasy in the Baltic Shield. In: D.A. Galson, S. Mueller, and B. Munch (eds.), First EGT Workshop, the Northern segment. European Science Foundation, Strasbourg, 53–66.

Balling N, 1995. Heat flow and thermal structure of lithosphere across the Baltic Shield and northern Tornquist Zone. Tectonophysics, Vol. 244, pp 13–50.

Bamber J L, Layberry R L, Gogenini S P, 2001. A new ice thickness and bed data set for the Greenland ice sheet 1: Measurement, data reduction, and errors. Journal of Geophysical Research 106 (D24): 33773–33780.

Bard E, Hamelin B, Fairbanks R G, 1990. U-Th ages obtained by mass spectrometry in corals from Barbados: sea-level during the past 130,000 years. Nature 346 (6283), 456–458.

Bard E, Hamelin B, Arnold M, Montaggioni L, Cabioch G, Faure G, Rougerie F, 1996. Deglacial sea-level record from Tahiti corals and the timing of global meltwater discharge. Nature 382 (6588), 241–244.

Bassett S E, Milne G A, Mitrovica J X, Clark P U, 2005. Ice sheet and solid earth influences on far-field sea-level histories. Science 309 (5736), 925–928.

Beardsmore G R, Cull J P, 2001. Crustal heat flow. A guide to measurement and modelling. Cambridge University Press, Cambridge. 324 pp.

Benson C, 1961. Stratigraphic studies in the snow and firn of the Greenland Ice Sheet. Folia Geographics Danica. 9, 13–37.

Berger A, 1978. Long-term variations of daily insolation and Quaternary climatic changes, Journal of the Atmospheric Sciences 35: 2362–2367.

Berger A, Loutre M F, 2002. An exceptionally long interglacial ahead? Science 297: 1287–1288.

Bills B G, James T S, 1996. Late Quaternary variations in relative sea level due to glacial polar wander. Geophysical Research Letters 23, 3023–3026.

Birch F, Roy R F, Decker E R, 1968. Heat flow and thermal history in New England and New York. In: Zen, E-an (Ed.): Studies of Appalachian Geology: Northern and Maritime. 437–451.

BIOCLIM, 2001. Deliverable D3: Global Climatic Features over the Next Million Years and Recommendation for Specific Situations to be Considered, ANDRA, Parc de la Croix Blanche, 1/7 rue Jean Monnet, 92298 Châtenay-Malabry, France.

BIOCLIM, 2003. Continuous climate evolution scenarios over western Europe (1000 km scale), Deliverable D7. Work package 2: Simulation of the future evolution of the biosphere system using the hierarchical strategy. 88 p.

Björck S, 1995. A review of the history of the Baltic Sea, 13.0–8.0 ka BP. Quaternary International 27, 19–40.

Bogren J, Gustavsson T, Loman G, 1998. Klimatförändringar Naturliga och antropogena orsaker. Studentlitteratur, Göteborgs universitet.

Boulton G S, Payne A, 1992. Simulation of the European ice sheet through the last glacial and prediction of future glaciation. SKB technical report 93-14: 139 pp, Svensk Kärnbränslehantering AB.

Boulton G S, Kautsky U, Morén L, Wallroth T, 2001a. Impact of long-term climate change on a deep geological repository for spent nuclear waste. SKB TR-99-05, Svensk Kärnbränslehantering AB.

Boulton G S, Zatsepin S, Maillot B, 2001b. Analysis of groundwater flow beneath ice sheets. SKB TR-01-06, Svensk Kärnbränslehantering AB.

Brantberger M, Zetterqvist A, Arnbjerg-Nielsen T, Olsson T, Outters N, Syrjänen P, 2006. Final repository for spent nuclear fuel. Underground design Forsmark, Layout D1. SKB R-06-34, Svensk Kärnbränslehantering AB.

Breemer C W, Clark P U, Haggerty R, 2002. Modelling the subglacial hydrology of the late Pleistocene lake Michigan Lobe, Laurentide Ice Sheet. GSA Bulletin 114: 665–674.

Broecker, 1991. In Climate change 1995, Impacts, adaptations and mitigation of climate change: scientific –technical analyses, contributing of working group 2 to the second assessment report of the intergovernmental panel on climate change, UNEP and WMO, Cambridge university press, 1996.

Buffer and backfill process report, 2006. Buffer and backfill process report for the safety assessment SR-Can. SKB TR-06-18, Svensk Kärnbränslehantering AB.

Burroughs W J, 2001. Climate change – a multidisciplinary approach, Cambridge University Press.

Burt T P, Williams P J, 1976. Hydraulic conductivity in frozen soils: Earth Surface Processes 1: 349–360.

Bäckblom G, Stanfors R, 1989. Interdisciplinary study of post-glacial faulting in the Lansjärv area northern Sweden. SKB TR-89-31, Svensk Kärnbränslehantering AB.

Bøggild C E, Mayer C, Podlech S, Taurisano A, Nielsen S, 2004. Towards an assessment of the balance state of the Greenland Ice Sheet. Geological Survey of Denmark and Greenland Bulletin 4, 81–84.

Čermák V, Balling N, Kukkonen I, Zui V I, 1993. Heat flow in the Baltic Shield – results of the lithospheric geothermal modelling. Precambrian Research 64(1–4): 53–65.

Chappell J, Polach H, 1991. Postglacial sea-level rise from a coral record at Huon Peninsula, Papua-New-Guinea. Nature 349 6305, 147–149.

Chappell J, Omura A, Esat T, McCulloch M, Pandolfi J, Ota Y, Pillans B, 1996. Reconciliation of late Quaternary sea levels derived from coral terraces at Huon Peninsula with deep sea oxygen isotope records. Earth and Planetary Science Letters 141 (1–4), 227–236.

Church J A, 35 others, 2001. Greenland and Antarctic Ice Sheets, in Houghton, J.T. (ed.), Climate Change 2001: the Scientific Basis (chap. 11.2.3), New York: Cambridge Univ. Press, 881 p.

Clark J A, Farrell W E, Peltier W R, 1978. Global changes in postglacial sea level: a numerical calculation. Quaternary Research 9, 265–287.

Clark P U, Alley R B, Keigwin L D, Licciardi J M, Johnsen S J, Wang H X, 1996. Origin of the first global meltwater pulse following the last glacial maximum. Paleoceanography 11(5), 563–577.

Clark P U, Mix A C, 2002. Ice sheets and sea level of the Last Glacial Maximum. Quaternary Science Reviews 21 (1–3), 1–7.

Clauser C, Huenges E, 1995. Thermal conductivity of rocks and minerals. In Handbook of Physical Constants: Rock Physics and Phase Relations, AGU Reference Shelf Series, Vol. 3, pp 105–126.

Coope G R, Lemdahl G, Lowe J J, Walkling A, 1998. Temperature gradients in northern Europe during the last glacial-Holocene transition (14-9 14C kyr BP) interpreted from coleopteran assemblages. Journal of Quaternary Science 13: 419–433.

Cubash U, Meehl G A, 2001. Projections of future climate change, In Climate Change 2001: The Scientific Basis. Houghton et al. (eds.) Cambridge University Press. New York.

Cutler P M, MacAyeal D R, Mickelson D M, Parizek B R, Colgan P M, 2000. A numerical investigation of ice-lobe-permafrost interaction around the southern Laurentide ice sheet: Journal of Glaciology 46: 311–325.

Dansgaard W, Johnsen S J, Clausen H B, Dahl-Jensen D, Gundestrup N S, Hammer C U, Hvidberg C S, Steffensen J P, Sveinbjörnsdottir A E, Jouzel J, Bond G, 1993. Evidence for general instability of past climate from a 250-kyr ice-core record. Nature 364: 218–220.

Data report, 2006. Data report for the safety assessment SR-Can. SKB TR-06-25, Svensk Kärnbränslehantering AB.

Davis J L, Mitrovica J X, 1996. Glacial isostatic adjustment and the anomalous tide gauge record of eastern North America. Nature 379 (6563), 331–333.

Davis J L, Mitrovica J X, Scherneck H G, Fan R, 1999. Investigations of Fennoscandian glacial isostatic adjustment using modern sea level records. Journal of Geophysical Research 104 (2), 2733–2747.

Denton G H, Hughes T J (eds), 1981. The Last Great Ice Sheets: New York, John Wiley and Sons, 484 p.

Duval P, Ashby M F, Anderman I, 1983. Rate-controlling processes in the creep of poly-crystalline ice. Journal of physical chemistry 87(21): 4066–4074.

Dziewonski A M, Anderson D L, 1981. Preliminary reference earth model (PREM). Physics of the Earth and Planetary Interiors 25, 297–356.

Engelhardt H, Humphrey N, Kamb B, Fahnestock M, 1990. Physical conditions at the base of a fast moving Antarctic ice stream. Science: 248: 57–59.

Engelhardt H F, Kamb B, 1998. Basal sliding of Ice Stream B, West Antarctica. Journal of Glaciology 44(147): 223–230.

EPICA community members, 2004. Eight glacial cycles from an Antarctic ice core. Nature 429: 623–628.

Eronen M, Gluckert G, Hatakka L, Van De Plassche O, Van Der Plicht J, Rantala P, 2001. Rates of Holocene isostatic uplift and relative sea-level lowering of the Baltic in SW Finland based on studies of isolation contacts. Boreas 30 (1), 17–30.

ETOPO2, 2001. Global Digital Elevation Model (ETOPO2) representing gridded (2 minute by 2 minute) elevation and bathymetry for the world. Data were derived from the National Geophysical Data Center (NGDC) ETOPO2 Global 2’ Elevations data set from September 2001.

Fairbanks R G, 1989. A 17,000-year glacio-eustatic sea level record: influence of glacial melting rates on the Younger Dryas event and deep-ocean circulation. Nature 342, 637–642.

Farrell W E, Clark J A, 1976. On postglacial sea level. Geophysical Journal of the Royal Astronomical Society 46, 647–667.

Fastook J L, Chapman J E, 1989. A map plane finite-element model: Three modelling experiments. Journal of Glaciology 35(119): 48–52.

Fastook J L, 1990. A map-plane finite-element program for ice sheet reconstruction: A steady-state calibration with Antarctica and a reconstruction of the Laurentide ice sheet for 18,000 BP. In Brown H.U., ed. Computer Assisted Analysis and Modelling on the IBM 3090. IBM Scientific and Technical Computing Department, White Plains, New York.

Fastook J L, 1994. Modelling the Ice Age: The Finite-element method in glaciology. Computational Science and Engineering 1(1): 55–67.

Fastook J L, Holmlund P, 1994. A glaciological model of the Younger Dryas event in Scandinavia. Journal of Glaciology 40(134), 125–131.

Fastook J L, Prentice M, 1994. A finite-element model of Antarctica: sensitivity test for meteorological mass-balance relationship. Journal of Glaciology 40(134): 167–175.

Fenton C H, Adams J, Halchuk S, 2006. Seismic hazard assessment for radioactive waste disposal sites in regions of low seismic activity, Geotechnical and Geological Engineering 24: 579–592, doi 10.1007/s10706-005-1148-4.

FEP report, 2006. FEP report for the safety assessment SR-Can. SKB TR-06-20, Svensk Kärnbränslehantering AB.

Fleming K, Johnston P, Zwartz D, Yokoyama Y, Lambeck K, Chappell J, 1998. Refining the eustatic sea-level curve since the Last Glacial Maximum using far- and intermediate-field sites. Earth and Planetary Science Letters 163, 327–342.

Flowers G E, Clarke G K C, 2002a. A multicomponent coupled model of glacier hydrology. 1. Theory and synthetic examples. J. Geophys. Res. 107 (B11), doi:10.1029/2001JB001122.

Flowers G E, Clarke G K C, 2002b. A multicomponent coupled model of glacier hydrology. 2. Application to Trapridge Glacier, Yukon, Canada. J. Geophys. Res. 107 (B11), doi:10.1029/2001JB001124.

Forsstrom P L, Sallasmaa O, Greve R, Zwinger T, 2003. Simulation of fast-flow features of the Fennoscandian ice sheet during the Last Glacial Maximum. Annals of Glaciology 37: 383–389.

Fotiev S M, 1997. Permafrost groundwater Russian Literature Review. In: Haldorsen S, Liebman M, Nelson G, van Everdingen R O, Boike J, 1997: State-of-the-art Report on saturated water movement in permafrost areas. Report No 4/97 (lnr 54). Agricultural University of Norway.

Fountain A G, Walder J S, 1998. Water flow through temperate glaciers. Rev. Geophys. 36 (X), 299–328.

Fountain A G, Jacobel R W, Schlichting R, Jansson P, 2005a. Fractures as the main pathways of water flow in temperate glaciers. Nature. 433 (7026): 618–621.

Fountain A G, Schlichting R, Jansson P, Jacobel R W, 2005b. Observations of englacial flow passages – a fracture dominated system. Ann. Glaciol. 40: 25–30.

French H M, 1996. The Periglacial Environment. Second edition. Addison Wesley Longman Limited.

Fronval T, Jansen E, 1996. Late Neogene paleoclimates and paleoceanography in the Iceland-Norwegian Sea: evidence from the Iceland and Vøring plateaus. In: Thiede, J., Myhre, A.M, Firth, J.V, Johnson G.L. and Ruddiman, W.F. (eds.), Proceedings of the Ocean Drilling Program, Scientific Results 151: 455–468.

Funder S, Demidov I, Yelovicheva Y, 2002. Hydrography and mollusc faunas of the Baltic and the White Sea-North Sea seaway in the Eemian. Paleogeography, Paleoclimatology, Paleoecology 184(3–4), 275–304.

Furlong K P, Chapman D S, 1987. Crustal heterogeneities and the thermal structure of the continental crust. Geophysical Research Letters 14(3):314–317.

Gascoyne M, 2000. A review of published literature on the effects of permafrost on the hydrogeochemistry of bedrock. SKB R-01-56, Svensk Kärnbränslehantering AB.

Geosphere process report, 2006. Geosphere process report for the safety assessment SR-Can. SKB TR-06-19, Svensk Kärnbränslehantering AB.

Giovinetto M B, Zwally H J, 2000. Spatial distribution of net surface accumulation on the Antarctic ice sheet. Annals of Glaciology 31: 171–178.

Glen J W, 1955. The creep of polycrystalline ice. Proceedings of the Royal Society, London, A228 (1175): 519–538.

Goodess C M, Palutikof, J P, Davies T D, 1992. The Nature and Causes of Climate Change: Assessing the Long Term Future, Belhaven Press, London.

Gregory J M, Huybrechts P, Raper S C B, 2004. Threatened loss of the Greenland ice sheet. Nature 428: p. 616.

Greve R, Hutter K, 1995. Polythermal three-dimensional modelling of the Greenland Ice Sheet with varied geothermal heat flux. Annals of glaciology 21: 8–12.

Grollimund B, Zoback M D, 2000. Post glacial lithospheric flexure and induced stresses and pore pressure changes in the northern North Sea, Tectonophysics, 327, 61–81.

Hambrey M J, Barrett P J, Ehrmann W U, Larsen B, 1992. Cainozoic sedimentary processes on the Antarctic continental margin and the record from deep drilling. Zeitschrift für Geomorphologie, Supplementband 86: 77–103.

Han D, Wahr J, 1989. Post-glacial rebound analysis for a rotating Earth, in 'Slow Deformations and Transmission of Stress in the Earth', pp 1–6, eds. Cohen, S. and P. Vanicek. AGU Mono. Series 49. American Geophysical Union, Washington D.C.

Hanebuth T, Stattegger K, Grootes P M, 2000. Rapid flooding of the Sunda Shelf: A late-glacial sea-level record. Science 288 (5468), 1033–1035.

Haq B U, Hardenbol J, Vail P R, 1987. Chronology of fluctuating sea levels since the Triassic. Science 235: 1156–1165.

Hartikainen J, 2004. Permafrost modeling in DECOVALEX III for BMT3. In Eloranta, E ed., DECOVALEX III, 1999–2003. An international project for the modelling of coupled thermo-hydro-mechanical processes for spent fuel disposal. Finnish national contributions. STUK-YTO-TR 209. Helsinki.

Hartikainen J, 2006. Numerical modelling of permafrost development at Forsmark and Laxemar. SKB XX-XX-XX, in prep, Svensk Kärnbränslehantering AB.

Hartikainen J, in prep. Work report of the project Numerical modelling of permafrost. To be published in SKB report. Svensk Kärnbränslehantering AB.

Heinrich H, 1988. Origin and consequences of cyclic ice rafting in the northeast Atlantic Ocean during the past 130,000 years. Quaternary Research 29: 142–152.

Hindmarsh R C A, Boulton G S, Hutter K, 1989. Modes of operation of thermo-mechanically coupled ice sheets. Annals of Glaciology 12: 57–69.

Hoaglund III J R, Kolak J J, Long D T, Larson G J, 2004. Analysis of modern and Pleistocene exchange between Saginaw Bay (Lake Huron) and the Saginaw Lowlands area. GSA Bulletin, 116: 3–15.

Hock R, 1998. Modelling of glacier melt and discharge. Zürcher Geographische Schriften. 70, 140 pp.

Hock R, 2005. Glacier melt: a review of processes and their modelling. Progr. Phys. Geogr. 29(3), 362–391.

Hock R, Jansson P, 2005. Modelling glacier hydrology. In: Anderson, M. G, and McDonnell, J. (eds.), Encyclopedia of Hydrological Sciences. John Wiley and Sons, Chichester. 4, 2647–2655.

Hock R, Jansson P, Braun L, 2005. Modelling the response of mountain glacier discharge to climate warming. In: U. M. Huber, H. K. M. Bugmann, and M. A. Reasoner (Eds.), 2005: Global Change and Mountain Regions (A State of Knowledge Overview), Springer, Dordrecht. 243–252.

Hohl V, 2005. Northern European long term climate archives. SKB TR-05-01, Svensk Kärnbränslehantering AB.

Hohmann M, 1997. Soil freezing – the concept of soil water potential. State of the art. Cold Reg. Sci. Technol., 25(2): 101–110.

Holmlund P, Fastook J, 1995. A time dependent glaciological model of the Weichselian ice sheet. Quaternary International 27: 53–58.

Hooke R LeB, 1977. Basal temperatures in polar ice sheets: a qualitative review: Quaternary Research 7: 1–13.

Hooke R LeB, 1984. On the role of mechanical energy in maintaining subglacial conduits at atmospheric pressure. J. Glaciol. 30 (105), 180–187.

Hooke R LeB, 1989. Englacial and subglacial hydrology: a qualitative review. Arct. Alp. Res. 21 (3), 221–233.

Hooke R LeB, Lauman T, Kohler J, 1990. Subglacial water pressures and the shape of subglacial conduits. J. Glaciol. 36 (122), 67–71.

Hooke R LeB, 1998. Principles of glacier mechanics. Prentice-Hall, Englewood Cliffs, N.J. 248 pp.

Hooke R LeB, 2004. Principles of glacier mechanics. Second edition. Cambridge: Cambridge University Press.

Hora S, Jensen M, 2005. Expert panel elicitation on seismicity following glaciation, Tech. Report SSI 2005:20, Swedish Radiation Protection Authority (SSI), Stockholm, Sweden.

Hubbard B, Nienow P, 1997. Alpine subglacial hydrology. Quat. Sci. Rev. 16 (X), 939–955.

Humlum O, Houmark-Nielsen M, 1994. Deglaciation rates in Denmark during the late Weichselian – implications for the palaeoenvironment. Geografisk Tidsskrift 94: 26–37.

Huybrechts P, 1990. A 3-D model for the Antarctic ice sheet: a sensitivity study on the glacial-interglacial contrast. Climate Dynamics 5(2): 79–92.

Huybrechts P, Letreguilly A, Reeh N, 1991. The Greenland ice sheet and greenhouse warming. Palaeogeography, Palaeoclimatology, Palaeoecology 89(4): 399–412.

Huybrechts P, T'siobbel S, 1995. Thermomechanical modelling of Northern Hemisphere ice sheets with a two-level mass-balance parameterization. Annals of Glaciology 21: 111–116.

Huybrechts P, Payne A J, EISMINT Intercomparison Group, 1996. The EISMINT benchmarks for testing ice sheet models. Annals of Glaciology 23, 1–12.

Huybrechts P, de Wolde J, 1999. The dynamic response of the Greenland and Antarctic ice sheets to multiple-century climate warming. Journal of Climatology 12: 2169–2188.

Huybrechts P, 2006. Numerical modeling of ice sheets through time. In: Knight, P.G. (ed.): Glacier Science and Environmental Change, Blackwell Publishing (Oxford), 406–412.

Håkansson R, 2000. Beräkning av nuklidinnehåll, resteffekt, aktivitet samt doshastighet för utbränt kärnbränsle. SKB R-99-74, Svensk Kärnbränslehantering AB.

Hökmark H, Fälth B, 2003. Thermal dimensioning of the deep repository. Influence of canister spacing, canister power, rock thermal properties and near-field design on the maximum canister surface temperature. SKB TR-03-09, Svensk Kärnbränslehantering AB.

Hökmark H, Fälth B, Wallroth T, 2006. T-H-M couplings in rock. Overview of results of importance to the SR-Can safety assessment. SKB R-06-88, Svensk Kärnbränslehantering AB.

Imbrie J, Hays J D, Martinson D G, McIntyre A, Mix A C, Morley J J, Pisias N G, W L Prell, Shackleton N J, 1984. The orbital theory of Pleistocene climate: support from a revised chronology of the marine $\delta^{18}O$ record. In: Berger A L et al. (Eds.), Milankovitch and Climate. Reidel, pp 269–305. Reidel Publishing Company.

IPCC, 2001. Climate Change 2001: The Scientific Basis. Contribution of Working Group I to the Third Assessment Report of the Intergovernmental Panel on Climate Change. Eds: Houghton, J.T,Y. Ding, D.J. Griggs, M. Noguer, P.J. van der Linden, X. Dai, K. Maskell, and C.A. Johnson. Cambridge University Press, Cambridge, United Kingdom and New York, NY, USA, 881 pp.

Isaksen K, Holmlund P, Sollid J L, Harris C, 2001. Three deep alpine-permafrost boreholes in Svalbard and Scandinavia. Permafrost and Periglacial Processes Vol. 12, pp 13–26.

Iverson N R, Hanson B, Hooke R LeB, Jansson P, 1995. Flow mechanism of glaciers on soft beds. Science 267:80–81.

Jansen E, Sjøholm J, 1991. Reconstruction of glaciation over the past 6 Myr from ice-borne deposits in the Norwegian Sea. Nature 349:600–603.

Jansson, P, 1997. Longitudinal coupling effects in ice flow across a subglacial ridge. Ann. Glaciol. 24: 169–174.

Jansson P, Hock R, Schneider T, 2003. The concept of glacier storage – A review. J. Hydrol. 282 (1–4): 116–129.

Jansson P, Näslund J O, Rodhe L, 2006. Glacial hydrology and eskers. A review of ice sheet hydrology. TR-06-34, Svensk Kärnbränslehantering AB.

Jaquet O, Siegel P, 2006. Simpevarp 1.2 – Regional groundwater flow model for a glaciation scenario. SKB R-06-100, Svensk Kärnbränslehantering AB.

Johansson J M, Davis J L, Scherneck H-G, Milne G A, Vermeer M, Mitrovica J X, Bennett R A, Jonsson B, Elgered G, Elósegui P, Koivula H, Poutanen M, Rönnäng B O, Shapiro I I, 2002. Continuous GPS measurements of postglacial adjustment in Fennoscandia, 1. Geodetic results. Journal of Geophysical Research 107, 400–428.

Johnsen S J, Dahl-Jensen D, Dansgaard W, Gundestrup N, 1995. Greenland palaeo-temperatures derived from GRIP bore hole temperature and ice core isotope profiles. Tellus, 47B(5): 624–629.

Johnson J, 1994. A basal water model for ice sheets. PhD thesis, University of Minnesota. 187 pp.

Johnson J, 2004. Estimating Basal Melt Rate in Antarctica. International Symposium on Ice and Water Interactions: Processes across the phase boundary, Portland, 2004.

Johnston A C, 1987. Suppression of earthquakes by large continental ice sheets, Nature, 330, 467–469.

Johnston A C, 1989. The effect of large ice sheets on earthquake genesis, in Earthquakes at North Atlantic Passive Margins: Neotectonics and Postglacial Rebound, edited by S. Gregersen and P. Basham, pp 581–599, Kluwer, Dordrecht.

Johnston, P, 1993. The effect of spatially non-uniform water loads on predictions of sea level change. Geophysical Journal International 114, 615–634.

Johnston P, Wu P, Lambeck K, 1998. Dependence of horizontal stress magnitude on load dimension in glacial rebound models, Geophys. J. Int., 132, 41–60.

Joughin I, Tulaczyk S, 2002. Positive mass balance for the Ross Ice Streams, West Antarctica. Science 295: 476–480.

Joughin I, Abdalati W, Fahnestock M, 2004. Large fluctuations in speed on Greenland's Jakobshavn Isbrae glacier. Nature 432, Dec 2 2004: 608–610.

Kamb B, Echelmeyer K A, 1986. Stress-gradient coupling in glacier flow: IV. Effects of the "T" term. J. Glaciol. 32, 342–349.

Kamb B, 1987. Glacier surge mechanism based on linked cavity configuration of the basal water conduit system. J. Geophys. Res. 92 (B9), 16585–16595.

Kamb B, Engelhardt H, 1987. Waves of accelerated motion in a glacier approaching surge: the mini-surges of Variegated Glacier, Alaska, USA. J. Glaciol. 33 (113), 27–46.

Kamb B, 2001. Basal zone of the West-Antarctic ice streams and its role in their rapid motion. In: The West Antarctic Ice Sheet- Behaviour and Environment, R. B. Alley and R. A. Bindschadler (eds.). Washington DC. AGU 77:157–200.

Karunaratne K C, Burn C R, 2004. Relations between air and surface temperature in discontinuous permafrost terrain near Mayo, Yukon Territory. Canadian Journal of Earth Sciences, Vol. 41, pp 1437–1451.

Kaufmann G, Wu P, Wolf D, 1997. Some effects of lateral heterogeneities in the upper mantle on postglacial land uplift close to continental margins. Geophys. J. Int., 128, 175–187.

Kaufmann G, Wu P, Li G Y, 2000. Glacial isostatic adjustment in Fennoscandia for a laterally heterogeneous earth. Geophysical Journal International 143 (1), 262–273.

Kaufmann G, Lambeck K, 2002. Glacial isostatic adjustment and the radial viscosity profile from inverse modeling. Journal of Geophysical Research 107 (11), art. 2280.

Kaufmann G, Wu P, Ivins E R, 2005. Lateral viscosity variations beneath Antarctica and their implications on regional rebound motions and seismotectonics, J. Geodyn., 39.

Kendall R A, Mitrovica J X, Milne G A, 2005. On post-glacial sea level – II. Numerical formulation and comparative results on spherically symmetric models. Geophysical Journal International 161, 679–706.

Kinck J J, Husebye E S, Larsson F R, 1993. The Moho depth distribution in Fennoscandia and the regional tectonic evolution from Archean to Permian times. Precambrian Research 64, 23–51.

King L, 1984. Permafrost in Scandinavia results from Lapland, Jotunheimen and Dovre/ Rondane. Department of Geography, University of Heidelberg. (In German).

Kleman J, Hättestrand C, Borgström I, Stroeven A, 1997. Fennoscandian palaeoglaciology reconstructed using a glacial geological inversion model. Journal of Glaciology 43(144): 283–299.

Kleman J, Hättestrand C, 1999. Frozen-based Fennoscandian and Laurentide ice sheets during the last glacial maximum. Nature 402: 63–66.

Klemann V, Wolf D, 1998. Modelling of stresses in the Fennoscandian lithosphere induced by Pleistocene glaciations, Tectonophysics, 294, 291–303.

Klemann V, Wolf D, 1999. Implications of a ductile crustal layer for the deformation caused by the Fennoscandian ice sheet, Geophys. J. Int., 139, 216–226, 1999.

Klene A E, Nelson F E, Shiklomanov N I, Hinkel K M, 2001. The N-factor in natural landscapes: Variability of air and soil-surface temperatures, Kuparuk River Basin, Alaska. Arctic, Antarctic, and Alpine Research, Vol. 33, pp 140–148.

Kohler J, 1995. Determining the extent of pressurized flow beneath Storglaciären, Sweden, using results of tracer experiments and measurements of input and output discharge. J. Glaciol. 41 (138), 217–231.

Kotilainen A, Hutri K-L, 2004. Submarine Holocene sedimentary disturbances in the Olkiluoto area of the Gulf of Bothnia, Baltic Sea: a case of postglacial palaeoseismicity, Quat. Sci. Rev., 23, 1125–1135, 2004.

Krabill W, Abdalati W, Frederick E, Manizade S, Martin C, Sonntag J, Swift R, Thomas R, Wright W, Yungel J, 2000. Greenland ice sheet; high elevation balance and peripheral thinning. Science 289 (5478): 428–430.

Kuivamäki A, Vuorela P, Paananen M, 1998. Indications of postglacial and recent bedrock movements in Finland and Russian Karelia, Tech. Rep. YST-99, Geological Survey of Finland, 1998.

Kujansuu R, 1964. Nuorista siirroksista Lappissa. Summary: Recent faults in Lapland, Geologi, 16, 30–36.

Kukkonen, I, 1989. Terrestrial heat flow and radiogenic heat production in Finland, the central Baltic Shield. Tectonophysics 164: 219–230.

Lachenbruch A H, 1968. Preliminary geothermal model of the Sierra Nevada. Journal of Geophysical Research 75: 3291–3300.

Lagerbäck R, 1988. The Veiki moraines in northern Sweden – widespread evidence of an Early Weichselian deglaciation. Boreas 17(4): 469–486.

Lagerbäck R, 1979. Neotectonic structures in northern Sweden, Geol. Fören. Stockholm Förh., 100, 263–269.

Lagerbäck R, 1990. Late Quaternary faulting and paleoseismicity in northern Fennoscandia, with particular reference to the Lansjärv area, northern Sweden, Geol. Fören. Stockholm Förh., 112, 333–354.

Lambeck K, Nakada M, 1990. Late Pleistocene and Holocene sea level change along the Australian coast. Palaeogeography, Palaeoclimatology and Palaeoecology 89, 143–176.

Lambeck K, Smither C, Johnston P, 1998. Sea-level change, glacial rebound and mantle viscosity for northern Europe. Geophysical Journal International 134 (1), 102–144.

Lambeck K, 1999. Shoreline displacements in southern-central Sweden and the evolution of the Baltic Sea since the last maximum glaciation. Journal of the Geological Society, London 156, 465–486.

Lambeck K, Chappell J, 2001. Sea level change through the last glacial cycle. Science 292 (5517), 679–686.

Lambeck K, Yokoyama Y, Purcell T, 2002. Into and out of the Last Glacial Maximum: Sea-level change during Oxygen Isotope Stages 3 and 2. Quaternary Science Reviews 21, 343–360.

Lambeck K, Purcell A, 2003. Glacial rebound and glacial stress in Finland, Tech. Rep. 2003-10, Posiva Oy, Olkiluoto, Finland.

Landström O, Larsson, S A, Lind G, Malmqvist D, 1979. Geothermal investigations in the Bohus granite area in southwestern Sweden. Tectonophysics 64: 131–162.

Lang H, 1987. Forecasting meltwater runoff from snow-covered areas and from glacier basins. In: Kraijenhoff, D. A, and Moll, J. R, (eds.), River flow modelling and forecasting. Reidel, Dordrecht. 99–127.

Lang, C, Leuenberger, M, Schwander, J, Johnsen S, 1999. 16°C rapid temperature variation in central Greenland 70,000 years ago. Science 286:934–937.

Latychev L, Mitrovica J X, Tamisiea M E, Tromp J, Moucha R, 2005. Influence of lithospheric thickness variations on 3-D crustal velocities due to glacial isostatic adjustment, Geophys. Res. Lett., 32.

Latychev K, Mitrovica J X, Tromp J, Tamisiea M E, Komatitsch D, Christara C C, 2005a. Glacial isostatic adjustment on 3-D Earth models: a finite-volume formulation. Geophysical Journal International 161 (2), 421–444.

Latychev K, Mitrovica J X, Tamisiea M E, Tromp J, Moucha R, 2005b. Influence of lithospheric thickness variations on 3-D crustal velocities due to glacial isostatic adjustment. Geophysical Research Letters 32 (1), L01304.

Lemdahl G, 1988. Palaeoclimatic and Palaeoecological studies based on subfossil insects from Late Weichselian sediments in southern Sweden. Doctoral Dissertation, Lund University, Lund, 11 pp.

Lidmar-Bergström K, 1996. A long-term perspective on glacial erosion. Earth Surface Processes and Landforms 22, 297–306.

Lisiecki L E, Raymo M E, 2005. A Pliocene-Pleistocene stack of 57 globally distributed benthic $\delta^{18}O$ records. Paleoceanography 20: 1–17.

Lokrantz H, Sohlenius G, 2006. Ice marginal fluctuations during the Weichselian glaciation in Fennoscandia, a literature review. SKB TR-06-36, Svensk Kärnbränslehantering AB.

Lockwood J G, 1979. Causes of Climate. Edward Arnold, London.

Lokrantz, H, Sohlenius G, 2006. Ice marginal fluctuations during the Weichselian glaciation in Fennoscandia, a literature review. SKB TR-06-36, Svensk Kärnbränslehantering AB.

Lundqvist J, 1992. Glacial stratigraphy in Sweden. Geological Survey of Finland Special Paper 5, p. 43–59.

Lythe M, Vaughan D G, BEDMAP Consortium, 2001. BEDMAP: a new ice thickness and subglacial topographic model of Antarctica. Journal of Geophysical Research, 106(B6), 11335–11351.

Lunardini V J, 1978. Theory of n-factors and correlation of data. In Proceedings of the 3rd International Conference on Permafrost,10–13 July 1978, Edmonton, Alta. National Research Council of Canada, Ottawa, Ont., Vol.1, pp 40–46.

Lunardini V J , 1981. Heat Transfer in Cold Climates. Van Nostrand Reinhold. New York.

Lund B, Zoback M D, 1999. Orientation and magnitude of in situ stress to 6.5 km depth in the Baltic Shield, Int. J. Rock. Mech. Min. Sci., 36, 169–190.

Lund B, 2005. Effects of deglaciation on the crustal stress field and implications for end-glacial faulting: A parametric study of simple Earth and ice models. SKB TR-05-04, Svensk Kärnbränslehantering AB.

Lund B, 2006. Stress variations during a glacial cycle at 500 m depth in Forsmark and Oskarshamn: Earth model effects. SKB R-06-95. Svensk Kärnbränslehantering AB.

Mai H, Thomsen T, 1993. Permafrost studies in Greenland. In: Sixth international conference proceedings on permafrost (Vol 2). South China University of Technology Press.

Malmqvist D, Larson S A, Landström O, Lind G, 1983. Heat flow and heat production from the Malingsbo granite, central Sweden. Bull. Geol. Inst., Uppsala univ., 9: 137–152.

Marchant D R, Denton G H, Sugden D E, Swisher C C, 1993. Miocene glacial stratigraphy and landscape evolution of the western Asgard Range, Antarctica. Geografiska Annaler, 75A(4): 303–330.

Martinec Z, 2000. Spectral-finite element approach to three-dimensional viscoelastic relaxation in a spherical earth, Geophys. J. Int., 142.

McIntyre K, Delaney M L, Ravelo A C, 2001. Millennial-scale climate change and oceanic processes in the late Pliocene and early Pleistocene. Paleoceanography 16: 535–543.

McConnell R K, 1968. Viscosity of the mantle from relaxation time spectra of isostatic adjustment. Journal of Geophysical Research 73(22), 7089–7105.

Milne G A, 1998. Refining models of the glacial isostatic adjustment process. Ph. D. Thesis, University of Toronto, Toronto.

Milne G A, Mitrovica J X, 1998. Postglacial sea-level change on a rotating Earth. Geophysical Journal International 133, 1–10.

Milne G A, Mitrovica J X, Davis J L, 1999. Near-field hydro-isostasy: the implementation of a revised sea-level equation. Geophysical Journal International 139, 464–482.

Milne G A, Davis J L, Mitrovica J X, Scherneck H G, Johansson J M, Vermeer M, Koivula H, 2001. Space-geodetic constraints on glacial isostatic adjustment in Fennoscandia. Science 291 (5512), 2381–2385.

Milne G A, Mitrovica J X, Schrag D P, 2002. Estimating past continental ice volume from sea-level data. Quaternary Science Reviews 21 (1–3), 361–376.

Milne G A, Mitrovica J X, Scherneck H G, Davis J L, Johansson J M, Koivula H, Vermeer M, 2004. Continuous GPS measurements of postglacial adjustment in Fennoscandia: 2. Modelling results. Journal of Geophysical Research 109 (2), B02412.

Ministry of the Environment, 2001. Sweden's third national communication on Climate Change – Under the United Nations Framework Convention on Climate Change. Ministry of the Environment, Sweden. Ds 2001:71. 288 pp.

Mitrovica J X, Peltier W R, 1991. On post-glacial geoid subsidence over the equatorial oceans. Journal of Geophysical Research 96, 20053–20071.

Mitrovica J X, Davis J L, Shapiro I I, 1994a. A spectral formalism for computing 3-dimensional deformations due to surface loads. 1. Theory. Journal of Geophysical Research 99 (4), 7057–7073.

Mitrovica J X, Davis J L, Shapiro I I, 1994b. A spectral formalism for computing 3-dimensional deformations due to surface loads. 2. Present-day glacial isostatic-adjustment. Journal of Geophysical Research 99 (4), 7075–7101.

Mitrovica J X, Forte A M, 1997. Radial profile of mantle viscosity: Results from the joint inversion of convection and postglacial rebound observables. Journal of Geophysical Research 102 (2), 2751–2769.

Mitrovica J X, Tamisiea M E, Davis J L, Milne G A, 2001a. Recent mass balance of polar ice sheets inferred from patterns of global sea-level change. Nature 409 (6823), 1026–1029.

Mitrovica J X, Milne G A, Davis J L, 2001b. Glacial isostatic adjustment on a rotating earth. Geophysical Journal International 147, 562–579.

Mitrovica J X, Milne G A, 2002. On the origin of late Holocene sea-level highstands within equatorial ocean basins. Quaternary Science Reviews 21, 2179–2190.

Mitrovica J X, 2003. Recent controversies in predicting post-glacial sea-level change. Quaternary Science Reviews 22 (2–4), 127–133.

Mitrovica J X, Milne G A, 2003. On post-glacial sea level: I. General theory. Geophysical Journal International 154, 253–267.

Mitrovica J X, Forte A M, 2004. A new inference of mantle viscosity based upon joint inversion of convection and glacial adjustment data. Earth and Planetary Science Letters 225 (1–2), 177–189.

Moberg A, Sonechkin D M, Holmgren K, Datsenko N M, Karlén W, 2005. Highly variable Northern Hemisphere temperatures reconstructed from low- and high-resolution proxy data. Nature 433: 613–617.

Moberg A, Gouirand I, Wohlfarth B, Schoning K, Kjellström E, Rummukainen M, de Jong R, Linderholm H, Zorita E, 2006. Climate in Sweden during the past millennium – Evidence from proxy data, instrumental data and model simulations. SKB TR-06-35, Svensk Kärnbränslehantering AB.

Montagnat M, Duval P, 2000. Rate controlling processes in the creep of polar ice, influence of grain boundary migration associated with recrystallization. Earth and Planetary Science Letters 183: 179–186.

Muir-Wood R, 1995. Reconstructing the tectonic history of Fennoscandia from its margins: The past 100 million years. SKB TR-95-36, Svensk Kärnbränslehantering AB.

Munier R, Fenton C, 2004. Review of postglacial faulting, Appendix 3 in Munier R and Hökmark H, Respect distances. Rationale and means of computation. SKB R-04-17, Svensk Kärnbränslehantering AB.

Müller F, 1962. Zonation in the accumulation area of the glaciers of Axel Heiberg Island, N.W.T, Canada. J. Glaciol. 4, 302–313.

Mörner N-A, 2004. Active faults and paleoseismicity in Fennoscandia, especially Sweden. Primary structures and secondary effects, Tectonophysics, 380, 139–157.

Nakada M, Lambeck K, 1989. Late Pleistocene and Holocene sea-level change in the Australian region and mantle rheology. Geophysical Journal International 96, 497–517.

Nansen F, 1922. The Strandflat and Isostasy. VidenskapsSelskapets Skrifter I, Matematisk-Naturvitenskapelig Klasse 1921. No 11. Kristiania (Oslo). 313 pp.

NAS, 2002. Abrupt Climate Change: Inevitable Surprises, National Academy Press, Washington D.C.

Nicholls R J, Lowe J A, 2006. Climate stabilisation and impacts of sea-level rise. IN Schellnhuber, H. J., Cramer, W., Nakicenovic, N., Wigley, T. M. L. & Yohe, G. (Eds.) Avoiding Dangerous Climate Change. Cambridge: Cambridge University Press.

Nienow P, Sharp M, Willis I, 1998. Seasonal changes in the morphology of the subglacial drainage system, Haut Glacier d'Arolla, Switzerland. Earth Surf. Proc. Landf. 23, 825–843.

NSF, 2000. Directorate for Geosciences 2000 Full Report, National Science Foundation, NSF 00-27.

Nye J F, 1976. Water flow in glaciers: jökulhlaups, tunnels and veins. J. Glaciol. 17, 181–207.

Näslund J O, 1997. Subglacial preservation of valley morphology at Amundsenisen, western Dronning Maud Land, Antarctica. Earth Surface Processes and Landforms 22: 441–455 and 703.

Näslund, 1998. Ice sheet, climate, and landscape interactions in Dronning Maud Land, Antarctica. PhD thesis. Dissertation series 11, Department of Physical Geography, Stockholm University. 109 p.

Näslund J O, Fastook J L, Holmlund P, 2000. Numerical modelling of the ice sheet in western Dronning Maud Land, East Antarctica: impact of present, past, and future climates. Journal of Glaciology 46 (152): 54–66.

Näslund J O, 2001. Landscape development in western and central Dronning Maud Land, East Antarctica. Antarctic Science 13(3): 302–311.

Näslund J O, Rodhe L, Fastook J, Holmlund P, 2003. New ways of studying ice sheet flow directions and glacial erosion by computer modelling – examples from Fennoscandia. Quaternary Science Reviews 22: 245–258.

Näslund J O, Jansson P, Fastook J L, Johnson J, Andersson L, 2005. Detailed spatially distributed geothermal heat flow data for modelling of basal temperatures and melt water production beneath the Fennoscandian ice sheet. Annals of Glaciology 40: 95–101.

Olesen O, 1988. The Stuoragurra Fault, evidence of neotectonics in the Precambrian of Finnmark, northern Norway, Norsk Geologisk Tidsskrift, 68, 107–118.

Olesen O, Henkel H, Lile O B, Mauring E, Rønning J S, 1992. Geophysical investigations of the Stuoragurra postglacial fault, Finnmark, northern Norway, J. Appl. Geophys., 29, 95–118.

Olesen O, Lundin E, Nordgulen Ø, Osmundsen P T, Skilbrei J R, Smethurst M A, Solli A, Bugge T, Fichler C, 2002. Bridging the gap between the Nordland onshore and offshore geology. Norwegian Journal of Geology 82, 243–262.

O'Neill K, Miller R D, 1985. Exploration of rigid ice model of frost heave. Water Resour. Res. 21(3): 281–296.

Paananen M, Ruskeeniemi T, 2003. Permafrost at Lupin: Interpretation of SAMPO electromagnetic soundings at Lupin. Geological Survey of Finland, Nuclear Waste Disposal Research, Report YST-117.

Padilla F, Villeneuve J P, 1992. Modelling and experimental studies of frost heave including solute effects. Cold Reg. Sci. Technol. 20 (2): 183–194.

Paillard D, 2001. Glacial cycles: Toward a new paradigm. Reviews of Geophysics 39, 325–346.

Paillard D, Parrenin F, 2004. The Antarctic ice-sheet and the triggering of deglaciations. Earth and Planetary Science Letters 227, 263–271.

Paterson W S B, 1994. The physics of glaciers. 3rd edition. New York: Pergamon/Elsevier Science Ltd. 480 p.

Pattyn F, Huybrechts P, Decleir H, 1989. Modelling glacier fluctuations in the Sør Rondane, Dronning Maud Land, Antarctica. Zeitschrift fur Gletscherkunde und Glazialgeologie 25(1): 33–47.

Pattyn F, 2003. A new three-dimensional higher-order thermomechanical ice sheet model: basic sensitivity, ice-stream development and ice flow across subglacial lakes. Journal of Geophysical Research (Solid Earth), 108 (B8), 2382:EPM4-1-EPM4-15.

Pattyn F, De Smedt, B, Souchez R, 2004. Influence of subglacial Lake Vostok on the regional ice dynamics of the Antarctic ice sheet: a model study. Journal of Glaciology 50 (171): 583–589.

Paulson A, Zhong S, Wahr J, 2005. Modelling post-glacial rebound with lateral viscosity variations. Geophysical Journal International, 163. 357–371.

Payne A J, 1995. Limit cycles in the basal thermal regime of ice sheets. Journal of Geophysical Research 100(B3): 4249–4263.

Payne A J, Baldwin D J, 1999. Thermomechanical modelling of the Scandinavian ice sheet: Implications for ice-stream formation. Annals of Glaciology: 28: 83–89.

Payne A J, Huybrechts P, Abe-Ouchi A, Calov R, Fastook J L, Greve R, Marshall S J, Marsiat I, Ritz C, Tarasov L, Thomassen M P A, 2000. Results from the EISMINT model intercomparison: the effects of thermomechanical coupling. Journal of Glaciology, 46(153): 227–238.

Peltier R, 1974. The impulse response of a Maxwell Earth, Rev. Geophys. Space Phys., 12, 649–669.

Peltier W R, Farrell W E, Clark J A, 1978. Glacial isostasy and relative sea level: a global finite element model. Tectonophysics 50, 81–110.

Peltier W R, 1994. Ice Age Palaeotopography. Science 265, 195–201.

Peltier W R, 1998. Postglacial variations in the level of the sea: Implications for climate dynamics and solid-earth geophysics. Reviews of Geophysics 36 (4), 603–689.

Peltier W R, 2002. On eustatic sea level history: Last Glacial Maximum to Holocene. Quaternary Science Reviews 21 (1–3), 377–396.

Peltier W R, Drummond R, 2002. A 'broad shelf effect' upon postglacial relative sea level history. Geophysical Research Letters 29, 10.1029/2001GL014273.

Peltier W R, 2005. On the hemispheric origins of meltwater pulse 1a. Quaternary Science Reviews 24 (14–15), 1655–1671.

Pérez-Gussinyé M, Lowry A R, Watts A B, Velicogna I, 2004. On the recovery of effective elastic thickness using spectral methods: Examples from synthetic data and from the Fennoscandian Shield. Journal of Geophysical Research 109, B10409, doi:10.1029/2003JB002788.

Piotrovsky J A, 1997. Subglacial hydrology in north-western Germany during the last glaciation: groundwater flow, tunnel valleys and hydrological cycles. Quaternary Science Reviews, 16: 169–185.

Pollack H N, Hurter S J, Johnson, J R, 1991. A new global heat flow compilation. Data from International Heat Flow Commission web site.

Pollack H N, Hurter S J, Johnson J R, 1993. Heat flow from the Earth's interior: Analysis of the global data set. Rev. Geophys. 31(3): 267–280.

Påsse T, 2001. An empirical model of glacio-isostatic movements and shore level displacement in Fennoscandia. SKB R-01-41, Svensk Kärnbränslehantering AB.

Quinlan G, 1984. Postglacial rebound and the focal mechanisms of eastern Canadian earthquakes, Can. J. Earth Sci., 21, 1018–1023.

Raab B, Vedin H, 1995. Climate, Lakes and Rivers. National Atlas of Sweden. Almqvist & Wiksell international. 315 p.

Radtke U, Grun R, Schwarz H P, 1988. Electron-spin resonance dating of the Pleistocene coral-reef tracts of Barbados. Quaternary Research 29 (3), 197–215.

Raymo M E, Ganley K, Carter S, Oppo D W, McManus J, 1998. Millennial-scale climate instability during the early Pleistocene epoch. Nature 392: 699–702.

Raymond C F, Harrison W D, 1975. Some observations on the behaviour of the liquid and gas phases in temperate glacier ice. J. of Glaciology 14(71): 213–234.

Remy F, Minster J F, 1993. Precise altimetric topography in ice sheet flow studies. Annals of Glaciology 17: 195–200.

Richardson S D, Reynolds J M, 2000. Degradation of ice -cored moraine dams: implications for hazard development. In Raymond, C.F.,Fountain, A., and Nakawo, M., (eds.), Debris-covered glaciers (proceedings of a workshop held at Seattle, Washington,USA, September 2000. IAHS Publication 264: 187–207.

Richardson C, 2004. Spatial characteristics of snow accumulation in Dronning Maud Land, Antarctica. Global and Planetary Change 42(1–4): 31–43.

Riddihough R P, 1972. Regional magnetic anomalies and geology in Fennoscandia: a discussion. Canadian Journal of Earth Sciences 9(3): 219–232.

Ritsema J, van Heijst H J, 2000. Seismic imaging of structural heterogeneity in Earth's mantle: evidence for large-scale mantle flow. Science Progress 83, 243–259.

Ritsema J, van Heijst H J, Woodhouse J H, 2004. Global transition zone tomography. Journal of Geophysical Research 109 (2), B02302.

Roberts M J, Russell A J, Tweed F S, Knudsen O, 2000. Ice fracturing during jökulhlaups: implications for englacial floodwater routing and outlet development. Earth Surface Processes and Landforms 25(13): 1429–1446.

Roberts M J, 2005. Jökulhlaups: a reassessment of floodwater flow through glaciers. Reviews of Geophysics 43:1–21

Ruddiman W F, 2000. Earth's climate past and present, W. H. Freeman and Company.

Rummukainen M, 2003. The Swedish regional climate modeling program, SWECLIM, 1996–2003. Final report. Reports Meteorology and Climatology 104, Swedish Meteorological and Hydrological Institute, Norrköping, Sweden, 47 pp.

Ruskeeniemi T, Paananen M, Ahonen L, Kaija J, Kuivamäki A, Frape S, Moren L, Degnan P, 2002. Permafrost at Lupin: Report of Phase I. Geological Survey of Finland, Nuclear Waste Disposal Research, Report YST-112.

Ruskeeniemi T, Ahonen L, Paananen M, Frape S, Stotler R, Hobbs M, Kaija J, Degnan P, Blomqvist R, Jensen M, Lehto K, Moren L, Puigdomenech I, Snellman M, 2004. Permafrost at Lupin: Report of Phase II. Geological Survey of Finland, Nuclear Waste Disposal Research, Report YST-119.

Röthlisberger H, 1972. Water pressure in intra- and subglacial channels. J. Glaciol. 11 (62), 177–204.

Röthlisberger H, Lang H, 1987. Glacial hydrology. In: Gurnell, A., and Clark, M. J., (eds.), Glacio-fluvial sediment transfer. New York, Wiley and Sons.

Schlesinger M E, Yin J, Yohe G W, Andronova N G, Malyshev S, Li B, 2006. Assessing the risk of a collapse of the Atlantic thermohaline circulation in Avoiding Dangerous Climate Change, Cambridge University Press, Cambridge, Chapter 5.

Schneider T, 2000. Hydrological processes in the wet-snow zone of glaciers: a review. Z. Gletscherk. Glazialgeol. 36 (1), 89–105.

Seipold U, 1995. The variation of thermal transport properties in Earth's crust, Journal of Geodynamics, Vol. 20, pp 145–154.

Shackleton N J, Kennett J P, 1975. Paleotemperature history of the Cainozoic and the initiation of Antarctic glaciation: oxygen and carbon analyses in DSDP sites 277, 279, and 281. In: J.P. Kennett and R. Houtz (Editors): Initial reports of the Deep Sea Drilling Project, 29: 743–755.

Shreve R S, 1972. Movement of water in glaciers. J. Glaciol. 11 (62), 205–214.

Shur Y L, Slavin-Borovskiy V B, 1993. N-factor maps of Russian permafrost region. Permafrost, Proceedings of the 6th International Conference, Beijing China, July, 564–568.

Siddall M, Rohling E J, Almogi-Labin A, Hemleben Ch, Meischner D, Schmelzer I, Smeed D A, 2003. Sea level fluctuations during the last glacial cycle. Nature 423, 853–858.

Siegert M J, Dowdeswell J A, 1996. Spatial variations in heat at the base of the Antarctic ice sheet from analysis of the thermal regime above subglacial lakes. Journal of Glaciology 42(142): 501–509.

Simons M, Hager B H, 1997. Localization of the gravity field and the signature of glacial rebound. Nature 390 (6659), 500–504.

SKB, 2004a. Interim main report of the safety assessment SR-Can. SKB TR-04-11, Svensk Kärnbränslehantering AB.

SKB, 2005a. Preliminary Site Description. Forsmark area – version 1.2. SKB R-05-18, Svensk Kärnbränslehantering AB.

SKB, 2006a. Preliminary Site Description. Laxemar subarea – version 1.2. SKB R-06-10, Svensk Kärnbränslehantering AB.

SKB, 2006b. Site descriptive model Laxemar. SKB R-06-22. Svensk Kärnbränslehantering AB.

SKB 2006c. Layout Laxemar. SKB R-06-36, Svensk Kärnbränslehantering AB.

SKB, 2006d. The Biosphere at Forsmark. SR-Can. R-06-xx, Svensk Kärnbränslehantering AB.

SKB, 2006e. The Biosphere at Laxemar. SR-Can. R-06-xx, Svensk Kärnbränslehantering AB.

Slunga R, 1991. The Baltic Shield earthquakes, Tectonophysics, 189, 323–331.

SMHI, 2001. Temperaturen och nederbörden i Sverige 1961–1990, referensnormaler. Utgåva 2. Meteorologisk rapport nr 99 år 2001.

Smith M W, Riseborough D W, 1996. Permafrost monitoring and detection of climate change, Permafrost and Periglacial Processes, Vol. 7, pp 301–309.

Spring U, Hutter K, 1981. Numerical studies of jökulhlaups. Cold. Reg. Sci. Technol. 4, 227–244.

SR-Can Main Report, 2006. Long-term safety for KBS-3 repositories at Forsmark and Laxemar – a first evaluation. Main Report of the SR-Can project. SKB TR-06-09, Svensk Kärnbränslehantering AB.

Staiger J W, Gosse J C, Johnson J V, Fastook J, Gray J T, Stockli D F, Stockli L, Finkel R, 2005. Relief generation by polythermal glacier ice, Earth Surface Processes and Landforms 30(9): 1145–1159.

Stein S, Sleep N H, Geller R J, Wang S C, Kroeger G C, 1979. Earthquakes along the passive margin of Eastern Canada, Geophys. Res. Lett., 6, 537–540.

Sundberg J, 1988. Thermal properties of soils and rocks. Geologiska Institutionen Publ. A 57, Chalmers Tekniska Högskola.

Svendsen J I, Mangerud J, 1987. Late Weichselian and Holocene sea-level history for a cross-section of western Norway. Journal of Quaternary Science 2: 113–132.

Svendsen J I, Astakhov V I, Bolshiyanov D Y, Demidov I, Dowdeswell J A, Gataullin V, Hjort C, Hubberten H W, Larsen E, Mangerud J, Melles M, Möller P, Saarnisto M, Siegert M J, 1999. Maximum extent of the Eurasian ice sheets in the Barents and Kara Sea region during the Weichselian. Boreas 28, 234–242.

Tamisiea M E, Mitrovica J X, Milne G A, Davis J L, 2001. Global geoid and sea level changes due to present-day ice mass fluctuations. Journal of Geophysical Research 106 (12), 30849–30863.

Tamisiea M E, Mitrovica J X, Davis J L, Milne G A, 2003. Long wavelength sea level and solid surface perturbations driven by polar ice mass variations: Fingerprinting Greenland and Antarctic ice sheet flux. Space Science Reviews 108 (1–2), 81–93.

Tarasov L, Peltier W R, 2004. A geophysically constrained large ensemble analysis of the deglacial history of the North American ice-sheet complex. Quaternary Science Reviews 23(3–4): 359–388.

Tarbuck E J, Lutgens F K, 1999. Earth: An introduction to physical geology: Prentice Hall, Upper Saddle River, NJ, 638 p.

Taylor A E, 1995. Field measurements of n-factors for natural forest areas, Mackenzie Valley, Northwest Territories. Geological Survey of Canada, Current Research, 1995-B, pp 89–98.

Taylor A E, 2001. Relationship of ground temperatures to air temperatures in forests.Geological Survey of Canada, Bulletin 547, pp 111–117.

Thomsen H H, Thorning L, Braithwaite R, 1989. Applied glacier research for planning hydro-electric power, Ilulissat/Jakobshavn, West Greenland. Annals of Glaciology, 13: 257–261.

Thorne M C, Kane P, 2006. Climate and Landscape Change within Tools for Optioneering of Remediation and Decommissioning Solutions. Report to Nexia Solutions Ltd. MTA/ P0013/2006-1: Issue 2. Mike Thorne and Associates Limited.

Tjernström M, Rummukainen M, Bergström S, Rodhe J, Persson G, 2003. Klimatmodellering och klimatscenarier ur SWECLIMs perpektiv. Reports Meteorology and Climatology 102, Swedish Meteorological and Hydrological Institute, Norrköping, Sweden, 101 pp.

Turcotte D L, 1980. On the thermal evolution of the Earth. Earth and Planetary Science Letters 48(1): 53–58.

Tushingham A M, Peltier W R, 1991. ICE-3G: a new global model of late Pleistocene deglaciation based on geophysical predictions of post-glacial relative sea level change. Journal of Geophysical Research 96, 4497–4523.

Van Heijst H J, Ritsema J, Woodhouse J H, 1999. Global P and S velocity structure derived from normal mode splitting, surface wave dispersion and body wave travel time data (abstract). Eos Trans. AGU, Spring Meet. Suppl., S221.

Van Tatenhove F G M, Huybrechts P, 1996. Modelling of the thermal conditions at the Greenland ice sheet margin during Holocene deglaciation: boundary conditions from moraine formation. Geografiska Annaler 78A (1), 83–99.

Vidstrand P, 2003. Surface and subsurface conditions in permafrost areas – a literature review. SKB TR-03-06, Svensk Kärnbränslehantering AB.

Waddington E D, 1987. Geothermal heat flux beneath ice sheets. In: E.D. Waddington, and J.S. Walder (Eds.): The physical basis of ice sheet modelling. International Association of Hydrological Research (IAHS) publication 170:217–226.

Wagner W, Saul A, Pruß A, 1994. International equations for the pressure along the melting and along the sublimation curve of ordinary water substance. J. Phys. Chem. Ref. Data 23 (3): 515–527.

Walcott R I, 1970. Isostatic response to loading of the crust in Canada, Can. J. Earth sci., 7, 716–727.

Washburn A L, 1979. Geocryology. Edward Arnold, London.

Waelbroeck C, Labeyrie L, Michel E, Duplessy J C, McManus J F, Lambeck K, Balbon E, Labracherie M, 2002. Sea-level and deep water temperature changes derived from benthic foraminifera isotopic records. Quaternary Science Reviews 21 (1–3), 295–305.

Walder J S, Fowler A, 1994. Channelized subglacial drainage over a deformable bed. J. Glaciol. 40 (134), 3–15.

Watts A B, 2001. Isostasy and Flexure of the Lithosphere, Cambridge University Press, Cambridge.

Weart S R, 2003. The discovery of global warming, Harvard University Press.

Weertman J, 1972. General theory of water flow at the base of a glacier or ice sheet. Rev. Geophys Space Phys. 10 (1), 287–303.

Whitehouse P, Latychev K, Milne G A, Mitrovica J X, Kendall K, 2006. Impact of 3-D Earth structure on Fennoscandian glacial isostatic adjustment: Implications for space-geodetic estimates of present-day crustal deformations. Geophysical Research Letters 33, L13502, doi:10.1029/2006GL026568.

Williams P J, Smith M W, 1989. The Frozen Earth. Cambridge University Press.

Witt A, Schumann A Y, 2005. Holocene climate variability on millennial scales recorded in Greenland ice cores. Nonlinear Processes in Geophysics 12: 345–352.

Wu P, Peltier W R, 1983. Glacial isostatic adjustment and the free air gravity anomaly as a constraint on deep mantle viscosity. Geophysical Journal of the Royal Astronomical Society 74, 377–449.

Wu P, Hasegawa H S, 1996a. Induced stresses and fault potential in eastern Canada due to a disc load: a preliminary analysis, Geophys. J. Int., 125, 415–430.

Wu P, Hasegawa H S, 1996b. Induced stresses and fault potential in eastern Canada due to a realistic load: a preliminary analysis, Geophys. J. Int., 127, 215–229.

Wu P, 1997. Effect of viscosity structure on fault potential and stress orientations in eastern Canada, Geophys. J. Int., 130, 365–382.

Wu P, Johnston P, Lambeck K, 1999. Postglacial rebound and fault instability in Fennoscandia, Geophys. J. Int., 139, 657–670.

Wu P, Johnston P, 2000. Can deglaciation trigger earthquakes in N. America? Geophys. Res. Lett., 27, 1323–1326.

Wu P, van der Wal W, 2003. Postglacial sea-levels on a spherical, self-gravitating viscoelastic earth: effects of lateral viscosity variations in the upper mantle on the inference of viscosity contrasts in the lower mantle, Earth Planet. Sci. Lett., 211, 57–68.

Wu P, 2004. Using commerical finite element packages for the study of earth deformations, sea levels and the state of stress, Geophys. J. Int., 158, 401–408.

Wu P, Wood R, Stott P, 2004. Does the recent freshening trend in the North Atlantic indicate a weakening thermohaline circulation? Geophysical Research Letters 31, L02301, doi:10.1029/2003GL018584.

Wu P, Wang H, Schotman H, 2005. Postglacial induced surface motions, sea-levels and geoid rates on a spherical, self-gravitating laterally heterogeneous earth. Journal of Geodynamics 39, 127–142.

Yershov E D, 1998. General Geocryology. Cambridge University Press.

Yin J, Schlesinger M E, Andronova N G, Malyshev S, Li B, 2006. Is a shutdown of the thermohaline circulation irreversible? Journal of Geophysical Research, 111, D12104, doi:10.1029/2005JD006562, 2006.

Yokoyama Y, Lambeck K, de Dekhar P, Johnston P, Fifield L K, 2000. Timing of the last glacial maximum from observed sea level minima. Nature 406, 713–716.

Zwally H J, Abdalati W, Herring T, Larson K, Saba J, Steffen K, 2002. Surface melt-induced acceleration of Greenland ice-sheet flow. Science. 297, 218–222.

Zweck C, Huybrechts P, 2003. Modeling the marine extent of Northern Hemisphere ice sheets during the last glacial cycle. Annals of Glaciology 37:173–180.

Zoback M D, Townend J, 2001. Implications of hydrostatic pore pressures and high crustal strength for the deformation of intraplate lithosphere, Tectonophysics, 336, 19–30.

ISSN 1404-0344
CM Digitaltryck AB, Bromma, 2005